Department of Chemical Engineering
Faculty of Engineering and Science

Plantwide Control and Simulation of Sulfur-Iodine Thermochemical Cycle Process for Hydrogen Production

Noraini Mohd

This thesis is presented for the Degree of
Doctor of Philosophy
of
Curtin University

July 2018

To the best of my knowledge and belief this thesis contains no material previously published by any other person except where due acknowledgment has been made.

This thesis contains no material which has been accepted for the award of any other degree or diploma in any university.

Signature: 

Date: 27th July 2018

Acknowledgements

All praises to Almighty Allah Who had given me the strength, endurance and patience in completing this Doctoral Philosophy (PhD) dissertation. Without His will, this dissertation will never be completed. I would like to express my warmest appreciation to my supervisor, Associate Professor Dr. Jobrun Nandong, for his continuous support, motivation and guidance as well as his constructive comments and suggestions throughout my PhD adventure. I can't thank him enough for all he had done, which sparked my curiosity, excitement and determination in completing this PhD adventure.

I would like to extend my appreciations to my thesis committee, Associate Prof. Dr. Chua Han Bing, Associate Prof. Dr. Zhuquan Zang and Dr. Ujjal K. Ghosh for their insightful comments and encouragement throughout my PhD research. I would like to thank the Higher Degrees by Research (HDR) team of Curtin Malaysia Graduate School represented by Prof. Marcus Lee and Prof. Clem Kuek, and the Faculty of Engineering and Science, represented by Prof. Lau Hieng Ho, for their valuable supports. The list of my acknowledgement goes to all the lecturers and staffs involved in both faculties.

I acknowledge the financial supports given by Curtin University, Curtin Malaysia Research Institution (CMRI) and Ministry of Higher Education (MOHE).

I would like to express my sincere appreciation to my process control teammates, especially to Dr. Seer Qiu Han, Dr. Saw Shuey Zi, Dr. Tiong Ching Ching, and my CMRI colleagues Khizar Abid, Wan Nur Firdaus, Kok Ka Yee, Evelyn Chiong, Tan Kei Xian, Chan Bun Seng, Ignatius, Timothy, Angie, Luke and to all HDR members for their warm friendship, continuous support, ideas sharing, useful advices and for all the fun we have had. To my dearest Solehah's, Muslimat's, Masturat's and friends in Miri, Sarawak, thank you for always making me feel like being with my family with their care, kindness, helps and moral support during my study.

Last but not least, I dedicate my heartiest gratitude to my adored parents Mr. Noh Mat and Mrs. Nor Azizah Awang, my parent in laws, Mr. Khaleb Mohamad and Mrs. Zainab Mohamad, also to my siblings Jeffry, Nurul Naziral, Mohamad Aiman Amsyar and my sibling in laws for their prayers and encouragements. The most special gratitude goes to my beloved husband, Mohamad Izuan Khaleb for his understanding, encouragement, endless love, prayers and supports for me. Not forgotten to my beloved son, Muhammad Naufal Khalis Mohamad Izuan, who is the most precious motivation throughout this journey. Finally, I would like to thanks to those who have indirectly contributed to this research, their kindness means a lot to me. I dedicate this thesis to all of you.

Noraini Mohd, July 2018.

Abstract

Driven by the urgency to address the growing threats of energy security and global warming issues, extensive researches across multi-disciplinary fields have been conducted to develop novel technologies for the alternative fuel production. Amongst several alternative fuels, hydrogen has been identified as one of the most promising energy vectors as well as the potential to serve as key technologies for future sustainable energy systems in the stationary power, transportation, industrial and residential sectors. Despite its tremendous potential as a fuel, presently, hydrogen only accounts for 2% of the global primary energy usage where over 90% of this hydrogen is generated from fossil fuels. Therefore, the current production of hydrogen is still considered unsustainable because it depends on non-renewable sources, e.g., coal and natural gas. It is important to note that, the actual impact of hydrogen fuel on the environment depends on the technological option and raw materials used to produce the fuel. Ideally, hydrogen should be produced from water in order for its production to be sustainable. One option to realize this idea is through the Sulfur-Iodine Thermochemical Cycle (SITC) process. Although a number of studies related to the SITC process have been conducted, very little of these studies have addressed the design, optimization and control aspects of the process. As such it remains to be answered whether the SITC process is viable or not at an industrial scale in terms of the economic and controllability grounds. The goal of this PhD study is to address this important gap, and more specifically to focus on the controllability of the entire SITC plant. This plantwide control study has now become possible because of the availability of data on the chemical reactions taking place in the process. Before the plantwide control and simulation study can be performed, the dynamic model of a pre-defined SITC flowsheet is first established via mass and energy balances. MATLAB (R2014) programs are developed in order to enable simulation of the process model, which includes a number of unconventional reaction schemes and configurations, some of which prohibits the simulation to be conducted using the Aspen Plus software (version 8.6). The SITC

flowsheet is divided into three major sections: Bunsen Section, H_2SO_4 Decomposition Section and HI Decomposition Section. As far as the proposed SITC flowsheet is concerned, there are four major challenges in the SITC plant operation and control. First, the HIx (HI-I_2-H_2O mixture) solution from the Bunsen Section must be controlled well above an azeotropic composition; otherwise, the proposed separation scheme using a flash tank will not work. Second, the H_2SO_4 decomposition section must be supplied with a high-temperature heating medium to keep the reactor temperature in the range of 800^oC to 1000^oC. Third, the HI decomposition section which is of a high endothermic reaction must be maintained at a temperature in the range of 450^oC to 500^oC. This heat is supplied via a direct heat integration scheme between the H_2SO_4 and HI decomposition sections. The fourth process control challenge of the SITC plant arises from the multiple mass and energy recycles used in the system, which can potentially lead to a "snowball" effect.

In order to address the aforementioned operational challenges, a plantwide control (PWC) strategy is carefully designed using the Self-Optimizing Control (SOC) structure approach, in combination with the Principal Component Analysis (PCA) and Response Surface Methodology (RSM) techniques. In the plantwide control strategy, both decentralized Proportional Integral Derivative (PID) control and multivariable Model Predictive Control (MPC) schemes are adopted. One of the important results from the plantwide control simulation shows that a nonlinear MPC is recommended to be used for controlling the HI decomposition section. One reason for this is that a decentralized PID control scheme is unable to prevent the violation of input constraints in the reactor. It is worth highlighting that, the proposed plantwide control strategy can effectively handle all of the above-mentioned challenges, which results in the achievement of 68.6% thermal efficiency at a maximum hydrogen production of 2,400 kg/hr. This is the highest thermal efficiency ever reported so far for the SITC plant. Furthermore, a few new contributions are made in the present work where one of them is the development of the modified PWC methodology incorporating SOC structure, PCA and RSM techniques. Another

contribution of the work is a novel Loop Gain Controllability (LGC) index. The LGC index can be used to determine an operating condition having favourable controllability property.

Keywords: Hydrogen; Sulfur-Iodine Thermochemical Cycle; Plantwide Control; Modelling; Controllability

List of Publications and Presentations

Publications

1) Noraini Mohd and Jobrun Nandong. “Multi-Scale Control of Bunsen Section in Iodine-Sulphur Thermochemical Cycle Process for Hydrogen Production”. Chemical Product and Process Modelling. 2016. (accepted).
2) Noraini Mohd and Jobrun Nandong. “Routh-Hurwitz tuning method for stable/unstable time-delay MIMO processes.” Int. Conf. on Process Engineering & Advanced Materials (ICPEAM 2018), Kuala Lumpur, Malaysia, 13-15 Aug. 2018. (accepted).
3) Noraini Mohd, Jobrun Nandong and Ujjal K. Ghosh. “Plantwide Design and Control of Sulfur-Iodine Thermochemical Cycle Plant.” Submitted to a journal (under review).
4) Noraini Mohd and Jobrun Nandong. “Self-Optimizing Control Structure of Sulfur-Iodine Thermochemical Cycle Plant for Hydrogen Production.” Submitted to a journal (under review).
5) Noraini Mohd, Jobrun Nandong and Syamsul Rizal Abd Shukor. “Simulation Studies of Sulphur-Iodine Thermochemical Cycle Process for Renewable Hydrogen Generation: A Review”. (to be submitted to a journal).
6) Noraini Mohd and Jobrun Nandong. “Dynamic Controllability Analysis Method for Decentralized PID Controller: Application to Patented H_2SO_4 Decomposition Reactor”. (to be submitted to a journal).

Presentations

1) Symposium of Malaysian Chemical Engineers (SOMChE) 2016, Miri, Sarawak, Malaysia. Presentation title: “Multi-Scale Control of Bunsen Section in Iodine-Sulphur Thermochemical Cycle Process for Hydrogen Production”.
2) North Borneo Research Colloquium (NBRC) 2016, Curtin University Malaysia, Malaysia. Presentation title: “Simulation Study on Bunsen Section in Hydrogen Production via Sulfur-Iodine Thermochemical Cycle Process”.
3) Symposium of Malaysian Chemical Engineers (SOMChE) 2017, Kuala Lumpur, Malaysia. Presentation title: “Dynamic Modelling and Controllability Analysis of Intensified Reactor: High Temperature Sulphuric Acid Decomposition in a Hydrogen Production via Thermochemical Cycle process”.
4) One Curtin Postgraduate Conference (OCPC) 2017, Curtin University Malaysia, Malaysia. Presentation title: “Rigorous Dynamic Modelling of Flash Tank for Sulphuric Acid and Water Separation in a Sustainable Alternative Fuel Production Cycle”.
5) 5^{th} Postgraduate Borneo Research Colloquium, 2017, University Malaysia Sarawak, UNIMAS, Kuching, Sarawak, Malaysia. Presentation title: “Modelling of High Temperature SO_3 Decomposer in Section II of Thermochemical Cycle Process for Hydrogen Production”.
6) One Curtin Postgraduate Conference (OCPC) 2018, Curtin University Malaysia, Malaysia. Presentation title: “Dynamic Simulation and Control of Sulfuric Acid Decomposition in Integrated Boiler-Superheater-Decomposer Reactor”.

Table of Contents

List of Tables

List of Figures

List of Abbreviations

FFNN	Feed forward neural network
GMC	Generic Model Control
LGC	Loop Gain Controllability index
ISE	Integrated Squared Error
LMPC	Linear MPC
LP	Linear programming
MIMO	Multi input multi output
MPC	Model Predictive Control
MSE	Means Squared Error
MAE	Means Absolute Error
MSC	Multi Scale Control
NARX	Nonlinear autoregressive model with exogenous input
NLP	Nonlinear programming
NMPC	Nonlinear Model Predictive Control
NN-MPC	Neural Network model based on Model Predictive Control
ODEs	Ordinary Differential Equations
OPPWIDE	Optimal-Practical Plantwide optimization
PID	Proportional Integral Derivative controller
QP	Quadratic programming
SISO	Single input single output
SS-MPC	State space model based on Model Predictive Control
SSE	Sum Squared Error
SITC	Sulfur-Iodine Thermochemical Cycle

1 Introduction

Sulfur-Iodine Thermochemical Cycle (SITC) process has emerged as a promising alternative technology to produce environmental friendly hydrogen fuel. Its strong potential is currently being studied at the lab-scales and pilot plant scales. To date, the SITC plant is not yet available anywhere at the industrial scale. This chapter provides a brief research background and problem identification, which is to be addressed in this research project. This introduction presents descriptions on the research motivation and objectives, as well as the novelty, contribution and significance of the proposed study, followed by brief research procedures and finally, the thesis structure.

1.1 Overview

Hydrogen has been recognized as an environmentally friendly alternative to other fuels in both transportation and non-transportation usages. Recent publications have advocated the potential of hydrogen fuel usage as an effective mitigation method to decrease the rate of anthropogenic greenhouse gas emissions, which have been identified responsible for increasing global warming issue (Cipriani et al., 2014; Gupta and Pant, 2008a; Moriarty and Honnery, 2009; Satyapal and Thomas, 2008). Over the last few decades, considerable research efforts have been dedicated to addressing renewable hydrogen production technologies, hence realizing the Hydrogen Economy (Kasahara et al., 2017). In this regard, the production of hydrogen fuel should be based on a renewable sources, non-fossil, and one that produces clean environmentally benign by-products; see (Almogren and Veziroglu, 2004; Duigou et al., 2007; Levene et al., 2007). Based on these criteria, hydrogen production is considered a clean, environment-friendly energy carrier if it is produced from water via thermal route using a renewable energy source (Nowotny and Veziroglu, 2011). So far, water represents the main feedstock for clean hydrogen production via the thermal route, which has recently established itself as a strong potential candidate to realizing the Hydrogen Economy (Funk, 2001; Schultz, 2003).

Some of the ways to produce hydrogen from water via the thermal route includes the electrolysis method, thermochemical water splitting method and hybrid cycle method. Unlike the conventional electrolysis, which needs electrical energy to split water molecules, the thermochemical cycle can split water molecules into hydrogen and oxygen directly using thermal energy (Huang and T-Raissi, 2005). Since the thermal energy can be obtained from solar or waste heat from a high temperature nuclear reactor, the thermochemical cycle has a potential to significantly reduce the cost of hydrogen production from water. There are more than 350 thermochemical cycles, which have been identified and evaluated in 2011 by the DOE-EERE Fuel Cell Technologies Program, Sandia National Laboratories, under a project called Solar Thermochemical Cycles for Hydrogen production (STCH) (Perret, 2011a). An extensive report by Perret (2011b) summarizes that the Sulfur-Iodine Thermochemical Cycle (SITC) has demonstrated the most promising performance in terms of experimental and technical feasibility, efficiency and stability when compared to other types of thermochemical cycles.

Even though the use of 'renewable' hydrogen as a substitute for the non-renewable fossil fuels appears to be an attractive way to address global warming and energy security issues, none of the currently available hydrogen production technologies are anywhere near to a point of economic viability (Abbasi and Abbasi, 2011). Consequently, it has been envisioned that the development of optimized plant designs and engineering methods that are able to improve overall system efficiency, reduce system complexity, increase controllable properties, and lower the capital cost are imperative for the systems-level improvements of a hydrogen production plant. So far, most mainstream works related to the SITC process have focused on experimental studies with some heavy attention to chemical reaction behaviours (Xu et al., 2017a). Presently, only a limited study on modelling of hydrogen production via the SITC process has been reported, partly due to the complex nature of this process, particularly when it is desired to be operated at a commercial-scale. Furthermore, existing research on the modelling has been done rather

disparately, confined to certain sections or equipment of the thermochemical cycle process, i.e., not on the entire plantwide process.

At the plantwide level, various mechanisms and process interactions are expected to come into play in determining the process dynamics and performance of the SITC process. One important factor in determining the efficiency of the SITC plant is the formation of different immiscible phases which can occur in the Bunsen Section (Guo et al., 2012). At the heart of SITC operation is the Bunsen Section, in which the reaction yield must be high enough to achieve compositions well above that of azeotropic compositions. Meeting this objective is crucial as to enable smooth operations of the subsequent sulfuric acid and hydrogen iodide decomposition sections. Other challenges can also arise from the high temperature requirement in the Sulfuric Acid Decomposition Section and the high thermal energy demand in the Hydrogen Iodide Decomposition Section (Wang et al., 2014a). Furthermore, the presence of more than a few serial reactions, together with the mass and heat recycle streams in the SITC plant are expected to pose some challenges to controlling the plant. All of the above-mentioned challenges contribute to inherent complexity in the plantwide SITC dynamics, hence to its plantwide design and control.

Due to the presence of multiple constraints in the SITC process, the conventional PID-based control system alone may not be able to provide sufficient performance in controlling the whole plant. Furthermore, the plant nonlinearity may impose a big challenge to the control system design, e.g., dynamic nonlinearity in the separation columns or equipment operated under critical conditions, loads of recycle lines, non-stationary behaviour in some of the sub-systems, and time delays of the sensors (Rodriguez-Toral et al., 2000). Despite the expected complex dynamics of SITC plant, the application of conventional PID controllers is still desirable because the control system can be applied without that much need on knowledge of advanced process modelling and control technique. However, for a certain part/s where complex dynamics and process constraints arise, it is may be necessary to apply some advanced control techniques to control this part of the plant. Thus, a practical

plantwide control system for the SITC plant are expected to be of a mix of PID and advanced controllers, e.g., nonlinear model predictive control (NMPC).

As a holistic methodology to improve performance, a plantwide control strategy has until now remained underutilized to address some of the difficulties encountered in a thermochemical process design. In the present study, one of the focal idea is to build a systematic procedure of plantwide control strategy, which takes into account multiscale information from across multiscale layers of units in the plant. In other words, data and dynamic behaviours of each equipment in every section are combined into an integrated model, which should offer enhanced predictions and interpretations of the system emergent properties – thus, to preserve system level properties such as robustness and flexibility. It is worth highlighting that process control and optimization along with the plant design are preferably addressed systematically within a plantwide framework. This then should allow simultaneous considerations of the economic and controllability analysis of the SITC plant. Overall, by applying the plantwide control strategies, the integration of advanced and conventional ways can be formulated into a practical solution for the complex and new SITC process.

1.2 Problem Statements

The motivation for this study is driven by two important research gaps in the existing studies related to the SITC process:

a) There has been no study on the plantwide control (PWC) structure development of the entire SITC plant.
b) There has been study on the design, simulation and optimization of an industrial scale SITC plant.

In view of the aforementioned research gaps, the present study aims to answer the following questions:

a) Is the industrial scale SITC process viable on the controllability and economic grounds?
b) Which section/s in the SITC plant will impose the most difficult challenge/s to operation and control?
c) Will the heat integration between Sulfuric Acid Decomposition and Hydrogen Iodide Decomposition Sections be feasible?
d) What is the workable plantwide control structure of the industrial SITC plant?

Relating to the first motivating factor, the control structure problem is the central issue to be resolved in modern process control which is an integral part of a plant design. An integrated plant design and plantwide control study of the SITC process has so far, received very little attention from research community. Besides, there has been no report of the complete industrial scale SITC process. Bear in mind that, an integrated system design is essential to address the key operational problems in all of the three sections in the SITC process. The primary goal of the plantwide control structure analysis is to achieve both economically feasible and dynamically controllable flow sheet design. This integrated study so far, has not been performed on the SITC process. Hence in this research work, the goal is to develop a design that can achieve an optimal compromise between steady-state economic and dynamic controllability performance criteria for the entire SITC plant.

As for the second motivation factor, existing research on the modelling, optimization and controllability of an industrial scale SITC process, remains very limited. In particular, the controllability study for the SITC process is currently not available in the open literature. In short, a rigorous system engineering study (robustness, flexibility and optimal operation) of the industrial scale SITC process has not yet been done. It is believed that, the system engineering study is a crucial step toward the commercialization of the SITC process for hydrogen production.

1.3 Research Objectives

The overall goal of the research project is to study an industrial scale SITC plant design to meet a production rate of at least 1,000 kg of hydrogen per hour. To attain the aforementioned goal, the following specific objectives are pursued:

1) To develop a flowsheet of an industrial scale SITC plant. Based on the designed flowsheet, a plantwide model of the SITC system will be established and utilized in objective (ii) and (iii) of this study.
2) To optimize the plantwide SITC process using the constructed model (objective (i)) aiming to achieve an optimal trade-off between steady-state economic and dynamic controllability performance criteria. Aspen Plus software will be used for conducting steady-state simulation and to generate data for steady-state optimization. The controllability performance evaluations will be conducted using the plantwide SITC model implemented in MATLAB environment.
3) To design plantwide control strategy (hybrid of PID controller and NMPC) for the SITC process. To address the high nonlinear characteristic in certain parts of the plant, the NMPC scheme will be used to control the parts involved. Conventional PID controllers designed based on the Multi-Scale Control (MSC) scheme will be used to control other parts which demonstrates mild dynamic nonlinearity or behaviours.

1.4 Novelty, Contributions and Significance

The novelty of the proposed research project lies in the adoption of thorough system engineering approach to hydrogen production via the SITC process, which attempts to address steady-state and dynamic operability performance issues. As far as the thermochemical cycle process is concerned, such an integrative research approach has not

yet been reported in the open literature. The main contributions of this work can be summarized as follows.

From the novelty perspectives:

1) New idea of combining MSC-PID and NMPC schemes in an integrated plantwide control (PWC) structure.
2) Application of system engineering approach incorporating controllability, robustness, flexibility and optimal operations of the thermochemical cycle process.
3) A unified methodology taking into accounts both steady-state performance and dynamic controllability criteria in the plantwide optimization.

From the scientific contributions perspectives:

1) A new controllability index is developed to help analyze the controllability property of the SITC process.
2) Some new insights into the design and operating condition influences on the SITC system-level properties, which answer the aforementioned research questions.
3) Novel procedure to develop a hybrid MSC-PID and advanced NMPC strategy for effective plantwide control of a complete process plant.

The significance of the proposed study can be viewed as follows:

1) Provide some new insights into the operation and control of SITC process at an industrial scale, which should serve as an essential reference in the thermochemical cycle research topic.
2) Provide some new research directions in the development of thermochemical cycle technology as an intensified approach to high-performance, economic and environmentally friendly of hydrogen production.
3) This project contributes to the Malaysian *National Key Area* (NKA): Oil, Gas & Energy, and Education sectors. The improvement in this process has the potential

in opening a new opportunity for the energy industry in Malaysia, i.e., to venture into a new technology to producing environmentally friendly as well as economically feasible alternative fuel for utility in the transportation sector.

It is worth highlighting that, to date, the plantwide modelling and control research remains an open problem that has become increasingly important in recent years. The reason for this arises from the need of process industries to meet tighter environmental regulations and product qualities. It has been recognized that the linkage of plant layout information (plantwide model) with the advancement in process control is a key to effectively using improved standards for achieving specified process performances. For some new underdeveloped processes, such as the SITC, a novel approach is required to addressing the design and control problems in the process.

1.5 Thesis Structure

This thesis is arranged into nine chapters. In all chapters, a relatively short background on the main subject of the chapter is presented in the introduction section.

Chapter 2 includes the background review of the SITC process scheme. The chapter illustrates the main concern on the control issues in the whole process plant, along with a discussion of research, modelling, control and plant design opportunities. Finally, a general framework is suggested for the case study.

Chapter 3 presents the methodology. This chapter provides all the basic and preliminaries to the subsequent chapters. It is then followed by the step-by-step procedures of the proposed methodology up to the controller performance evaluation procedure.

Chapter 4 presents the process description, modelling, controllability analysis, process controller design and the result evaluation of the Bunsen Section in the SITC plant.

Chapter 5 presents the process description, modelling, controllability analysis, process controller design and the result evaluation of the Sulfuric Acid Section in the SITC plant.

Chapter 6 presents the process description, modelling, controllability analysis, process controller design and result evaluation of the Hydrogen Iodide Section in the SITC plant.

Chapter 7 presents the complete flowsheet development of the industrial scale SITC plant.

Chapter 8 details the plantwide control structure development of the SITC plant.

Chapter 9 provides main conclusions. Figure 1-1 shows the overall thesis structure.

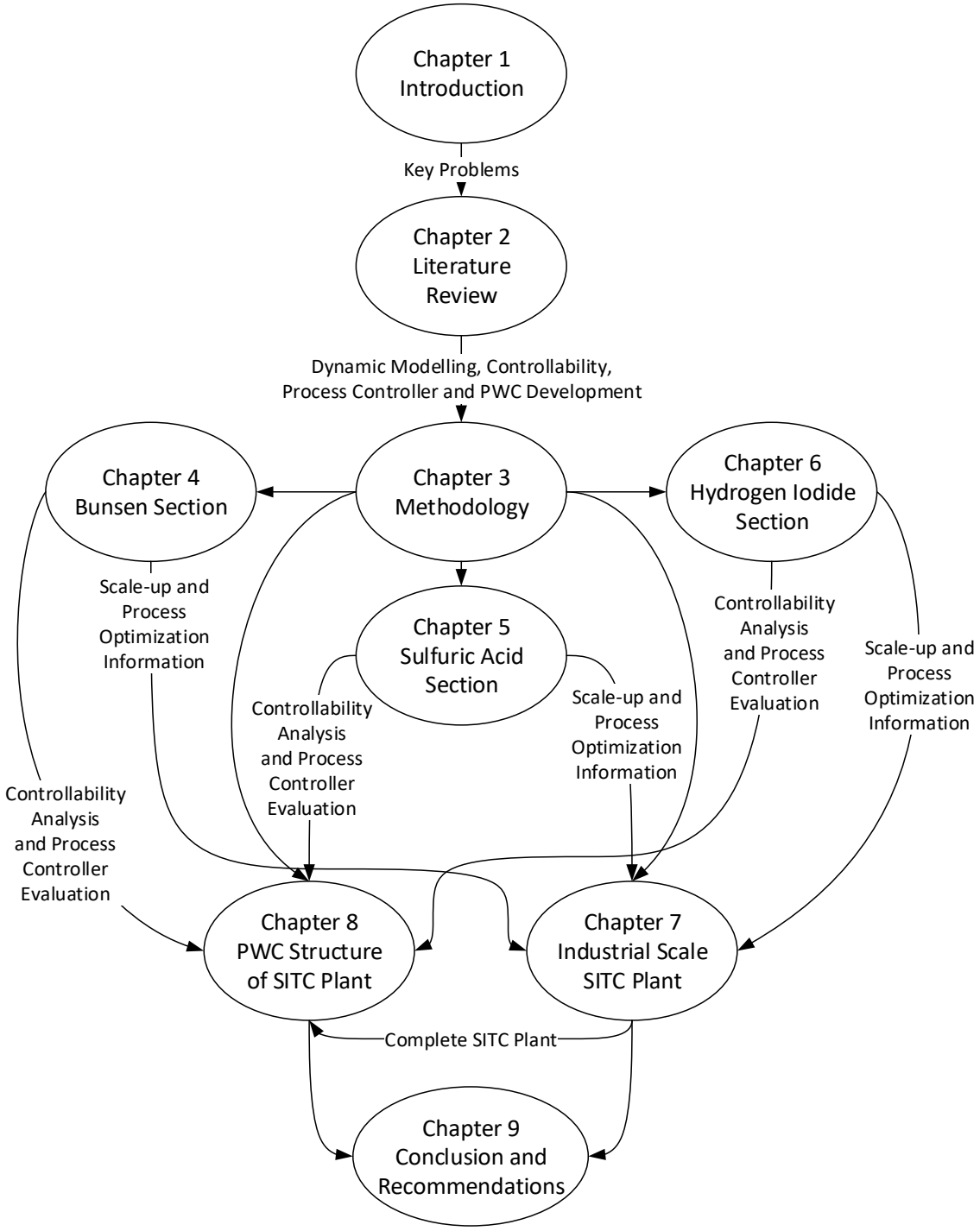

Figure 1-1: Flowchart of overall thesis structure

2 Recent Progress and Future Breakthrough of SITC Process

Modelling and process control, which accounts for major portions in the development of process models, controllers and optimization techniques have been increasingly implemented to improve product quality and productivity, and at the same time, to optimize the safety and economic performances of a given chemical plant. Efficient modelling and process control are crucial for complex processes that exhibit nonlinear behaviour, involve variable constraints, time delays and unstable reaction. The main objective of this chapter is to explore and review the existing research studies reported in literature, which are related to the modelling and process control development of the hydrogen production via Sulfur-Iodine Thermochemical Cycle (SITC) process. Additionally, the chapter summarizes the latest findings and makes some recommendations on promising research directions at the end of the chapter. The suggested framework in this chapter serves as a roadmap to the plantwide control structure development and simulation of SITC process in the subsequent stage of this thesis.

2.1 Background

Hydrogen is a superior energy carrier and its efficiency is comparable to electricity, which can be used with almost zero emission at the point of use (Gupta and Pant, 2008b). It has been technically established that hydrogen can be utilized for transportation, heating, power generation, and could replace current fossil fuel in their present use. Moreover, hydrogen can be produced from both renewable and non-renewable sources.

There are four different conventional ways of producing hydrogen: (i) from natural gas through steam reforming, (ii) from processing oil (catalytic cracking), (iii) from coal gasification and, (iv) from electrolysis using different energy mixes. The first to third

methods use fossil fuels as their raw materials (Vitart et al., 2006). Steam-methane reforming pathway represents the current leading technology for producing hydrogen in large quantities, which essentially extracts hydrogen from methane. However, this reaction causes a side production of carbon dioxide and carbon monoxide, which are greenhouse gases that contribute to global warming phenomenon. For each tonne of hydrogen produced from hydrocarbons, approximately 2.5 tonnes of carbon is released as carbon dioxide (CO_2) (Gupta and Pant, 2008b). Meanwhile, in the cases of hydrogen being produced from coal, approximately 5 tonnes of CO_2 is emitted per tonne of hydrogen produced to the atmosphere (Gupta and Pant, 2008b). These two pathways undeniably contribute to high greenhouse gas emissions and are a large fraction of air pollutions.

As today's world face an urgency to combat global warming, developing renewable fuel technologies are becoming more important, a factor that motivates the development of alternative methods of hydrogen production from renewable sources. Many recent publications presented the potential of hydrogen as transportation fuel (Gupta and Pant, 2008a; Moriarty and Honnery, 2009; Satyapal and Thomas, 2008) and mostly are focusing on the production of hydrogen from renewable energy (Duigou et al., 2007; Levene et al., 2007). In this respect, hydrogen is a clean, renewable energy carrier if it is produced from water using thermal energy by utilizing renewable energy source.

2.2 Production of Hydrogen from Water via Thermal Energy Method

A well-known method for generating renewable hydrogen is via thermal method using water as the feedstock. The water molecule is a natural and abundant source of hydrogen. It presents as a high volume resource from seawater and fresh water, especially in tropical regions like Malaysia. However, high capacities of thermal energy are required to split its molecule. There are a few ways to produce hydrogen from water using thermal energy, which are:

1. Electrolysis
2. Thermochemical water splitting
3. Hybrid cycles

Electrolysis is an established hydrogen production via thermal energy method consuming water as the feedstock. At present, electrolysis is widely used as the renewable hydrogen energy production (Gupta and Pant, 2008b). Besides electrolysis, SITC process was found to be promising for large-scale hydrogen production (Y. Guo et al., 2014; Paul et al., 2003a; Smitkova et al., 2011a; Zhang et al., 2010a). Unlike the conventional electrolysis, SITC process can convert thermal energy directly into chemical energy by forming hydrogen and oxygen (Huang and T-Raissi, 2005). The potential of SITC process is supported by abundance of quality publications and researches from a number of well-known research institutions in United States (General Atomic), Italy (ENEA), Japan (JAEA), China (INET), Korea (KAIST), and many other institutions that are currently working toward commercialisation of the SITC process.

2.3 Sulfur-Iodine Thermochemical Cycle (SITC) Process

A few factors presented by Zhang et al., (2010b) brought up the possibilities for commercialisation of the SITC process. Firstly, the SITC process is a purely thermal process, so the industrial scale is estimated to be very economic. Secondly, SITC process is proven to have high thermal efficiency, which is 50% at average; henceforth, this is good indication for the large-scale hydrogen production. Thirdly, SITC process is an all-fluid process, which makes it easier to be scaled up and consequently, realising continuous operation. There are a few challenges in the SITC process as listed in Table 2-1, including the cost of raw material, the energy source and the highly corrosive chemical reaction. The challenges, however, may be overcome with continuous research and development efforts.

Table 2.1: Advantages and challenges of SITC process (Perret, 2011a)

Advantages	**Challenges**
Sulfur and water are cheap and abundant	Iodine is scarce and expensive
Liquid/ gas stream; continuous flow process; separations are relatively easy	Corrosive chemicals
Thermal heat well-matched to advanced power tower	Non-ideal solutions prevent theoretical prediction of equilibrium states
Thermal storage concept is simple	Heat exchanger for solid particle thermal medium not demonstrated

In the thermochemical cycle process, there are three main reactions involved: Section I involves the Bunsen reaction in producing hydrogen iodide (HI) and sulfuric acid (H_2SO_4). In Section II, the H_2SO_4 decomposition occurs to produce sulfur dioxide (SO_2) and O_2, and in Section III, the HI is decomposed to generate hydrogen. Equations (2.1) to (2.3) show the general chemical reactions involved (Kubo et al., 2004):

Section I, Bunsen reaction: Exothermic Reaction, ΔH = -165 kJ/mol

$$I_2 + SO_2 + 2H_2O \leftrightarrow H_2SO_4 + 2HI \quad (2.1)$$

Section II, Sulfuric acid decomposition: Endothermic Reaction, ΔH = +371 kJ/mol

$$H_2SO_4 \leftrightarrow SO_2 + \frac{1}{2}O_2 + H_2O \quad (2.2)$$

Section III, Hydrogen iodide decomposition: Endothermic Reaction, ΔH = +173 kJ/mol

$$2HI \leftrightarrow H_2 + I_2 \quad (2.3)$$

Figure 2-1 shows an overview depicting the interconnections of the three sections in the SITC process. In this figure, the water decomposition is carried out via chemical reactions using intermediary elements: sulfur and iodine that are recycled from Section II and Section III, respectively. In order to study the operation of a process, it is important to

investigate which parameters are involved in the process operation. The inlet parameters/variables and outlet of each section are listed as in Table 2.2. At least more than ten input and output variables, respectively, are involved in the SITC process. Each variable plays a significant role in determining the dynamic controllability of the SITC plant and needs to be optimized accordingly to meet the desired plant objective.

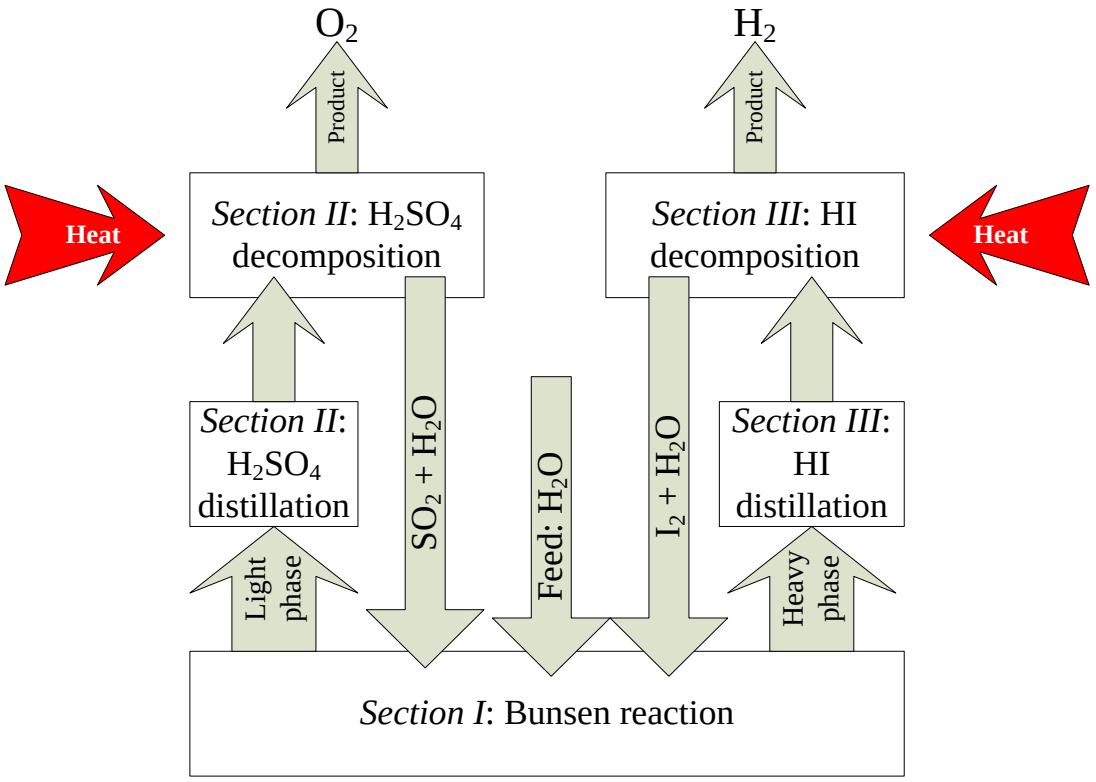

Figure 2-1 : SITC process flow diagram, Section I, Section II, and Section III (Sakaba et al., 2006)

Table 2.2: Potential input and output variables of SITC process

Section	**Input**	**Output**
I-Bunsen	1. Feed iodine flow rate 2. Feed sulfur dioxide flow rate 3. Feed water and iodine mixture flow rate 4. Feed sulfur dioxide gas flow rate 5. Feed temperature 6. Feed cooling water temperature 7. Feed cooling water flow rate	1. Sulfuric acid flow rate 2. Hydrogen iodide flow rate 3. Trace of iodide concentration 4. Water flow rate 5. Trace of sulfur dioxide concentration 6. Outlet temperature 7. Outlet cooling water temperature
II-H_2SO_4	1. Feed sulfuric acid flow rate 2. Feed sulfuric acid concentration 3. Feed temperature 4. Feed heating element temperature 5. Feed heating element flow rate	1. Oxygen flow rate 2. Outlet temperature 3. Sulfuric acid conversion 4. Sulfur dioxide flow rate 5. Sulfur trioxide flow rate
III-HI	1. Feed hydrogen iodide concentration 2. Feed flow rate of hydrogen iodide 3. Feed temperature 4. Feed heating element temperature 5. Feed heating element flow rate	1. Hydrogen flow rate 2. Outlet temperature 3. Hydrogen yield 4. Water/iodine flow rate

2.3.1 Bunsen Section (Section I)

The Bunsen Section consists of the mixing-reacting process. In this section, the objectives are to produce the desired product and to do the separation of the products. The reaction process is carried out by a continuous-stirred tank reactor (CSTR) for the liquid phase reaction (Zhang et al., 2014), while a liquid-liquid (L-L) separator is used for product separation. The Bunsen reactor is initially operated at selected steady-state conditions and assumed to be perfectly mixed. Consequently, there is no time dependence or position dependence of the temperature, concentration or reaction rate inside the reactor. This means every variable is the same at every point inside the Bunsen reactor. Thus, the concentration is identical everywhere in the reaction vessel; concentrations or temperatures are the same as the exit point as they are elsewhere in the tank. A mixture of excess iodine and water is initially fed into the Bunsen reactor and mixed with sulfur dioxide. The products formed are H_2SO_4 and HI. The H_2SO_4 solution in the lighter phase is diluted with water, while the HIx solution is in the heavier phase. These solutions are then sent to an L-L separator to be separated into two different liquid mixtures.

2.3.2 Sulfuric Acid Section (Section II)

From the L-L separator in the Bunsen Section, the aqueous light phase H_2SO_4 solution is pumped into a separator in Section II, where water is separated from the solution and recycled back to the Bunsen Section. From the separator, the enriched H_2SO_4 is sent to an evaporator, where the acid is decomposed into SO_3 and water. SO_3 is further heated up in a decomposer to separate the SO_2 and it is recycled back into the Bunsen Section. In general, this section usually consists of three main equipment: a separator, an H_2SO_4 concentrator/evaporator and an SO_3 decomposer. Section II is where the highest temperature reaction occurs in the SITC plant, where the decomposition process of SO_3 into SO_2 requires a supercritical temperature.

2.3.3 Hydrogen Iodide Section (Section III)

From the Bunsen Section, the heavy phase, which is the HIx solution, is sent to a separator in the Section III prior to entering the HI decomposer. In Section III, water will be distilled from HI solution and the remaining HI will be decomposed into hydrogen and iodine. The iodine will be recycled back into Section I. The main issue of Section III is the selection of a few choices of comparable methods. Without carefully analyzing the right chemical reaction and equipment, Section III is prone to deal with an azeotropic HI solution. Hence, the method chosen to deal with the HI solution is very crucial from the beginning of SITC process design.

2.3.4 Energy Sources to Power the Industrial Scale SITC Process

The easiest way to produce hydrogen in the SITC process is to heat the reactants with an adequate temperature so that the change of Gibbs energy is less than or equal to zero (Yadav and Banerjee, 2016a). Two energy sources that are available and currently being developed to power the SITC process are the nuclear and solar energy. Nuclear energy is the preferred heat source for the SITC introduced by GA in 1980's (O'Keefe et al., 1982). Solar energy was proposed later but has now become the focus as it is safer and more practical in certain aspects when compared to nuclear energy (Schultz, 2003). In this section, the potential of hydropower as the heat supply for the SITC process will be presented.

2.3.4.1 Nuclear Power Plant

Nuclear energy is currently utilized to produce electricity worldwide (Adamantiades and Kessides, 2009; Fino, 2014; Lattin and Utgikar, 2009; World Nuclear Association, n.d.). A number of countries have benefited from the co-generation and heat production using nuclear reactors. In 2016, more than 9 GW of new nuclear capacity was commissioned

around the world; this was the largest annual increase in the last 25 years (World Nuclear Association, n.d.).

The main process of the reactor core in a nuclear power plant is to convert nuclear energy into heat. A nuclear power plant, when coupled with a high temperature reactor, is capable of producing very high-pressure steam. It is reported that the SITC process, if combined with a nuclear energy source could achieve a thermal cycle efficiency of 52% (Schultz, 2003). At present, the main SITC research institutions in the East Asia region are following in the steps of the GA by designing and utilizing nuclear power plant facilities to supply heat for the SITC process (Cho et al., 2009; Kasahara et al., 2017; Wang et al., 2014a).

2.3.4.2 Solar Power Plant

Even though the SITC process was predominantly developed for hydrogen production with nuclear energy as the heat source, it can also be powered by solar energy (solar plant) as the required temperature for the cycle can be fulfilled by both sources. Solar hydrogen, which is considered an ultimate solution to energy and environmental problems, has received very intense research efforts globally (Bennur and Dhere, 2008; Liberatore et al., 2012; Perret, 2011b; Prosini et al., 2009; Ratlamwala and Dincer, 2014; Yadav and Banerjee, 2016b). A solar plant has the potential to produce hydrogen from water at a much larger scale in the near future. Some centers, worldwide, that are working on the solar thermochemical cycle are listed in Table 2.3. The solar plant capacity can be expanded solely by increasing the number of plant units which can be achieved by setting up solar plant units in areas where solar energy and water supply are readily available (Baykara, 2004). The only drawback of solar energy is that it is either too costly, or it faces a deficiency of high energy efficiency for the commercialisation of the SITC plants (Bennur and Dhere, 2008; Liberatore et al., 2012; Perret, 2011b).

Table 2.3: Outdoor research facilities and demonstration plants on solar thermochemical processes (Yadav and Banerjee, 2016b)

No	Centre (region)	Facility
1	CSIRO (Australia)	25kW(dish), 500kW, 1200kW(solar towers) solar methane reforming plants
2	University of Miyazak (Japan)	100kW beam down concentrator
3	IU and KIER (South Korea)	5kW dish concentrator, 45kW solar furnace
4	CAS (China)	10kW multi-dish concentrator
5	Masdar Institute (UAE)	100kW beam down facility
6	NREL (USA)	10kW solar furnace
7	IER-UNAM (Mexico)	30kW solar furnace
8	PSA (Spain)	5kW vertical axis solar furnace, 40kW and 60kW solar furnace, 7MW and 2.7MW solar towers
9	PROMES-CNRS (France)	1MW solar furnace
10	PSI (Switzerland)	40kW solar furnace
11	UCB, SuF (USA)	1MW solar biomass gasification plant
12	SNL (USA)	16kW solar furnace
13	DLR (Germany)	25kW solar furnace
14	Academy of Sciences (Uzbekistan)	1MW solar furnace

2.3.4.3 Hydro Power Plant

The potential of hydro technology is dependent on three factors: resource accessibility, minimum cost and technology enhancement. Some authorities proposed the use of hydro

power as the energy source of renewable ‘carbon-free’ hydrogen (Abbasi and Abbasi, 2011). The advantage of hydro power plant is that it has a very high ramp-up rate, which makes it particularly useful in peak load and emergency situations. Nevertheless, the SITC technology stands a good chance to be integrated with mega hydro power stations, where the high-temperature thermal energy required can be supplied via a high-temperature solar concentrator technology built at the dam site. The open space of the hydro lakes can be used as a cost-effective solar field to generate the high-temperature thermal energy supplied to Section II in the SITC plant. Water required in Section I of the SITC plant can be provided directly from the stream leaving the dam. Nevertheless, the efficiency of the SITC process combined with hydro power has yet to be achieved at this point of time.

2.3.5 SITC Pilot-Scale Research Projects

This section seeks to give an overview on important SITC pilot-scale projects and their progress. Japan, South Korea and China, through their specialised institutions, are now leading research and development of the SITC technology. In the past three decades, these countries have been working on the SITC projects on a laboratory scale and until today, they have achieved continuous production in a bench scale with the average hydrogen production rate of 10 NL/hr to 60 NL/hr. Now, these countries are moving forward to the next project, which is the scaling-up of the SITC process to industrial scale (Kasahara et al., 2017; Ping et al., 2016a).

2.3.5.1 Japan Atomic Energy Agency (JAEA) (formerly known as Japan Atomic Energy Research Institute)

2.3.5.1.1 Institution background

The JAEA has been doing research on the atomic since June 1956 (“Japan Atomic Energy Agency (JAEA),” 2017), while research and development of the SITC process started in the early 1990’s. Since then, the JAEA has arranged researches of SITC in a systematic

manner. The construction and operation of a test apparatus of an entire cycle has been the absolute objective of each procedure. When the operation of the test apparatus succeeded, research and development progressed to the next step for a larger scale test. In February 2010, a center called the High-Temperature Gas-Cooled Reactor (HTGR) Hydrogen and Heat Application Research Centre, located at the JAEA Oarai site was set up for hydrogen production. It hosted a High-Temperature Engineering Test Reactor (HTTR), which is the largest size with a capacity of 30 MWth, and is the highest temperature (950℃) reactor currently operating in the world (Sakaba et al., 2012). Due to its advantage over other water-splitting hydrogen production processes using heat from the HTGR, the SITC process has been selected by the JAEA as an important research priority for future energy technology (Sato et al., 2011).

2.3.5.1.2 Description and current facilities

At JAEA, Bunsen reaction experiments for Section I was carried out to investigate the effect of SO_2 pressure and temperature on HI concentration in the HIx phase. The Bunsen reaction condition was in the range of 323-363 K and 0.01–0.599 MPa. In the case of high SO_2 pressure and high temperature, HI molar ratio ($[HI]/([HI] + [H_2O]$)) was higher. The highest molar ratio was 18.4 ± 0.8 mol% (Kubo et al., 2012). The vapour-liquid equilibrium (VLE) data of $HI - H_2O$ and $HI - H_2O - I_2$ mixtures were measured (Hodotsuka et al., 2008). In Section II, the JAEA fabricated a H_2SO_4 decomposer bayonet reactor for H_2SO_4 vapourisation and SO_3 decomposition. The reactor was composed of silicon carbide (SiC), ceramic tubes and one SiC thermocouple sheath tube on the nest (Kasahara et al., 2017). Sealing was made of gold, and tie rods and springs were used for the connection to a pressure vessel to absorb thermal expansion. The thermal stress of the heat exchanger was analyzed, where maximum stress (126 MPa) was about half of the average tensile strength of SiC material (249 MPa) (Kubo et al., 2012). For Section III, a combination of electro-electrodialysis (EED) and conventional distillation was selected by the JAEA from several

proposed separation methods. The distilled HI vapour was decomposed thermally with a heat of 450–500℃ in the HI decomposition part.

An overview of the research and development activities on the SITC process in the JAEA is presented in Table 2.4. The research started on a small scale and was powered by electric heat supply. The first step was the laboratory-scale test, which was carried out until 1998 (Kubo et al., 2012). The JAEA then started a bench scale facility of the SITC research in 1998, which achieved a continuous closed loop operation in 2004. In 2007, one of a constructed pilot plant had successfully operated for a week with a capacity of 30 Nm^3/hr of hydrogen. In 2014, the JAEA planned to produce approximately 1,000 Nm^3/hr of hydrogen via an HTTR-IS industrial scale project. The HTTR-IS plant would be driven by the sensible heat of high-pressure helium gas, whose highest temperature reached 900℃ (Terada et al., 2007). Based on the current test facility of the industrial materials constructed by the JAEA, a 150 L/hr hydrogen production was successfully achieved. The test, with the objective of seeking for components and stability, has demonstrated a stable production rate of oxygen and hydrogen by the H_2SO_4 decomposer and HI decomposer (Kasahara et al., 2017).

Table 2.4: Overview of the research and development of the SITC process in JAEA

Research and Development Stage	**Lab stage middle of 1980s to 1997 (Sakaba et al., 2007)**	**Bench stage 1998 to 2005 (Sakaba et al., 2007)**	**Pilot stage 2007 to 2016 (Kasahara et al., 2017)**	**HTTR-IS stage 2016 to now (planned)**
Hydrogen production (Nm^3/hr)	±0.001	±0.05	±0.1	±1000
Heat supply	Electric	Electric	Helium heated electrically	Helium heated by HTTR
Material	Glass	Glass	Industrial materials	Industrial materials
Process pressure	Atmospheric	Atmospheric	High pressure	High pressure

2.3.5.2 SITC research institutes in South Korea

2.3.5.2.1 Institution background

More than one institute in South Korea are currently focused on the SITC research and development. The Korea Institute of Energy Research (KIER), the Korea Atomic Energy Research Institute (KAERI), the Korea Advanced Institute of Science and Technology (KAIST), and the Korea Electric Power Research Institute (KEPRI) have been

concentrating on the development of the technology for domestic nuclear hydrogen production since 2005.

2.3.5.2.2 Description of current research and facilities

The KAERI, through the Nuclear Hydrogen Development and Demonstration (NHDD) program, has established a plan to demonstrate the substantial production of hydrogen via a high-temperature reactor by the early 2020's (Jonghwa et al., 2007). In 2008, the KAERI developed a hybrid-design SO_3 decomposer, which could withstand severe operating conditions in Section II of the SITC process (Kim et al., 2008). The KAERI developed four main equipment to decompose the sulfuric acid, which are: an H_2SO_4 distillation column, an H_2SO_4 vaporizer, an H_2SO_4 decomposer, and an SO_3 decomposer. At the KIER, apart from reporting their conceptual design of SITC, is also studying hydrogen production from the SITC using heat from solar energy. At the KAIST, researchers (Lee et al., 2009, 2008a) have developed an upgraded flow sheet for low-pressure operating conditions of the SITC. To cope with the underlying drawbacks of conventional SITC, researchers in KAIST (Cho et al., 2009; Yoon et al., 2015) have proposed new operating windows for Section I of the SITC process and a flow sheet, which includes a flash distillation.

In a joint venture research, the KAIST and the KAERI conducted mechanical assessments to investigate suitable materials for the high-temperature HI decomposition in Section III of the SITC process (Choi et al., 2014a). In another project, both the KIER and the KAERI are working on embedding an electrodialysis cell and a membrane reactor in the SITC process. In 2012, a SITC test facility operated in a pressurized environment was constructed by the KAERI, the KIER, the KAIST, and Pohang Steel Company (POSCO), with an estimated capacity of 50 NL/hr of hydrogen production (Chang et al., 2012).

2.3.5.3 Institute of Nuclear and New Energy Technology (INET)

2.3.5.3.1 Institution background

From the 1970s, high-temperature gas-cooled reactor (HTGR) technology experienced advanced expansion in China. The Institute of Nuclear and New Energy Technology (INET) of Tsinghua University China is a body that has been initiated to carry out fundamental studies on nuclear hydrogen production since 2005. Prior to the venture in hydrogen production, the INET began with a nuclear reactor design. In 2000, the INET had successfully produced a 10 MW test reactor (HTR-10) with spherical fuel elements. In 2003, the reactor achieved its full power operation, in which a number of safety-related experiments were conducted on the HTR-10. A commercial demonstration plant project set up by the INET, namely, HTR-PM (Pebble Module) has led to the interest of the central government of China in nuclear hydrogen production research, which finally gave its approval to support the project (Ping et al., 2016b).

2.3.5.3.2 Description of current research and facilities

Unlike other institutions, the INET studied the separation characteristic of the Section I products in terms of phase equilibrium. The Bunsen reactor in Section I was studied under simulated closed-cycle conditions; the reaction between $I_2/HI/H_2O$ solution and SO_2 (Guo et al., 2012; Lan et al., 2013). For Section II, the Pt/SiC catalyst was chosen for the H_2SO_4 decomposition process. An electro-electrodialysis (EED) process was chosen for Section III to decompose the HI solution over pseudo-azeotropic conditions. The INET carried out several series of research on Section III, focusing on the catalyst selection for the HI decomposer. It is hard for HI to decompose without catalysts, even at 500℃. In the last three decades, INET's research on HI decomposition catalyst was conducted with Pt-based catalyst. The Pt/CNT catalyst was found to have the highest performance, which revealed that the dispersion and particle size of Pt on the supports played a significant role in the catalyst activity. The active carbon was selected to support Pt to catalyse the HI

decomposition in the IS-10, which reached a conversion of up to 20% with 10 L/h of hydrogen production (Wang et al., 2012).

For bench scale, the INET chose a new catalyst, the platinum-based iridium active carbon (Pt-Ir/ C), which produced 60 NL/hr of hydrogen. Further study on the catalyst by INET may be retrieved in the work of Wang et al., (2014b, 2012), Xu et al., (2017b) and Zhang et al., (2010a). The INET research center had essential facilities for the process studies of nuclear hydrogen. The HTR-10 constructed in the INET provided a proper nuclear reactor facility for upcoming research and development of nuclear-powered hydrogen production technology. A proof-of-concept facility (IS-10) (Zhang et al., 2010a) and an integrated lab-scale facility (IS-100) were constructed in consequence. From 2010 to 2014, supported by the National S&T Major project of the Ministry of Science and Technology, the INET carried out studies on the key technology of hydrogen production from HTGR. The bench-scale facility IS-100 with a hydrogen production rate 100 NL/hr was designed and built. Demonstration of continuous production of 60 NL/hr was achieved by the end of 2014 (Xu et al., 2017b). Table 2.5 presents a summary of the current and future phase research plans on the SITC process by the INET.

Table 2.5: The current and future phase research on SITC process by INET

Phase	**1**	**2**	**3**	**4**	**5**
Year	2006 to 2010	2011 to 2015	2016 to 2020	2021 to 2025	Beyond 2030
Research focus	Fundamental study and process verification of nuclear hydrogen process	Integrated laboratory-scale test	Develops the key technologies of pilot scale demonstration	Coupling the SITC technology with the nuclear reactor, nuclear hydrogen production safety and the pilot-scale test.	Aims at the commercialization of nuclear hydrogen production in China

2.4 Process Modelling and Controller Development of Thermochemical Cycle Processes

Safety is of paramount importance in the SITC plant. In the discussion of previous section, JAEA, KAIST and INET have shown a significant effort in the research and development of a stable and safe SITC process. In this respect, the control system components play an important role to ensure safety as well as a consistent operation of the overall SITC plant. Thus, the impact of control system components failure on the consistency of the hydrogen production plant must be studied (Sato et al., 2011). A good control system should be able to cope with complex dynamics such as inverse response, dead time, process uncertainties, and strong nonlinearities as well as to deal with changing operational conditions in the presence of unmeasured disturbances. In this section, discussion of the four sub-sections will be presented, they are: 1) Process controller development, 2) Process modelling development, 3) Process controller application, 4) Controllability analysis method.

2.4.1 Process Controller Development

Currently, the Proportional-Integral-Derivative (PID) controllers are most widely used to control industrial processes. Various PID controller tuning methods were developed in the past few decades. A few researchers have also studied the use of PID controllers in various thermochemical processes. A multiple input-single output (MISO) Proportional-Integral (PI) controller was developed by Sack et.al, (2012, 2015) (Säck et al., 2012), in which it was reported that the hydrogen iodide decomposition reactor unit in Section III SITC was prone to overheating due to the presence of constraints. It was reported that the control scheme to control the heat source generation of the plant developed by Sato et al. (2011) (Sato et al., 2011) was able to compensate for the disturbances, but its validation remains to be seen in further work. Al Dabbagh et al. (2010) (Al-Dabbagh and Lu, 2010) developed a different control scheme using a network control system and found that the scheme was capable of capturing the system behaviour and interaction in the controlled system.

However, verification and validation studies of the system to ensure the credibility of the method have yet to be conducted. Table 2.6 lists the recent controller schemes developed for the thermochemical cycle processes.

It is important to note that the presence of multiple constraints in the SITC process makes the PID-based controller less effective in controlling the whole plant. Furthermore, plant nonlinearity often imposes a big challenge to the control system design, e.g., the presence of nonlinearity in the separation columns or equipment operating under critical conditions, loads of recycle lines, non-stationary behaviour in the systems, and time delay of the sensors (Rodriguez-Toral et al., 2000). In general, the cost of modelling and the fact that feedback control might be designed without much need for models has motivated the use of PID control locally, but it will not be effective when applied to the entire plantwide system. In addition, model-free methods, which often lack detailed information on a given process, might lead to a low-performance controller (Ashoori et al., 2009).

As mentioned earlier, it is very difficult to achieve an effective control system design for the SITC process reactors due to the presence of constraints and nonlinearities. Due to these difficulties, the study of advanced control strategy, particularly on a model-based controller to control these systems has generated a growing attention in recent years (Ashoori et al., 2009; Costa et al., 2002). Among the well-known model-based control strategies are the Internal Model Control (IMC), the Generic Model Control (GMC) and the Model Predictive Control (MPC) (Ashoori et al., 2009; Deshpande et al., 2009; Garcia et al., 1989; Henson, 2003; Zhu et al., 2000).

Table 2.6: Controllers developed and applied in various parts of thermochemical cycle processes for hydrogen production.

No	Authors	Process	Controller	Controlled Variable	Manipulated Variable
1	Sack et al. (2015)	Thermochemical water splitting cycle using metal oxides (Simulation)	PI Controller	Temperature	Solar input power, fluid temperature of the preheating gas
2	Sato et al. (2011)	Thermochemical cycle process integrated with VHTR (Simulation)	Conventional feedback controller	Inlet turbine temperature, turbine speed	Bypass flow, coolant feed flow rate
3	Al Dabbagh et al. (2010)	Thermochemical Copper-Chlorine (Cu-Cl) Cycle (Simulation)	Network Control System (NCS)	Hydrogen production rate and hydrogen level in the storage tank	Feed flow of HCl gas, Cu particles and cooling water

2.4.1.1 Nonlinear Model Predictive Controller (NMPC)

MPC refers to a class of control algorithms, in which a dynamic process model is used to predict and optimize process performance. An important advantage of this type of controller is its ability to cope with input and output constraints, time delay, non-minimum phase behaviour and multivariable systems (Temengfl et al., 1995). The majority of chemical processes (e.g. reactors, distillation columns) are multivariable in nature, where cross-coupling effects are strong and cannot be neglected in the control design.

An extensive review on linear and nonlinear MPCs was reported by Morari and Lee (1999). Despite the fact that most real processes are approximately linear within only a limited operating window, linear MPC approaches with linear models embedded are used in the majority of applications (Morari and Lee, 1999), with the feedback mechanism of the MPC compensating for prediction errors due to a structural mismatch between the model and the process. In addition, a linear model controller is acceptable when the process operates at a single set-point and the primary use of the controller is for the rejection of disturbances. However, many processes do not operate at a single set-point, rather, in different conditions depending on market requirements.

When linear models are not sufficiently accurate because of process nonlinearities, the process can be controlled with nonlinear model predictive controllers (NMPC). In recent years, a nonlinear MPC (NMPC) has been used in several industrial processes (Ramaswamy et al., 2005). The NMPC possesses its own specialty in coping with important issues in the chemical process. It is a versatile controller, where it copes satisfactorily with a few critical fermentation issues such as nonlinearity behaviour, time delay, inverse response, multivariable system, constraint, and optimization (future prediction based on calculations), which could not cope through a conventional controller that has no models. The NMPC uses a nonlinear model and current plant measurements to calculate future moves in the independent variables (e.g. feed flow rate, inlet concentration). The nonlinear model used may be in the form of an empirical data fit or a

high fidelity model based on fundamentals such as mass, species and energy balances. The NMPC is well suited for high performance control of constrained multivariable processes such as the SITC process because the explicit pairing of input and output variables is not required and the constraints can be integrated directly into the related open loop optimal control formulation.

2.4.1.2 Multi-scale Controller (MSC)

Even though several more advanced controller techniques than the PID control have been developed over the last few decades, it is interesting to note that the PID is still the most frequently used control technique in the chemical process due to historical factors and implementation facilities. For this reason, developing and embedding a control technology that is more practical for the industry is crucial. For instance, part of the control strategies for the plant can be built based on the latest control PID-based approach, i.e., the multi-scale control (MSC) scheme, developed recently by Nandong and Zang (2013) (Nandong and Zhuquan, 2013). The MSC scheme has shown reliable performance in various processes, including multivariable processes (Nandong, 2015).

The details of the multi-scale control scheme can be found in (Nandong and Zang, 2013a). It was shown that the multi-scale control scheme could be used to synthesise practical PID controller augmented with a filter. It is interesting to note that the multi-scale control scheme can provide significant performance and robustness improvement over the conventional PID control for processes with long dead time and inverse-response behaviour. The basic idea of the multi-scale control scheme is to decompose a given plant into a sum of basic factors with distinct response speeds-multi-scale modes. A set of sub-controllers is designed based on the basic modes, which are then combined in such a way to enhance co-operation among these different modes-vital to good performance and robustness.

2.4.2 Process Controller Application

There is scarce information on the controller application applied on the SITC plant or its equipment. Hence, this section will serve as a reference analysis on the process controller applications on the other processes equipment that is similar to the equipment in the SITC plant. There are four types of major equipment in the SITC plant, which are continuous stirred-tank reactor (CSTR), liquid-liquid (L-L) separator, flash tanks, and tubular reactor or decomposers.

2.4.2.1 Continuous Stirred Tank Reactor (CSTR)

CSTR is widely used in chemical industry. The demand of global economy and increase in competition are forcing chemical processes to operate under multiple constraints. To address this requirement, research has been carried out by Pan et al. (2007) through the application of Lazy Learning-Based Online Identification and Adaptive PID Control on a CSTR system. The simulation was carried out in an AAS simulator to control the output concentration by manipulating the cooling jacket temperature. A two-layer PID according to GMV criteria has been proposed. The results show that the control system drives the controlled variable to its desired setpoint with better accuracy as compared with tuning scheme based on RHW and conventional PID method.

Seki and Naka (2008) had designed a controller scheme for CSTR with one recycle line. They applied a self-optimising control structure and selected an MPC for the supervisory layer. A PI controller is developed for the regulatory layer to control the reactor level. Both MPC and PI show good performances in controlling the nominated layer. This work can be a good reference on the PWC application on CSTR.

Prakash and Srinivan (2009) designed a nonlinear PID and an NMPC scheme to control output concentration of a stand-alone CSTR. The nonlinear process or system is represented as a family of local linear state-space model. The proposed PID and NMPC are

designed based on the local linear models. The controller performance is compared with Analytical Model-Based LMPC and NMPC. The proposed nonlinear PID has shown good set-point tracking, disturbance rejection capability at nominal and shifted operating points, and is comparable to the performance of Analytical Model-Based NMPC.

Zhao et al. (2015) had designed a terminal sliding mode controller for CSTR. By using sliding mode principles, a finite time stability observer to measure the unmeasurable states was designed. Compared to the existing terminal sliding controller, the proposed controller shows stronger robustness to external disturbance and can eliminate the error in setpoint tracking.

In 2016, Mohd and Aziz had designed the NMPC controller to control an integrated CSTR system. NARX-Based NMPC was designed to control the CSTR. In comparison to LMPC (using state-space model) and conventional PID controller, the NMPC has outperformed the other controllers in setpoint tracking, disturbance rejections and robustness tests. It can be seen that the accuracy of the model has an important role on the control of the controller action performance.

Deepa and Baraniligesan (2017) had developed a Neural Network-Based NMPC. A deep learning neural network MPC was designed and the performance of CSTR was analyzed. A hybrid article swarm optimization-gravitational search is employed to tune the weight of the neural network model. The result revealed that the controller is able to achieve minimal ISE in comparison to other types of Neural Network-Based MPC.

2.4.2.2 Liquid-liquid (L-L) separator

Designing separation equipment for two immiscible liquids is important in SITC plant. The challenge is in the fluctuations of the feed stream that inhibit the system to achieve the desired product level. Chonwattana et al. (2018) carried out an experimental work on the dynamic modelling and control of a liquid-liquid separator, or also known as a decanter.

The decanter is a bench-scale palm oil/water separator. They proposed a feedback controller to control the interface level of the liquid by manipulating the feed flow rate. The proposed controller performance was compared with the LQR and PI controllers. The experimental results showed that integrating the real-time estimation of the unmeasured disturbance into the control strategy (proposed controller) shows obvious controller improvement as compared to the LQR and PI controller. The proposed technique proved that the real-time dynamic behaviour of the decanter plays a significant role in determining good controller performance.

2.4.2.3 Flash tank

Rangaiah et al. (2002) in a study of the controller design for industrial four-stage evaporator system addressed the importance of dynamic model onto controller design. Since systems with moderate to strongly nonlinear dynamics are often encountered in the separation processes, there is a need for nonlinear model-based controller to achieve a desired system controller performance. In their study, Rangaiah et al. (2002) had designed an NMPC to control an MIMO system of an integrated flash tank. A stable control is obtained initially but steady-state offset was observed. A simple parameter adaptation technique is proposed and successfully applied to offset-free control. The result showed that NMPC is better than the PID-type controller. However, both controllers are comparable since they can be tuned to achieve the desired setpoints.

Zhang et al. (2018) carried out a study on integrating feedback control and safety systems. Their work focuses on two case studies, including one flash tank to elucidate the dynamic interaction between feedback control and safety system. In the flash tank case, they regulated temperature, level and pressure by applying a PID-type controller. Using a large-scale dynamic model simulator, they demonstrate that modifying the PID-type controllers (in this case, a PI) lead to improved close-loop performance compared to fixing the controller parameters regardless the actions of the safety system.

2.4.2.4 Tubular reactor/ decomposer

A tubular flow reactor is a vessel through which flow is continuous. The flow is usually at steady state, and configured so that conversion of the chemicals and other dependent variables are functions of position within the reactor rather than of time. Tubular flow reactors are mainly used in chemical industry and wastewater discharged units. Control of output variables is very challenging because due to the presence of high time delay in these types of reactors. Vural et al. (2015) presented an application of pH control to a tubular flow reactor. A comparison of a conventional PID controller, self-tuning PID and a PID system using fuzzy model is carried out. The excellent performance of fuzzy-based PID controller is verified as compared to the conventional PID. However, when compared to the self-tuning PID, the conventional PID shows better performance. It is worth highlighting that controlling pH via PID controller is an established method in industry. The question is, can PID control the other output variables of tubular reactor such as temperature?

Arefi et al. (2008) presented a Neural Wiener Based MPC to control a tubular reactor temperature. The performances of Neural Wiener Based MPC (NWMPC), LMPC and PID controllers are compared. The setpoint tracking behaviour system with NMPC shows good tracking speed and low overshoot for all operating points. Since the process has strong nonlinearity and wide range of operating points, it makes the PID and LMPC techniques unsuitable and hence, demanding a more complex identification and controller design procedure such as NMPC.

Another study by Puebla et al. (2013) presented a spatiotemporal pattern control by manipulating the fluid velocity of tubular reactor. The controller is implemented via numerical simulations in three benchmark tubular reactors. The proposed robust feedback controller embedded in a state estimator showed adequate performance in regulating the output and tracking the spatiotemporal pattern at a desired position. However, the concept of suppression of the complex dynamics through control at a single position does not seem

feasible to many systems. Table 2.7 presents the summary of the process controller application on CSTR, L-L separator, flash tank, and tubular reactor of various processes discussed above.

From these controller application reviews, it can be seen that the first principle mathematical model is the most popular model chosen. Even though theoretically rigorous models are more realistic and would probably lead to better results, the excessive complexity of the first principle model hinders the determination of the optimal result. This issue was asserted earlier by Willis (2000) and Willis et al. (1991), who reported that the development of the white box model (first principle model) is complicated and costly due to deficient understanding of the actual processes. In addition, these models may be too difficult to be practical because computational loads or assumptions involved will degrade the model accuracy in real-time applications (Pearson, 1995).

The black-box (empirical model) and the grey-box models (hybrid model) possess their own specialty. They are able to simplify the calculation burden of the white-box model by replacing some equations using empirical relationships, yet still fulfilling excellent performance requirement. For the nonlinear black-box model, researchers have mainly focused on NARX models and the Neural Network model. However, due to the generic structure of Neural Network, this model usually requires the estimation of a large number of parameters. Problems related to computational procedures are necessary to achieve good results, including the definition of the Neural Network dimension, the choice of nonlinear activation functions and the search for the optimum weight set, are still drawbacks to a wider use of Neural Network (Dote and Ovaska, 2001; Haykin, 1999).

On the other hand, the implementation of the NARX model is easier, where the model parameters can be verified using the information matrix, the covariance matrices or able to evaluate the model prediction error using a given final prediction error criterion. Another preferable property of the NARX model based MPC algorithm is the availability of tuning parameters that enables the adjustment of the control law and as a consequence, allows for

adjustments in controller behaviour (Mjalli and Al-asheh, 2005). In addition, it provides a great presentation for real process analysis, modelling and prediction due to its strength in accommodating the dynamic, complex and nonlinear nature of the actual process application (Harris and Yu, 2007; Mu et al., 2005). Therefore, it can be seen that the NARX model based MPC is an excellent option to represent a nonlinear or an unstable process.

Table 2.7: Summary of the process controller application on CSTR, L-L separator, flash tank and tubular reactor of various processes

No	Year	Author/s	Process Controller	Manipulated and Controlled variables (MVs and CVs)	Research category
CSTR					
1	2007	Pan et al., 2007	Lazy-Learning identification according to general minimum variance (GMV) criterion based PID controller.	MV: Cooling jacket temperature CV: Output concentration	Simulation of a stand-alone CSTR in AAS simulator system.
2	2008	Seki and Naka, 2008	PI controller and linear MPC (applied in a self-optimizing control structure)	MVs: Reactor feed flow, reflux ratio CVs: Reactor holdup, reactor temperature	Simulation of an integrated CSTR.
3	2009	Prakash and Srinivasan, 2009	Nonlinear PID, nonlinear MPC and linear MPC	MV: Coolant flowrate CV: Output concentration	Simulation of a stand-alone CSTR
4	2015	Zhao et al., 2015	Terminal sliding mode controllers (TSMC)	MV: Coolant flowrate	Simulation of a stand-alone CSTR

				CV: Output concentration, reactor temperature	
5	2016	Mohd and Aziz, 2016	Multi input multi output NARX-MPC, linear MPC and PID controller	MVs: Feed flowrate, Cooling water flowrate CVs: Product concentration, Reactor temperature.	Simulation of an integrated CSTR.
6	2017	Shakeri et al., 2017	Focker-Plank observer based MPC	MV: Coolant flowrate CV: Output concentration, reactor temperature (via a probability density function (PDF) relation)	Simulation of a stand-alone CSTR
7	2017	Deepa and Baranilingesan, 2017	Deep learning neural network MPC (DLNNMPC) and PID controller	MV: Feed temperature CV: Output concentration, reactor temperature	Simulation of a stand-alone CSTR
L-L Separator					
8	2018	Chonwattana et al, 2018	LQR, PI and a proposed model-based controllers	MVs: Water flow rate, oil flow rate CVs: Interface level, total height in the separator	Experimental and Simulation of a stand-alone separator.
Flash Tank					

9	2002	Rangaiah et al, 2002	Nonlinear MPC (NMPC) and PI controllers	MVs: Feed flow rate, feed temperature, feed density CVs: Tank level, outlet flow rate, outlet density	Simulation of integrated flash tanks.
10	2018	Z. Zhang et al, 2018	PI controller	MVs: Cooling water flow rate, outlet flow rate CVs: Tank level, tank temperature	Simulation of a stand-alone flash tanks.
Tubular reactor/ decomposer					
11	2008	Arefi et. al, 2008	PID, LMPC and NMPC	MV: Coolant flow rate CV: Reactor temperature	Simulation of a stand-alone reactor
12	2013	Puebla et.al, 2013	Robust Feedback Controller	MV: Fluid velocity CV: Spatiotemporal pattern	Simulation of a stand-alone reactor
13	2015	Vural et al, 2015	PID	MV: Feed base flowrate CV: pH	Experimental and Simulation of a stand-alone reactor

2.4.3 Process Modelling Development

Referring to the SITC challenges as mentioned earlier, the development of a precise and consistent model taking into account the critical immiscible-phase regions that will probably occur is essential in the SITC process. Also, the intricacy to deal with electrolytic behaviour, liquid-liquid immiscibility, and optimum temperature can be overcome with a well-founded process modelling. It is undeniably that the natural progression from a scratch idea to steady-state simulator to decisions on PWC is centered upon the modelling (Downs, 2012). Process modelling is well known as an invaluable tool for process cycle analysis; for flowsheet development, designing controller, performing cycle improvements, and minimizing costly experimental procedures as mentioned above. Thus, model-based control should be used when the modelling effort gives enough payback in terms of simplicity and improved performance, especially to increase the production efficiency, and this will usually be at the higher layers in the plantwide control hierarchy.

Previous control studies on thermochemical cycle process have focused on the cycle efficiency improvements, more specifically, the studies of static characteristics (Goldstein et al., 2005; Kasahara et al., 2007; Lee et al., 2008a; Paul et al., 2003a). Very little attempts have been made to investigate the process dynamics and modelling of the entire SITC plant. Recently, Singh and co-workers (Singh et al., 2012) worked on the two nonlinear models comparison without optimizer in the real-time of fault propagation analysis for the dynamic of the Cu-Cl thermochemical cycle. Their results have shown that the accuracy of the NARX model is better than the Genetic Programming (GP) in the prediction of the selected process variable behaviour and identifying the variable's interrelationship pattern. Yoon et al. (2008) also developed a nonlinear model without an optimizer by improving a Neumann's model for the SITC. The improved nonlinear model gave a result with less performance deviation as compared to the other models.

Meanwhile, Revankar et al. (2010) and Sato et al. (2011) had carried out an investigation on the dynamics of heat cogeneration systems for the thermochemical cycle process as well as investigating a control scheme that enables continuous operation of the reactors against unusual events. The simulation results demonstrated that the efficacy and technical feasibility of their proposed control scheme for continuous operation of the reactor and power conversion unit against load change events in the plant. All these phenomena are independent and must be considered in an integrated process design if it is to produce meaningful results. Table 2.8 summarizes the types of models developed for the various thermochemical processes.

Table 2.8: Type of models developed for various thermochemical cycle processes

No	Authors	Type of Model	Model	Input / Output and model source	Optimizer
1	Hossam et al. (2014)	NARX and Genetic Programming (GP)	Nonlinear	SISO* Valve Opening Percentage/Reactor Pressure. EXPERIMENTAL	NIL
2	Thanh et al. (2014)	Langmuir–Hinshelwood	Linear	MISO** I_2 feed flow rate, current flow (co and counter) of heating medium/HI conversion. EXPERIMENTAL	NIL
3	Sack et al. (2012)	State-space	Linear	MIMO*** Solar input power, fluid temperature of the gas preheating / Temperature, H2 Concentration. EXPERIMENTAL	NIL
4	Singh et al. (2012)	State- space	Linear	SISO Steam flow rate/ Temperature. SIMULATION AND EXPERIMENTAL	NIL
5	Ahmad et al. (2010)	Dynamic Flow graph Methodology (DFM)	Linear	MIMO 4 flow rate/temperature HCl and Cu. SIMULATION	NIL
6	Yoon et al. (2008)	Neumann-NRTL Thermochemical model vs. KAIST model (improved Neumann's)	Nonlinear	MIMO Temperature and HI concentration /Total pressure, hydrogen production. SIMULATION	YES

2.4.3.1 Dynamic Modelling of Separation Process

In the dynamic modelling of separation processes, to calculate the phase equilibria, there are two available methods: (1) Based on activity coefficient, and (2) Using fugacity coefficient. Before computers became readily available, the fugacity coefficient method is the preferred one, until the last six decades when the activity coefficient method took over the cumbersome calculations via computing technology. The activity coefficient can be estimated from a few models such as Pitzer, Van Laar, NRTL, UNIQUAC, Margules, and Wilson models. The NRTL and UNIQUAC models have been widely used for almost thirty years, superseding the equations of Margules, van Laar, and Wilson models (Prausnitz and Tavares, 2004).

Besides the need for choosing the right phase equilibrium estimation model, the properties of pure components and mixtures must also be estimated appropriately for a reliable simulation work. In fact, selecting the proper method for determining properties is one of the most important steps that will affect the simulation output. As a result, it is vital to carefully consider appropriate techniques to estimate different properties used in the separation model. Due to the scarcity of thermodynamic data, a lot of effort has been made to determine these properties from a known molecular structure. There are three mainstream techniques (but are not limited to) available to estimate thermodynamic properties, which are UNIFAC, Equation of State (EOS) and Langmuir.

Recently, a simulation has been carried out by Chao et al. (2017) by employing the UNIFAC method for modelling an ionic liquid process to estimate the thermodynamic properties involved at a room temperature and atmospheric pressure. Based on their findings, it was demonstrated that the UNIFAC model is adequate to estimate the thermodynamic properties at low temperature and pressure conditions. Note that for a process under supercritical conditions, the EOS approach is more frequently used. Among the popular EOS-based methods, especially for the hydrocarbon and gas processing

systems, are the Peng-Robinson (PR) and Soave-Redlich-Kwong (SRK). A new approach exploiting the PR method was presented by Deilamani and Assar (2015), which is based on a black oil separation process. It was verified that for the particular crude oil separation, the PR is efficient in identifying the gas phases as well as for two- or three-phase flash calculations. Although the EOS (PR) has been widely used, there are a few drawbacks under certain cases; it is unable to define the standard states for the high temperature and pressure conditions. Due to this limitation, a number of studies based on the mixture of different EOS methods have been carried out. For an example, Costa et al. (2009) performed a study of polyethylene separation case; they showed that the mix EOS of SRK-van der Waals (VDW) is good enough for estimating the thermodynamic of polyethylene in industrial separators. However, it is not as accurate as the single EOS method, which was also proposed in the aforementioned work. It is worth highlighting that the dynamic modelling is the best model presentation of any separation equipment, including flash tank.

In the SITC plant, flash tanks play a significant role to separate both sulfuric and Hydroiodic acids from their mixtures. To estimate the phase equilibria and thermodynamic properties of a flash tank, a pre-simulation in the Aspen Plus software shall be carried out. Once the phase equilibria and desired thermodynamic properties are obtained, the dynamic modelling of the flash tank can be performed via the MATLAB simulation. The reason for performing such modelling in MATLAB is to enable the use of many tools available in this software for optimization, nonlinear analysis and control studies–in Aspen, such studies can be limited.

2.4.3.2 Commercial Product Used for Process Modelling

The systematic method of the SITC process development via simulation consists of the modelling of the principal reactor, cooling systems, heating equipment, and separators. In evaluating the credibility of any proposed flowsheet, a few types of simulation tools were used by researchers. For instance, PROSIM software was used by Neumann (1987) to study

the activity coefficient of HI decomposition system in Section III SITC process (Cho et al., 2009). INET used OLI software to analyze the SITC electrolyte system and designed equipment model (Guo et al., 2011). Chart FX, Spread 7.0, and ActiveX control software programs were also used by INET conjointly. Nagarajan et al. (2008,2014) (Nagarajan et al., 2009) utilized the FLUENT and CFD software to model the H_2SO_4 decomposer in Section II SITC process. The JAEA utilized the dynamic simulation codes in RELAP5 software to model the HTTR-IS system (Sakaba et al., 2012). On top of it all, Aspen Plus and Aspen HYSIS are mostly used in the modelling and simulation of the SITC process (Doizi et al., 2007; Gabbar et al., 2014; Zhang et al., 2010b).

Embedding Aspen Plus and Aspen HYSIS in the modelling, design and simulation of the SITC process has now become a worldwide trend among researchers (Park et al., 2013; Schultz, 2003; Smitkova et al., 2011b). Gabbar et al. (2014) (Gabbar et al., 2014) proposed a hazard identification and risk assessment method based on the Fault Semantic network. In this work, they extracted data of the Cu-Cl thermochemical cycle (CuCl-TC) from Aspen HYSIS and carried out variable interaction analysis for the CuCl-TC process using the proposed method. Conjoining Aspen HYSIS and the FSN, researchers have successfully achieved reasonable detection and prediction of the process variables interaction. Park et al. (2013) (Park et al., 2013) had developed a best-fit electrolyte dynamic model for Section II SITC process via Aspen Plus simulation. The chosen model is the electrolyte NRTL combined with an ideal gas EOS for the phase fugacity coefficient. The conversions and heat transfers in the designed decomposer sections were found to have acceptable agreement with the experimental data. This work is useful as the foundation for further simulation on the sulfuric acid decomposition section at high pressure and temperature. Smitkova et al. (2011) (Smitkova et al., 2011b) compared the Westinghouse and the SITC methods. They carried out a life cycle analysis (LCA) via Aspen Plus simulation. The LCA results confirm that the SITC process is an attractive method for hydrogen production due to its low environmental impact. If solar energy is utilized as the heat source, any harmful environment impact will further decrease. The researchers found

a major problem to be addressed in the SITC process, which is recycling iodine. Shin et al. (2012) (Shin et al., 2012) embedded an electrodialysis cell (EDC) and a membrane reactor (MR) model in a preliminary SITC flowsheet simulation via the Aspen Plus. The EDC and MR models were designed for the HI decomposition section (Section III). The researchers calculated the thermal energy and electric energy required per unit of equipment for the entire SITC process via the simulation method. It was found that the overall thermal efficiency of hydrogen production of up to 39.4% could be expected if both EDC and MR are implanted in the process. In INET, Aspen Plus software combined with the OLI thermodynamics database was used to simulate Section III. Some parameters in the Aspen Plus databank were reviewed based on available data and models in the OLI databank to solve the HI decomposition problems and the reliability of the simulation was verified with published data (Guo et al., 2011).

A summary of simulation research carried out via Aspen Plus and Aspen HYSIS for various thermochemical cycle processes is shown in Table 2.9.

Table 2.9: Application of Aspen Plus and HYSIS in various thermochemical processes modelling and simulation

No	Authors	Simulation detail	Software	Simulation section (if SITC)
1	Rosen, 1996	Comparing few hydrogen production processes; Steam methane reforming (SMR), Thermochemical Cycle (TC) and integrated processes via exergy analysis simulation.	Aspen Plus	
2	Rosen and Scott, 1998 (Rosen, 1998)	Comparing few hydrogen production processes; SMR, TC (ispra-mark 10) and integrated process via efficiency assessments simulation	Aspen Plus	
3	Paul and Brown, 2003	Thermodynamic study of SITC process using simulation	Aspen Plus	Section I, II and III
4	Schultz et.al, 2003	Design a GA SITC process (experiment verification is needed) and compare solar and nuclear energy source for the SITC	Aspen Plus	Section III
5	Huang and Raissi, 2005	Simulation for Section II SITC process. Resulted in a simpler, more stable, and yield higher conversion efficiencies.	Aspen HYSIS	Section II

6	Yoon et.al, 2008	Thermodynamic study of SITC process using by simulation	Aspen Plus	Section III
7	Andress et .al, 2009	Simulation using Aspen algorithm for the conceptualization, reaction cluster synthesis, process integration and performance evaluation for the Fe-Cl TC. Achieved efficiency 35% to 49%.	Aspen Plus	
8	Cho et.al, 2009	Simulation of SITC process using ELECNRTL for evaluation of state and activity model. Design a model for EED coupled for HI section (applied Redlich-kwong EOS properties and Henry constant for partial pressure)	Aspen Plus	Section III
9	Anantharaman et.al, 2010	Model gasification of CO_2 and H_2 purification and compression, for the Integrated Gasification Combined Cycle (IGCC) process.	Aspen HYSIS	
10	Zhang et.al, 2010	Simulation for a HI decomposition model referring to experimental work of IS-10 by INET. Produced hydrogen at a rate 10 NL/hr., (catalyst used = Platinum on activated carbon and copper chromite)	Aspen Plus	Section III
11	Guo et.al, 2014	Simulated SITC process as reported by Brown (2003)	Aspen Plus	Section III

12	Perret,2011	Compared few conceptual design; SITC, Hybrid Sulfur, Photolytic Sulfur, Zinc Oxide, Cadmium Oxide, Sodium Manganese, Hybrid Copper Chloride).	Aspen Plus	Section II and III
13	Smitkova et.al, 2011	Compared Westinghouse and SITC method. Carried out a life cycle analysis (LCA). Found a major problem with recycling iodine in SITC process.	Aspen Plus	Section I, II and III
14	Shin et.al, 2012	Simulated a membrane reactor od the HI decomposition section	Aspen Plus	Section I, II and III
15	Park et.al, 2013	Develop best-fit electrolyte dynamic model and compare with experimental work	Aspen Plus	Section II
16	Gabbar et.al, 2014	Extract data from Aspen Hysys and carried out variable interaction analysis for CuCl-TC process.	Aspen HYSIS	

2.4.4 Controllability Analysis Methods

Most industrial process control applications involve a set of output (controlled) and manipulating variables. These processes with multiple inputs and outputs often lead to complicated transfer function models (Seborg et al., 2004). For complex units such as the separation column, the input-output variables are often interrelated, which poses a challenging problem to control engineers (Seferlis and Georgiadis, 2004). In two-input two-output (TITO) process, two input variables may affect one controlled variable or two controlled variables may be affected by one manipulated variable. This is known as the process interaction or coupling, which plays a critical role in the process controller design. As the interaction gets severe, it becomes more difficult to control the given process. Conventionally, controllability index is utilized to determine input-output interaction as well as controller pairing, where it is an essential step prior to the process controller development.

The currently available controllability analysis methodologies range from pure mathematical programming techniques (e.g. Heath, Kookos, & Perkins, 2000; Wang & McAvoy, 2001) to heuristic-based methods (e.g. Luyben, Tyreus, & Luyben, 1999) (Kookos and Perkins, 2002). There are three categories of controllability methods: (1) Steady-state, (2) Linear dynamic, and (3) Nonlinear dynamic model-based (Karami et al., 2015).

Relative Gain Array (RGA) by Bristol (1966) is the most widely steady-state type controllability analysis method used over the past fifty years. Although there are other more advanced controllability methods, the RGA is still used as an initial screening tool to avoid impractical pairings based on some criteria such as reliability and robustness (Rangaiah and Kariwala, 2012). The steady-state RGA analysis is based on the open-loop gains of the given process. It provides a relatively simple way to evaluate the severity of process interaction and its impact on controller pairings. For a decentralized control based on the RGA analysis, one should pair the manipulated variable, u_j with the controlled variable, y_i such that λ_{ij} is positive and close to 1. Based on the RGA, the best pairings should meet two rules: i) The pairings along the diagonal shall have the RGA matrix close to unity at frequencies around the closed-loop bandwidth, and ii) The

steady-state RGA elements are positive (avoid negative elements, if possible). Note that several variants of the Bristol's RGA have been developed, e.g. dynamic RGA, RNGA, et cetera. Rigorous analysis and discussion on the process controllability was presented by Shen et al., (2010). The authors laid down some rules in the pairings of manipulated and controlled variables for a decentralized control system as follows:

1) All paired RGA elements are positive.
2) Niederlinski Index (N_I) is positive.
3) All paired relative normalized gain array (RNGA) elements are closest to 1.
4) Large RNGA elements are avoided.

Since the controllability analysis involves the RNGA, RGA and N_I criteria, the result should give a more thorough understanding of the issue affecting the decentralized control design. Here, the RNGA is used to measure the loop interactions whilst the RGA and NI are used to rule out closed-loop unstable pairings. Just like the RGA, the N_I can also be used alone to analyze controller pairings for multi-loop SISO controllers, but this only gives partial understanding on the controllability. As RGA does not use information about the process dynamics, it can sometimes lead to incorrect pairings.

A number of methods have been proposed to overcome this restriction of RGA, which uses RGA-type mapping. Unlike RGA, the resulting matrix for some of such recently proposed methods has no associated physical interpretation. An obvious reason for the success of the RGA-type mapping is that repeated application of this mapping can identify diagonally dominant elements of a matrix, provided such elements exist. On the other hand, methods such as μ-interaction measure and those based on controllability and observability analysis are theoretically more sound; their use has however, been limited (Moaveni and Kariwala, 2012).

2.4.4.1 Research Gap in Controllability Analysis

An interesting quote made by Downs (2012), "*A theoretically correct but persistently time-consuming approaches will depreciate their implementation by the process control design community*" (Downs, 2012). Inspired by this quote, it is understood that any controllability analysis methods should be simple but efficient.

When we come across an unstable model or a nonlinear model, it is common to jump straight forward onto a model-based controller. Similarly, for a stable or linear model it is always decided to use a PID controller. In regard to this issues, a few questions aroused,

1) To what extent does an unstable or a nonlinear model is unable to be control by a PID controller?
2) Is there a way to know the possibility whether an unstable or a nonlinear type of model is controllable by a PID controller?
3) Is it true that a stable or linear model is surely controllable by a PID controller?
4) How reliable is the RGA index interpretation in articulating the level of a model controllability?

Essential in a controllability analysis is that the adopted method should, in theory:

a) Enable the determination of the input-output pairings in the presence of process interaction, and
b) Estimate the maximum achievable controller performance.

However, none of the aforementioned controllability indices can simultaneously meet these two criteria, i.e., determination of controller pairings and estimation of the maximum achievable controller performance. Many of the existing controllability analysis methods address the controller pairings based solely on the steady-state process gains.

The past thirty years have seen rapid advances in the process controller development that utilizes process dynamic behaviour and to a certain extent, this has led to a more efficient process operation; see (Alberto et al., 2010; Chin et al., 2010; Froisy, 2006; Mohd and Aziz, 2016; Shafiee et al., 2008). The advancement in the process controller design has spurred a renewed interest to improve the controllability analysis method based on the dynamic behaviour of the process model. Compared to the steady-state controllability analysis method, the dynamic model-based method can give significantly improved performance.

In order to fulfill the aforementioned gap, a controllability analysis index has been developed recently. The Loop Gain Controllability (LGC) is a controllability index that utilizes the loop gain information of a control loop, seeking for the upper and lower limit of the process controller. An advantage of the proposed LGC index is that it is not only straightforward, but can utilize both steady-state and dynamic information from the given process. The index estimates the impacts of process interaction, dead time and time constants on the maximum achievable controller performance. Hence, it not only assesses the pairings, but also estimates the controller performance achievable from a given pairing. Both the stability and performance margins of the single-input single-output (SISO) controller can be inferred from the LGC index. LGC can efficiently evaluate the performance of a control scheme without performing controller design and closed-loop simulation. Table 2.10 lists the function-feature comparison between the LGC index and the RGA and N_I indices. Noticeably, the LGC can provide a more comprehensive controllability analysis than the RGA and N_I-LGC capable of determining the best pairing as well as estimating controller performance limit.

Table 2.10: Function and feature comparison between RGA, NI and LGC

Controllability Indices	**Function-feature**	**Objective**	**Interpretation**
Relative Gain Array (RGA) (Bristol, 1966)	Based on λ_{ii} derived from process gains. Steady-state approach'	To determine input-output pairings based on the diagonal matrix.	If $\lambda_{ii} = 1$, the corresponding input-output pairing has no control effect on the output. If $0 < \lambda_{ii} < 1$, closed loop interaction is more severe the smaller the value. Interaction is most severe at $\lambda = 0.5$. For $\lambda_{ii} > 1$, the interaction becomes severe as the value increases, so more difficult to control. Pairing on negative λ should be avoided.
Niederlinski Index (Niederlinski, 1971)(Niederlinski, 1971)	Ratio of a determinant of the process gain matrix to the product of the diagonal elements. Steady-state approach	To determine if multi-loop SISO controllers with integral action can control the system.	The negative value means that the closed-loop system is unstable under PI control with positive loop gain and integral action.
Loop Gain Controllability (LGC) (present work)	Function of k, τ, θ and λ_{ii}. Dynamic approach	Use to estimate controller performance of multi-loop SISO controllers.	The positive value indicates the selected pairing is controllable by PID controller. While negative value means that the loop is uncontrollable. The larger the value means the higher the achievable controller performance. If two systems have comparable LGC values, then the performance will also be comparable.

2.5 Plantwide Control Structure

Since the SITC process has many measurements and control loops, the strategy of Plantwide Control (PWC) is proposed in this work. The PWC design has attracted a lot of research interest in the process control community over the last four decades, since the pioneering work by Buckley (1964). In definition, the PWC refers to a control philosophy of the overall plant emphasizing on the structural decisions. The PWC calculates optimal values for the set of selected manipulated variables in order to maximize a plantwide profitability objective function instead of just maintaining a set of controlled outputs at the predefined setpoint. The PWC considers the entire aspects such as feed changes and interaction between processes affecting the safety and optimal operation of the entire plant (Rangaiah and Kariwala, 2012). The structural decision comprises the selection or placement of manipulators and measurements along with the classification and breakdown of the total problem into smaller sub-problems (the control configuration) (Larsson and Skogestad, 2000).

Luyben and Tyreus (1997) presented nine steps of the PWC design. Steps 1 and 2 establish the objectives of the control system and the available degrees of freedom. Step 3 ensures that any production of heat (entropy) within the process is properly dissipated. Steps 4 and 5 are to satisfy the business objectives concerning production rate, product quality and safety. Step 6 involves total mass balance control, whereas in Step 7, it ensures that non-conserved chemical components are accounted for. In Step 8, complete the control systems for individual unit operations. Finally, Step 9 uses the remaining degrees of freedom for optimization and improves dynamic controllability. It should be highlighted that most of these steps required experience-based knowledge. Hence, in this work, these nine steps will be used as the general guideline for PWC structure design.

Larrson and Skogestad (2000) introduced a new PWC method, which is a hybrid between process- and mathematically-oriented approaches. The PWC method inspired by the Luybens procedure is known as Skogestad Self-Optimizing Control (SOC). SOC is a stepwise PWC procedure of seven-step and divided into a top-down part and a bottom-up part.

2.6 Research Challenges in SITC Process

In the last few decades, the exploration of the SITC process has grown rapidly. This is evident by the increasing number of research that has been published. Nevertheless, there is scarce information on the rigorous dynamic modelling and process controller development of the entire SITC process or research on the complete SITC process flowsheet particularly on an industrial scale. This includes overall mass and energy balances and presenting the focal operating conditions such as temperature, pressure and composition in the process, equipment design, process controllability analysis, and cost (capital and operating) estimates. It is indisputable that the actual implementation of the SITC process is much more complex than the simple presentation of its chemical reactions. The entire SITC process is closely attached with many recycle streams. Therefore, the reliability of a designed flowsheet is difficult to evaluate by means of experimentation tools.

At this point, a requirement to build an effective design, modelling and process control system by dint of a simulation tool to evaluate the reliability of the designed flowsheet is important. A number of tools can be used for HI and H_2SO_4 decomposition; however, there are no available tool to simulate the entire cycle (Ping et al., 2016a). There are a few major constraints to be addressed in the modelling and process control development of the SITC process:

a) The chemical species includes strong acids (HI and H_2SO_4) that are immiscible (Paul et al., 2003b). During the operation, the ratio of HI and H_2SO_4 in the reactor involved must be kept above a threshold value for optimum separation. The ratio of these two species is very sensitive to changes in the operating conditions induced by disturbances. Also, it is important to feed iodine and sulfur to the reactor at an optimum composition ratio. An analysis of thermodynamics by Baykara (2004) (Baykara, 2004) suggests that at 1 bar and 2500 K, only 2.69% of water is decomposed into hydrogen and this will increase to 25% at a lower pressure of 0.05 bar. Hence, the optimum operating pressure and temperature must be studied.

b) Two main elements for the simulation of the Section I are the prediction of the phase states and the calculation of the phase compositions (Guo et al., 2012). In the Bunsen Reactor, the HI, I_2, H_2O, and H_2SO_4 co-exist. The evaluation of the phase states has to be portrayed with an appropriate modelling method. There are three possible states in the Bunsen Reactor: homogeneous phase, two-liquid phase, and two-liquid phase with I_2 precipitation. All states are possible to be simulated by a simulation software. For instance, if the two-phase state is selected, then the accurate calculation of the solution composition is essential. For a control system design, it is essential to control the feed of SO_2 pressure as well as the H_2O feed flow rate in order to produce optimum amounts of HI and H_2SO_4(Mohd and Nandong, 2017).

c) Section II has units that operate at very high temperatures (around 800℃ or more) that go beyond the critical temperature of water (374℃), which is the H_2SO_4 decomposer (Kim et al., 2008; Nagarajan et al., 2014). Since the H_2SO_4 decomposer runs endothermic reaction, the temperature and energy supplied to the system must be sufficient. As a rule of thumb, a higher temperature tends to favors greater efficiency. However, the energy (heat) must be controlled below 1140℃ to prevent a dangerous process runaway reaction from occurring. If the temperature can be decreased to some extent, but at the same time keeping the operational efficiency at the same level, or even higher, then a great deal of many resources can be saved with better safety conditions. Interestingly, that is a challenge to be addressed in order to design Section II effectively and to make sure that a high conversion is achievable by the designed H_2SO_4 decomposer. The next constraint is the type and efficiency of the available energy source, which requires an in-depth study on the thermodynamic properties of the heat supply that include the heat capacity of the design material. The efficiency of the sulfuric acid and water separation system prior to entering the H_2SO_4 decomposer should also be realistic. Since the SITC process occurs in a cycle, failure to remove water will affect the cycle efficiency, hence reducing the hydrogen production (Lee et al., 2009).

d) Section III often encounters the complex nonlinear behaviour of the $HI - I_2 - H_2O$ system, which includes various liquid phases, azeotropes and possible solid precipitation. From the thermodynamic point of view, the current understanding of Section III has so far remained limited compared to Sections I and II. The binary ($HI - H_2O$) and ternary ($HI - I_2 - H_2O$) mixtures in the HI section are strongly non-ideal solutions and partially immiscible systems, which are difficult to model and predict their thermodynamic behaviours. In addition, the presence of an azeotrope in the binary mixture $HI - H_2O$ prevents a high concentration of HI, which causes the incomplete and slow decomposition of HI into H_2 and I_2, and leads to a very large energy demand due to the substantial calorific capacity of the HI mixture containing large amounts of iodine and water.

All of the constraints above must be overcome for the SITC to move forward to the commercialization stage. In this work, fundamental and empirical models will be developed to describe the dynamic behaviour of the thermochemical cycle process. Aspen Plus simulation will be utilized to extract the required data and parameters that are not available in the literature. An integrated MSC and NMPC scheme will be designed in MATLAB environment and implemented to control the SITC process. A new controllability analysis method will be implemented prior to process controller design. All controllers developed in this work will be implemented in the PWC strategy and the proposed approach will be evaluated based on its efficiency, economic and operability, while demonstrating the benefits of using the proposed PWC strategy.

2.7 Summary

In this chapter, the background of SITC process has been reviewed and summarized as follows:

a) SITC process has received a remarkable attention worldwide due to its high potential as a renewable hydrogen production in a large scale.

b) The availability of renewable energy sources such as from a nuclear, solar and hydro power would increase the potential of SITC process toward its commercialization.

c) SITC process to date has received little research attention in the area of modelling and process controller design. Thus, this lack of study opens a new opportunity for fresh new ideas and innovative researches in this area.

d) The dynamic modelling, process controller design and PWC structure development present a bright prospective to optimize the energy usage of SITC plant, and achieve trade-off between economic and dynamic plant controllability; therefore, producing an optimal STIC plant.

3 Methodology: From Process Modelling to PWC Structure Development

In Chapter 2 it has been substantiated that the dynamic modelling, process controller design and PWC structure development have a bright prospective in the development of SITC plant. In regard to that, Chapter 3 will provide several further basics and preliminaries, including methodology for the process modelling, controller design for subsequent works in this research. This chapter is laid down as follows - starting with SITC flowsheet design, process modelling and finally the PWC structure design. The details and summaries of the Loop Gain Controllability index and its related analysis, the PWC structure optimization procedure and its control approach, as well as the Multi-Scale Control and Model Predictive Control schemes are also presented.

3.1 Overview

Controlling the Bunsen Section, Sulfuric Acid Section and Hydrogen Iodide Section are crucial in SITC process. In the past, many researchers only focused on the study of the process behaviour rather than study on the process control development of the SITC process. Until now, there is no research has been carried out to study which section impose the most difficult challenges to operation and control. Moreover, no work has been reported to improve the controllability of the given SITC process. Therefore, dynamic modelling of the entire plant of the SITC process will be develop prior to the controllability analysis and process controller design. The process controller development will be assembled in a systematic PWC structure. One of the task in this work is to embark the SITC plant scale-up procedure since there is none industry scale of SITC plant available. The SITC process will be scale-up from laboratory scale to an industrial plant scale prior to PWC structure development.

The overall process methodology in this work consisted of preliminary work, modelling and simulation study, plant scale-up, process controller design and development, plantwide model, plantwide optimization, plantwide control structure

design, and finally the performance evaluation. The detail of each methodology are presented as follows. An overall summary of process methodology is presented by a flowchart in Figure 3-1.

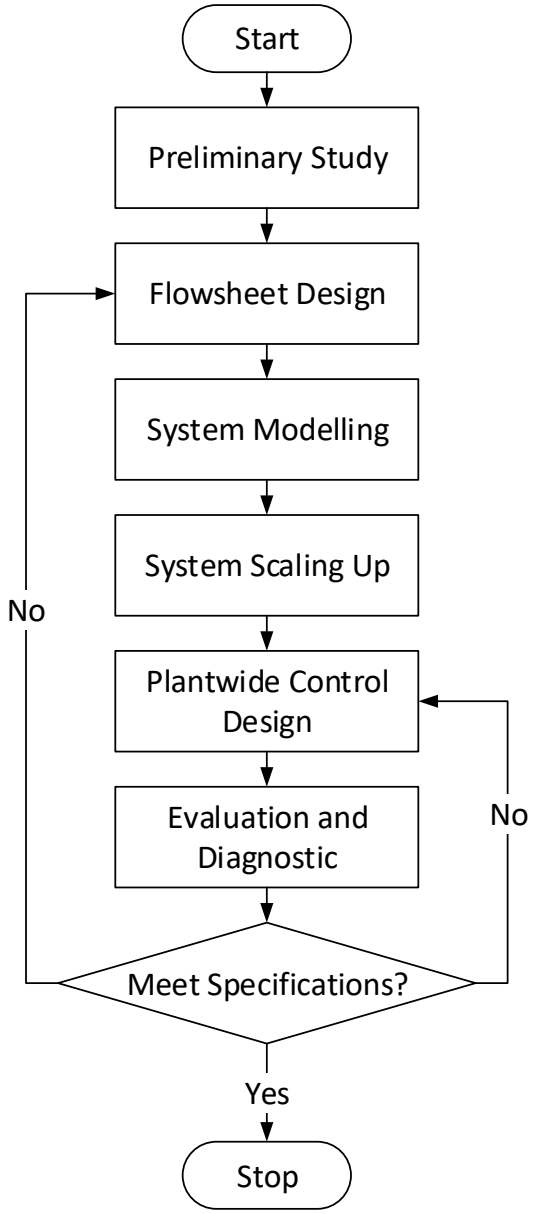

Figure 3-1: Flowchart of overall research methodology

3.2 Overall Process Methodology

3.2.1 Preliminary Work

Literature related to the SITC process including the process behaviour and control strategies will be collected, and the most suitable theoretical process models will be selected and adapted to the current research work. A practical flowsheet design will be chosen for Section I, Section II and Section III of the SITC process. The main information sources such as published literature, manufacturers, and researchers working actively in the SITC process area will be consulted in order to obtain relevant information and data.

3.2.2 Modelling

In this work, mathematical and empirical models will be developed to describe the process behaviour of SITC process using Aspen Plus and MATLAB. The model is developed based on the fundamental mass and energy balances. The process data from Aspen Plus simulation will be extracted to synthesize the control system for SITC process using MATLAB. Furthermore, an empirical model will be developed based on the data generated from mathematical model run in Aspen Plus which is to be embedded into the process control scheme, i.e., to be used in the model-based control strategy. Simulation studies will be carried out both in the Aspen Plus and MATLAB environments for the SITC process system. The flowsheet design of the system will take into account the recycled parts of the process. The result of simulation studies will be compared with available experimental results, and the model will be validated using data from the literature. Figure 3-2 summarized the overall modelling methodologies for each unit in the SITC plant. It should be noted that, the tremendous impact that simulation has had on the chemical process industry is due to the following benefits:

1) Economic desirability. It is usually cheaper to use simulation techniques incorporating fundamental laboratory data into the mathematical model than it is to build numerous different-sized pilot plants.

2) It is a convenient way to investigate the effects of the system parameters and process disturbances upon operating.
3) Simulations are the reasonable way of extrapolating performance, but only for scaling up processes (e.g.: lab scale process to plant scale process).
4) It provides a better understanding of the important process behaviour and mechanisms.

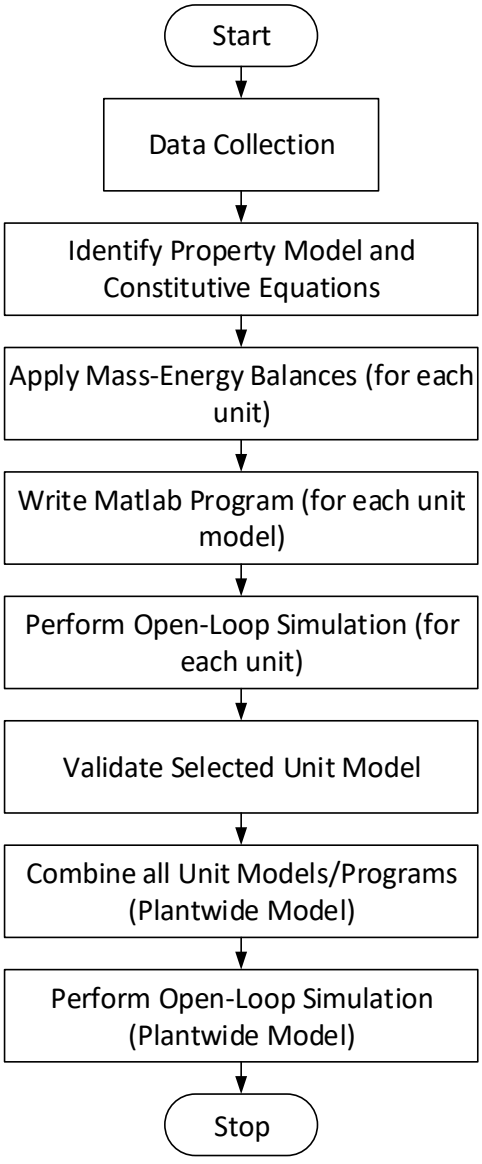

Figure 3-2: Flowchart of overall modelling methodologies

3.2.3 Plant Scale-up

In this work the SITC plant scale-up procedure will be carried out since there is none industry scale of SITC plant available. The scale-up will be done by unit based. Scale-up chemical processes are well-known to be complicated area of chemical engineering, and can be costly when it goes wrong. It is an art of designing using limited data. In this work, specific types of challenges have been address include the following physical and chemical elements of a scale-up of process technology:

1) Reaction kinetics: SITC system involve a number of reaction kinetic parameters. In system with good reaction kinetics, molecules from each element mix efficiently and quickly together, reaching a state of equilibrium for the solution. Unsuitable changes in physical and chemical factors can prevent the molecules of the mixture from mixing and colliding correctly. This can create bad reaction kinetics without proper system design. For SITC, the reaction kinetic parameters are assumed to be similar between laboratory scale and plant scale.
2) Chemical equilibrium: a reaction is not productive until chemical equilibrium is reached, which does not occur immediately. It is observed that as increased quantities of chemicals are mixed, the time for SITC reactions to reach equilibrium increases at a nonlinear rate.
3) Material properties: incorrectly selected materials can influence the reaction, erode over time, or make the system unnecessarily expensive. The material of construction for SITC plant are collected from reliable literature studies.
4) Thermodynamics: heat loss and gain can play a major role in chemical reactions. Controlling reaction temperature is important to a successful plant scale up. Most of control loop in the SITC will be focusing on the temperature control.
5) Equipment selection and design: the ratio of surface area to mixture volume determines how quickly heat can be discharged from the system. If the tank is the incorrect size, it will be difficult to control the chemical reaction, which will begin escalating quickly. In addition, a correct size will inhibit the snowball effect to the plant. Practical methods from the established procedures will be

used for equipment selection and size scale-up. The detail scale-up information will be presented in Chapter 4, 5 and 6.

3.2.4 Process Controller Design and Development (by Section)

The MSC and the NMPC algorithm will be formulated for controlling the SITC plant. The constraints imposed by the nonlinear model will be identified while the input and output variables information gathered from the previous stage will be considered during the controller development stage. Prior to the process controller design, a dynamic controllability analysis is proposed. The analysis is based on Loop Gain Controllability (LGC) index, a type of dynamic controllability analysis to analyze the extent of PID controller performance on the particular pairing and operating condition. The details of LGC will be presented in Section 3.3. The flowchart of overall dynamic controllability methodology is presented in Figure 3-3.

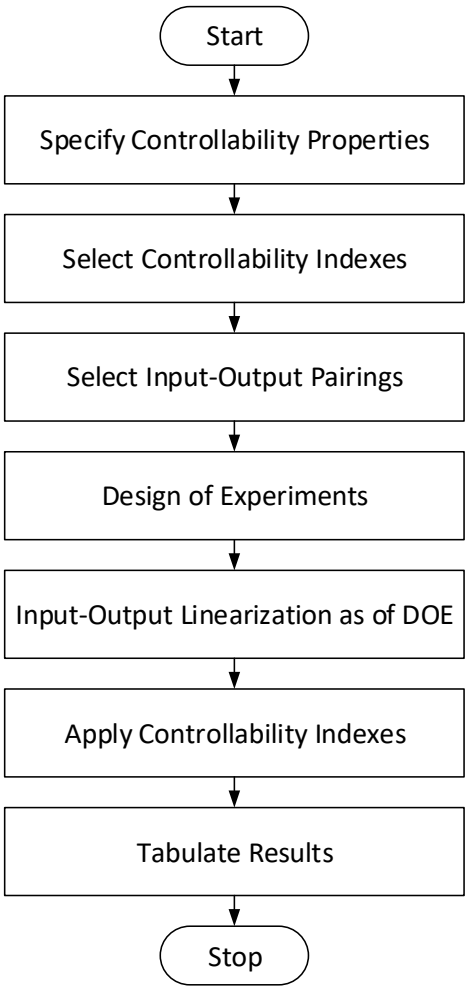

Figure 3-3: Flowchart of overall methodology for dynamic controllability analysis.

3.2.4.1 Input Signal Selection for NMPC

Particularly for the development of NMPC, the selection of the input excitation sequence is very important especially in the empirical modeling development stage. The modeling must use the initial data that have comprehensive process input-output information over the entire nonlinear operating range. Pseudo-Random Binary Signal (PRBS) sequence is often used as inputs to a system in order to produce representative sets of data to be analyzed (Arefi et al., 2008). It is one of the input excitation which is traditionally and successfully used in a linear identification. However, it is not a good choice for a nonlinear system since it only applies two input magnitudes and does not excite the process over a broad enough range of inputs (Hong et al., n.d.). In this work,

the multi-level input sequence was used because it was implemented successfully in a nonlinear identification (Proll and Karim, 1994)

The steps of multi-level input development are explained below. The multi-level input sequences were generated in the range [0, 0.5] of random values as follows (Hong et al., n.d.):

a) Type 1: If the value is higher than 0.5, the multi-level sequence applied is uniform distribution form upper and lower bounds. The maximum magnitudes used in the uniform distribution are 2% to 3% of the steady states for u_1 and u_2. For example, let the steady state value for u_1 is 42 m^3/h while u_2 is 52 m^3/h.
b) Type 2: If the value is in the range [0.25, 0.5], the Type 1 multi-level procedure is repeated except that maximum magnitudes are assigned to 10% of the steady states.
c) Type 3: If the value is within [0, 0.25], Type 1 multi-level procedure is repeated except that the bounds for u_1 and u_2 are [37, 47] and [47, 57], respectively.
d) Type 4: If the value is lower than 0, the Type 1 multi-level procedure is repeated with [34, 50] and [42, 62] as the bounds for u_1 and u_2, respectively.

The initial data was generated by exciting the first principle model to the multi-level input sequences.

3.2.5 Plantwide Model

The plantwide modelling is the development of dynamic model for the entire plant. In this work, the plantwide model is the combination of the dynamic model of Section I, Section II and Section III in the SITC plant. The final part of plantwide modeling is the process model optimization.

3.2.5.1 Process Model Optimization

In this work Response Surface Methodology (RSM) is selected as the process optimization methodology. RSM is a type of sensitivity study method is advantageous in minimising the number of trials and predicting interactions between the variables of

interest, which in turn improves the operational performance of the process. It is widely used in processing several factors where it is necessary to study the interaction effects of the factors on a response. It serves as a good tool to determine potential MV and CV. In RSM, an analysis of process variables is designed in such a way where there are two or more factors, each with possible distinguished values or 'levels', and whose experimental or simulation responses take on all possible combinations of these factors. The RSM analysis is carried out via Design Expert (v9) software. Besides RSM, PCA method will be also incorporate to analyze the input-output of the SITC plant. The detail on PCA method is available in the literature (Nandong and Samyudia, 2009). The proposed sensitivity study and analysis procedure via RSM and PCA are summarized in a systematic procedure as follows:

1) **Step 1** – Generation of operating regimes. Select a nominal (0) operating level, and for each nominal level apply step input changes to produce a set data for lower (-1) and higher level (+1). The magnitude of perturbed input selection of the levels is based on the variable's constraint in the process.

2) **Step 2** – Data generation. Compute the responses of the quality variables corresponding to each level.

3) **Step 3a** – RSM Analysis. Gather and combine all the generated data on the process parameters, input-output variables and the computed response variables in Step 2. Analysis of Variance, ANOVA and optimum operating conditions are determined. Based on ANOVA result, the significant factors are selected as potential MVs while the significant response are selected as potential CVs.

4) **Step 3b-** PCA analysis. Gather and combine all the generated data on the process parameters, input-output variables and the computed response variables in Step 2. The principle components (2D and 3D) as well as the Pareto will be plotted. Based on these plots, the significant factors are selected as potential MVs while the significant response are selected as potential CVs

3.2.6 Plantwide Control Structure Development

The overall summary of the PWC structure development is shows in Figure 3-4. The PWC structure will be design in a systematic procedure as follows:

1) Identification of control objectives and constraints.
2) Input-output identification. Input-output identification is generally part of modelling and simulation procedure. Process model optimization and sensitivity study method are used to identify the potential input as manipulated variable (MV) and the output as controlled variable (CV); see Section 3.2.5.
3) Selection of control structure; decentralized or centralized or mixed of both.
    a. Decomposition into major plant sections.
    b. Selection of control laws and synthesis methods, e.g., IMC-PID, MSC-PID, NMPC, etc.
    c. Evaluation of each section or unit via simulation study.
4) Assembling PWC structure. The control strategies of each sections (i.e., in step 3) are assemble to develop a complete PWC structure. The Skogestad Self-Optimizing Control (SOC) is chosen as the PWC structure methodology. The details of PWC structure will be presented in Section 3.4.
5) Plantwide optimization. The developed PWC structure is optimized (steady-states and dynamics). The details of the plantwide optimization formulation will be presented in Section 3.5.
6) Pre-evaluation of the PWC structure.
7) Enhancement of the PWC structure.
8) Evaluation of the refined control strategy.
9) Stop after meeting all control objectives and constraints.

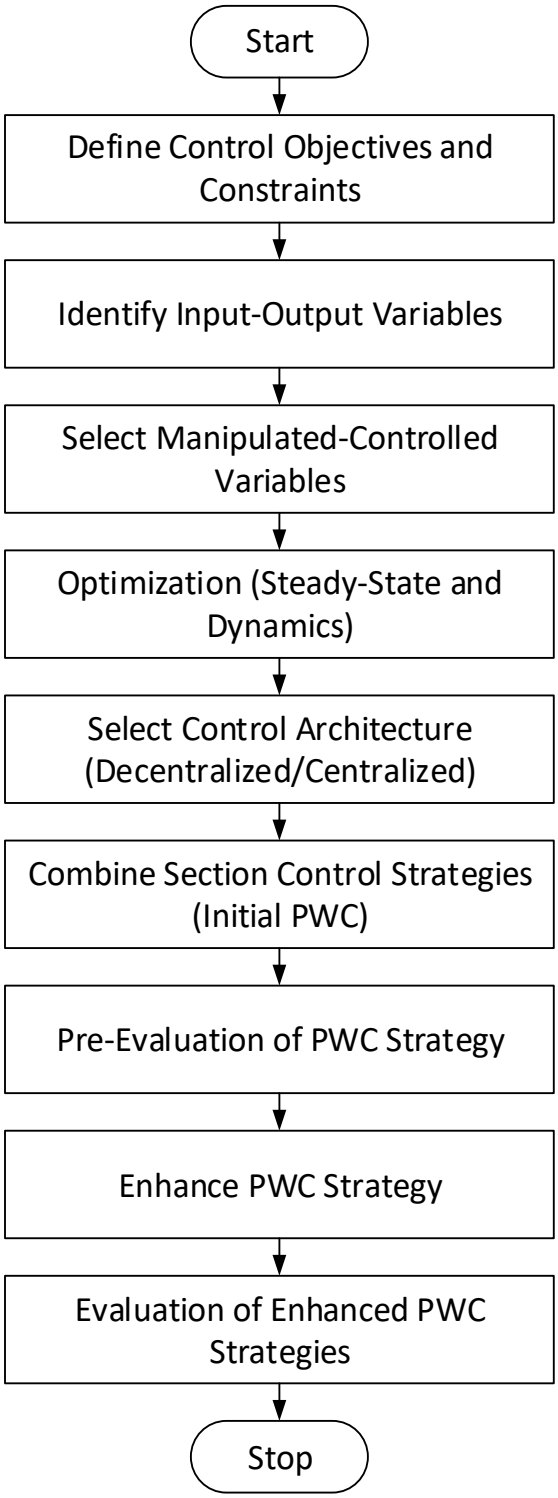

Figure 3-4: Flowchart of overall PWC structure development

3.2.7 Process Controller Performance Evaluation

The built controller's configurations of each section in the SITC plant will be evaluated via simulation for performance and robustness. The performance criteria for controller will be assessed via Integrated Absolute Error (IAE) while for the model, Mean Squared Error (MSE) will be used. They are defined as:

$$IAE = \int_0^\infty |e(t)| dt \tag{3.1}$$

where e is the differences between the output profile and the desired profile.

$$MSE = \frac{\sum_{i=1}^{nt} (y_i - f_i)^2}{nt} \tag{3.2}$$

where y is the desired profile, f is the output profile and nt is the number of samples.

The economic and the thermal efficiency assessment of the SITC plant will be performed.

3.3 Loop Gain Controllability (LGC) Index

3.3.1 Fundamental of LGC

Loop Gain Controllability analysis is proposed to seek the extent of controllability of any model regardless the model type, by giving an index value. Figure 3-5 shows the standard single-loop feedback control structure consisting of a controller and process model (including actuator and sensor). In Figure 3-5, the dashed area represents the proposed LGC calculation for the given loop. The idea of LGC is to utilize both the controller and process model data collectively in defining the controllability index. In the present study, the LGC is derived for a two-input two-output (TITO) model.

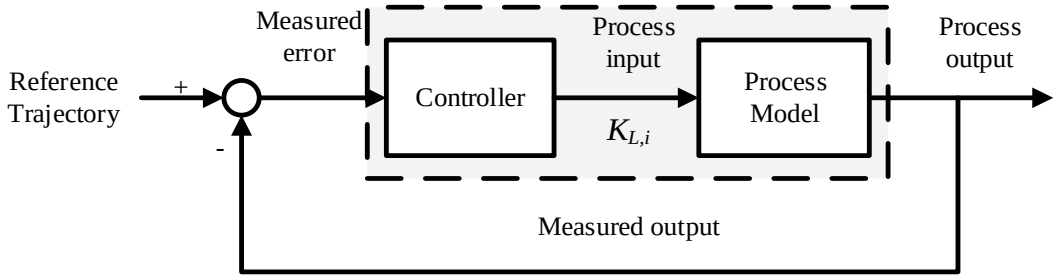

Figure 3-5: Loop gain (dashed square area) of a general control loop structure

Essentially, the LGC index is directly related to the minimum upper limit ($\overline{K}_{i,min}$) and maximum lower limit ($\underline{K}_{i,max}$) on the loop gain for a given i^{th}-loop, i.e., $K_{L,i} = K_{c,i}k_{ii}$ where $K_{c,i}$ and $k_{eff,ii}$ denote the control gain and effective open-loop process gain respectively. For closed-loop stability, the loop gain must be placed in the range of

$$\underline{K}_{i,\max} < K_{L,i} < \overline{K}_{i,\min} \tag{3.3}$$

Figure 3-6 illustrates the main idea behind the LGC index. For a process under PID control, there exist several upper and lower limits on the loop gain (Seer and Nandong, 2017a) the closed-loop system is stable between these two limits. The distance between these two limits represents the LGC index. For a TITO process with two loops, the LGC calculation attempts to first find the minimum upper limit, $\overline{K}_{i,min}$ and the maximum lower limit, $\underline{K}_{i,max}$. The LGC index, δ is given by:

$$\delta = \overline{K}_{\min} - \underline{K}_{\max}, \quad for\ \underline{K}_{\max} > 0 \tag{3.4}$$

else,

$$\delta = \overline{K}_{\min}, \quad for\ \underline{K}_{\max} < 0 \tag{3.5}$$

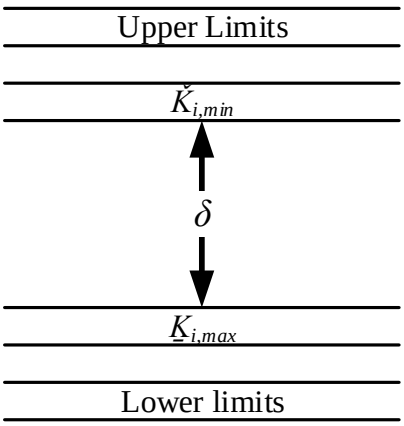

Figure 3-6: Upper and lower limits concept behind the LGC approach

Note that, the larger the value of δ, the larger is the robustness margin as well as the maximum achievable performance. For a first order plus dead time (FOPDT) model, the LGC function is a function of process gain k, dead time θ and time constant τ, i.e.:

$$\delta = f(k, \theta, \tau) \tag{3.6}$$

The following section presents the derivation of LGC index for a TITO process.

3.3.2 Derivation of LGC Index

Consider a $2x2$ (TITO) process given as follows

$$\mathbf{P(s)} = \begin{bmatrix} g_{11}(s) & g_{12}(s) \\ g_{21}(s) & g_{22}(s) \end{bmatrix} \tag{3.7}$$

where the transfer function g_{ij} for $i = 1, 2$ and $j = 1, 2$ takes the form of

$$g_{ij}(s) = \frac{k_{ij} \exp(-\theta_{ij} s)}{\tau_{ij} s + 1} \tag{3.8}$$

In (3.8), k_{ij}, τ_{ij} and θ_{ij} denote the process gain, time constant and deadtime respectively. Note that, the transfer function matrix (3.7) can be written in the decoupled form as follows

$$\mathbf{P(s)} = \begin{bmatrix} g_1^{eff}(s) & 0 \\ 0 & g_2^{eff}(s) \end{bmatrix} \tag{3.9}$$

where the decoupled effective open-loop transfer function (EOTF) is given by

$$g_i^{eff}(s) = g_{ii}(s) - \frac{g_{ij}(s)g_{ji}(s)}{g_{jj}(s)} \tag{3.10}$$

Upon simplification, the EOTF can be written as follows

$$g_i^{eff}(s) = k_{ii}\left[\frac{\exp(-\theta_{ii}s)}{\tau_{ii}s+1} - \left(\frac{k_{ij}k_{ji}}{k_{ii}k_{jj}}\right)\left(\frac{(\tau_{jj}s+1)\exp(-\theta_{I_i}s}{(\tau_{ij}s+1)(\tau_{ji}s+1)}\right)\right] \tag{3.11}$$

where $\theta_{I_i} = \theta_{ij} + \theta_{ji} - \theta_{jj}$.

Consider the loop 1, we can express (3.11) in term of the diagonal RGA element λ_{11}

$$g_1^{eff}(s) = k_{11}\left[\frac{\exp(-\theta_{11}s)}{\tau_{11}s+1} - \psi_1\left(\frac{(\tau_{22}s+1)\exp(-\theta_{I_1}s}{(\tau_{12}s+1)(\tau_{21}s+1)}\right)\right] \tag{3.12}$$

Here, ψ_1 is defined as

$$\psi_1 = \frac{k_{12}k_{21}}{k_{11}k_{22}} = \frac{\lambda_{11}-1}{\lambda_{11}} \tag{3.13}$$

The RGA matrix corresponding to (3.13) assuming direct pairings is

$$\Lambda = \begin{bmatrix} \lambda_{11} & 1-\lambda_{11} \\ 1-\lambda_{11} & \lambda_{11} \end{bmatrix} \tag{3.14}$$

where

$$\lambda_{11} = \frac{k_{11}}{k_{11} - \frac{k_{12}k_{21}}{k_{22}}} \tag{3.15}$$

Based on the EOTF, the closed-loop set-point transfer function for the loop 1 is

$$H_{R_1}(s) = \frac{g_{c_1}(s)g_1^{eff}(s)}{1 + g_{c_1}(s)g_1^{eff}(s)} \tag{3.16}$$

By approximating the dead time term using first-order Padé formula and assuming P-only controller is used, the closed-loop characteristic equation for (3.12) becomes

$$1 + \frac{K_{L_1}\left(\tau_{I_1}s + 1\right)}{\tau_{I_1}s}\left\{\frac{1 - \alpha_{11}s}{\left(\tau_{11}s + 1\right)\left(\alpha_{11}s + 1\right)} - \psi_1\left[\frac{\left(1 - \alpha_{I_1}s\right)\left(\tau_{22}s + 1\right)}{\left(\tau_{12}s + 1\right)\left(\tau_{21}s + 1\right)\left(\alpha_{I1}s + 1\right)}\right]\right\} = 0 \tag{3.17}$$

where $\alpha_{ii} = 0.5\theta_{ii}$ and the loop gain is $K_{L_1} = k_{c_1}k_{11}$.

Equation (3.17) can be simplified into a polynomial form as proposed by (Seer and Nandong, 2017a):

$$\begin{aligned} &f_6 s^6 + \left(f_5 + K_{L_1}h_5\right)s^5 + \left(f_4 + K_{L_1}h_4\right)s^4 + \left(f_3 + K_{L3}h_3\right)s^3 + \ldots \\ &\left(f_2 + K_{L_2}h_2\right)s^2 + \left(f_1 + K_{L_1}h_1\right)s + K_{L_1}h_0 = 0 \end{aligned} \tag{3.18}$$

From (3.18), we may write general equations as in (3.19) and (3.20)

$$f_k = \left(a_{k-2}\tau_{11} + a_{k-1}\right)\tau_{I_1} \quad for\, k = 1, 2, \ldots 6 \tag{3.19}$$

$$h_k = \tau_{I_1}\left(b_{1(k-1)} - \psi_1 b_{2(k-1)}\right) + b_{1k} - \psi_1 b_{2k} \quad for\, k = 0, 1, \ldots 5 \tag{3.20}$$

The parameters in (3.18) - (3.20) are presented in the Appendix A. By adapting the PID stability theorem in (Seer and Nandong, 2017a), a set of upper and lower limits on the loop gain can be obtained. As the PID stability theorem is based on Routh-Hurwitz stability criteria, both the necessary and sufficient conditions will yield upper and lower

limits on the loop gain. Considering all of these limits, the value of LGC index δ_1 is then calculated as in (3.4) or (3.5).

In the present study, the LGC index is based on the P-only controller. Following a similar procedure, we can also derive the LGC index based on the PI or full PID controller but this will lead to a higher order characteristic polynomial (seventh-order for PI and eighth-order for PID). For the derivation of limits on loop gain based on the PID controller applied to a fourth-order nonminimum-phase system, refer to (Seer and Nandong, 2017b). Note that, a limitation of the LGC index derived in this work is that the total dead time $\theta_{I_i} > 0$. The LGC calculation is not valid when $\theta_{I_i} < 0$. When $\theta_{I_i} > 0$, the following interpretations can be made of the δ value:

a) The positive δ value indicates the selected pairing is controllable. While $\delta \leq 0$ means that the loop is uncontrollable (unstable closed loop).
b) Larger δ value means a higher maximum achievable control performance of the given pairing.
c) If two systems have comparable values of LGC, then the controllability performance of the systems should also be comparable even though the systems have different orders, e.g., one first-order and another fourth-order.

The LGC index can also be derived based on the FOPDT model (3.8) for purely single-loop case. By approximating the dead time term using first-order Padé formula, it can be readily shown that the LGC index based on g_{ii} is given by

$$\delta_{ii} = \frac{\tau_{ii} + 0.5\theta_{ii}}{0.5\theta_{ii}} \tag{3.21}$$

Figure 3-7 depicted the overall methodology to determine LGC of a system as well as the step to apply the LGC testing in a closed-loop simulation.

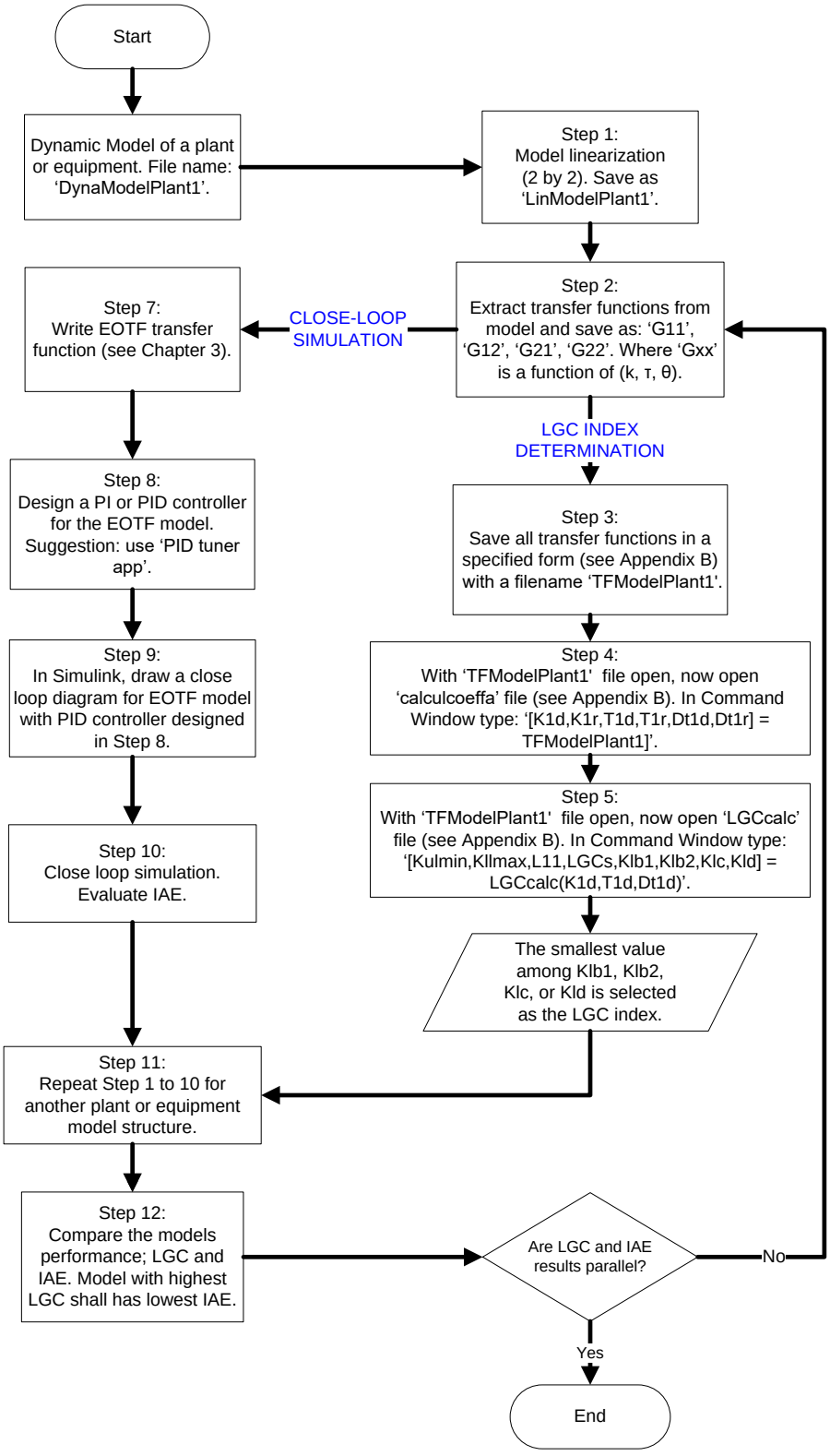

Figure 3-7: Overall methodology of LGC index determination and closed-loop simulation.

3.3.3 Illustrative Examples – Evaluation of Dynamics via LGC Index

This section demonstrates the applications of the LGC analysis to two familiar processes, namely a binary distillation column (benzene-toluene separation) and interacting liquid tanks. Both of the TITO processes are simulated in the Control Station's Loop-Pro Trainer software. The baseline of both systems are presented in Tables 3.1 and 3.2. The transfer functions are obtained using $\pm 10\%$ single-direction step tests and presented in Table 3.3. Both of the processes are nonlinear so the transfer functions obtained vary with direction of the step tests. Each linearized system is evaluated based on the LGC (δ) index as well as RGA and N_I indices for benchmarking purposes. Based on linearized systems, the controllability indices are obtained as in the Tables 3.4, 3.5, 3.6 and 3.7. By using a multi-loop PI controller, simulation study is carried out in MATLAB environment. The PI controller performances are evaluated against sequential step changes of 1 unit each in the setpoint of y_1 and y_2.

Table 3.1. Baseline conditions for the Distillation Column (DC)

Parameters	**Value**
Reflux R (%) = u_1	50
Steam S (%) = u_2	47
Feed flow (kg/min)	596
Top purity X_d (%) = y_1	94.5
Bottom purity X_b (%) = y_2	2.6%

Table 3.2. Baseline conditions for the Interacting Tanks (IT)

Parameters	**Value**
Feed flow 1 (m^3/min) = u_1	61.5
Feed flow 2 (m^3/min) = u_2	61.5
Disturbance 1 (m^3/min)	1.0
Liquid Level 1 (m) = y_1	3.46
Liquid Level 2 (m) = y_2	3.26

Table 3.3. Transfer Functions for the DC and IT processes.

Model	g_{11}	g_{12}	g_{21}	g_{22}
Distillation Column - step up (DC_{SU}): Model 1	$\frac{0.415e^{-22.4s}}{41.9s+1}$	$\frac{-0.919e^{-24.8s}}{43.2s+1}$	$\frac{1.049e^{-44.6s}}{63.2s+1}$	$\frac{-0.161e^{-7.6s}}{28.7s+1}$
Interaction Tanks - step up (IT_{SU}): Model 3	$\frac{0.0755e^{-5.91s}}{16.4s+1}$	$\frac{0.042e^{-6.75s}}{15s+1}$	$\frac{0.0361e^{-6.77s}}{17.1s+1}$	$\frac{0.0767e^{-7.57s}}{16.1s+1}$
Distillation Column - step down (DC_{SD}): Model 2	$\frac{1.056e^{-32.6s}}{36.2s+1}$	$\frac{-0.333e^{-18.7s}}{40.7s+1}$	$\frac{0.146e^{-21.7s}}{21.7s+1}$	$\frac{-0.984e^{-31.7s}}{60.9s+1}$
Interaction Tanks - step down (IT_{SD}): Model 4	$\frac{0.0673e^{-6.11s}}{13.7s+1}$	$\frac{0.0404e^{-5.95s}}{14.2s+1}$	$\frac{0.034e^{-6.84s}}{14.9s+1}$	$\frac{0.0697e^{-6.81s}}{14.6s+1}$

3.3.3.1 Distillation Column

Distillation column is a nonlinear process. Advanced model-based process controller is always a preferable choice to control the distillation column due to its high nonlinearity behaviour (Pearson, 2003). In this section, the objective is to seek the controllability of the distillation column. Table 3.4 and 3.5 show the LGC values for Model 1 and 2 of distillation column. The LGC of Model 1 (1st order DC_{11SU}) is 4.741 while DC_{22SU} is

8.553. Comparison of both LGC values for loop 1 and 2 using Model 1 (1^{st} order DC_{11SU} and DC_{22SU}) results revealed that,

a) The preferable pairing is DC_{22SU} since it has the highest LGC value.
b) The LGC indices are not in parallel with RGA which is -0.0746 and N_I which is 0.1386 where both indices suggested indirect pairing.
c) For Model 1, 5^{th} order, the results of LGC are smaller than the 1^{st} order. The LGC for Model 1, 5^{th} order DC_{11SU} is 2.8463 is smaller than DC_{22SU} which is 2.9769. The smaller the value of LGC at 5^{th} order model indicates that the interaction is high and it is quite challenging to be controlled by a PID controller. However, it is still controllable since the LGC is positive.

The profiles of both Model 1 and 2 are shown in Figure 3-8. For both Model 1 and 2, the best performance of controller can be obtained by $DC_{22.}$ It is shown that for certain case, instead of suggesting for indirect pairing, one may still use direct pairing by changing the diagonal position (from G_{11} to using G_{22}) to see whether it is controllable. The question is, if both are controllable which one will produce higher controller performance if controlled by a PID controller?

a) The answer is given by the LGC value, where for a SISO controller, it is revealed that DC_{22SU} should have a higher achievable controller performance. Meanwhile, with regard to the TITO system, the choice of DC_{22SD} shall produce a higher achievable controller performance.
b) In conclusion based on the LGC index, the distillation column is controllable by a conventional PID controller.

Table 3.4: Distillation Column Model 1: feature comparison among RGA, N_I and LGC.

Control Loop	**1st Order Model**			**5th Order (EOTF) Model**				
	LGC	PI controller	IAE	LGC	PI controller	IAE	RGA	N_I
DC_{11SU} Loop 1	4.74	$K_{c1} = 2.262$ $\tau_{I_1} = 42$	98.1	Direct pairing: 2.846	$K_{c1} = 0.161$ $\tau_{I_1} = 94$	298.5	Direct pairing: -0.0746	Direct pairing: 0.1386
DC_{22SU} Loop 2	8.55	$K_{c2} = -11.87$ $\tau_{I_2} = 29$	33.6	Direct pairing: 2.977	$K_{c2} = 0.294$ $\tau_{I_2} = 64$	225.2		

Table 3.5: Distillation Column Model 2: feature comparison among RGA, N_I and LGC.

Control Loop	**1st Order Model**			**5th Order (EOTF) Model**				
	LGC	PI controller	IAE	LGC	PI controller	IAE	RGA	N_I
DC_{11SD} Loop 1	3.22	$K_{c1} = 0.538$ $\tau_{I_1} = 37$	140.6	Direct pairing: 3.111	$K_{c1} = 0.899$ $\tau_{I_1} = 46$	145.4	Direct pairing: 1.049	Direct pairing: 0.0936
DC_{22SD} Loop 2	4.84	$K_{c2} = -1.202$ $\tau_{I_2} = 69$	129.6	Direct pairing: 4.719	$K_{c2} = -1.293$ $\tau_{I_2} = 76$	138.6		

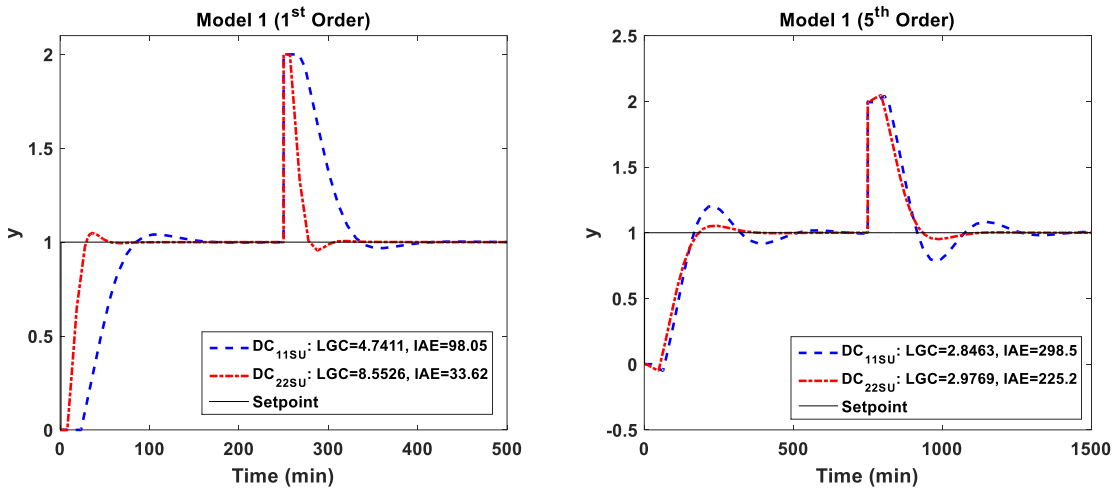

(a)

(b)

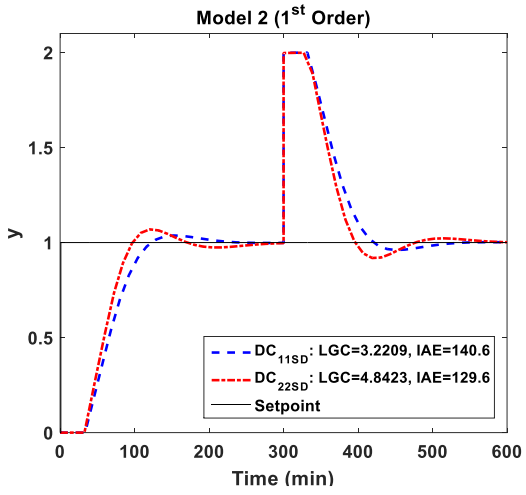

(c)

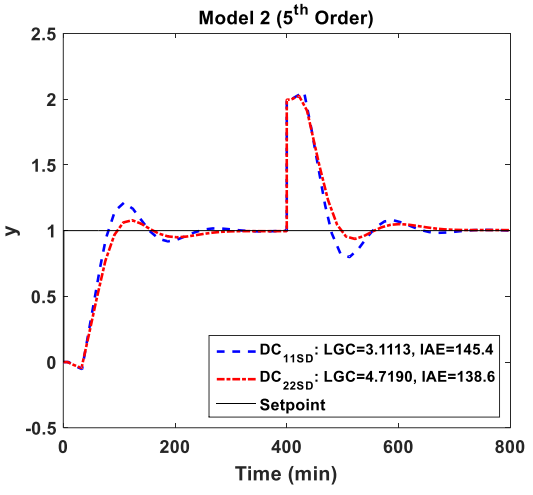

(d)

Figure 3-8: LGC analysis of distillation column for step up and step down models: a) Model 1, 1st order, b) Model 1, 5th order, c) Model 2, 1st order, d) Model 2, 5th order.

3.3.3.2 Interacting Tanks

Model 3 and 4 represent the interacting tanks (IT) systems. The IT system consists of four interconnected tanks. Table 3.6 and 3.7 shows the LGC values for Model 3 and Model 4 respectively. Comparison of both LGC values for loop 1 and 2 using Model 1 (1st order IT_{11SU} and IT_{22SU}) results revealed that,

a) For the case where the interaction is ignored, notice that the LGC for the loop 1 (IT_{11SU}) is larger than that for the loop 2 (IT_{22SU}) indicating that the loop 1 should exhibit higher achievable performance. This is shown by the loop 1 has IAE value smaller than that of the loop 2.
b) For the case where the interaction is considered (i.e., based on the EOTF), the loop 1 also exhibits larger LGC value than that of the loop 2 suggesting that even when interaction is considered, the loop 1 shall have higher achievable performance than the loop 2. In fact, this confirmed by the IAE for the loop 1 is smaller than for the loop 2.
c) For comparison between two systems with different orders, consider the loop 2. Notice that the LGC value based on the FOPDT (without interaction) and fifth-order EOTF (with coupling), the former has larger LGC than the latter, hence indicating that the coupling effect has reduced the achievable control performance. Again this result is confirmed by the IAE value of the system without coupling (based on G_{11}) is smaller than that of the system with coupling (based on EOTF- 5^{th} Order).
d) The LGC index for Model 3 (1^{st} Order) is in parallel with RGA which is 1.3547 and N_I which is 0.5237 where all indices suggested direct pairing.
e) For the Model 3, 5^{th} order, the results of both LGC showing high values. The LGC for IT_{11SU} is 4.9674 which is higher than IT_{22SU} which is 4.0170. The higher the value of LGC indicates that the interaction is low and it is easier to be controlled by a PID controller. The profiles of both Model 3 and 4 are shown in Figure 3-9. For both Model 1 and 2 either for SISO or TITO controller, the best performance of controller can be obtained by $IT_{11SU.}$

An additional LGC calculation was carried out for the Model 3 if the IT system uses the indirect pairing. As shown in Table 3.6, the indirect pairing of Model 3 Loop 1 produced 5.3921 which is slightly higher than direct pairing which is high LGC index, 5.1067. Denoted that if the LGC is comparable than the control performance is estimated to be comparable. Meanwhile the indirect pairing of Model 3 Loop 2, the LGC is 5.9012 which is higher that the direct pairing LGC of 4.017. The higher LGC value of the indirect pairing is indicating a higher control loop performance. Next, both

loops were test with process controller performance and the result are plotted. Figure 3-10 shown the result of both direct and indirect pairing of loop 1 and loop 2 of Model 3 IT system. From the plot in Figure 3-10 it is proven that the indirect pairing of IT system Model 3 Loop 2, produced a better controller performance as compared to the direct pairing.

Table 3.6: Interacting Tanks Model 3: Features comparison between RGA, N_I and LGC

Control Loop	**1st Order Model**			**5th Order (EOTF) Model**				
	LGC	PI controller	IAE	LGC	PI controller	IAE	RGA	N_I
IT_{11SU} Loop 1	6.550	$K_{c1} = 19.7$ $\tau_{I_1} = 16$	24.8	Direct pairing: 5.1067 Indirect pairing: 5.3921	Direct pairing: $K_{c11} = 37.62, \tau_{I_{11}} = 28$ Indirect pairing: $K_{c21} = -10.13, \tau_{I_{21}} = 16$	Direct pairing: 26.2 Indirect pairing: 25.9	Direct pairing: 1.3547	Direct pairing: 0.5237
IT_{22SU} Loop 2	5.254	$K_{c2} = 18.8$ $\tau_{I_2} = 14$	25.7	Direct pairing: 4.017 Indirect pairing: 5.9012	Direct pairing: $K_{c22} = 21.73, \tau_{I_{22}} = 18$ Direct pairing: $K_{c12} = -13.22, \tau_{I_{12}} = 18$	Direct pairing: 34.19 Direct pairing: 28.7		

Table 3.7: Interacting Tanks, Model 4: Features comparison between RGA, N_I and LGC

Control Loop	**1st Order Model**			**5th Order (EOTF) Model**				
	LGC	PI controller	IAE	LGC	PI controller	IAE	RGA	N_I
IT_{11SD} Loop 1	5.484	$K_{c1} = 19.50$ $\tau_{I_1} = 15$	26.6	Direct pairing: 3.586 Indirect pairing: 4.4054	Direct pairing: $K_{c11} = 28.12, \tau_{I_{11}} = 24$ Indirect pairing: $K_{c21} = -10.95, \tau_{I_{21}} = 13$	Direct pairing: 35.3 Direct pairing: 27.1	Direct pairing: 1.4141	Direct pairing: 0.5857
IT_{22SD} Loop 2	5.288	$K_{c2} = 14.81$ $\tau_{I_2} = 14$	30.61	Direct pairing: 3.893 Indirect pairing: 5.9012	Direct pairing: $K_{c22} = 19.95, \tau_{I_{22}} = 19$ Indirect pairing: $K_{c12} = -12.22, \tau_{I_{12}} = 14$	Direct pairing: 38.2 Indirect pairing: 30.6		

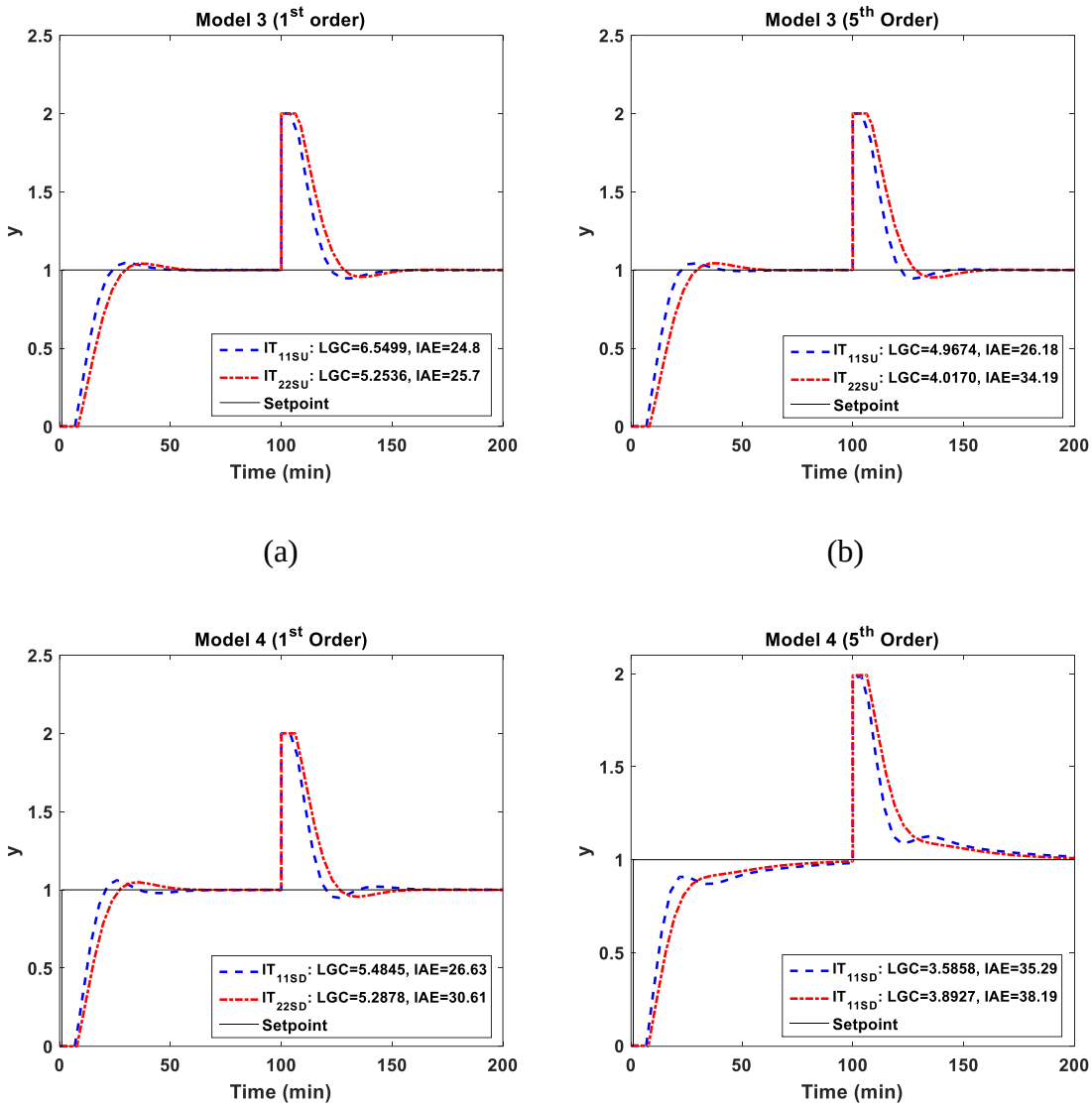

Figure 3-9: LGC analysis of interacting tanks for step up and step down models: a) Model 3, 1st order, b) Model 3, 5th order, c) Model 4, 1st order, d) Model 4, 5th order

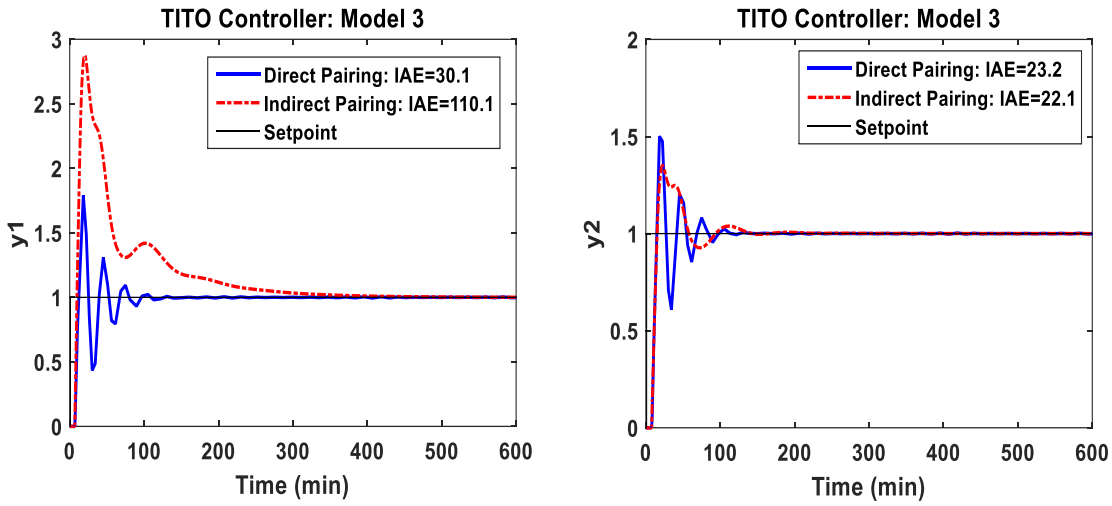

(a) (b)

Figure 3-10: LGC analysis of interacting tanks Model 3, Loop 1 (y1) and Loop 2 (y2) for direct and indirect pairings.

Up to this section, the LGC has been introduced and its application has been validated. In the next chapter the LGC will be applied onto each sections in SITC plant and the entire plant eventually.

3.4 Plantwide Control Approach

The control system of a plant usually divided into several layers. Typically, layers consisted of scheduling (weeks), site-wide optimization (day), local optimization (hour), supervisory (minutes) and regulatory control (seconds). The Skogestad SOC method (Skogestad, 2012) consists of the following steps:

Top-down part (focus on steady-state optimal operation)

1) Step S1. Define operational objectives (economic cost function and constraints)

2) Step S2. Identify steady-state degrees of freedom and determine the optimal steady-state operation conditions, including active constraints.

3) Step S3. Identify candidate measurements and select primary controlled variables.

4) Step S4. Select the location of throughput manipulator (TPM).

Bottom-up part (focus on the control layer structures).

1) Step S5. Select the structure of regulatory (stabilizing) control layer.
2) Step S6. Select the structure of the supervisory control layer.
3) Step S7. Select structure of (or assess need for) optimization layer. The OPPWIDE optimization is proposed for optimization layer.

3.5 Optimal-Practical Plantwide (OPPWIDE) Optimization

The multilayer control system structure is typically used in the advanced process control. The layer comprised of the basic control layer which is responsible for safe operation of the process, the supervisory control layer and the set-point optimization layer. The standard multilayer system structure applied in this work is depicted in Figure 3-11.

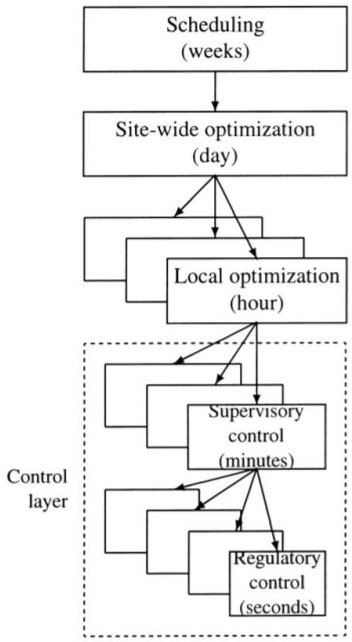

Figure 3-11: Control hierarchy of a chemical plant (Skogestad, 2000a)

The basic control layer is the lowest layer of the process. The second layer which is the supervisory control layer calculates on-line setpoint for the basic control layer. The third layer which is the optimization layer calculates on-line economically optimal set-points for the supervisory control layer in such a way that the production profit is maximized and constraints are satisfied (Ławrynczuk, 2010).

In this work, the OPPWIDE optimization will be embedded into the third layer of the plantwide control system. Following are the steps used to construct the OPPWIDE optimization formulation. These steps will be applied onto the developed PWC structure of SITC plant.

1) Step 1: Specify desired performance measures. For the selected flowsheet, the optimization objective is measured as follows,

$$\Psi = \left[\varphi_1, \varphi_2\right] \tag{3.22}$$

where

$\varphi_1 = optimality\ performance\ measure$

$\varphi_2 = practicality\ performance\ measure$

In this work the optimality performance is defined as the optimum profit, *P* achievable by controlling the primary variable.

$$P = -J = cost\ feed + cost\ utilities\ (energy) - value\ products \tag{3.23}$$

In brief, the optimality performance shall directly proportional to the primary controlled variable of the plant (e.g. $\varphi_1 \equiv \dot{m}_{H_2}$). Where $\dot{m}_{H_2}$ is mass flowrate of hydrogen. The primary controlled variable will only be established in the later chapter of the thesis. Meanwhile, the practicality performance φ_2 will be represented by the LGC index. These criteria are used to measure the overall performances of the SITC plant.

2) Step 2: Selection of decision variables, U_1. From the given process flowsheet and model, select the decision variables which consist of operating or/and design parameters. The selection is made based on the final structure of the developed plant flowsheet. Assuming that $U_1 \in u^r$ is a row vector with a total r number of operating and design parameters.

$$U_1 = [u_1, u_2 \ldots u_r] \tag{3.24}$$

3) Step 3: Determination of constraints. All constraints imposed on the selected decision variables as well as other (outputs) constraints must be identified and their values specified. It is assumed that the decision variables are bounded as follows

$$U_{1,\min} < U_1 < U_{1,\max} \tag{3.25}$$

where $U_{1,min}$ and $U_{1,max}$ denote the lower and upper constraint limits on U_1 respectively.

4) Step 4: Selection of baseline condition. The baseline or nominal condition represents the nominal values of operating and design parameters selected in Step 2. The baseline condition can be selected based on prior knowledge obtained from previous study or literature reports. Alternatively, if one has a dynamic process model corresponding to the desired flowsheet, numerical or simulation study can be first conducted in order to determine a viable baseline condition.
5) Step 5: Magnitude of input perturbations. Select the magnitude of perturbation of each decision variable. The magnitude of perturbation should not be so large or so small. A 10% to 20% of perturbation is advised (Mohd and Aziz, 2016) but must not violate the constraints imposed on that particular variable.
6) Step 6: Formation of dataset, X. Based on Step 5 and 6 and by using the developed process model, a series of simulation runs is conducted. For each simulation run, calculate the values of optimality and practicality performance measures as specified in Step 1.

3.6 Multi-scale Control Scheme

The basic control layer in the PWC structure which is also known as regulatory layer is responsible for safe operation of the process. Contrasting to the other layers, this layer has direct access to input variable of the process. PID controllers are usually used in this layer (Ławrynczuk, 2010). In this work MSC will be chosen to assist the lowest layer if it is not controllable by conventional PID controller. The controllability analysis of each loop or equipment will be done by determining LGC index.

Figure 3-12 shows the three types of MSC loops. As refer to Nandong & Zang, (2013b), the principle of the proposed MSC scheme is basically to utilize all dynamics information (represented as modes) of a plant with the purpose of improving cooperation among these different plant modes. To attain decent cooperation among the different plant modes, it is essential to assemble the sub-controllers based on the cascade configuration. Each controller can be deduced as being designed to control a specific plant mode where the slower mode commands the faster mode. By enhancing good cooperation among the different plant modes, a significant performance improvement can be made over that of the standard single-loop feedback control scheme. For the standard single-loop feedback control scheme where only a single controller is used, good cooperation among the different plant modes might not be achievable, and subsequently, this could result in rather poor closed-loop performance/robustness.

The overall multi-scale controller, $K_{msc,}$ can be expressed as,

$$K_{msc} = K_o(s)G_1(s)G_2(s) \tag{3.26}$$

Where, $G_1(s)$ and $G_2(s)$ are from the plant model transfer function called the augmented overall transfer function,

$$P_C(s) = G_1(s)G_2(s)P(s) \tag{3.27}$$

Where the inner-layer closed loop transfer function in equation (3.26) can be expressed as,

$$G_1(s) = \frac{U(s)}{C_o(s)} = \frac{K_1(s)}{1 + G_2(s)K_1(s)W_1(s)} \tag{3.28}$$

$$G_2(s) = \frac{U(s)}{C_1(s)} = \frac{K_2(s)}{1 + K_2(s)W_2(s)} \tag{3.29}$$

And the predictors are given by,

$$\begin{bmatrix} W_1(s) \\ W_2(s) \end{bmatrix} = \begin{bmatrix} P_1(s) \\ P_2(s) \end{bmatrix} \tag{3.30}$$

3.7 Model Predictive Control

In the optimizing layer, a model based control will be embedded. Model Predictive Control (MPC) is often used for the supervisory control in this layer (Ławrynczuk, 2010). The MPC technique started its development in the 1970s because conventional single loop controllers (e.g. PID) were unable to satisfy the increasingly stringent performance requirements. MPC is formulated as the repeated solution of a (finite) horizon open loop optimal control problem subject to plant dynamics and inputs and state constraints. To incorporate feedback, the optimal open loop control is implemented only at the next sampling time instant (Allgower *et.al*, 2004). A simplified block diagram of the typical MPC is shown in Figure 3-13.

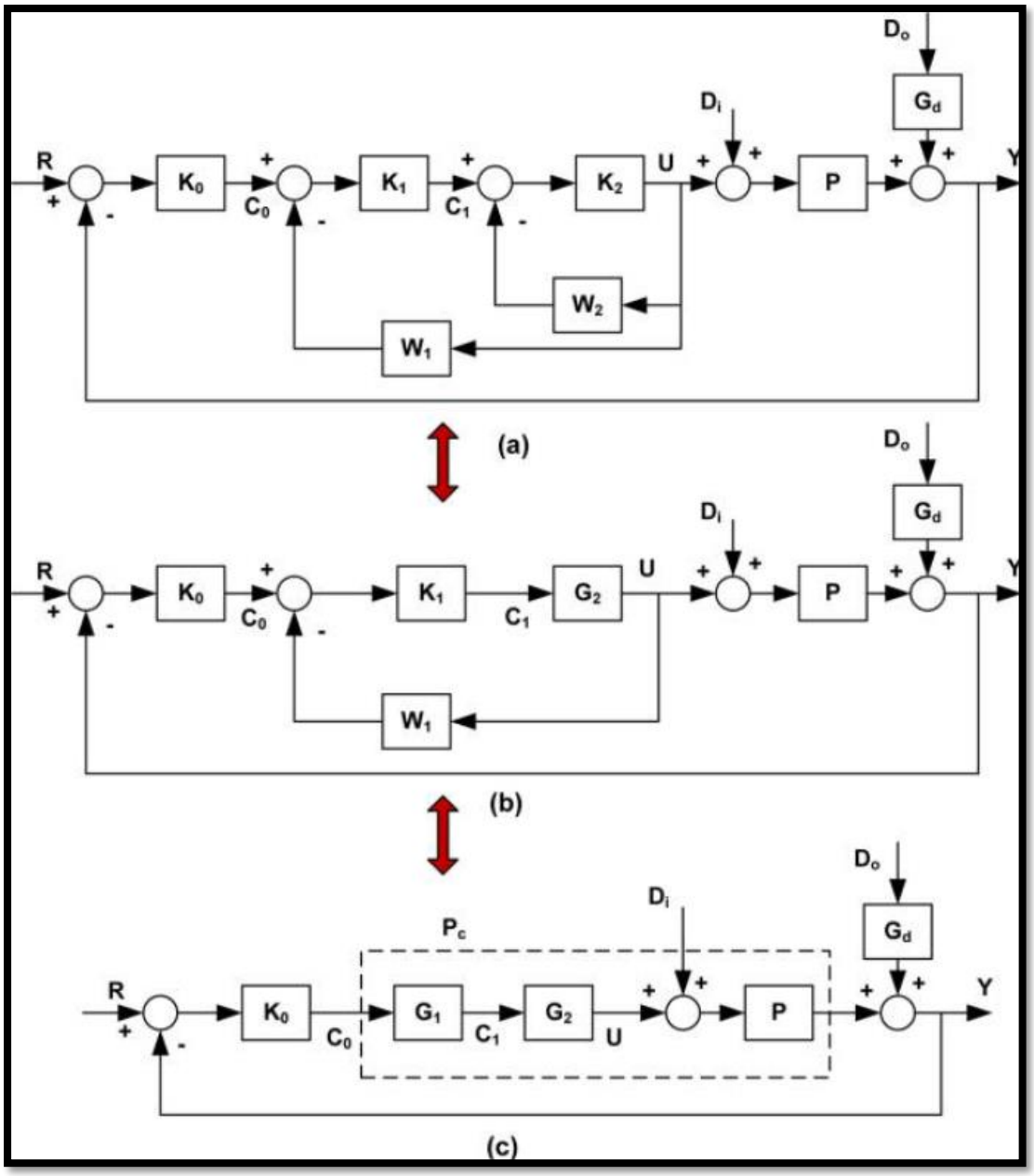

Figure 3-12: Multi-scale control scheme: (a) three-loop, (b) reduced two-loop, and (c) equivalent single-loop block diagrams (Nandong, 2014).

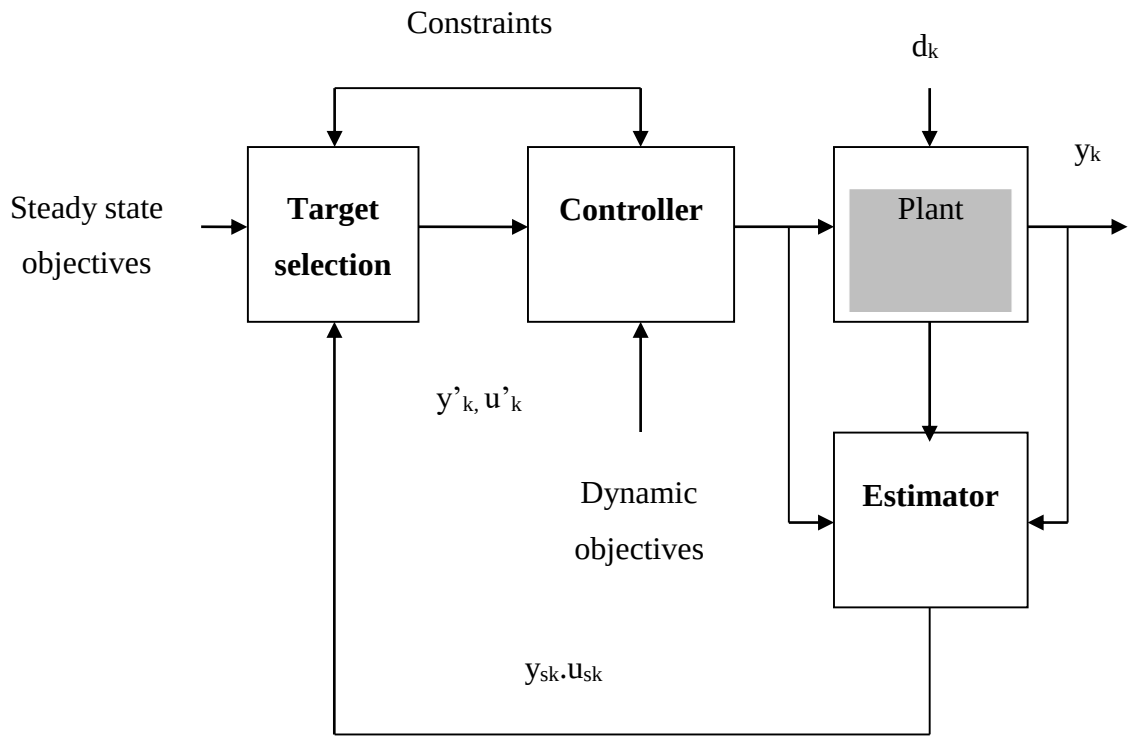

Figure 3-13: A simplified block diagram of the typical MPC

There are three common elements in the MPC system and their functions as explained below:

1) **Target selection**: Determines the best feasible, steady-state operating point for controlled outputs and manipulated inputs based on steady-state gains of the model. It can be implemented on the basis of minimising deviations from the desired steady-state or as the result of an economic-based steady-state optimization.
2) **Controller**: Determines optimal, feasible future inputs over a moving horizon to minimize predicted future controlled errors of controlled outputs from the targets determined by the target selection. Tuning parameters (e.g. weights) are used to establish the dynamic objectives.
3) **Estimator**: Updates the model predictions to account for unmeasured disturbances and model errors. It includes a deterministic part that models the effect of the controller manipulated variables on the process outputs, and a

stochastic part that models the effect of unmeasured disturbances on the process outputs. The simplest form for the disturbance estimator, corresponding to an integrating disturbance model driven by white noise, is the original MPC output correction where the current offset between the measurement and the model prediction is used to bias future model predictions.

A number of researchers have advocated an improved form of MPC which is a nonlinear control scheme as to overcome the process nonlinearity issues; one of such scheme is the Nonlinear MPC (NMPC) which has become a popular topic in recent years and has successfully been used in several industrial processes. The NMPC tool can be used for rapid prototyping and evaluation of an algorithm for any industrial process, hence making it a convenient means to broaden the acceptance of this technique in the industrial community (Nagy and Agachi, 1997; Nagy et al., 2007). The general NMPC formulation can be expressed as a nonlinear programming problem as follows:

$$J = \sum_{j=1}^{P} (e(k+j))^T Q(e(k+j)) + \sum_{j=0}^{M-1} (\Delta u(k+j))^T R(\Delta u(k+j)) \tag{3.31}$$

subject to

$$y_{pre} = F(y,u) \tag{3.32}$$

$$u_{\min} \le u(k+j) \le u_{\max} \quad for\ j = 0,1,\dots,M-1 \tag{3.33}$$

$$u(j) = u(k+M-1) \quad for\ j > k+M-1 \tag{3.34}$$

with

$$e(k+j) = y_{ref}(k+j) - y_{pre(k+j)},\ j = 1,2,\dots P \tag{3.35}$$

$$\Delta u(k+j) = u(k-j) - u(k+j-1)\ j = 0,1,\dots M-1 \tag{3.36}$$

where, $y_{ref}(k+j)$ is the vector of the setpoint, and $y_{pre(k+j)}$ signify the predicted controlled variable given by the model. P is the prediction horizon, M is the control

horizon, and ***Q*** and ***R*** are weighting matrices which are all adjustable parameters in MPC.

3.7.1 MPC tuning

Tuning an MPC is accomplished based on offline simulation and the actual performance of the online controller. The offline simulation done in this work is used to verify steady state behaviour (ensuring optimal operation for various constraint scenarios) and to determine, via trial and error, initial tuning values for the controlled variable and the manipulated variable weights. The objective functions of the MPC online optimization used are:

$$\min_{U[t|t],\ldots U[m+p|t]_{i=0}} J(Y(t),U(t)) \tag{3.37}$$

$$\min_{U[t|t],\ldots U[m+p|t]_{k=0}} \sum_{k=1}^{P} w_k (Y[t+k\,|\,t]-Y_{setpoint})^2 + \sum_{k=1}^{M} \Delta u' r_k \Delta u[t+k\,|\,t] \tag{3.38}$$

Where **Y** is the desired product, **U** is the input. P and M are the process output prediction and the manipulated process input horizons, respectively with P ≥ M and they are adjustable as well as and the weighting matrices **Q** and **R**. $U[t+k|t]_{k=0,\ldots,P}$ is the future process input values. In general, a longer control horizon will make the controller more aggressive. Meanwhile, the weighting matrix, **R**, allows the input variables to be weighted according to their relative importance. In **R**, the diagonal elements r_{ii} are referred to as move suppression factors. They provide convenient tuning parameters because increasing the value of r_{ii} tends to make the MPC controller more conservative by reducing the magnitudes of the input moves (Seborg et al. 2004).

3.8 Summary

A conceptual framework of an overall PWC structure for the SITC plant has been proposed and summarized as follows:

a) The PWC structure is modified by incorporating the RSM and PCA concepts to include input-output sensitivity studies. The modification relates the sensitivity analysis and process optimization of the SITC plant.
b) Prior to sensitivity analysis, dynamic modelling of each major sections in the SITC plant is completed and subsequently scaled-up. Scaling-up is carried out by unit based, and all sections will be finally assembled to form an industrial scale SITC plant. Practical methods from the established procedures will be used for equipment selection and dimensional scale-up. If the scale up result is incorrect, it will be difficult to control the chemical reactions involved, and can lead to failure to meet the minimum target production rate. In addition, a correct size will avoid the snowball effect from occurring in the plant. The detail scale-up information will be presented in Chapters 4, 5 and 6.
c) Controllers including MSC-PID and NMPC will be designed to control each sections in the plant.
d) The final step of PWC structure development is the plantwide optimization. A PWC optimization formulation, namely OPPWIDE optimization is proposed. The OPPWIDE is a function of optimality and practicality, which will be calculated based on the steady-state economic (optimality) and LGC index (practicality) indexes.

4 Bunsen Section: Dynamic Modelling and Controllability Analysis

This chapter covers fundamental modelling of the Bunsen Section (Section I), controllability analysis and evaluation of control strategies for the Bunsen Section. Prior to scaling up, the developed model was first validated using the data from a laboratory scale Bunsen reactor reported in the literature. The effects of input variables on output variables were analyzed and the process operating conditions were optimized. The controllability analysis for the Bunsen reactor was carried out via the LGC index to identify the operating condition that gives the most favorable dynamics. The dynamic modelling of the Liquid-liquid separator, which was part of the Bunsen Section was also presented. Some control strategies were proposed and evaluated for both Bunsen reactor and Liquid-liquid separator units. At the end of this chapter, a summary on the Bunsen Section is presented.

4.1 Fundamental of Bunsen Section

In the Bunsen Section, there are two main processes involved: Bunsen reaction and liquid-liquid separation of heavy, hydrogen iodide/iodine, HI/I_2 solution from the aqueous sulfuric acid, H_2SO_4 light solution. In the Bunsen reactor, H_2O reacts with iodine, I_2 and sulfur dioxide SO_2 to produce two immiscible liquid-aqueous phases: one phase mainly contains sulfuric acid and the other phase containing hydrogen iodide. Note that, the Bunsen Section is the most important part of the SITC process. The products quality from this section will influence the selection of equipment or process in the next section, and consequently can greatly affect the plant cost.

In view of various studies, there are three important criteria which must be fulfilled by the Bunsen reactor. These criteria are as follows:

a) The operating window for the reactor temperature should be between 330 K and 350 K. This range is the optimal temperature window proposed by (Lee et al., 2008b).
b) The feed molar ratio of I_2/H_2O should be between 0.333 and 0.538. If the I_2/H_2O molar ratio is outside of this range, the Bunsen reactor's heavy phase product will prone to be azeotropic.
c) The molar ratio of $HI/(HI + H_2O)$ should be kept in the range of 0.16 to 0.25 to ensure the solution composition is above the azeotropic condition. It is essential to produce an over-azeotropic solution composition to reduce the complexity of the separation process in Section II and III.

4.1.1 Reaction Mechanism

In this study, the main chemical reaction equation is taken to be the optimal Bunsen reaction as proposed by Lee et al. (Lee et al., 2008a). This is an exothermic reaction with $\Delta H = -165\ kJ/mol$ and can be presented as follows

$$13H_2O + 5I_2 + SO_2 \leftrightarrow [H_2SO_4 + 5H_2O] + [2HI + 4I_2 + 6H_2O] \quad (4.1)$$

Meanwhile, the predominant reaction steps are taken from Zhu et al. (2013) as follows:

$$I_2 + I^- \xrightarrow{k_2} I_3^- \quad (4.2)$$

$$SO_2 + I_2 + 2H_2O \xrightarrow{k_1} SO_2^{2-} + 2I^- + 4H^+ \quad (4.3)$$

$$SO_2 + I_3^- + 2H_2O \xrightarrow{k_3} SO_4^{2-} + 3I^- + 4H^+ \quad (4.4)$$

Where k_1 is the first step reaction rate coefficient, k_2 is the second step reaction rate coefficient which is solely represented the reaction kinetic on iodine, and k_3 is the third step reaction rate coefficient. All steps have different value of reaction kinetics.

Two main elements for the simulation of the Section I are the prediction of the phase states and the calculation of the phase compositions (Guo et al., 2012). In the Bunsen reactor, the HI, I_2, H_2O and H_2SO_4 co-exist. The evaluation of the phase states has to

be portrayed with an appropriate modelling method. There are three possible states in the Bunsen reactor: homogeneous phase, two-liquid phase, and two liquid phase with I_2 precipitation. All states are possible to be simulated by a simulation software. For instance, if the two-phase state is selected, then the accurate calculation of the solution composition is essential.

4.2 Bunsen Reactor

4.2.1 Modeling of Bunsen Reactor

According to literature reports, a continuous stirred tank reactor (CSTR) is often chosen for the laboratory scale experimental study of Bunsen reaction (Yoon et al., 2015). The schematic of CSTR used for conducting Bunsen reaction is shown in Figure 4-1.

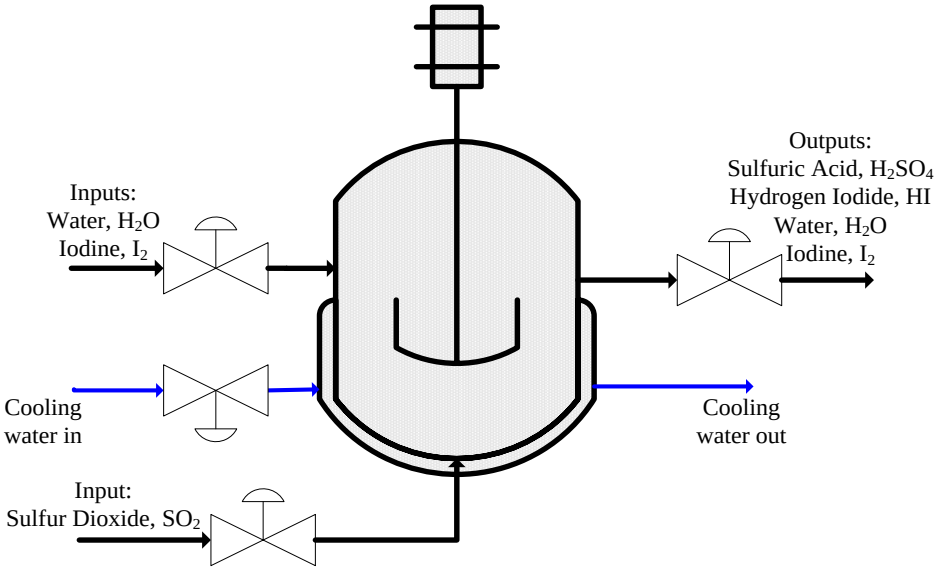

Figure 4-1: Bunsen reactor (jacket CSTR)

In order to model the CSTR shown in Figure 4-1, several state variables are required which include HI and H_2SO_4 molar flow rates, in addition to a number of kinetics parameters. In the experimental study, the reactor is initially started in a semi-batch mode. A certain amount of I_2 and H_2O are initially fed into the semi-batch reactor while SO_2 gas is continuously fed into the reactor at a specified flow rate from a storage tank.

After a certain period, all reactants feed flowrate are switched to a continuous mode when the state variables reach steady state responses. In the continuous mode, the products are taken out continuously from the reactor.

The following assumptions are made in the modelling of Bunsen reactor (Figure 4-1).

A.4.2.1: Complete mixing inside the reactor and jacket compartments, i.e., jacketed CSTR.

A.4.2.2: Constant liquid volume in the jacket compartment.

A.4.2.3: Kinetic information taken from Zhu et al., 2013.

A.4.2.4: Constant physical properties.

A.4.2.5: Reactor is in an adiabatic condition.

A.4.2.6: Iodine is fully dissolved in the solution.

A.4.2.7: The products form two immiscible liquids.

A.4.2.8: The reaction only takes place in the aqueous phase in which the iodine molecules and bisulphate anions come into contact.

4.2.1.1 Mass and Energy Balance

The kinetics and design parameters of the semi-batch mode can be retrieved from the experimental work of Zhu et al. (2013). The predominant reaction steps (Zhu et al., 2013) as represented by equations (4.5) – (4.8) are modified to develop mass balance of Bunsen reactor,

$$\frac{dc_{I_2}}{dt} = k_1 c_{I_2} c_{SO_2} + k_2 c_{I_2} c_{I^-} \tag{4.5}$$

$$\frac{dc_{I^-}}{dt} = 2k_1 c_{I_2} c_{SO_2} + 3k_3 c_{I_3^-} c_{SO_2} - k_2 c_{I_2} c_{I^-} \tag{4.6}$$

$$\frac{dc_{I_3^-}}{dt} = k_2 c_{I_2} c_{I^-} - k_3 c_{I_3^-} c_{SO_2} = 0 \tag{4.7}$$

$$\frac{dc_{SO_4^{2-}}}{dt} = k_1 c_{I_2} c_{SO_2} + k_3 c_{I_3^-} c_{SO_2} \tag{4.8}$$

where c_{I_2} is the I_2 concentration, c_{I^-} is the I^- concentration, $c_{I_3^-}$ is the I_3^- concentration, $c_{SO_4^{2-}}$ is the SO_4^{2-} concentration, and c_{SO_2} is the SO_2 concentration.

The developed species mol balances (mol/min) in the Bunsen reactor are represented by equations (4.9) – (4.21):

$$\frac{dn_{I_2}}{dt} = F_{I_2 o} - F_{I_2} + R_{I_2} V \tag{4.9}$$

$$\frac{dn_{HI}}{dt} = F_{HIo} - F_{HI} + R_{HI} V \tag{4.10}$$

$$\frac{dn_{SO_2}}{dt} = F_{SO_2 o} - F_{SO_2} + R_{SO_2} V \tag{4.11}$$

$$\frac{dn_{H_2SO_4}}{dt} = F_{H_2 so_4} - F_{H_2 so_4} + R_{H_2SO_4} V \tag{4.12}$$

$$\frac{dn_{H_2O}}{dt} = F_{H_2 Oo} - F_{H_2O} + R_{H_2O} V \tag{4.13}$$

Where n_{I_2} is the mol of I_2 ,n_{HI} is the mol of HI, n_{SO_2} is the mol of SO_2 , $n_{H_2SO_4}$ is the mol of H_2SO_4 and n_{H_2O} is the mol of water. F_x is the molar flowrate of component x, R_x is the reaction rate of component x, where $x = I_2, HI, SO_2, H_2SO_4 \; or \; H_2O$.

Note that, the reaction rates based on the predominant steps are given as follows

$$r_1 = k_1 C_{I_2} C_{SO_2} \tag{4.14}$$

$$r_2 = k_2 C_{I_2} C_{I^-} \tag{4.15}$$

$$r_3 = r_2 \tag{4.16}$$

While the species reaction rates are as follows

$$R_{I_2} = -r_1 - r_2 \tag{4.17}$$

$$R_{HI} = 2r_1 - r_2 + 3r_3 \tag{4.18}$$

$$R_{so_2} = -r_1 \tag{4.19}$$

$$R_{H_2SO_4} = r_1 + r_3 \tag{4.20}$$

$$R_{H_2O} = -14r_1 - r_3 \tag{4.21}$$

The energy balances are given by equations (4.22) – (4.23):

$$\frac{dT}{dt} = \frac{v_{SO_{2o}} \rho_g C_{pg} (T_o - T)}{V \rho_g C_{pg}} + \frac{\sum_{n=a}^{f} R(n) H_r - Q_j}{\rho C_p} \tag{4.22}$$

$$\frac{dT_j}{dt} = \frac{v_j (T_{jsp} - T_j)}{V_j} + Q_j \tag{4.23}$$

where T is the reactor temperature, v_{SO_2} is the volumetric flowrate of SO_2, ρ_g is the density of SO_2 gas, C_{pg} is the heat capacity of SO_2 gas, T_o is the feed temperature, V is the reaction volume, $\sum R\ (n)$ is the total reaction rates of iodine, hydrogen iodide, sulfur dioxide, sulfuric acid and water, H_r is the heat of reaction, Q_j is the jacket heat, ρ is the density of solution, C_p is the heat capacity of solution in the Bunsen reactor, T_j is the jacket temperature, v_j is the volumetric flowrate of cooling water, T_{jsp} is the desired jacket temperature, and V_j is the jacket volume. The heat transfer rate from the reactor to the jacket compartment is as follows

$$Q_j = \frac{U_r A_r \left(T - T_j\right)}{C_p \rho V_j} \tag{4.24}$$

where U_r is the overall heat coeffient, and A_r is the reaction area.

By applying the total mass balance on the reactor side, the holdup liquid level (HL) in a stand-alone Bunsen reactor is expressed as follows

$$\frac{dHL}{dt} = \frac{(F_{H_2Oo} - F_{H_2O})/A_r + R_{H_2O} HL}{c_{H_2O}} \tag{4.25}$$

For an integrated Bunsen reactor in the SITC plant, the reactor level is given as

$$A_r \rho_a \frac{dHL}{dt} = \dot{m}_1 + \dot{m}_2 - \dot{m}_3 - \dot{m}_4 \tag{4.26}$$

where $\dot{m}_1, \dot{m}_2, \dot{m}_3$ and $\dot{m}_4$ denote the mass flow rates of fresh feed of aqueous iodine, recycle SO_2 stream from the Section II, liquid reactor effluent containing HI and vapour reactor effluent respectively.

The average liquid density is calculated using the formula given by

$$\rho_a = \sum_{i=1}^{n} (x_i \rho_i) \tag{4.27}$$

where x_i and ρ_i denote the mass fraction and liquid density of i-component respectively.

Note that, the gaseous recycle stream of SO_2 also contains O_2 and some other minor impurities. This gaseous stream is directly bubbled (from the bottom of reactor) through the liquid in the reactor. The SO_2 component is dissolved in the liquid forming sulfuric acid while the insoluble O_2 gas leaves the Bunsen reactor to be store in a storage tank.

For the purpose of simulation study, the mass and energy balances are solved using numerical differentiation formulas (NDFs), ode15s in MATLAB environment. The

kinetic, design and physical parameter values and their units used for simulation are given in the Tables 4.1, 4.2 and 4.3.

Table 4.1: Kinetic parameters for the Bunsen reactor (Zhu et al., 2013)

Parameter	**Value or expression**
Frequency factor, A_1	$2.622\,\frac{L}{mol.min}$
Frequency factor, A_2	$43.9044\,\frac{L}{mol.min}$
Activation Energy, E_{a1}	$9212\ \frac{L.kpa}{mol.K}$
Activation Energy, E_{a2}	$23513\ \frac{L.kpa}{mol.K}$
Overall heat coefficient, U_r	$90\,\frac{J}{min.m^2.K}$

Table 4.2: Design parameters for the Bunsen reactor

Parameter	**Value or expression**
Area of reaction, A_r	$0.03\ m^2$
Reactor Volume, V	$0.5\ L$
Cooling Jacket Volume, V_j	$0.35V\ \ L$
Enthalpy change, ΔH_R	$E_{a1} - E_{a2}$

Table 4.3: Physical constants for the Bunsen reactor (Don and Perry, 1984)

Constant	**Value**
Gas constant, R	$8.314\ \frac{L.kpa}{mol.K}$
Density of liquid, ρ	$1000\ \frac{g}{L}$
Density of gas, ρ_g	$2.619\ \frac{g}{L}$
Specific heat capacity, C_p	$4.184e^3\,\frac{J}{g.K}$
Molecular weight of Water	$18\ \frac{g}{mol}$
Molecular weight of Iodine	$253.8\ \frac{g}{mol}$
Molecular weight of Sulphur Dioxide	$64.1\ \frac{g}{mol}$

4.2.1.2 Model Validation

A laboratory scale of Bunsen reactor is assumed and simulated based on the dynamic model and properties as presented in the previous Section 4.2.1. The simulation is performed until the process reaches an equilibrium. Then the simulated result is then compared with the data that obtained from the literature (Zhu et al., 2013). Table 4.4 displays the simulation parameters and the comparison between the model predictions and experimental data at three different operating temperatures: 336K, 345K and 358K. Note that, α_{SO2} denotes the total conversion of SO_2 gas.

Table 4.4: Bunsen Reactor Validation Parameters and Results

Set of operating conditions					α_{SO2}	
No	**T (K)**	**Feed SO_2 (L/min)**	**Feed Ratio (I_2/ H_2O)**	**Time (min)**	**Zhu et al. (2013)**	**Current work (2016)**
1	336	0.086	0.9/4.2	10	0.07	0.07
				20	0.10	0.18
				30	0.40	0.31
				50	0.60	0.60
				80	1.00	0.92
				100	1.00	1.00
2	345	0.086	0.9/4.2	10	0.05	0.08
				20	0.10	0.20
				30	0.30	0.34
				50	0.80	0.66
				80	1.00	0.95
				100	1.00	1.00
3	358	0.086	0.9/4.2	5	0.03	0.03
				30	0.45	0.40
				40	0.80	0.60
				50	0.90	0.77
				60	0.97	0.88
				90	1.00	1.00

Figure 4-2 (a), (b), and (c), shows the validation plots. With the average of mean squared error (MSE) equals to 0.12 and mean absolute error (MAE) equals to 0.03, it can be concluded that the developed model prediction is comparable with the experimental data from the literature. Therefore, the model can be used to conduct further studies, such as for process optimization and control.

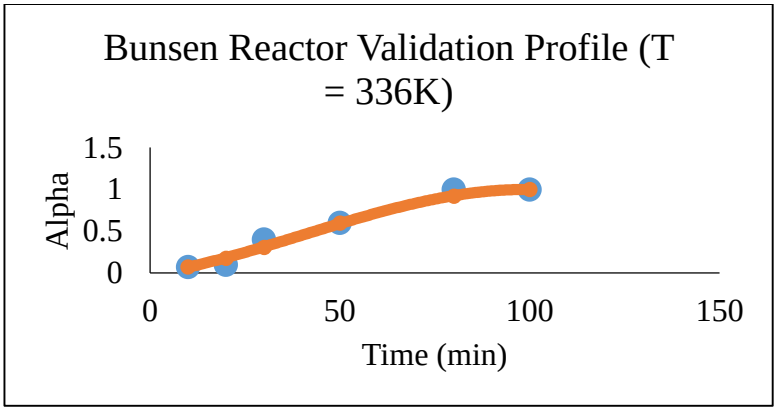

(a)

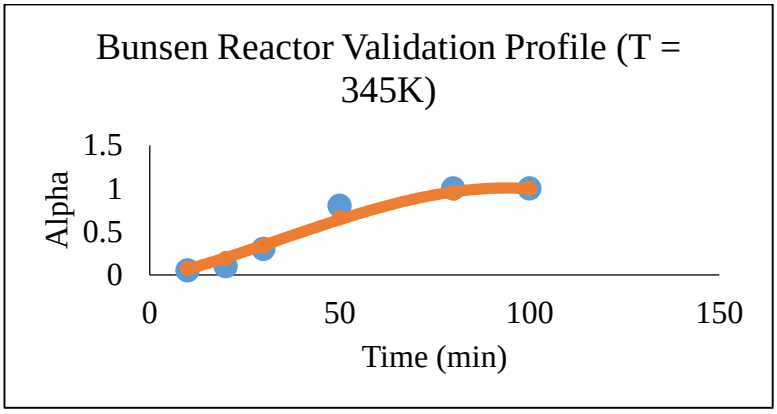

(b)

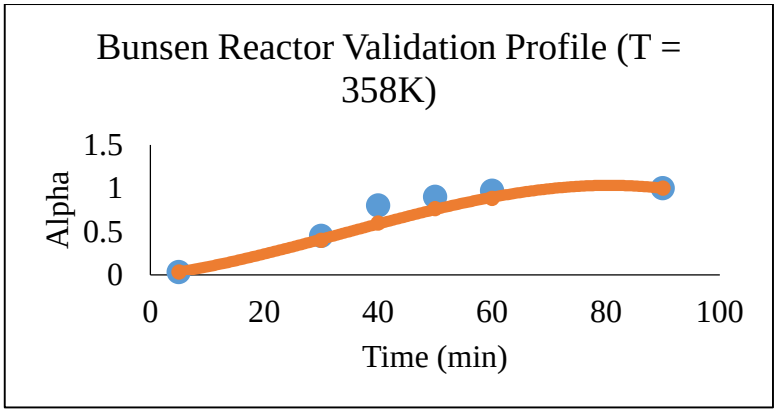

(c)

Figure 4-2: Bunsen Reactor Validation Plots: Simulation of Current Work (solid line) vs. Zhu et al. (2013) (dot marker). (a) Temperature 336K, (b) Temperature 345K, (c) Temperature 358K.

4.2.1.3 Sensitivity Analysis and Process Optimization of Bunsen Reactor

After validation of the model, sensitivity analysis and process optimization are carried out using the model. This analysis is particularly useful in the early stage of data processing for Bunsen reactor. In this analysis, more than two factors are considered: originally, there are eight factors to be investigated to assess the effects on the desired products in terms of the molar flow rates of HI and H_2SO_4. By using the RSM method (see Section 3.2.5), a contoured, 3D surface, and cube plots corresponding to the obtained functions at each optimum value can be analyzed, hence to explore the function in the factor (input) space. Also, an individual response (output) may be graphed to show the optimum point. The following steps are the simplified steps adopted in order to identify the main inputs on a certain response. Further details on the RSM methodology can be retrieved from Section 3.2.5.1.

1) Step 1: Generate an RSM equation for each output or response.

2) Step 2: Plot 3D diagram for each response against certain inputs.

3) Step 3: Analyze the plots.

Table 4.5 lists the nominal values of eight input variables used in the RSM analysis. The magnitude of input perturbation is chosen to be 30%. Note that, the Level -1 (-0.3) shows the values of the eight input variables after decreasing them by 30% from their nominal values. Level +1 (+0.3) denotes the values of the eight input variables after increasing them by 30% from their nominal values.

Table 4.5: Factors, levels and actual values for Bunsen reactor optimization

Factor	**Variable**	**Level -1 (-0.3)**	**Nominal values (0)**	**Level +1 (+0.3)**
A	SO_2 gas pressure, P (kPa)	140	200	260
B	SO_2 volumetric feed flow rate, υ_{SO2o} (L/min)	0.0602	0.086	0.1118
C	Iodine initial mol, n_{I_2} (mol)	0.63	0.9	1.17
D	Water initial mol, n_{H_2O} (mol)	2.94	4.2	5.46
E	Feed reactor temperature, T_o (K)	324	345	367
F	Feed jacket temperature, T_{jo} (K)	292	300	308
G	Cooling water volumetric feed flow rate, v_{jo} (L/min)	0.00252	3.60e-03	0.00468
H	Water volumetric feed flow rate, v_o (L/min)	0.00007	1.00e-04	0.00013

The first column of the experimental matrix is used to show the factor coding. The second column shows the variable based on the names of the factors or a combination of them which are taken at their high level (+1) during an experimental run. The third column holds the first factor levels in coded form -1. The forth column has the coded levels of the nominal and the last column to the right contains the high level with +1.

Please note that, the number of simulation (computer experimental) runs is determined via the Design of Experiment (DOE) based on the Box–Behnken experimental design method. The simulation runs are conducted in order to obtain enough data which shall systematically help evaluate the effects of operational parameters on the responses, which are the HI and H_2SO_4 molar flow rates.

In total, there are eight factors as reported in literature which have effects on the HI and H_2SO_4 molar flow rates: these include feed gas pressure, feed iodine molar flow rates, feed temperature, and total water feed flow rate to the reactor and cooling water flow rate to the jacket. These are independent variables which affect the kinetic of reactions and selectivity of the process, hence influencing the quantity and quality of products. The data generated from the computer experiments is then analyzed using statistical method in the Design Expert Software.

From the statistical data analysis, i.e., the ANOVA suggests that a quadratic order statistical model is sufficient to represent the effects of the aforementioned eight factors on the HI and H_2SO_4 molar flow rates. The adjusted *R-square* for the model is 0.99, thus indicating it is significant. There are four factors that cause the significant effects (p-value < 0.0001) on all responses, which are: (1) feed sulfur dioxide gas pressure, (2) feed iodine molar flow rate, (3) feed temperature, and (4) feed volumetric water flow rate.

Figure 4-3 shows the range of optimum condition (yellow region) of the two most significant factors in the Bunsen reactor. This range is obtained by setting the desired product molar flow rates to the maximum. Noted that, the statistical model is applicable over a wide region to produce the optimum value of both desired products. This wide region of optimal operation provides a good criterion for controller development.

The precise point of optimal values of P_{SO2} and v_{H2O} for the HI and H_2SO_4 are depicted in Figures 4-4 and 4-5 (3D plots) respectively. As can be seen in Figures 4-4 and 4-5, the upper plane representing the optimum surface is fairly flat. Significantly, the flat plane means that the optimum values of HI and H_2SO_4 flow rates (1.8 and 0.9 mol/min) are quite insensitive to the values of the manipulated variables, (P_{SO2} and v_{H2O}); thus, the input constraint implementation is usually easy (Skogestad, 2000b). In other words, there is no economic loss (e.g., on the HI production) occurred by adjusting the manipulated inputs (feed sulfur dioxide gas pressure and feed water flow rate), from the constant optimal values of both manipulated variables. On the contrary, the sharper the optimum surface as the manipulated inputs change, the bigger the economic loss will be when the inputs are adjusted (i.e., control purpose).

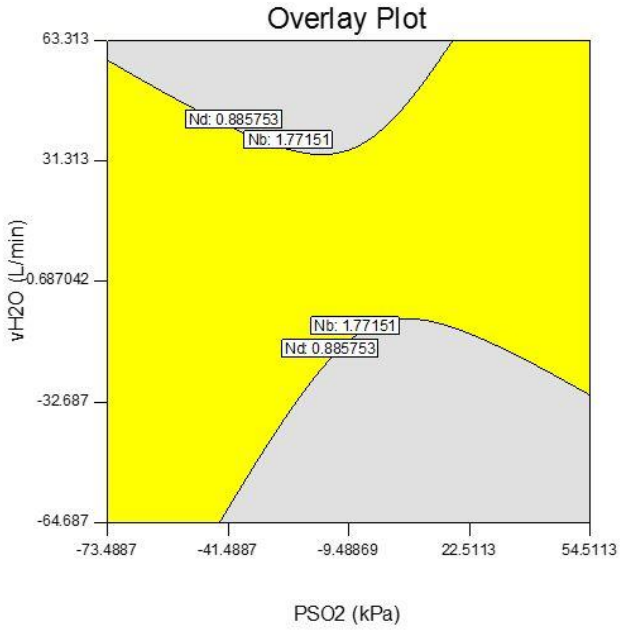

Figure 4-3: Overlay plot for HI and H_2SO_4 flow rates under optimum condition of the main input ranges

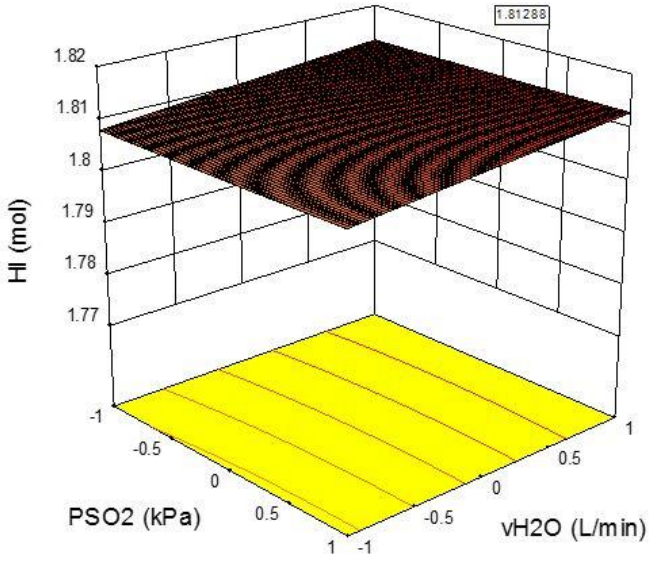

Figure 4-4: 3D Plot of optimum HI molar flow rate and operating condition: 1.8 mol

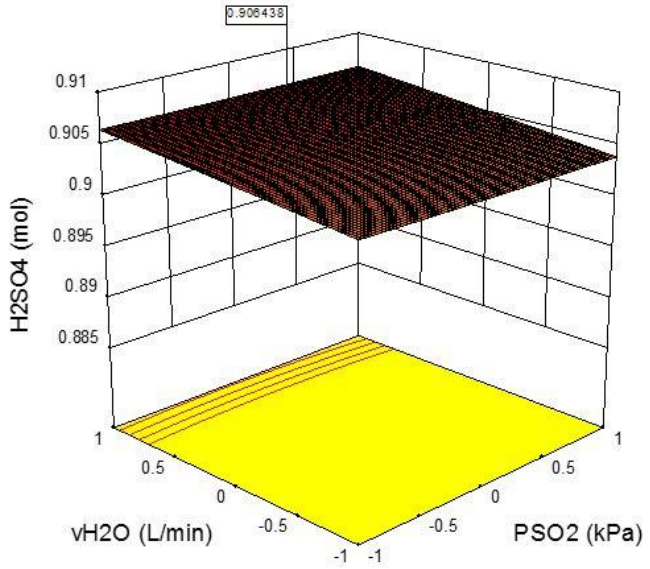

Figure 4-5: 3D Plot of optimum H_2SO_4 molar flow rate and operating condition: 0.9 mol

Table 4.6: Optimum values of parameters for Bunsen reactor

Coded Factor	**Variable**	**Value**
A	SO_2 gas pressure, P (kPa)	223
B	SO_2 volumetric feed flow rate, υ_{SO2o} (L/min)	0.1
C	Iodine initial mol, n_{I_2} (mol)	0.9
D	Water initial mol, n_{H_2O} (mol)	5.2
E	Feed reactor temperature, T_o (K)	345
F	Feed jacket temperature, T_{jo} (K)	300.8
G	Cooling water volumetric feed flow rate, v_{jo} (L/min)	3.79e-3
H	Water volumetric feed flow rate, v_o (L/min)	1.00e-04

4.3 Bunsen Reactor Scale-Up Procedure

The scaling-up procedure for the Bunsen reactor is carried out based on the objective to achieve more than 1,000 kg/hr of H_2 production. The scale-up calculation is done by backward calculation of the overall SITC chemical reaction equation as follows.

$$\underbrace{13H_2O + 5I_2 + SO_2}_{SectionI} \leftrightarrow \underbrace{\left[H_2SO_4 + 5H_2O\right]}_{SectionII} + \underbrace{\left[2HI + 4I_2 + 6H_2O\right]}_{SectionIII} \quad (4.28)$$

Figure 4-6 illustrates an example block diagram of SITC plant scale-up. A summary flow chart indicating the steps involved in the scaling up procedure is presented in Figure 4-7. Figure 4-8 depicts the idea of Bunsen reactor scaling up. By assuming 99% conversion in each Section II and Section III, the estimated total production rate of H_2SO_4 and HI mixture required is 9,500 $\frac{kg}{hr}$. This production rate shall be accomplished by setting the feed flow rates of water, iodine and sulfur dioxide

accordingly. Once the estimated feedstock amount is calculated, the size of the reactor including the area and height can be optimized based on the desired feed and production rates. The kinetic parameters used for both laboratory scale and plant scale are unchanged. Table 4.7 listed the kinetics, operating and design parameters of Bunsen reactor used in both laboratory scale and plant scale simulation studies.

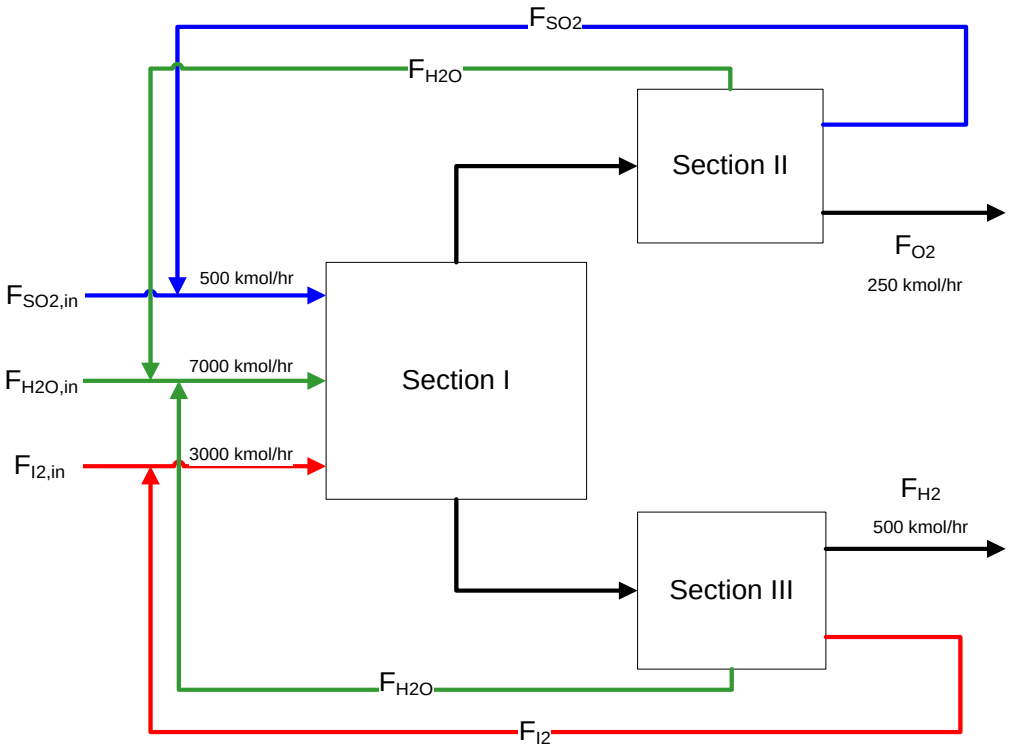

Figure 4-6: An example illustration block diagram of SITC plant scale-up.

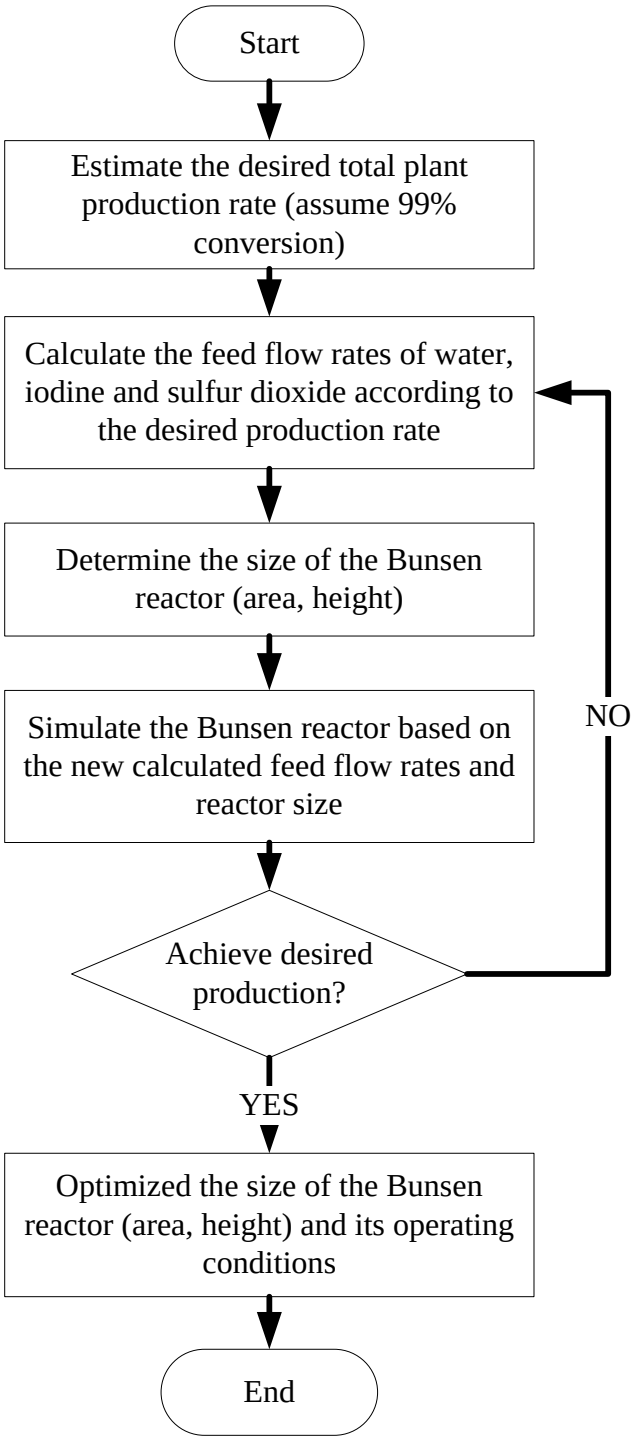

Figure 4-7: Flowchart of scaling up steps for Bunsen reactor

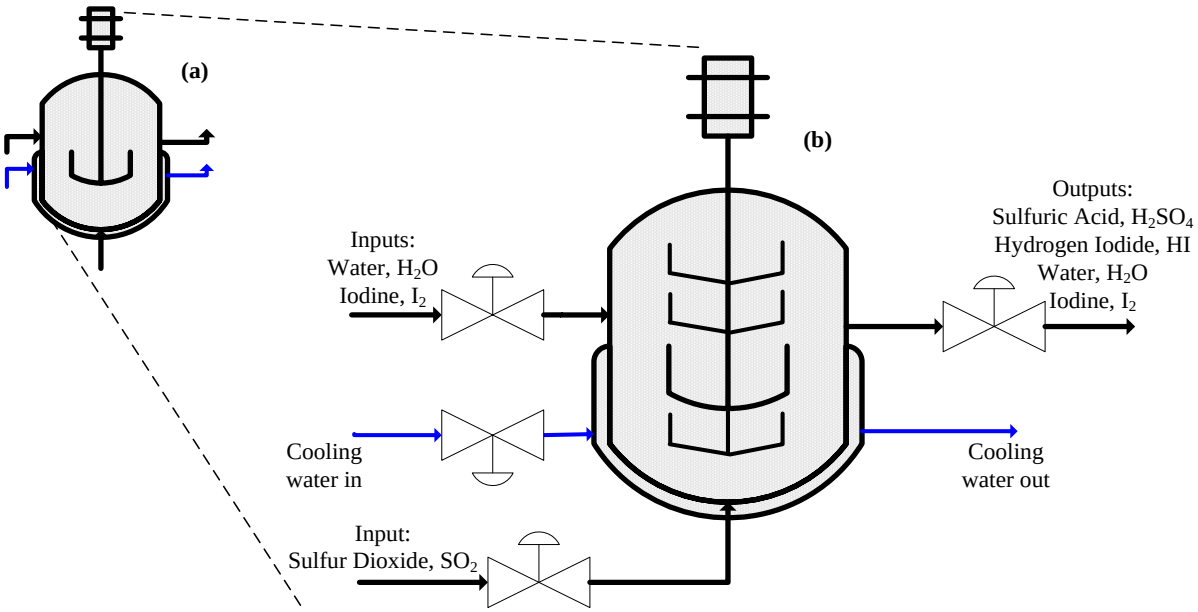

Figure 4-8: Scaling-up schematic diagram for Bunsen reactor: (a) the laboratory scale Bunsen reactor, (b) the plant scale Bunsen reactor.

Table 4.7: Bunsen reactor laboratory scale and plant scale parameters

Bunsen reactor Parameter	**Laboratory Scale**	**Plant Scale**
Cross section area, A_{rx}	$3.3e^{-3}\ m^2$	$20\ m^2$
Maximum height, H_T	$0.15\ m$	$25\ m$
Volumetric feed flow rate of water, v_o	$2.4e^{-4}\ \frac{m^3}{hr}$	$0.102\ \frac{m^3}{hr}$
Molar feed flow rate of iodine, n_{I_2}	$0.9\ mol/min$	$1425\ kmol/hr$
Volumetric feed flow rate of sulphur dioxide (gas), v_{SO2}	$9.6e^{-4}\ \frac{m^3}{hr}$	$0.48\ \frac{m^3}{hr}$
Volumetric feed flow rate of cooling water, v_{jo}	$2.28e^{-4}\ \frac{m^3}{hr}$	$1.466\ \frac{m^3}{hr}$
Iodine to water molar ratio	0.36	0.37
Temperature, T	$345\ K$	$338\ K$

4.4 Liquid-Liquid Separator

Liquid-liquid separator (LLS) is the second important equipment in the Bunsen Section. It is used to separate the two immiscible phases, which are the sulfuric acid and hydrogen iodide solutions. Figure 4-8 shows the schematic design of LLS used in the study.

There is one input line and two output lines. The input line consisting sulfuric acid and hydrogen iodide mixtures. The first output line consisted of light phase liquid which is sulfuric acid and water mixture. The second output line consisted of heavy phase liquid which is hydrogen iodide, water and iodine mixture. The LLS is designed for a plant-scale size.

For the LLS model simplification, assumptions have been made where few are referred to Chonwattana et al, (2018):

A.4.4.1: Both liquid solutions fed to the separator are immiscible and dispersed uniformly in the LLS separation chamber.

A.4.4.2: Densities of both liquid solutions are constant.

A.4.4.3: There is an adequate different between the two liquid densities for a phase separation.

A.4.4.4: The separator has a sufficient retention time to allow the immiscible mixtures to separate into two layers.

A.4.4.5: The emulsion layer between the two liquids formed in the separator is not considered in the developed model.

A.4.4.6: The heavy phase liquid solutions are always below the specified v-notch height. The v-notch angle is 60^{o}.

A.4.4.7: The process is always in a continuous mode.

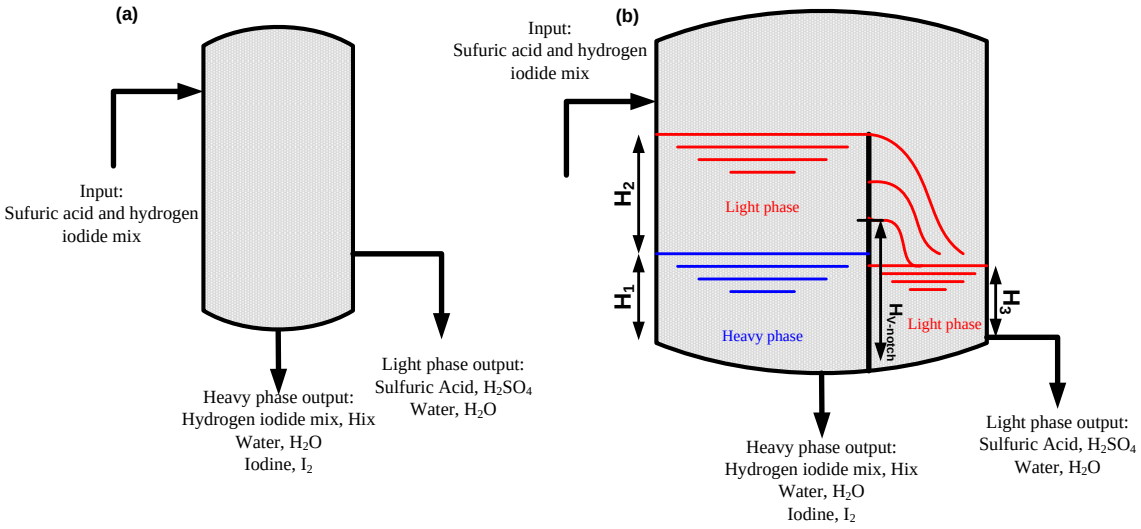

Figure 4-9: Liquid-liquid separator: (a) schematic diagram, and (b) internal view

4.4.1 Mass Balance

The proposed LLS dynamic model is developed by mean of mass balance for each phase to account for the levels of liquid phases. The objective of LLS modelling is to capture the light and heavy phase dynamics of liquid levels in the separation chamber, and the liquid level in the collecting (light phase) chamber. For the heavy phase liquid in the separation chamber, mass balance on the phase leads to

$$\frac{dH_1}{dt} = \frac{x_{in}\rho_{AV}\dot{m}_{in} - \rho_H \dot{m}_1}{\rho_H A_s} \tag{4.29}$$

where H_1 is the level of heavy phase solution, x_{in} is the feed fraction of the heavy phase solution, ρ_{AV} is the density of the mixture, $\dot{m}_{in}$ is the feed flow rate mixture, ρ_H is the density of heavy phase solution and A_s is the surface area of the separating chamber LLS. Mass balance on the light phase liquid in the separation compartment yields

$$\frac{dH_2}{dt} = \frac{(1-x_{in})\rho_{AV}\dot{m}_{in} - \rho_L Q_v}{\rho_L A_s} \tag{4.30}$$

where H_2 is the level of light phase solution, ρ_L is the density of light phase solution and Q_v is the flow rate at the v-notch of the LLS.

Meanwhile, the light phase liquid level in the collecting chamber of the LLS gives

$$\frac{dH_3}{dt} = \frac{Q_v - \dot{m}_2}{A_c} \tag{4.31}$$

where H_3 is the level of light phase solution in the collecting chamber, $\dot{m}_2$ is the outlet flow rate from collecting camber and A_c is the surface area of collecting chamber LLS.

Note that, parameters appear in the equations (4.29) – (4.31) above are expressed as follows:

$$\dot{m}_1 = kv_1 H_1 + 0.75 kv_1 H_2 \tag{4.32}$$

$$\dot{m}_2 = kv_2 H_3 \tag{4.33}$$

$$\begin{aligned} &for\, h > 0, \\ &Q_v = (4.28 m_{cv} C_v \frac{\theta}{2})(h_d + k)^{2.5}, \\ &else \\ &Q_v = 0 \end{aligned} \tag{4.34}$$

Where h is the height of light phase level in the separating chamber. If $h > 0$, the height is above the bottom of V-notch. If the level is below the V-notch, there will be no flow. On the other hand, it is essential to make sure that the heavy phase liquid level is always below the bottom of V-notch; otherwise, HI solution will go to the collecting chamber. The parameters of LLS dynamic model are listed in the Table 4.8. The parameters are based on the industrial scale.

Table 4.8: Parameters of LLS dynamic model

Parameters	**Value or expression**
Heavy phase density, ρ_H	$1300\ \frac{kg}{m^3}$

Light phase density, ρ_L	$1100\ \frac{kg}{m^3}$
Average density, ρ_{AV}	$\rho_H x_{in} + (1 - x_{in})\rho_L$
Area of separator, A_s	$20\ m^2$
Area of collecting chamber, A_c	$0.2A_s\ m^2$
Valve coefficient 1, kv_1	0.4
Valve coefficient 2, kv_2	1
Total liquid height, H_t	$H_1 + H_2$
V-notch height, $H_{v-notch}$	$13\ m$
Height above the V-notch bottom, h	$H_t - H_{v-notch}$
Total height of LLS, HHT	$25\ m$

4.5 Novel Procedure for Control System Design

In order to design a control system or strategy for the Bunsen reactor unit, the following procedure is applied:

Step 1: Determine control objectives. The explicit objectives of controlling the Bunsen reactor are to maintain the X and Y variables at constant optimal setpoint. The reasons of implicit objectives of controlling X and Y variables are maintained (i.e, keep HIx solution above azeotropic composition, etc).

Step 2: Determine potential manipulated variables. PCA and RSM analyses are adopted in order to determine which inputs are strongly correlated with the controlled variables X and Y. RSM analysis is used to determine which inputs that cause minimum economic loss (i.e., flat) when the inputs are used as manipulated variables.

Step 3: Determine favorable operating conditions and pairings. To determine a favorable operating conditions, the fundamental model is linearized at different operating points. A few sets of linearized models (2x2 transfer function matrices) are obtained, which are then analyzed for the controllability properties by using LGC and RGA indices.

Step 4: Select and design controller algorithms. Based on the LGC index, a suitable controller algorithm is chosen, e.g., either standard PID controller or MPC; the latter will be used if the LGC value is very small, which implies difficult to control the system using the standard decentralized PID control.

Step 5: Evaluate control strategy. The control strategy designed in Step 4 is evaluated for its servo and regulatory control performances. If the performances are not satisfactory, a new control strategy will be designed or a different controller law will be adopted.

The strength or advantage of the procedure is that it allows the simultaneous determination of suitable operating condition and controller pairing. In some existing methods, the operating condition is often pre-defined, or selected in ad-hoc manner. Avoiding an operating condition that gives poor controllability is just as important as selecting proper controller pairings in a decentralized control scheme. Poor controllability of the given operating condition will unavoidable lead to poor control performance regardless of the type of control law being used.

Another advantage of the proposed procedure is its ability to avoid an engineer from selecting unsuitable manipulated variables which can cause serious economic loss due to the adjustments of the inputs. This ability arises from the incorporation of PCA and RSM techniques in Step 2. Figure 4-10 presented the above step in a flowchart form. Step 1 to 3 will be presented in detail in Section 4.6. Step 4 will be presented in detail in Section 4.7 and Step 5 will be presented in detail in Section 4.8.

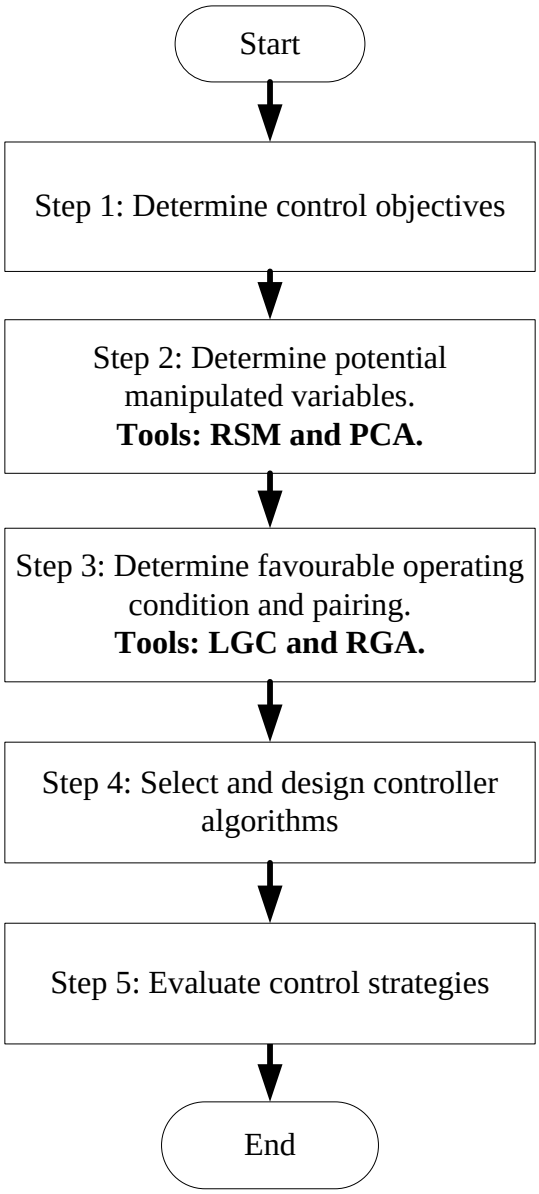

Figure 4-10: Flowchart of novel procedure for designing control system

4.6 Loop Gain Controllability Analysis

In this section, the LGC analysis will be carried out for the Bunsen reactor. Since Bunsen reactor is a multivariable process, controlling the reactor will require more than one control loops. Here, the LGC analysis can be used to determine:

a) Dynamically favorable operating conditions which give good controllability performance, i.e., to find the operating conditions, at which the reactor is easy to control even by using a simple PID control system.
b) The best sets of manipulated inputs and controlled outputs which can lead to the highest achievable control performance.

Based on the sensitivity analysis via RSM method, there are four potential manipulated input variables have been identified for the Bunsen reactor: (1) cooling jacket flow rate, (2) feed molar flow rate of iodine, (3) feed temperature, and (4) sulfur dioxide feed flow rate or pressure. Table 4.9 lists down the potential manipulated inputs (MVs) and controlled outputs or variables (CVs) for the Bunsen reactor. The LGC analysis results are also presented corresponding to the different sets of MVs and CVs. In this case the feed temperature is not chosen as the manipulated variable since it cannot be adjusted rapidly – its application as manipulated variable will be hampered by long time-delay, which is not desirable for closed-loop stability. Thus, in practice the feed temperature acts as one of the potential disturbance variables (DVs). Controlling the reactor holdup level is crucial as this directly leads to inventory control of the reactor to avoid potential unsafe conditions. If the reactor holdup level drops to a very low value, then this can cause cavitation of the pump installed beneath the reactor. On the contrary, if the reactor holdup level is not controlled, this can lead to a possible overflow of the reactor. To control the reactor holdup level, either the feed flow or outlet flow from the reactor can manipulated. In the present study, it is preferable to manipulate the outlet flow rate as to control the reactor holdup level. Alternatively, the reactor holdup level can be controlled indirectly by controlling the production rate. From the PCA analysis, it is found that the production rate and holdup level are positively correlated, which implies that if one of these variables are controlled, then this would indirectly control another variable.

In the Table 4.9, it is shown that the LGC value for the 2×2 MIMO Model 1 (set 1 of MV-CV) is higher than that of the Model 2. Note that, for Model 2 the LGC value is negative which implies very poor controllability property based on the sets of MV-CV selected.

Even though the RGA values between the Model 1 and Model 2 are comparable, hence indicating equally favorable input-output pairings, the negative LGC value of the Model 2 implies that it is not controllable. Therefore, the pairing as in the Model 1 is choose for the controller design of the Bunsen reactor.

Recall that, a positive LGC value but lower than unity suggests that the system is difficult to control using the conventional decentralized PID control. In this case the LGC value for Model 1 is less than one, which implies it is hard to control with PID-based controller. For this reason, the application of an advanced model based controller will be preferable, e.g., Nonlinear MPC.

Table 4.10 shows the transfer function models for Bunsen reactor which are derived via linearization of the fundamental model at some nominal operating conditions. Notice that the diagonal transfer functions for the Model 2 exhibit very large time-delays compared to that of the Model 1. Thus, the reason for the negative LGC value of the Model 2 (difficult to control) is due to the long time-delays. For a given system, as the time-delays become larger, the maximum achievable control performance becomes smaller.

Table 4.9: Controllability analysis based on 2x2 MIMO model of Bunsen reactor

Model BR	**Sensitivity analyzes**		θ_{eotf}	**LGC**	**RGA**
	Manipulated Input	**Controlled Output**			
Model 1	Outlet Flowrate	Reactor Level	10.62	0.9077	$\begin{bmatrix} 1.0151 & -0.0151 \\ -0.0151 & 1.0151 \end{bmatrix}$
	Jacket Flowrate	Reactor Temperature			
	Feed Flowrate Iodine, I_2 (MV1)	Product Flowrate (CV1)			
		Reactor Temperature			
	Feed Flowrate Sulphur Dioxide, SO_2 (MV2)	Product Flowrate			
		Reactor Temperature (CV2)			
	Feed temperature	Reactor Level			
		Reactor Temperature			
Model 2	Outlet Flowrate	Reactor Level	35.11	-0.9841	$\begin{bmatrix} 0.9815 & 0.0185 \\ 0.0185 & 0.9815 \end{bmatrix}$
	Jacket Flowrate (MV1)	Reactor Temperature (CV1)			
	Feed Flowrate Iodine, I_2 (MV2)	Product Flowrate (CV2)			
		Reactor Temperature			
	Feed Flowrate Sulphur Dioxide, SO_2	Product Flowrate			
		Reactor Temperature			
	Feed temperature	Reactor Level			
		Reactor Temperature			

Table 4.10: Transfer function models for the Bunsen reactor at nominal conditions.

No	Bunsen reactor Model	Input-Output Pairing
1	$Model\ 1 = \begin{bmatrix} \frac{1.0469e^{-0.8503s}}{20.32s+1} & \frac{0.031e^{-0.3978s}}{0.4105s-1} \\ \frac{-0.0047e^{-10.637s}}{51.14s+1} & \frac{-3.87\times10^{-5}e^{-0.4104s}}{0.4105s-1} \end{bmatrix}$	Feed Flowrate Iodine, I_2 (MV1) Feed Flowrate Sulfur Dioxide, SO_2 (MV2) Product Flowrate (CV1) Reactor Temperature (CV2)
2	$Model\ 2 = \begin{bmatrix} \frac{7.7084\times10^{-4}e^{-30.68s}}{154.29s+1} & \frac{381.25e^{-2.31s}}{59.66s+1} \\ \frac{0.00146e^{-63.52s}}{62.4s+1} & \frac{-13.574e^{-30.72s}}{154.11s+1} \end{bmatrix}$	Jacket Flowrate (MV1) Feed Flowrate Sulphur Dioxide, SO_2 (MV2) Reactor Temperature (CV1) Product Flowrate (CV2)

4.7 Process Controller Design for Bunsen Section

4.7.1 NMPC Design for Bunsen reactor

Based on the LGC analysis result (small index value less than 1) as well as the presence of unstable poles in the Model 1, it is can be anticipated that the Bunsen reactor is difficult to be control by using PID-based controllers. In view of this problem in this work a nonlinear MPC (NMPC) is chosen for controlling the Bunsen reactor. A NARX model is embedded into the MPC to form the NMPC. The significant of NARX model can be retrieved from (Mohd and Aziz, 2016).

For the NMPC scheme, the manipulated variables (MVs) used are iodine molar feed flow (MV1) and sulfur dioxide feed flow (MV2) while the controlled variables (CVs) are sulfuric acid flowrate (CV1) and reactor temperature (CV2).

4.7.1.1 Identification of NARX empirical model

A set of input-output data of Bunsen reactor corresponding to the Model 1 (from previous section) consisting of 16,455 samples is generated from the first principle Bunsen reactor model. The type of simulation input used is the multi-level input signal (see details in Section 3.2.4) to mimic the input of a real plant input. The generated data is then used for the development of NARX model using the System Identification Toolbox in MATLAB via, 'nlarx' nonlinear function. The NARX model order and delay; $[na, nb, nk]$; [3,2,3] are used. Figure 4-11 and 4-12 show the plotted NARX models for both input-output pairings. Table 4.11 tabulated the result from these figures. It is demonstrated that the nonlinearity estimator object '*sigmoidnet*' and '*wavenet*' shown the best fit NARX model for Bunsen reactor.

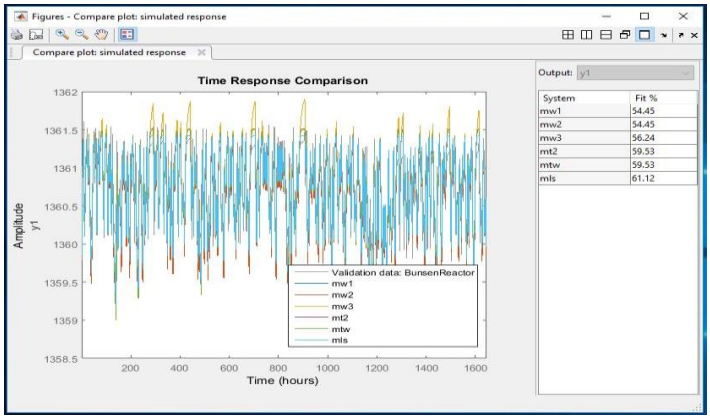

Figure 4-11: NARX model identification for $u_1 and\ y_1$

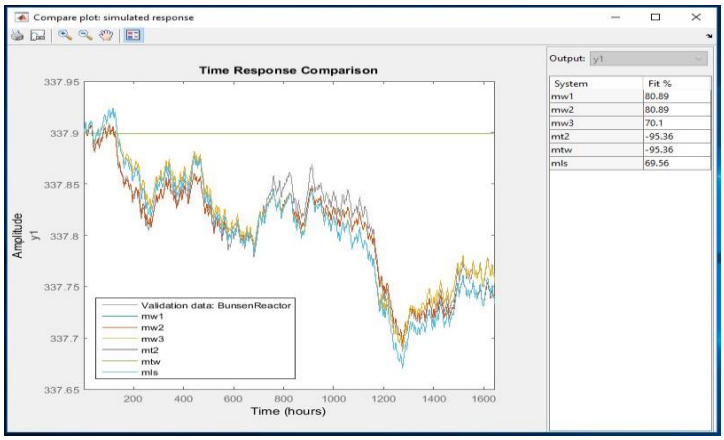

Figure 4-12: NARX model identification for $u_2\ and\ y_2$

Table 4.11: NARX model nonlinearity estimator object best fit value

Nonlinearity estimator object	**Best fit value**	
	Pairing 1	**Pairing 2**
Wavenet	54.45	80.89
Wavenet (high order)	54.45	80.89
Wavenet (custom order)	56.24	70.10
Treepartition	59.53	-95.36
Sigmoidnet	61.12	69.56

4.7.1.2 NMPC development

The NMPC is first tuned via an offline simulation. The objective functions of the NMPC given as follow,

$$\min_{N_I[t|t],\ldots N_I[m+p|t]_{i=0}} J(SA(t), N_I(t)) \tag{4.35}$$

$$\min_{v_{SO_2}[t|t],\ldots v_{SO_2}[m+p|t]_{i=0}} J(T(t), v_{SO_2}(t)) \tag{4.36}$$

$$\min_{N_I[t|t],\ldots N_I[m+p|t]_{k=0}} \sum_{k=1}^{P} w_k (SA[t+k\,|\,t] - SA_{setpoint})^2 + \sum_{k=1}^{M} r_k \Delta u[t+k\,|\,t]^2 \tag{4.37}$$

$$\min_{v_{SO_2}[t|t],\ldots v_{SO_2}[m+p|t]_{k=0}} \sum_{k=1}^{P} w_k (T[t+k\,|\,t] - T_{setpoint})^2 + \sum_{k=1}^{M} r_k \Delta u[t+k\,|\,t]^2 \tag{4.38}$$

where $\boldsymbol{SA}$ is the product flowrate and $\boldsymbol{T}$ is the temperature. $\boldsymbol{P}$ is process output prediction, $\boldsymbol{M}$ is manipulated input horizons and $\boldsymbol{Q}$ and $\boldsymbol{R}$ are the weighting matrices. $\boldsymbol{N_I[t+k|t]_{k=0\ldots P}}$ and $\boldsymbol{v_{SO_2}[t+k|t]_{k=0\ldots P}}$ are the set of future process input values.

The output prediction shall be more or equal than the manipulated input horizons, $\boldsymbol{P \geq M}$ where they are adjustable. In this work, the tuning test begins with $\boldsymbol{M = 1}$ and $\boldsymbol{P = 15}$. The weighting matrix $\boldsymbol{R}$ is a diagonal form as $\boldsymbol{r_k = diag(a, b, c, \ldots)}$ while $\boldsymbol{w_k = 2 \times 2}$ matrix. The tuning Set 2 with $\boldsymbol{M = 1}$ and $\boldsymbol{P = 20}$ produced the best performance. Table 4.12 listed the SSE values of various MPC tuning.

Table 4.12: SSE values for CV1 and CV2 of Bunsen reactor for various MPC tuning

Weighting matrices		**Set**	**Control horizon, *M***	**Prediction horizon, *P***	**SSE for CV1**	**SSE for CV2**
w_k	r_k					
$\mathbf{2 \times 2}$ matrix (input)	$\begin{bmatrix} \mathbf{2} & \mathbf{0} \\ \mathbf{0} & \mathbf{2} \end{bmatrix}$	1	1	15	14.5330	31.4951
		2	1	20	14.1726	31.0756
		3	2	15	14.1827	30.7564
		4	2	20	14.5787	30.4951
		5	3	15	14.5273	31.0756
		6	3	20	14.5330	31.0610

4.7.2 MSC-PID Design for Liquid-liquid separator

The details of the multi-scale control (MSC) scheme can be found in (Nandong and Zang, 2013a). The MSC scheme can be used to synthesize practical PID controller augmented with a filter. i.e., MSC-PID controller. It is interesting to note that, the MSC scheme can provide significant performance and robustness improvements for some processes with long dead time and inverse-response behaviors. The basic idea of the MSC scheme is to decompose a given plant into a sum of basic factors with distinct speeds of responses – multi-scale modes. A set of sub-controllers is designed based on the basic modes, which are then combined in such a way to enhance cooperation among these different modes. For the LLS unit, the MSC scheme will be used to design the required PID controllers for controlling liquid levels in the unit.

For the LLS effective operation, it is crucial to keep the level of each heavy phase and light phase liquid in the collection chamber at constant setpoint so that the separation process can be performed efficiently. Two SISO PID controllers are designed to achieve this purpose. The nominal conditions of the LLS at which the controllers are designed are shown in Table 4.13. The transfer function of a linearized LLS model (heavy phase) is as follows

$$G_{LLS} = \frac{0.06864\,s^2 + 0.0008062\,s - 9.353e^{-6}}{s^3 - 0.1326\,s^2 + 0.002153\,s} \tag{4.39}$$

Based on the transfer function of LLS, an MSC-PID controllers is obtained using the MSC scheme. The inner-loop P-only controller is first designed, and then the PI controller. The overall MSC-PID controllers are given as follows.

$$G_{MSC} = 2467\left(\frac{1+0.0189\,s}{0.1137\,s}\right)\left(\frac{2476\,s+46.73}{s+0.1137}\right) \tag{4.40}$$

Note that the MSC-PID controller above is compared with an IMC-PID controller. The IMC-PID controller setting (using MATLAB Control System Design) is given as follows.

$$G_{IMC} = -0.00083832\left(\frac{(1+96s)(1+1.5e3)}{s}\right) \tag{4.41}$$

Table 4.13: Nominal value of LLS levels

Variables	**Nominal value**
Heavy phase level, L_{HLS} (m)	5.997
Light phase level, L_{LLS} (m)	8.523
Collecting chamber level, L_{LCLS} (m)	2.244

4.8 Performance Evaluation of NMPC in Bunsen Reactor

4.8.1 NMPC Performance on Bunsen reactor

4.8.1.1 Setpoint tracking

Figures 4-13, 4-14, 4-15 and 4-16 show the results for the setpoint tracking of sulphuric acid flow rate (CV1), i.e., the primary controlled variable. The setpoint for the CV1 is changed from a nominal steady-state, 1,360 kg/hr to 1,385 kg/hr at 750th hour (in simulation unit), then from 1,385 kg/hr to 1,335 kg/hr at the 1200th hour, and finally set back to original point value for the rest of simulation. Meanwhile, the setpoint of temperature (CV2) is changed from a nominal steady-state, 338 K to 341 K at 750th

hour, then from 341 K to 335 K at the 1200th hour, and finally set back to the original nominal steady state value for the rest of simulation. For both CV1 and CV2, the NMPC is able to drive the controlled outputs to their desired setpoint smoothly with a fast response without any delay while the MVs are still within the desired boundaries. There is a small offset for CV1. However, the offset is less than 1.5 kg/hr which is insignificant to the overall flowrate of the plant.

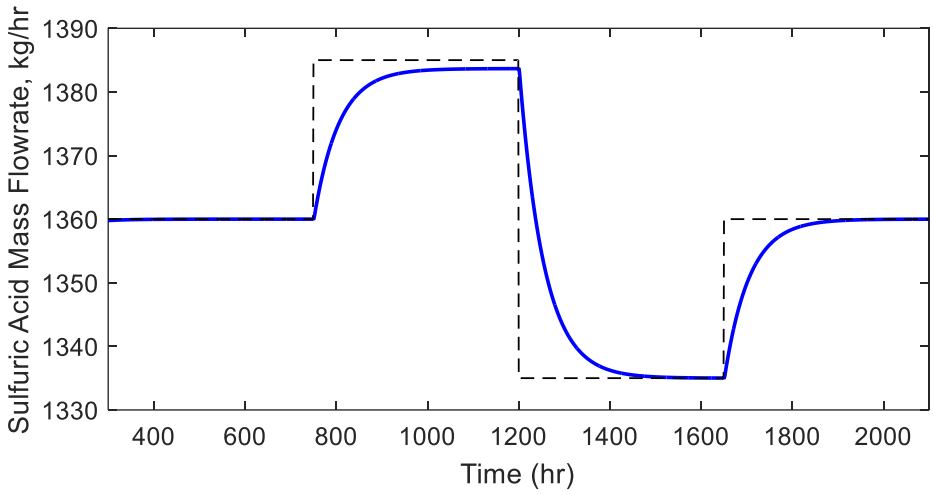

Figure 4-13: Response of NMPC for setpoint changes in CV1, sulfuric acid flowrate.

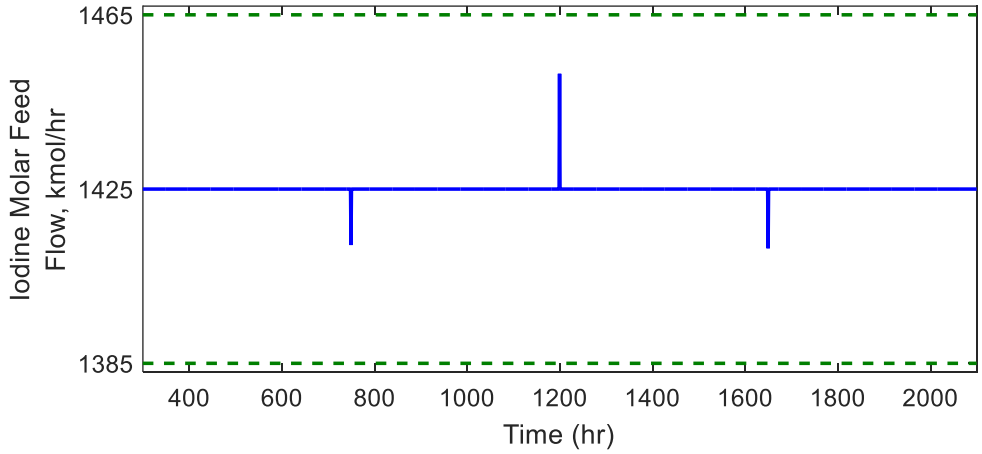

Figure 4-14: Response of iodine molar feed flow (MV1) under the setpoint changes in CV1.

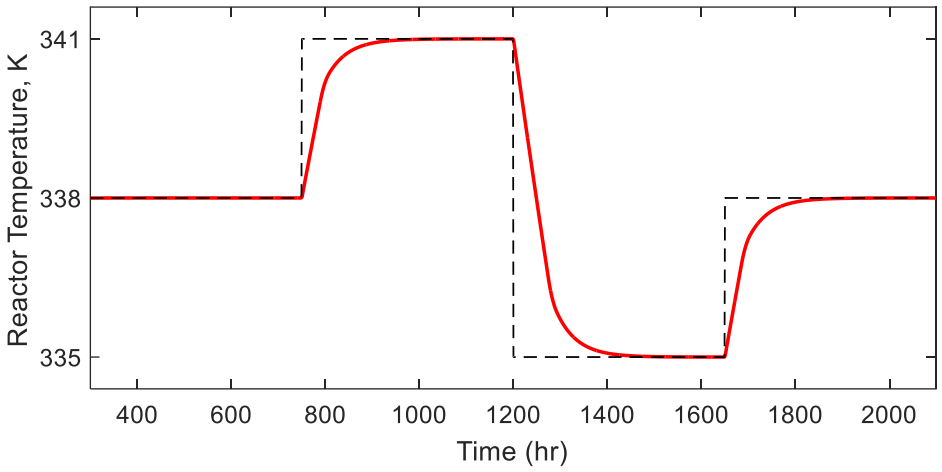

Figure 4-15: Response of NMPC for setpoint changes in CV2, Bunsen reactor temperature.

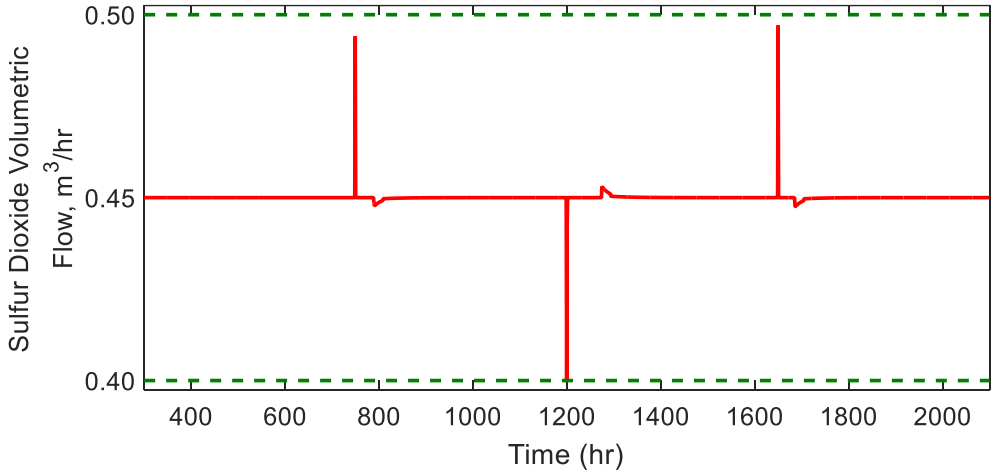

Figure 4-16: Response of sulfur dioxide volumetric flow rate (MV2) under the setpoint changes in CV2.

4.8.1.2 Disturbance Rejection Test

A disturbance test is introduced at the 400th hour for both CV1 and CV2. The feed temperature is increased by 5^{o}C for 5 hours and the disturbance rejection response of the NMPC is observed. Figure 4-17 shows that the disturbance affect the product flowrate with a very minimal fluctuation with magnitudes less than 0.05 kg/hr.

Meanwhile, Figure 4-18 shows that the NMPC is able to completely reject the disturbance after about 150 hours. Even though the rejection time is long; the reactor temperature is still kept within the optimal temperature window, i.e., $330\ K \leq T \leq 350\ K$.

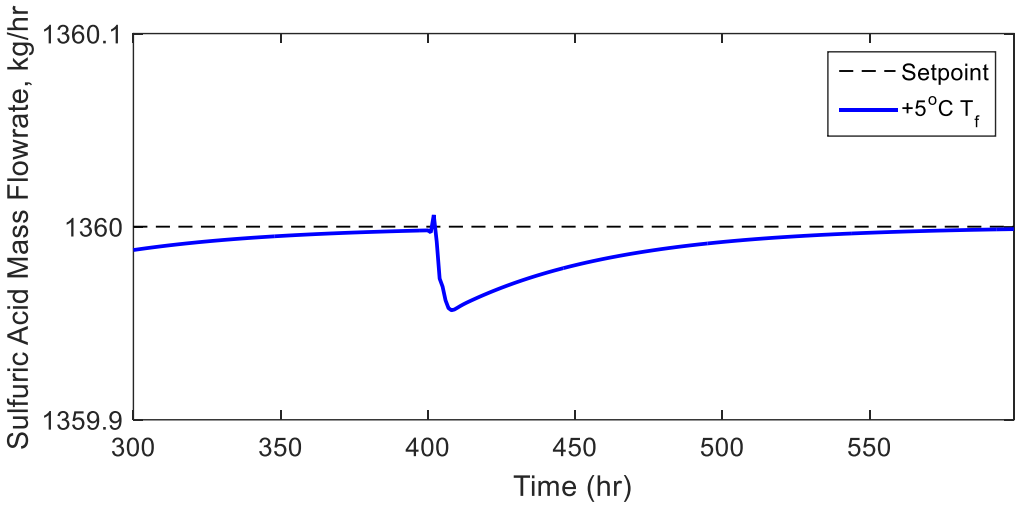

Figure 4-17: Response of NMPC for disturbance rejection test for CV1

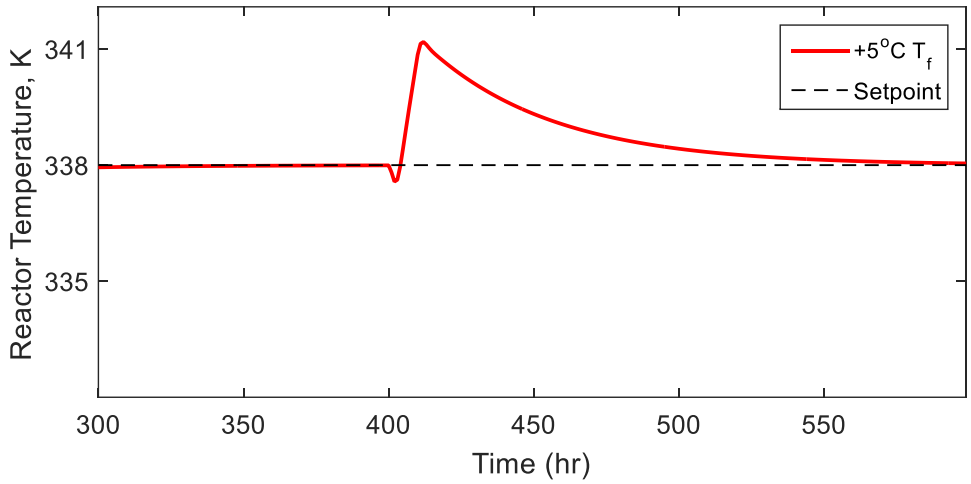

Figure 4-18: Response of NMPC for disturbance rejection test for CV2

Based on the setpoint tracking and disturbance rejection test, it is shown that the NMPC is able to fulfill all three keys criteria for Bunsen reactor:

a) The resulting feed molar ratio of I_2/H_2O is between 0.356 and 0.377, i.e., within the optimal operating range.
b) The resulting molar ratio of $HI/(HI + H_2O)$ lies between 0.16 and 0.25, i.e., at 0.23 where this will ensure the solution remains over azeotropic condition.

As a conclusion, the NMPC can provide satisfactory closed-loop performances for the Bunsen reactor, under both servo and regulatory control objectives.

4.8.2 MSC-PID Performance

4.8.2.1 Setpoint tracking

Figure 4-19 shows the results for the setpoint tracking of heavy phase level in the LLS separating chamber. The nominal setpoint is set at 5.6 m. It is shows that MSC-PID drives the heavy phase liquid level to the setpoint faster that IMC-PID which could not settle to the desired setpoint. The IAE for MSC-PID is very small which is only 0.0468 showing an efficient controller performance as compared to the IMC-PID with IAE of 121.4.

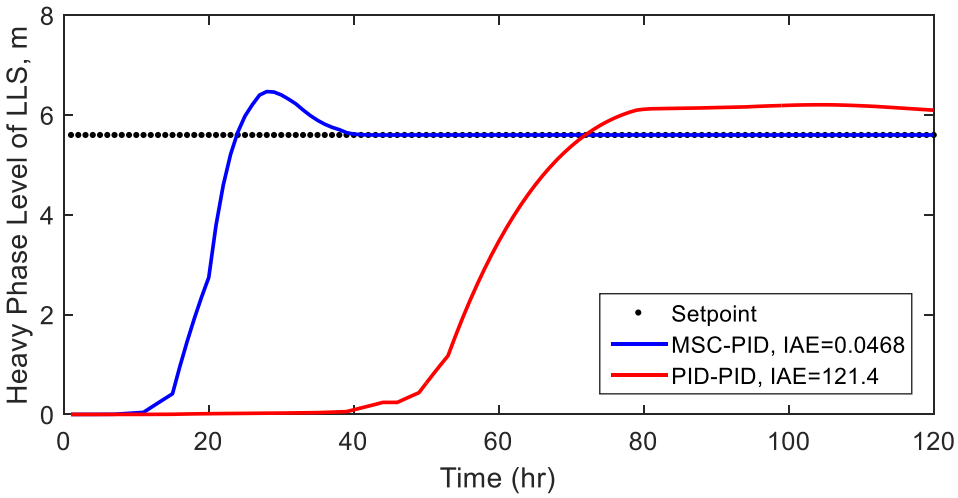

Figure 4-19: Response of MSC-PID and IMC-PID for setpoint tracking in CV, heavy phase level of LLS.

The setpoint tracking is continued with another setpoint change test. The CV changes from nominal steady state, to 7 m at 25th hour, 7 m to 3 m at the 50th hour and then set back to the steady state value for the rest of hours. Figure 4-20 reveals that the MSC-PID is able to drive the process output to its desired setpoint with a fast response with little delay, while the IMC-PID is not able to track the given setpoint changes.

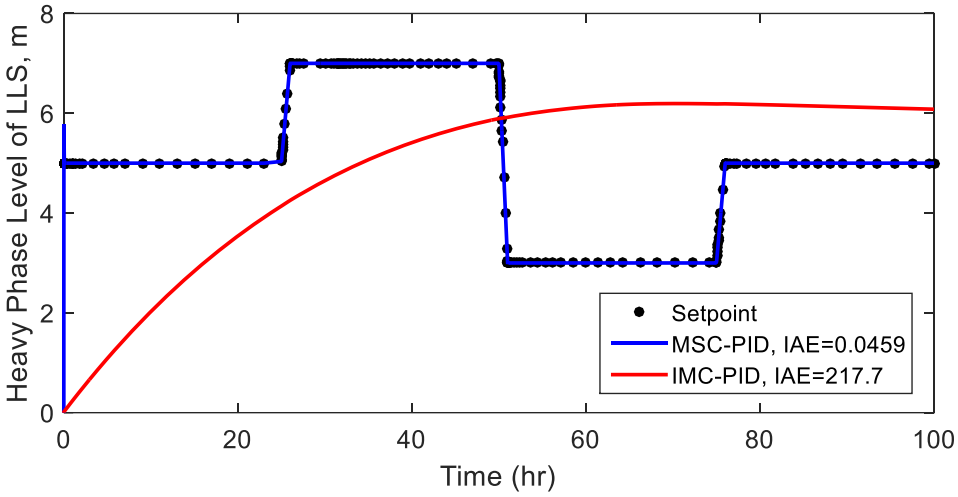

Figure 4-20: Response of MSC-PID and IMC-PID for setpoint changes in CV, heavy phase level of LLS.

4.8.2.2 Disturbance rejection test

A disturbance test is introduced at the 80th hour. The feed flowrate which is the upstream flow from the Bunsen reactor is increased by 20% for 1 hour and the disturbance rejection time of both controllers are observed. Figure 4-21 shows response of the MSC-PID controller, notice that the disturbance has only little effect on the heavy phase liquid level. On the contrary, Figure 4-22 shows that the IMC-PID is not able to reject the disturbance and which indicates instability behaviour of the controller. For both setpoint tracking and disturbance rejection tests, the MSC-PID show satisfactory performances as compared to the IMC-PID.

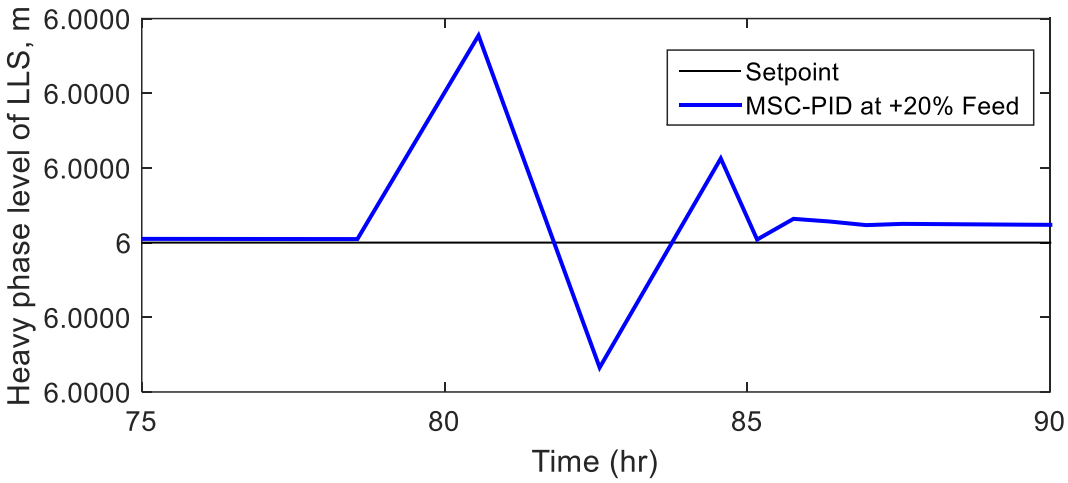

Figure 4-21: Response of MSC-PID for disturbance rejection test for CV.

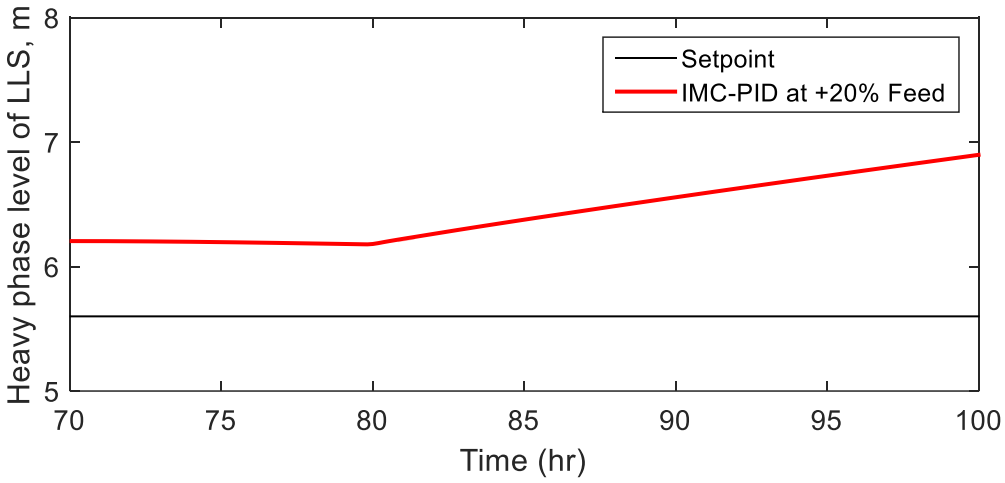

Figure 4-22: Response of IMC-PID for disturbance rejection test for CV.

4.9 Summary

To the best of our knowledge, to date, there has been no report on the detailed fundamental models and scale-up for the Bunsen reactor and L-L separator units of the SITC plant. The sensitivity analysis for Bunsen reactor reveals that the kinetics of Bunsen reaction in the CSTR:

a) Has little dependence on temperature changes within the specified optimal range.
b) Slightly sensitive to the changes in both feed flow rate of SO_2 gas and its partial pressure.
c) Changes in iodine and water molar feed flow rates have the most significant influences on the total output variables; sulfuric acid and hydrogen iodide flowrate.

It has been demonstrated that, the scaling up of the L-L separator presented a number of challenges, and must be addressed when selecting the area and height of weir. After the scaling up procedure, the controllability analyses were carried out via LGC index. Since the value of LGC based on the Model 1 is less than unity, this means that the system is very difficult to control using the standard decentralized PID control. Thus, for the Bunsen reactor, a NMPC is chosen. In view of the satisfactory servo and regulatory performances demonstrated by the NMPC, it can be concluded that the application of NARX model in the controller is adequate enough to capture the main nonlinear dynamics of the Bunsen reactor. Meanwhile, for the LLS, two PID controllers are developed and compared, which are designed based on the MSC-PID and IMC-PID approaches. Based on the setpoint tracking and disturbance rejection tests, it has been shown that the MSC-PID outperforms the IMC-PID controllers.

5 Sulfuric Acid Section (Section II): Dynamic Modelling and Controllability Analysis

This chapter covers aspects from fundamental to process controller performance evaluation of the Sulfuric Acid Section. Prior to plant scale-up, a preliminary simulation of a laboratory scale Sulfuric Acid Integrated Boiler Superheater Decomposer (SA-IBSD) reactor using kinetic parameters available in literature was carried out and validated. The effects of input variables on output variables were analyzed and the process operating conditions were then optimized. Meanwhile, the controllability analysis for the reactor was carried out based on the LGC method and the most controllable model (operating condition) is selected. The dynamic modelling of a flash tank for concentrating sulfuric acid solution was also presented. Suitable controller strategies were selected and designed for the SA-IBSD reactor, and their performances were evaluated. At the end of this chapter, a summary on the Sulfuric Acid Section is highlighted.

5.1 Fundamental of Sulphuric Acid Section

In the Sulfuric Acid Section there are two main processes :(1) sulfuric acid flashing, and (2) sulfuric acid decomposition processes. A sulfuric acid flash tank (SA-FT) is used to first concentrate the sulfuric acid solution from the Bunsen Section. It follows that the concentrated acid is then sent to an integrated reactor, i.e., Sulfuric Acid Integrated Boiler Superheater Decomposer (SA-IBSD) reactor to decompose the sulfuric acid.

The sulfuric acid mixture from the Bunsen Section is fed to the SA-FT to be concentrated to a desired concentration, which is more than 90% acid concentration. From the sulfuric acid solution, water vapor is eliminated as much as possible before the sulfuric acid is fed to the SA-IBSD reactor. In the SA-IBSD reactor, the sulfuric

acid is decomposed into sulfur dioxide and oxygen. Sulfur dioxide is recycled to Bunsen reactor while oxygen is collected as a byproduct.

5.1.1 Reaction Mechanisms

The overall chemical reaction of Sulfuric Acid Section is given as follows,

$$H_2SO_4(l) + 5H_2O(l) \rightleftharpoons SO_2(g) + 6H_2O(g) + \frac{1}{2}O_2(g) \quad (5.1)$$

The chemical reactions taking place in the SA-IBSD reactor are as follows,

Reaction 1: Evaporation

$$H_2SO(l)_4 \rightleftharpoons SO_3(g) + H_2O(g) \quad \Delta H_1 = +300 \text{ kJ/mol} \quad (5.2)$$

Reaction 2: Decomposition

$$SO_3(g) \rightleftharpoons SO_2(g) + \frac{1}{2}O_2(g) \quad \Delta H_2 = +274 \text{ kJ/mol} \quad (5.3)$$

Note that, the decomposition reaction is carried out in the presence of catalyst.

The SA-IBSD unit operates at a very high temperatures that goes beyond the critical temperature of water (374℃) (Kim et al., 2008; Nagarajan et al., 2014). Since the SA-IBSD reactor is an endothermic reaction, the reaction temperature and the thermal energy supplied to the system must be sufficient. As a rule of thumb, a higher temperature tends to favor greater efficiency. Please note that, however, it is desired to control the reaction temperature below 1140℃ to prevent a potentially dangerous process runaway reaction and catalyst deactivation.

5.2 Dynamic Modelling and Simulation

5.2.1 Sulfuric Acid Flash Tank (SA-FT)

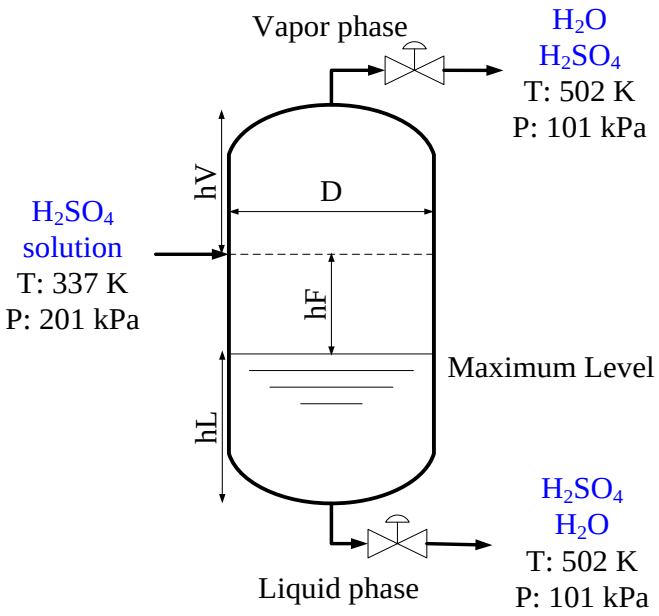

Figure 5-1: The schematic diagram of SA-FT (Watkins, 1967)

In this section, a dynamic model of the flash tank to concentrate sulfuric acid is presented. Figure 5-1 shows the schematic diagram of SA-FT, which is modified from the Watkins's separator and accumulator design (Watkins, 1967). The height or length of the SA-FT is given as follows

$$L = H_L + H_F + H_V \tag{5.4}$$

From Figure 5-1, H_L is the liquid level, H_F is the flooding level which is the distance between liquid level and feed nozzle, H_V is the vapor level, and D is diameter.

The essential rule of the flash tank design is that to specify the length-to-diameter (L/D) ratio, which shall lie between 3 and 5. This is based on the fact that, as the diameter decreases, the shell thickness decreases and vessel length increases. In addition to that, at some point between the L/D ratios of 3 and 5, a minimum vessel

weight can be found, and this will result in the minimum capital cost of the unit (Rao, 2012).

The sulfuric acid/water binary separation is a crucial unit operation in a SITC process for hydrogen production. In the dynamic modelling of the SA-FT unit, it is decided to estimate the activity coefficients for the binary mixture using the NRTL model whereas the thermodynamic properties are estimated via the EOS type, i.e. specifically the Peng-Robinson (PR) method. To estimate the phase equilibria and thermodynamic properties, a pre-simulation is first carried out in the Aspen Plus software. Once the phase equilibria and the desired thermodynamic properties are obtained, the dynamic modelling of the SA-FT can be performed via the MATLAB simulation. One of the reasons for conducting this modelling in MATLAB is to enable the use of many tools available in this software, e.g., for optimization, nonlinear analysis and control studies; in Aspen such studies are quite limited. The results of the SA-FT simulation are then compared with the available literature data.

From the liquid-liquid separation (LLS) unit in the Bunsen Section, the aqueous H_2SO_4 solution is fed into the SA-FT. The sulfuric acid stream is pre-heated and flashed in the SA-FT unit to remove water as much as possible. It is important to note that, the relative volatility of the components to be separated should be much larger than 1 for the single flash operation to be able to achieve the required separation. Since water has a lower volatility than the sulfuric acid, so the evaporation of water is much higher than the acid. Hence, the water is separated from the solution (as the light vapour phase) and it is recycled back to the Bunsen Section. The sulfuric acid is accumulated in the liquid phase during the flash process. Since the SITC plant involves a closed cycle, failing to remove most water from the acid stream prior to entering the SA-IBSD

reactor will affect the cycle efficiency, which in turn shall reduce the hydrogen production (Lee et al., 2009).

The proposed SA-FT dynamic model (mass and energy balances) and design procedure are summarized as follows:

Step SA-FT.1: Calculate the bubble point and the vapour pressure for the water/sulfuric acid mixture.

Step SA-FT.2: Find the steady-state value for each variable based on the derived differential equations. The steady-state is important to see the capability of the developed dynamic model to achieve stable output.

Step SA-FT.3: Simulate the SA-FT model in, i) stand-alone mode and ii) integrated mode. The model is simulated in the MATLAB Simulink environment.

5.2.1.1 Mass and Energy Balances

The following steps are applied in the modeling and simulation of SA-FT:

Step SA-FT.1 Bubble point and vapour pressure calculation

The following algorithm is applied to find the bubble-point.

Step SA-FT.1.1: Guess the flash tank temperature, e.g., $T = T_1$.

The liquid mass fractions are first estimated in addition to flash tank pressure. From this estimation, the bubble-point calculation is then continued as follows. Note that, the summation of mass fractions in either liquid or vapour phase must be unity, so that:

$$\sum_{i=1}^{m} y_i = \frac{1}{P}\left[\sum_{i=1}^{m}\left(x_i \gamma_i P_i^s\right)\right] = 1 \tag{5.5}$$

where y_i denote the the vapor fraction, x_i is the liquid fraction, γ_i is the liquid activity coefficient and P_i^s is the vapour pressure of i-th component.

From the equation (5.5), the mass fractions in liquid and vapour are related via the Vapour-Liquid Equilibrium relation:

$$\frac{y_i}{x_i} = \frac{\gamma_i P_i^s}{P} \tag{5.6}$$

Step SA-FT.1.2: Calculate the vapour pressure via Eqn. (5.7).

Vapour pressure P_i^s of the i-th component is calculated using the Antoine's equation

$$\log_{10} P_i^s = A_i - \frac{B_i}{C_i + T} \tag{5.7}$$

Step SA-FT.1.3: Calculate the activity coefficients via Eqn. (5.8) to (5.9)

The activity coefficients of two liquid mixtures can be calculated using the Non-Random Two-Liquid (NRTL) model (Prausnitz and Tavares, 2004) given by:

$$\ln \gamma_i = x_2^2 \left[\tau_{21} \left(\frac{G_{21}}{x_1 + x_2 G_{21}} \right)^2 + \frac{\tau_{12} G_{12}}{(x_2 + x_1 G_{12})^2} \right] \tag{5.8}$$

$$\ln \gamma_2 = x_1^2 \left[\tau_{12} \left(\frac{G_{12}}{x_2 + x_1 G_{12}} \right)^2 + \frac{\tau_{21} G_{21}}{(x_1 + x_2 G_{21})^2} \right] \tag{5.9}$$

The Gibbs energy equation is given as follows

$$\ln G_{12} = -\alpha_{12} \tau_{12} \tag{5.10}$$

$$\ln G_{21} = -\alpha_{21} \tau_{21} \tag{5.11}$$

The non-randomness parameter α_{ij} and the dimensionless interaction parameter τ_{ij} are extracted from the Aspen Plus simulation as described in the following section.

5.2.1.1.1 Aspen Plus Simulation

Table 5.1 lists the products of the flash tank according to the Aspen Plus simulation. From Table 5.1 it can be seen that 99% of water is evaporated while more than 80% of sulfuric acid is recovered from the aqueous solution. Note that, the output is comparable to the literature (Lee et al., 2009) hence the design of flash tank model in the Aspen Plus environment is acceptable. The next step is to extract the data of Vapour-Liquid Equilibrium (VLE) from the Properties Data in Aspen Plus. For each component in a binary mixture, one can easily plot a VLE diagram.

Table 5.1: Sulfuric acid flash tank output from the Aspen Plus simulation.

Flow rate (mol/s)	**Current Work**	**Reference (Lee et al., 2009)**
Vapour		
Water, H_2O	11.18	10.69
Sulfuric Acid, H_2SO_4	0.45	0.83
Liquid		
Water, H_2O	0.12	0.61
Sulfuric Acid, H_2SO_4	1.81	1.43

From the simulation in Aspen Plus, the non-randomness parameter, α_{ij} and the dimensionless interaction parameter τ_{ij} are extracted and tabulated in Table 5.2. Once α_{ij} and τ_{ij} are determined, then the Equations (5.10) and (5.11) can be solved completely in MATLAB to obtain the activity coefficients required for simulation of the SA-FT unit.

Step SA-FT.1.4: Calculate the summation in Eqn. (5.5).

If the summation in equation (5.5) is unity, then the bubble point is determined, otherwise, go to Step SA-FT.1.1 and repeat the previous procedure until the specified error tolerant is achieved.

Step SA-FT.2 Find the steady state based on differential equations

The differential equation for the holdup liquid level is determined by the amount of feed, evaporation and liquid product flow rate:

$$\frac{dH_L}{dt} = \frac{1}{A\rho_L}\left(F_f - F_{eva} - F_L\right) \tag{5.12}$$

Where the H_L is the liquid level in the flash tank, ρ_L is the liquid density, A is the surface area of the flash tank, F_f is the feed flowrate to the flash tank, F_{eva} is the flowrate of the evaporated vapor at the upper part of flash tank and F_L is the liquid flowrate at the bottom of flash tank.

Table 5.2: NRTL parameters for Sulfuric Acid/ Water separation in SA-FT.

Parameters (subscript: 1- H_2O, 2- H_2SO_4)	**Value**
Non-randomness parameter, α_{12}	272.6
Non-randomness parameter, α_{21}	170.9
Dimensionless interaction parameter, τ_{12}	0.3
Dimensionless interaction parameter, τ_{21}	0.3

The mass balance, M_T of the flash tank is expressed as the sum of feed flow minus the exit flows.

$$\frac{dM_T}{dt} = F_f - F_L - F_V \tag{5.13}$$

The mass fraction of liquid phase, x_i for each component is expressed in the form of

$$\frac{dx_i}{dt} = \frac{1}{AH_L\rho_L}\left[F_f\left(z_i - x_i\right) - F_{eva}\left(y_i - x_i\right)\right] \tag{5.14}$$

Where z_i is the total fraction of liquid and vapor.

Meanwhile, the mass fraction in the vapour phase is expressed in terms of the liquid phase changes and the relative volatility written as follows

$$\frac{dy_i}{dt} = \frac{\gamma_i P_i^*}{P}\left(\frac{dx_i}{dt}\right) \tag{5.15}$$

The energy balance representing the temperature change, is calculated according to

$$\frac{dT}{dt} = \frac{MWt}{C_{pA}M_T}\left\{\begin{array}{l}\dfrac{F_f\left(C_{pf}T_f - C_{pA}T\right) - F_V\left[\left(C_{pV} - C_{pA}\right)T + \lambda\right] - F_L\left(C_{pL} - C_{pA}\right)T}{MWt} \\ \ldots + Q_s\end{array}\right\} \tag{5.16}$$

where MWt is the average molar mass, C_{pA} is the average heat capacity, C_{pf} is the feed heat capacity, T_f is the feed temperature, C_{pV} is the vapor heat capacity, C_{pL} is the liquid heat capacity, λ is the sensible heat, and Q_s is the amount of heat supplied to flash tank.

The evolution of pressure, P with time is described as a function of temperature changes

$$\frac{dP}{dt} = R\rho_v\left[T\frac{d\left(\sum_i^n \frac{y_i}{MW_i}\right)}{dt} + \left(\sum_i^n \frac{y_i}{MW_i}\right)\frac{dT}{dt}\right] \tag{5.17}$$

Here, we assume that the vapour density ρ_v is taken from the previous time step $t-1$. Its value is recalculated after each time step as follows

$$\rho_{v(t-1)} = \frac{P(t-1)}{RT(t-1)\left(\sum_i^n \frac{y_i(t-1)}{MW_i}\right)} \tag{5.18}$$

For the exit liquid flow rate, it is assumed that the flow rate is given by a square root of liquid height in the tank,

$$F_L = k_L\sqrt{H_L} \tag{5.19}$$

where k_L denotes the valve coefficient. Note that, the exit flow rate of vapour is assumed to be linearly proportional to the pressure in the flash tank, i.e.:

$$F_V = k_v P \tag{5.20}$$

where k_v denotes the coefficient of valve attached to the vapour line. Since $X_V + X_L = 1$, we can express the average specific heat capacity in terms of

$$C_{pA} = X_L C_{pL} + (1 - X_L) C_{pV} \tag{5.21}$$

Note that, F_{eva} denotes the rate of evaporation due to the excess heat Q_{ex} defined by

$$Q_{ex} = Q_S - \underbrace{F_f C_{pf} (T - T_f)}_{\substack{sensible \\ heat}} \tag{5.22}$$

Significantly, the excess heat represents a balance of heat from steam, which is not used to heat up the cold feed; a portion to heat up the feed is called sensible heat. So, the rate of evaporation is given by the excess heat is as follows

$$F_{eva} = \frac{Q_{ex} MW}{\lambda} \tag{5.23}$$

where Q_S and λ denote the heat supplied by steam and the latent heat of evaporation, respectively. The heat supply is

$$Q_S = U_t A_w (T_S - T) \tag{5.24}$$

Step SA-FT.3 Simulation in the Simulink

The developed first principal model in the previous steps is simulated in the MATLAB environment. For analysis, the output profiles; tank level, outlet liquid sulfuric acid fraction and outlet vapor sulfuric acid fraction, of the system are then plotted. Figure 5-2(a) shows the liquid level of the SA-FT unit. The output profiles are plotted based on a start-up simulation. The liquid level which is set at an initial value reaches a steady state value which shows that the dynamic model met the desired constraint level, hence preventing the occurrence of flooding in the flash tank.

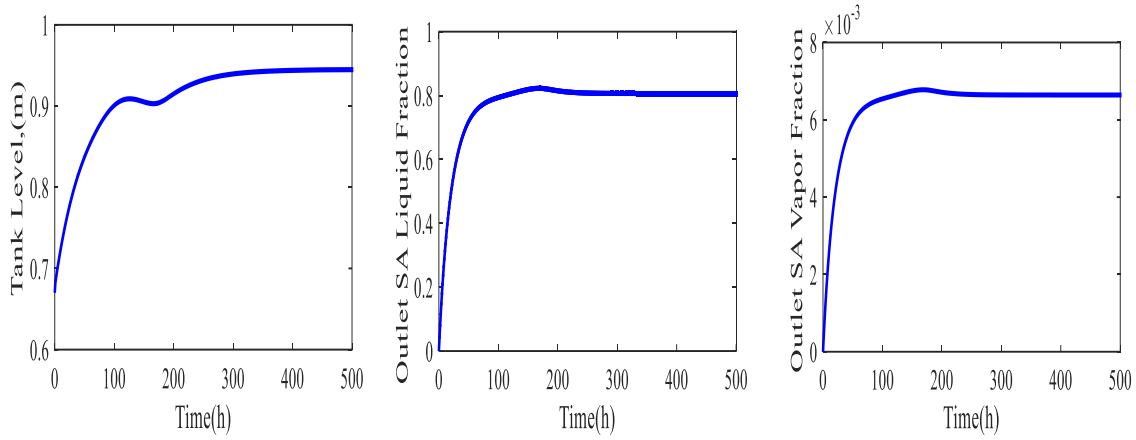

(a) (b) (c)

Figure 5-2: Output profiles, (a) Flash tank level, (b) Sulfuric acid liquid fraction (bottom outlet), (c) Sulfuric acid vapor fraction (upper outlet)

The desired output variables are presented in Table 5.3. Table 5.3 provided the output vapor and liquid fraction of the sulfuric acid as well as the pressure and temperature of the designed flash tank, in comparison to the experimental data from the literature (Lee et al., 2009). The output fraction profiles are also plotted and presented in Figure 5-2(b) and 5-2(c). As compared to the output data from the literature, the output sulfuric acid liquid fraction in this work is 15.7% higher where the amount of water effectively removed is 99% as compared to only 93% in the literature. While the outlet vapor fraction of the sulfuric acid is efficiently reduced to 85% as compared to the literature. Based on the result it is revealed that the developed flash tank model is reasonable and realistic for further simulation in the SITC plant.

Table 5.3: Flash tank dynamic modelling results vs. literature

Variables	**Current Work**	**Literature (Lee et al., 2009)**
Pressure	<10 bar	
Temperature	>100ºC	
L/D Ratio	3-5	NA
Bubble point (99% water evaporation)	a. 177 ºC (VLE diagram) b. 110-206 ºC (**Step SA-FT.1**)	NA
Feed Fraction (dimensionless)		
Water, H_2O	0.83	
Sulfuric Acid, H_2SO_4	0.17	
Outlet Vapor Fraction (dimensionless)		
Water, H_2O	0.99	0.93
Sulfuric Acid, H_2SO_4	0.01	0.07
Outlet Liquid Fraction (dimensionless)		
Water, H_2O	0.19	0.30
Sulfuric Acid, H_2SO_4	0.81	0.70

5.2.2 Sulfuric Acid Decomposition in SA-IBSD Reactor

Conventionally, Section II should consist of at least three major equipment; a flash tank, H_2SO_4 concentrator/ evaporator, and SO_3 decomposer. Usually, after the SA-FT unit the relatively flashed acid is first heated in a boiler unit, then followed by further heating in a superheater unit before finally decomposition in a catalytic fixed bed reactor unit. In this study, instead of using three separate units for the sulfuric acid evaporation, super heating and decomposition processes, an integrated boiler, superheater and decomposer (SA-IBSD) reactor is developed in this work. Please note that the required energy is obtained from an external high temperature reactor, e.g., nuclear reactor.

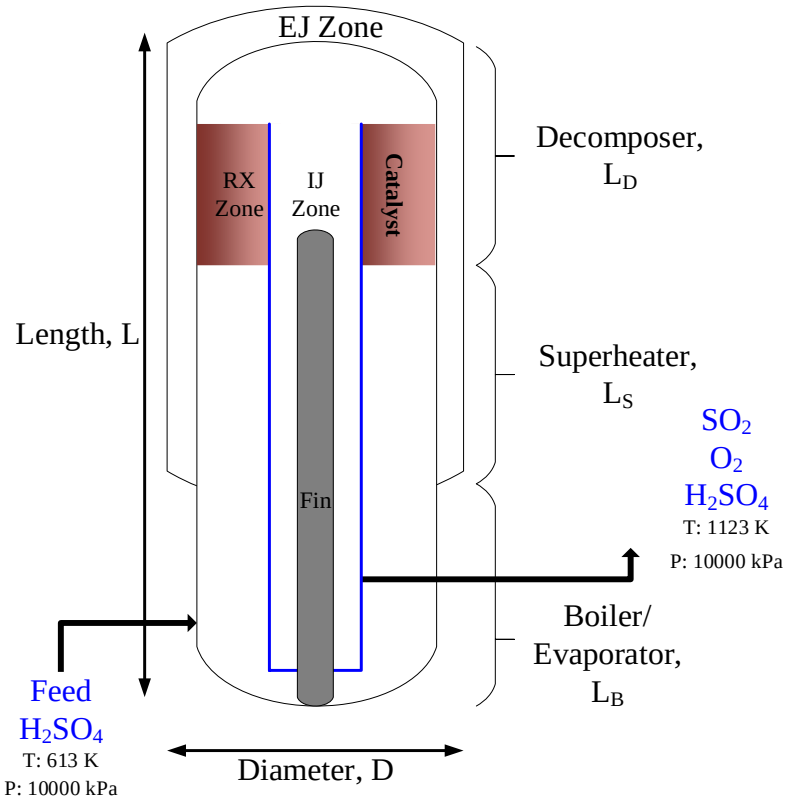

Figure 5-3: Schematic diagram of the modified SA-IBSD reactor (Moore et.al, 2011)

Bear in mind that, Section II involves the highest temperature in the SITC plant (up to 1000^{o}C). Such a high temperature operation poses a number of significant challenges that have led to several studies on the behaviour of the Section II, e.g., catalyst stability and overheating reactor (Rashkeev et al., 2009; Kim et al., 2013; Park et al., 2013; Noguchi et al., 2014).

The SA-IBSD apparatus was patented by Moore et.al, (2011). The reactor is constructed of ceramics and other corrosion resistant materials to decompose the H_2SO_4 into SO_2, O_2 and H_2O. The integrated reactor is designed with one part of it is packed with catalyst and the inner part with a fin to increase the recuperation efficiency of thermal energy. Figure 5-3 shows the schematic diagram of the modified version of a single cell SA-IBSD reactor. In a large scale operation, a number of cells are arranged in a single shell. The configuration resembles a shell and tube heat exchanger type reactor. Here, each tube is replaced with a reactor cell shown in Figure 5-3. In this study, a modification is made to enable scaling up of the SA-IBSD reactor, i.e., for an

industrial-scale production. The properties used in the patented SA-IBSD reactor (single cell) are described in Table 5.4.

Table 5.4: Parameters of the patented integrated reactor for sulfuric acid decomposition proposed by Moore et.al, 2011.

Parameter	**Value**
Length, L_T or H_T	4 ft. to 5ft, or 14 ft.
Ratio of length to diameter, L/D	10 to 100
Length of Decomposer, L_D	1/3 L_T
Length of Superheater, L_S	1/3 L_T
Length of Boiler, L_B	1/3 L_T
Sources of heat	Either nuclear, solar, electrical, and/or chemical combustion
Active catalyst	Either platinum, iron oxide, rhodium and metal oxides (chosen in this work is in form of pellets (Choi et al., 2014b))
Design material	Either ceramics, silicon carbide, silicon carbide alloys, alumina, quartz or glass
Operating pressure	Up to 100 bar or 10,000 kPa
Operating temperature	With Catalyst: 750 to 900 ^oC Without Catalyst: more than 1000 ^oC
Boiler temperature	340 ^oC
Superheater temperature	>700 ^oC
Decomposer temperature	700 to 900 ^oC or >1000 ^oC
Feed temperature, T_o	<100 ^oC
Feed H_2SO_4 concentration, C_{SAo}	20% to 100%
Maximum conversion of H_2SO_4	36%

In the proposed dynamic modelling, the SA-IBSD is divided into five zones which are:

a) Evaporator Zone

b) Superheater Zone

c) Decomposer Zone or Reaction (RX) Zone

d) Internal Jacket (IJ) Zone (acting as a central baffle to increase recuperation efficiency)

e) External Jacket (EJ) Zone

5.2.2.1 Model Assumptions

The assumptions made in the modelling and simulation of the SA-IBSD reactor are listed as follows; some are adopted from (Nagarajan et al., 2009):

A.5.2.1: The SA-IBSD is designed as a long catalytic packed bed reactor and considered having pseudo-homogenous reaction zone.

A.5.2.2: The mass of the catalyst is uniformly distributed throughout the packed bed (Reaction Zone) where the chemical reaction only occurs in the catalyst phase.

A.5.2.3: The flow is assumed to be in gas phase outside the catalyst pellets.

A.5.2.4: The pressure is assumed constant in all zones.

A.5.2.5: Well mixing in both IJ and EJ Zones, so the temperature is uniform in these two zones.

A.5.2.6: Well mixing in Evaporator, Superheater and Decomposer Zones.

5.2.2.2 Mass and Energy Balance

5.2.2.2.1 Evaporator Zone

This is the zone where the sulfuric acid from the Bunsen Section of the SITC plant enters the SA-IBSD reactor. In this zone, the sulfuric acid is first heated up to its boiling temperature before it is subsequently decomposed into SO_3 and H_2O as depicted in (5.25) - (5.26). The power law is used to represent the rate law. The reaction type follows reversible elementary second order kinetics:

$$H_2SO_4(l) \longrightarrow SO_3(g) + H_2O(g), \quad r_{af} = -k_{fa}C_a \tag{5.25}$$

$$SO_3(g) + H_2O(g) \longrightarrow H_2SO_4(l), \quad r_{ar} = k_{ra}C_a \tag{5.26}$$

where H_2SO_4, SO_3 and H_2O are denote as components a, b and c respectively.

The net rate of reaction is given by

$$r_a = r_{af} + r_{ar} \tag{5.27}$$

$$r_a = k_{fa}\left[C_a - \frac{C_b C_c}{K_{Eq}}\right] \tag{5.28}$$

$$K_{Eq} = \frac{C_b C_c}{C_a} \tag{5.29}$$

where r_a is the total reaction rate, r_{af} is the forward reaction rate, r_{ar} is the reverse reaction rate. K_{Eq} is the equilibrium constant, C_i is the concentration of component-i.

The general species mass balances considering input and output concentration (kmol/m^3.hr) is given by (5.30) - (5.32).

$$V_E \frac{dC_a}{dt} = \dot{M}_T\left(\frac{C_{a_i}}{\rho_{g_{Ei}}} - \frac{C_{a_o}}{\rho_{g_{Eo}}}\right) - r_a V_E \tag{5.30}$$

$$V_E \frac{dC_b}{dt} = \dot{M}_T \left(\frac{C_{b_i}}{\rho_{g_{Ei}}} - \frac{C_{b_o}}{\rho_{g_{Eo}}} \right) + r_a V_E \tag{5.31}$$

$$V_E \frac{dC_c}{dt} = \dot{M}_T \left(\frac{C_{c_i}}{\rho_{g_{Ei}}} - \frac{C_{c_o}}{\rho_{g_{Eo}}} \right) + r_a V_E \tag{5.32}$$

Meanwhile, the energy balances (kJ/hr) on the reactor and jacket sides are given as in (5.33) and (5.34) respectively.

$$\frac{V_E \rho_{g_{Eo}} C_{p_E}}{\overline{MW}} \frac{dT_E}{dt} = \dot{M}_T C_a \left(\frac{H_i}{\rho_{g_{Ei}}} - \frac{H_o}{\rho_{g_{Eo}}} \right) + r_a \Delta H_1 V_E + Q_{IJ} \tag{5.33}$$

$$\frac{V_{IJ} \rho_{IJout} C_{p_{IJ}}}{\overline{MW}} \frac{dT_{IJ}}{dt} = \dot{M}_{IJ} C_{IJ} \left(\frac{H_i}{\rho_{IJinE}} - \frac{H_o}{\rho_{IJoutE}} \right) - Q_{IJ} - Q_{Dfin} \tag{5.34}$$

where

$$Q_{IJ} = A_{r_D} U_{r_D} \left(T_{IJ} - T_E \right) \tag{5.35}$$

Notations: V_E is the volume of Evaporator Zone, $\dot{M}_T$ is the total feed flowrate, ρ_{gEi} is the density of the inlet mixture, ρ_{gEo} is the density of the outlet mixture, ΔH_1 is the reaction enthalpy, Q_{IJ} is the heat transfer from IJ Zone, Q_{Dfin} is the heat transfer from fin, A_{rD} is the heat transfer cros section area, U_{rD} is the iverall heat transfer coefficient, T_{IJ} is the temperature of the IJ zone, T_E is the temperature of the Evaporator Zone and $\overline{MW}$ is the average molecular weight. The subscript i and o denote the input and output respectively.

Table 5.5 shows the parameters and constants used in the simulation for the Evaporator Zone.

Table 5.5: Values of model parameters used in the simulation of the Evaporator Zone

Evaporator - Parameters or Constants	**Value**	**References**
Volume of evaporation section, V_E	$H_E \times A_E\ m^3$	
Heat capacity of feed mixture, CpE	$159\ kJ/kmol.K$	ASPEN PLUS Simulation
Height of evaporation section, H_E	$\frac{1}{3}H_T$	(Moore et al., 2011)
Average Molecular weight, MW	$51\ kg/kmol$	ASPEN PLUS Simulation
Diameter of tank, D_E	$0.57\ m$	
Total height of SA-IBSD, H_T	$4\ m$	
Area of tank, A_E	$0.25\pi DE2\ m^2$	
Wall area for heat transfer, A_{rE}	$0.13\ A_E$	
Arrhenius Constant, ARH_E	$3.275e^3$	(Choi et al., 2014b)
Activation energy, E_{aE}	$62.798\ kJ/mol$	(Choi et al., 2014b)
Enthalpy, H_{RE}	$5882\ kJ/mol$	ASPEN PLUS Simulation

5.2.2.2.2 Superheater zone

In the superheater region, the vapour is superheated to more than 700℃ before is subsequently sent to the third region, i.e., the decomposer zone. The energy balances for the superheater are given as follows:

$$\frac{P_T V_{EJ}}{RT_{EJ}}\frac{dT_{EJ}}{dt} = \frac{C_{p_{EJ}}\left(F_{EJ_i}T_{EJ_i} - F_{EJ_o}T_{EJ_o} - q_{hot}\right)}{C_{v_{EJ}}} - \left(F_{EJ_i} - F_{EJ_o}\right)T_{EJ} \tag{5.36}$$

$$\frac{P_T V_S}{RT_S}\frac{dT_S}{dt} = \frac{C_{p_S}\left(F_{S_i}T_{S_i} - F_{S_o}T_{S_o} + q_{cool}\right)}{C_{vs}} - \left(F_{S_i} - F_{S_o}\right)T_S \tag{5.37}$$

$$\frac{\rho_w C_{p_w} V_S}{A_S} \frac{dT_w}{dt} = h_{hot} \Delta T_{w_{hot}} - h_{cool} \Delta T_{w_{cool}} \tag{5.38}$$

where,

$$q_{hot} = \frac{h_{hot} A_{EJ}}{MW_{EJ}} \Delta T_{EJ} \tag{5.39}$$

$$q_{cool} = \frac{h_{cool} A_S}{MW_S} \Delta T_S \tag{5.40}$$

where C_{PEJ} is the heat capacity of the EJ Zone, P_T is the total pressure of the reactor, T_{EJ} is the EJ Zone temperature, V_{EJ} is the volume of EJ Zone, F_{EJ} is the flowrate in the EJ Zone, V_S is the volume of Superheater Zone, T_S is the temperature of Superheater Zone, C_{PS} is the heat capacity of the mixture in Superheater Zone, T_w is the wall temperature, q_{cool} is the heat transfer from Superheater Zone to EJ Zone, q_{hot} is the heat transfer from EJ Zone to Superheater Zone, A_{EJ} is the heat transfer area of EJ Zone, A_S is the heat transfer area of Superheater Zone, MW_{EJ} is the molar mass of EJ Zone, MW_S is the molar mass of Superheater Zone, ΔT_S and ΔT_{EJ} are the log mean temperature different.

Table 5.6: Values of parameters used in the simulation of the Superheater Zone

Parameters or Constants	**Value**
Feed molar flowrate of mixture, F_{2o}	$(\dot{M}_T)/MW2o$
Molar flowrate of mixture, F_2	$(\dot{M}_T)/MW2$
Feed molar flowrate of EJ, F_{EJo}	$(\dot{M_{TEJo}})/MW_{EJo}$
Molar flowrate of EJ, F_{EJ}	$(\dot{M_{TEJ}})/MW_{EJ}$
Density at the wall, ρ_w	$(MW_2/Tw)(P/R)\ kg/hr$
Molar heat capacity of feed mixture, Cp_2	$3.7\ kJ/kg.K$
Molar heat capacity of feed mixture, Cp_{EJ}	$2.47\ kJ/kg.K$
Gas molar heat capacity of feed mixture, Cv_2	$Cp_2 - (R/MW2)$
Steam molar heat capacity of feed mixture, Cv_{EJ}	$Cp_{EJ} - (R/MWEJ)$
Hot side heat transfer coefficient, h_{hot}	$1200\ kJ/hr.m^2.K$
Cool side heat transfer coefficient, h_{cool}	$1200\ kJ/hr.m^2.K$

5.2.2.2.3 Decomposer Zone

The decomposition zone is the upper part of the SA-IBSD reactor which is packed with catalyst pellets. In this zone, the sulfur trioxide is decomposed catalytically into SO_2 and O_2 molecules. This region required the highest temperature in the whole reactor.

For simplicity the power law is used to derive the rate law of the decomposition reaction. Here, it is considered that the reaction type follows a reversible elementary first order kinetics as proposed by Choi et al., (2014b).

$$SO_3(g) \rightleftharpoons SO_2(g) + \frac{1}{2}O_2(g) \tag{5.41}$$

The net chemical rate law is as follows. Notation b, d and e denote SO_3, SO_2 and O_2 components respectively:

$$r_b = -r_d = -2r_e \tag{5.42}$$

$$r_b = k_{AD} A_{catD} P_1 \tag{5.43}$$

where by using Dalton's Law, the partial pressure is given by

$$P_1 = P_T \frac{n_1}{n_T} \tag{5.44}$$

Here A_{catD} is the surface area of catalyst is, $n_1$is the mol of species 1 and n_T is the total moles of all species.

The species mass balances considering the input and output concentrations (kmol/m^3.hr) are given by the following equations.

$$V_D \frac{dC_b}{dt} = \dot{M}\left(\frac{C_{b_i}}{\rho_{g_{Di}}} - \frac{C_{b_o}}{\rho_{g_{Do}}}\right) - r_b W_{cat} \tag{5.45}$$

$$V_D \frac{dC_d}{dt} = \dot{M}\left(\frac{C_{d_i}}{\rho_{g_{Di}}} - \frac{C_{d_o}}{\rho_{g_{Do}}}\right) + r_b W_{cat} \tag{5.46}$$

$$V_D \frac{dC_e}{dt} = \dot{M}\left(\frac{C_{e_i}}{\rho_{g_{Di}}} - \frac{C_{e_o}}{\rho_{g_{Do}}}\right) + 0.5 r_b W_{cat} \tag{5.47}$$

where the volume of gas and total volume are

$$V_D = \varepsilon V_{RX} \tag{5.48}$$

$$V_{TD} = n V_{RX} \tag{5.49}$$

Notations: C is concentration, $\dot{M}$ is the mass flowrate to the Decomposer Zone, ρ_{gD} is the density of Decomposer Zone mixture, W_{cat} is the weight of catalyst, ε is the voidage factor, and V_{RX} is the volume of the reaction zone.

The volumetric flowrate v, m^3/hr is given by

$$v = \frac{\dot{M}}{\rho} \tag{5.50}$$

Meanwhile, the average density, $\bar{\rho}$ is derived from the ideal gas equation:

$$P_T V_D = n_T R T_D \tag{5.51}$$

$$n_T = \frac{\dot{M}}{\overline{MW}} \tag{5.52}$$

$$P_T V_D = \frac{\dot{M}}{\overline{MW}} R T_D \tag{5.53}$$

$$\frac{\dot{M}}{V_D} = \rho = \left(\frac{\overline{MW}}{T_D}\right)\left(\frac{P_T}{R}\right) \tag{5.54}$$

Note that, the average molecular weight, $\overline{MW}$ is calculated as follows:

$$y_i = \frac{n_i}{\Sigma_{i=1}^{3} n_i} \tag{5.55}$$

$$\overline{MW} = \left(\frac{1}{\Sigma_{i=1}^{3} c_i}\right)\left(\Sigma_{i=1}^{3}\ C_i MW_i\right) \tag{5.56}$$

Finally, the energy balances (kJ/hr) are given as follows

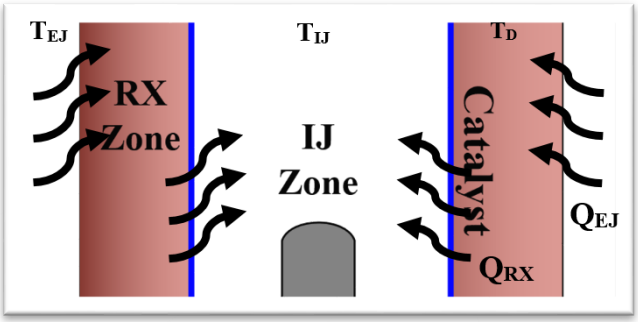

Figure 5-4: Zoom in diagram for the reaction zone in the SA-IBSD reactor cell.

Figure 5-4 displays the zoom in diagram of the Reaction (RX) Zone; the heat flows from the EJ Zone into the RX Zone, which subsequently flows into IJ Zone. In term of the defined variables, the energy balances involved can be written as follows.

For the energy balance in the reaction zone (catalyst region), the differential equation is expressed as

$$\frac{\varepsilon V_D \rho_{gD_o} C_{p_o}}{\overline{M}\overline{W}} \frac{dT_D}{dt} = \dot{M}_T \left(\frac{C_{p_i} T_{D_i} C_b}{\rho_{gD_i}} - \frac{C_{p_o} T_D C_b}{\rho_{gD_o}} \right) - r_b W_{cat} \Delta H_D + Q_{EJ} - Q_D \tag{5.57}$$

For the internal jacket zone, i.e., IJ Zone:

$$\frac{\varepsilon V_{IJ} \rho_{IJo} C_{pIJ}}{\overline{M}\overline{W}} \frac{dT_{IJ}}{dt} = \dot{M}_{IJ} C_b \left(\frac{C_{p_i} T_{IJ_i}}{\rho_{IJ_i}} - \frac{C_{p_o} T_{IJ_o}}{\rho_{IJo}} \right) + Q_D - Q_{Dfin} \tag{5.58}$$

where

$$\dot{M}_{IJ} = \rho_{IJ} V_{IJ} \tag{5.59}$$

$$Q_{Dfin} = M \frac{\sinh mL + \left(\frac{h}{mk} \right) \cosh mL}{\cosh mL + \left(\frac{h}{mk} \right) \sinh mL} \tag{5.60}$$

The parameters M and m are calculated using the following equations

$$M = \sqrt{h P_f k A_c T_D} \tag{5.61}$$

$$m = \sqrt{\frac{h P_f}{k A_c}} \tag{5.62}$$

where h and k, are the heat transfer coefficients, P_f is the perimeter of the fin cross-section, and A_c is the cross section area of fin.

For the external jacket zone, i.e., EJ zone:

$$\frac{V_{EJ} \rho_{EJo} C_{pEJ}}{\overline{M}\overline{W}_{EJ}} \frac{dT_{EJ}}{dt} = \dot{M}_{EJ} C_b \left(\frac{C_{pS} T_{EJ_i}}{\rho_{EJ_i}} - \frac{C_{pS} T_{EJ_o}}{\rho_{EJo}} \right) - Q_{EJ} \tag{5.63}$$

where

$$Q_{EJ} = A_{EJ} U_{EJ} (T_{EJ} - T_D) \tag{5.64}$$

$$\dot{M}_{EJ} = \rho_{EJ} V_{EJ} \tag{5.65}$$

Table 5.7: Values of parameters used in the simulation of the decomposition zone

Parameters or Constants	**Value**	**Reference**
Feed volumetric flowrate, v_D	0.025 m^3/hr	Aspen Plus Simulation
Gas constant, R	8.314×10^{-3} m^3.kPa/K.mol	
Molar heat capacity of feed mixture, Cp_D	93 kJ/kmol.K	Aspen Plus Simulation
Height of decomposition section, H_D	$\frac{1}{3} H_T$	Aspen Plus Simulation + Flash Tank Design and Rules
Diameter of tank, D_D	0.57 m	(Moore et al., 2011)
Area of tank, A_D	$0.25\pi D_D^2$ m^2	(Moore et al., 2011)
Overall heat transfer coefficient, U_{rD}	1.8×10^7 kJ/hr.m^2.K	
Arrhenius Constant, ARH_D	4.54×10^9 m^3/m.hr	(Kim et al., 2013)
Activation energy, E_{aD}	141400 kJ/kmol	(Kim et al., 2013)
Enthalpy, H_{rD}	273760 kJ/kmol	Aspen Plus Simulation
Bed porosity, ε_{bed}	0.8	(Str??hle et al., 2014)
Area of a catalyst, Fe_2O_3, A_{catD}	1.17 m^2/g	(Kim et al., 2013)
Diameter of a catalyst pellet, D_{cat}	0.006 m	(Kim et al., 2013)
Bulk density of catalyst, ρ_{bulk_cat}	2320 kg/m^3	(Kim et al., 2013)
Mass of Catalyst, Fe_2O_3, Wcat	2800 g	(Kim et al., 2013)

5.2.2.3 Validation of the SA-IBSD Reactor Model

Note that, the model of the SA-IBSD reactor developed previously is based on a single cell. The model is validated using available literature data (Moore et al., 2011). Figure 5-5 shows the result of the model validation. As can be seen in Figure 5-5, the temperature profiles given by the simulation and literature are comparable. Comparison between the simulated and experimental data yields a small value of Mean Squared Error (MSE) of 0.25, which demonstrates that the developed model is reliable to be used for further research, e.g. for optimization and control purposes.

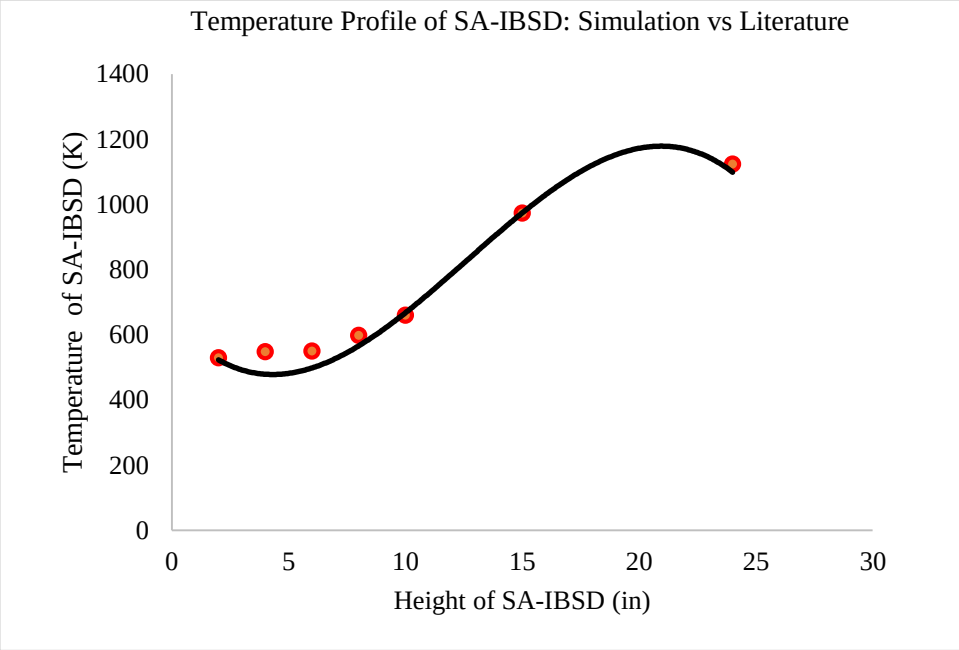

Figure 5-5: Validation plot of temperature profile of SA-IBSD reactor: Simulation (solid line) vs. Literature (Moore et.al, 2011) (dotted)

5.2.2.4 SA-IBSD Scale-up Procedure

The scaling-up process for the SA-IBSD reactor is carried out based on the objective to achieve more than 1000 kg/hr of H_2 production. Figure 5-6 depicted the idea of SA-IBSD reactor scaling up process. Given the product flow rate from the Bunsen Section, the size of Section II equipment is adjusted accordingly.

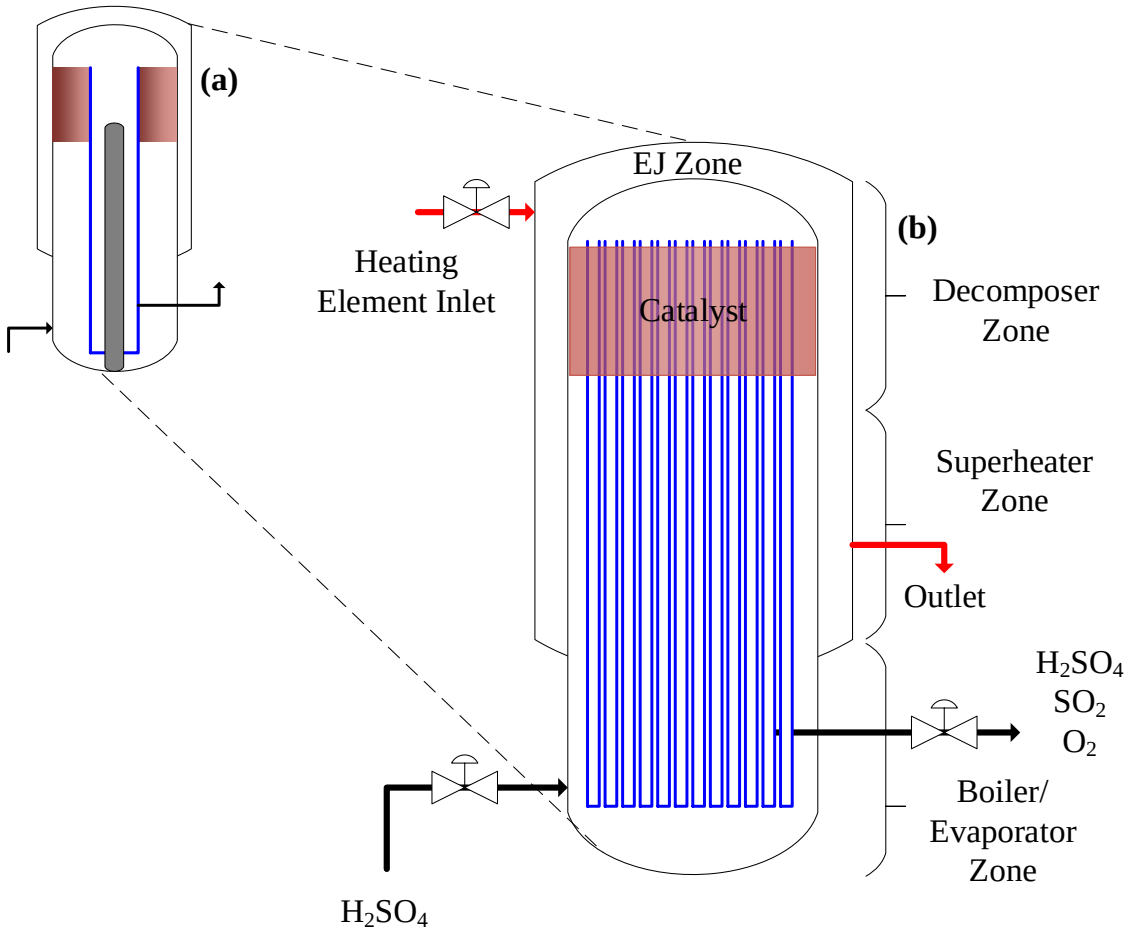

Figure 5-6: Scaling-up illustrative diagram for SA-IBSD reactor: a) the laboratory scale SA-IBSD reactor cell, b) the plant scale multi-cell SAIBSD reactor.

The hydrogen production amount shall be accomplished by setting the feed flow rate and operating conditions accordingly. Once the estimated feedstock amount to achieve the target production rate is calculated, the dimension of the reactor including the area and height are optimized based on the desired feed and production rates. The kinetic parameters used for both laboratory scale and plant scale are kept the same, except for the amount of catalysts. The height is scaled based on the L/D ratio proposed by Moore, et.al (2011). The total cross section area is calculated based on the area of the total tubes in the SA-IBSD reactor. The number of tubes is calculated based on trial-and-error simulation. The chosen number of tubes is the one that can produce the desired minimum production rate. The catalyst weight is scale based on the total catalyst of 150

tubes or cells in the SA-IBSD. The calculation of catalyst weight is done using the following equations

$$V_{tube} = L_{tube}\left(\frac{D_{tube}^2}{4}\right)\pi \tag{5.66}$$

$$W_{catT} = N_{tube}V_{tube}\rho_{bed} \tag{5.67}$$

$$\rho_{bed} = \varepsilon\rho_{cat} \tag{5.68}$$

where V_{tube} is the volume of tube (SA-IBSD Decomposition Zone), m^3, L_{tube} is the tube length, m, D_{tube} is the tube diameter, W_{catT} is the total catalyst weight, kg, ρ_{bed} is the density of catalyst bed, kg/m^3, and ρ_{cat} is the density of catalyst, kg/m^3. Table 5.8 listed the parameters of SA-IBSD reactor both for the laboratory scale and plant scale units.

Table 5.8: SA-IBSD reactor laboratory scale and plant scale parameters

SA-IBSD reactor Parameters	**Laboratory Scale**	**Plant Scale**
Number of tube or cell	1	150
External Jacket diameter, D_{EJ}	0.0397 m	2.07 m
Tube diameter, D_D	0.0381 m	0.0381 m
Total reaction cross section area, A_{rx}	$1.14e^{-3}$ m^2	0.17 m^2
Maximum height, H_T	4 m	20.7 m
Feed flow rate of sulphuric acid	$8.04e^{-4}$ $\frac{m^3}{hr}$	1400 $\frac{kg}{hr}$
Total mass of catalyst, Fe_2O_3, W_{catT}	2.8 kg	$\pm$1857 kg
Overall sulfuric acid conversion	0.39	0.41
External jacket temperature, T_{EJ}	1203 K	1203 K
Reactor temperature, T	1123 K	1073 K
Reactor pressure, P	1000 kPa	10000 kPa

5.3 Loop Gain Controllability Analysis of SA-IBSD Reactor

Based on the sensitivity study, there are three significant inputs and two significant outputs in the SA-IBSD reactor. The LGC is used as a tool to find the favorable dynamic controllability property for TITO model of SA-IBSD reactor. Prior to LGC analysis, the SA-IBSD simulation is carried out in MATLAB Simulink. Ode15s solver is chosen since the SA-IBSD reactor dynamics exhibit that of a stiff ODE system. A few SA-IBSD transfer function models (linearized) are presented in Table 5.9. The pairings are shortlisted based on a sensitivity study analysis. The best model is indicating by the highest LGC value as well as RGA index which in this case is Model 1 as presented in Table 5.10. The controller setting for SA-IBSD is then designed based on the Model 1. The question is, what is the suitable controller to design for SA-IBSD reactor? To answer this question, on may refer to the LGC index where in this case LGC index less than 1. This value indicating the model is hardly controllable by a conventional PID-based controller.

Table 5.9: SA-IBSD transfer function models and its input-output pairing

No	SA-IBSD reactor Model	Input-Output pairing
1	$Model\ 1$ $= \begin{bmatrix} \frac{0.002e^{-5.18\times10^{-5}s}}{1.002s+1} & \frac{-0.3572e^{-5.18\times10^{-5}s}}{0.6159s+1} \\ \frac{0.001e^{-3.27\times10^{-5}s}}{6.71e^{-5}s+1} & \frac{-0.2694e^{-3.27\times10^{-5}s}}{0.8506s+1} \end{bmatrix}$	Feed Flowrate (MV1) Feed Jacket Temperature (MV2) Product Flowrate (CV1) Reactor Temperature (CV2)
2	$Model\ 2$ $= \begin{bmatrix} \frac{0.0018e^{-5.18\times10^{-5}s}}{s+1} & \frac{-0.442e^{-5.18\times10^{-5}s}}{1.328s+1} \\ \frac{0.001e^{-3.27\times10^{-5}s}}{s+1} & \frac{-0.55e^{-3.27\times10^{-5}s}}{s+1} \end{bmatrix}$	Feed Flowrate (MV1) Feed Temperature (MV2) Product Flowrate (CV1) Reactor Temperature (CV2)

Table 5.10: Controllability analysis for SA-IBSD reactor

Model SAIBSD	**Sensitivity Study Analysis**		θ_{eotf}	**LGC**	**RGA**
	Significant Input	Significant Output			
Model 1	Feed Flowrate (MV1)	Product Flowrate (CV1)	5.18e-5	0.3684	$\begin{bmatrix} 2.3253 & -1.3253 \\ -1.3253 & 2.3253 \end{bmatrix}$
		Reactor Temperature			
	Feed External Jacket Flowrate (MV2)	Product Flowrate			
		Reactor Temperature (CV2)			
	Feed temperature	Product Flowrate			
		Reactor Temperature			
Model 2	Feed Flowrate (MV1)	Product Flowrate (CV1)	5.18e-5	0.3643	$\begin{bmatrix} 47.82 & -46.82 \\ -46.82 & 47.82 \end{bmatrix}$
		Reactor Temperature			
	Feed External Jacket Flowrate	Product Flowrate			
		Reactor Temperature			
	Feed temperature (MV2)	Product Flowrate			
		Reactor Temperature (CV2)			

5.4 Process Controller Design of SA-IBSD Reactor

The control objectives of the SA-IBSD reactor are:

a) To achieve a desired production flowrate.
b) To keep the temperature as minimum as possible without violating the constraints (minimum temperature limit of the SA-IBSD reactor at 1073 K).

A SISO controller will be developed for the SA-IBSD reactor. The SISO type controller is chosen because it is shown by the sensitivity study (see Chapter 7) that the jacket feed flow rate has a direct impact on both oxygen production rate and the reactor temperature. Hence, by controlling one CV; reactor temperature is sufficient which can indirectly affect the other CV. For the SA-IBSD, a PID-based controller is designed which of an MSC-PID type, i.e., PID designed using multi-scale control (MSC) scheme. The chosen MV is the external jacket flow rate and the CV is the reactor temperature. Table 11 listed the nominal values and the constraints of the output variables.

Table 5.11: Nominal values and the constraints of the SA-IBSD reactor output variables.

Variables	**Nominal value**	**Constraints**
Reactor temperature, $T_{SA-IBSD}$ (K)	1123	Min: 1073 , Max: 1140
Oxygen flowrate, m_{O2} (kg/hr)	450	Min: 350

The details of the multi-scale control scheme can be found in (Nandong and Zang, 2013a). The basic idea of the multi-scale control scheme is to decompose a given plant into a sum of basic factors with distinct speeds of responses – multi-scale modes. A set of sub-controllers is designed based on the basic modes, which are then combined in such a way to enhance cooperation among these different modes.

The MSC-PID control is designed using the multi-scale control scheme: the inner-loop is based on a P-only controller and outer-loop based on a PI controller. The MSC-PID controllers are given as follows.

$$G_{MSC} = -18.561\left(\frac{1+1.33s}{0.1137\,s}\right)\left(\frac{-18.561s - 21.82}{s + 7.054}\right) \tag{5.69}$$

The MSC-PID controller is compared with an IMC-PID controller. The IMC-PID controller setting is given as follows

$$G_{IMC} = -4.85e^{10}\left(\frac{(1+2.7e^{-6}s)(1+1.5e3)}{s}\right) \tag{5.70}$$

5.5 Controller Performance of SA-IBSD Reactor

The setpoint tracking is carried out via a setpoint change test. The reactor temperature (CV1) is changed from the nominal steady state value, 1073 K to 1083 K at 200th hour, 1083 K to 1063 K at the 400th hour and then set back to the steady state value for the rest of hours. Figures 5-7 and 5-8 demonstrate that the MSC-PID is able to drive the temperature output to its desired setpoint with a fast response and little delay. On the other hand, the IMC-PID controller is not even able to track the given setpoint changes. Figure 5-9 shows that the MSC-PID does not violate the MV constraints.

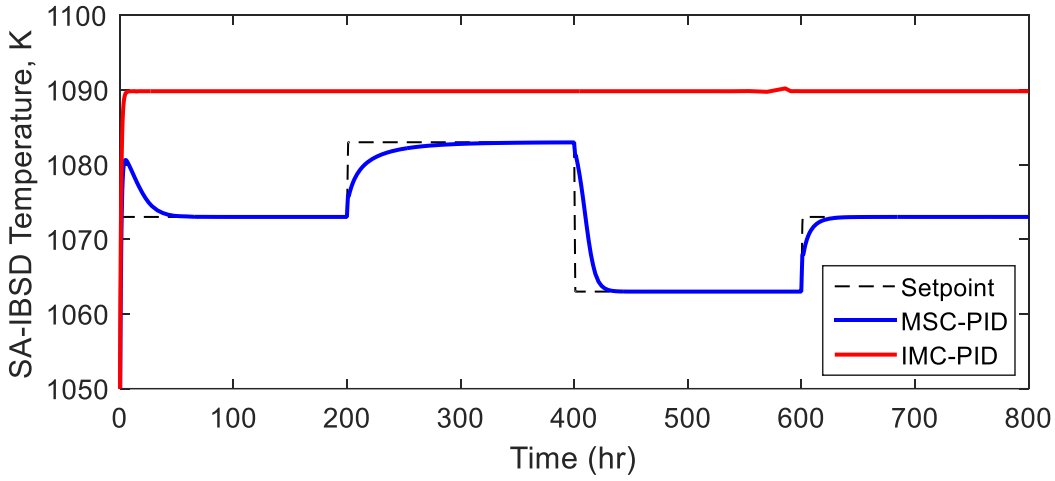

Figure 5-7: Response of MSC-PID and IMC-PID for setpoint changes in CV1, temperature of SA-IBSD reactor.

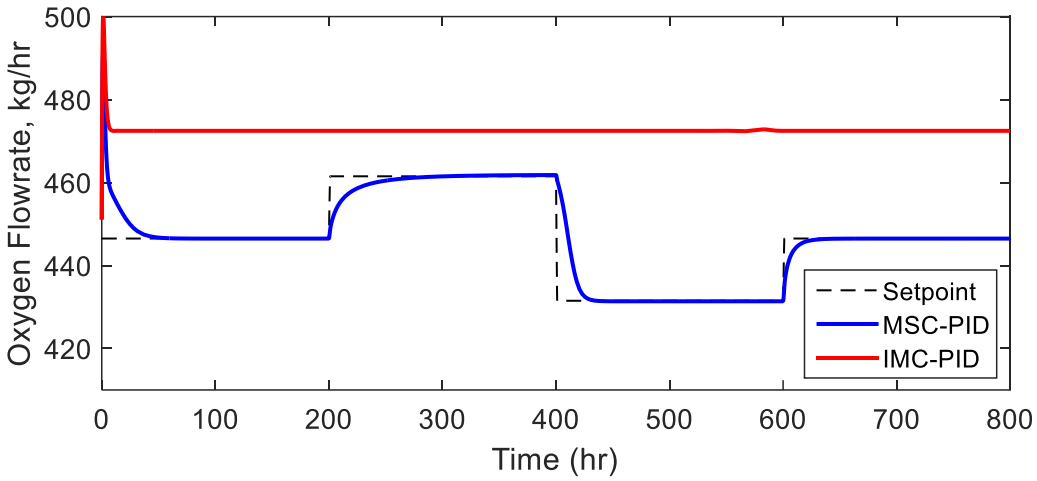

Figure 5-8: Response of MSC-PID and IMC-PID for setpoint changes in CV2, product flowrate of SA-IBSD reactor.

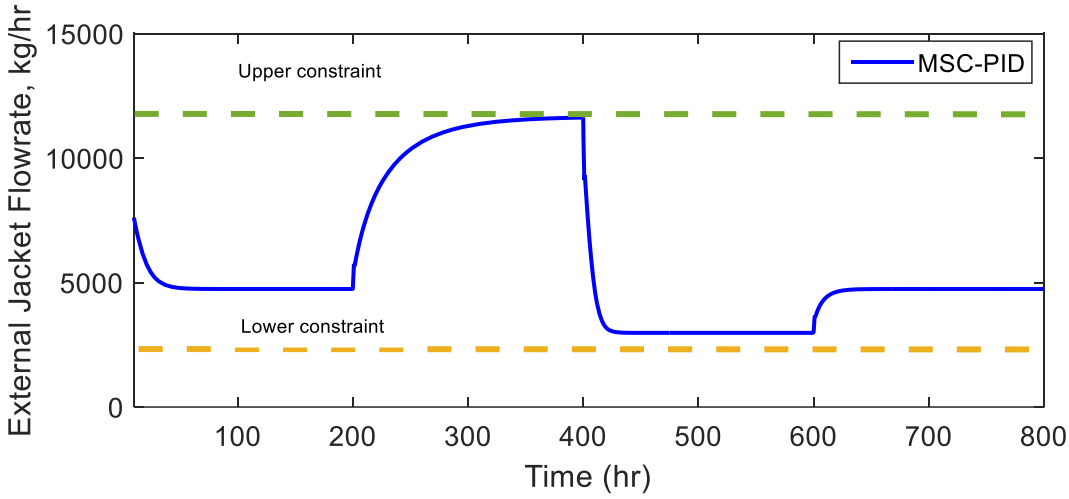

Figure 5-9: Response of MSC-PID and IMC-PID for setpoint changes in MV2, external jacket flowrate of SA-IBSD reactor.

A disturbance is introduced at 100th hour. The feed temperature from the upstream flow of SA-FT is disturbed by ±5^{o}C for 1 hour and the disturbance rejection times of both CVs by one controller are observed. Figure 5-10 shows that with the MSC-PID controller, the disturbance on the reactor temperature is successfully rejected after about 20 hours.

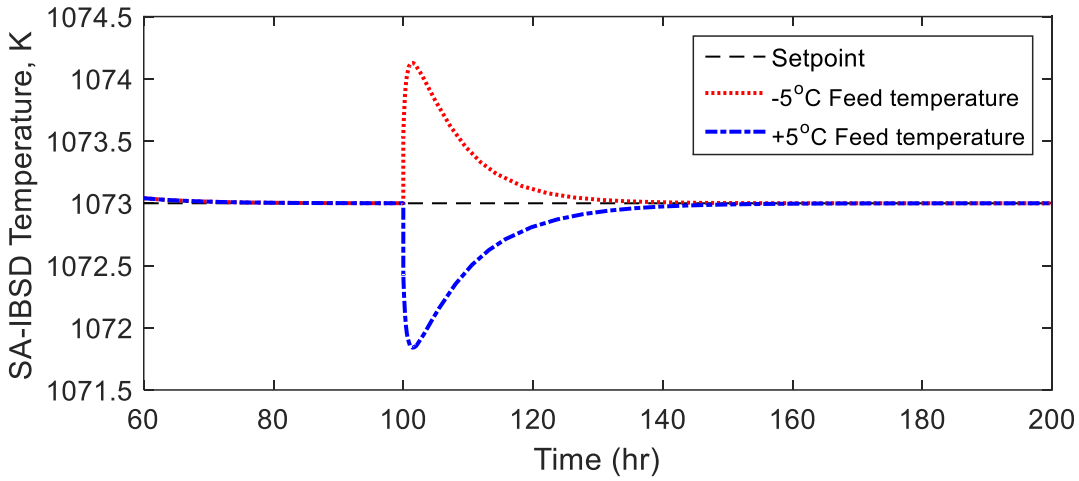

Figure 5-10: Response of MSC-PID for disturbance rejection test for SA-IBSD temperature, CV1.

MSC-PID is developed based on a careful selection and derivation of fast and slow mode of the transfer function model. Hence MSC-PID is able to capture the behaviour of the process better than the conventional PID.

5.6 Summary

Dynamic modelling and design of the SA-FT and SA-IBSD reactor units in the Section II of the SITC plant have been presented in this chapter. The summary is as follows,

a) To meet the minimum cost design criteria, the flash tank is successfully designed using the developed fundamental model with a length over diameter (L/D) ratio within the recommended range, i.e., between 3 and 5.
b) Data on the kinetic and physical-chemical properties for the model development have been obtained from Aspen Plus package and some literature reports.
c) Based on the dynamic simulation, the output liquid fraction of sulfuric acid obtained was 15.7% higher than the value reported in literature. Overall, the comparisons between the simulation and experimental data showed that the proposed model can satisfactorily predict the separation characteristics of the system under the designed temperature and pressure. The results demonstrated that the selected NRTL model and PR thermodynamic data are appropriate for

the sulfuric acid/water separation simulation. The accuracy of the model was confirmed via a careful comparison between the simulation results and experimental data collected from the open literature. Significantly, this flash tank model can be used for the flash tank design, optimization and control studies in the other chemical plant.

d) A Sulfuric Acid Integrated Boiler Superheater and Decomposer (SA-IBSD) reactor has been designed based on a patented reactor design, and the model has been successfully validated.

e) The simulated dynamic model exhibited stable outputs of oxygen flowrate and reactor temperature. The SA-IBSD was then scaled-up to a plant-scale size consisting of 150 tubes, with an overall conversion of 41%.

f) The LGC analysis has been carried out for the selected input-output pairings of SA-IBSD reactor. Model 1 of SA-IBSD reactor was chosen to represent the SA-IBSD reactor temperature and was then used for the PID controller design via the multi scale control scheme (i.e., MSC-PID). Unlike the internal model control (IMC-PID) controller, the MSC-PID controller can successfully drive the SA-IBSD reactor temperature to its desired setpoints in addition to showing good performance on the disturbance rejection tests.

6 Hydrogen Iodide Section: Dynamic Modelling and Controllability Analysis

This chapter covers the fundamentals of Hydrogen Iodide Section including process controller performance evaluation. Prior to plant scale-up, a preliminary simulation of a laboratory scale Hydrogen Iodide Decomposition (HI-DE) was carried out. The controllability analysis for the reactor was carried out using the LGC method, and the most controllable model (or pairings and operating conditions) was selected. The dynamic modelling of a flash tank for hydrogen iodide vaporization was also presented. Suitable process controllers were designed for the HI-DE reactor and their performance were evaluated. At the end of this chapter, a summary on the Hydrogen Iodide Section is highlighted.

6.1 Fundamental of Hydrogen Iodide Section

In this section there are two main processes involved: hydrogen iodide concentration and decomposition processes. Two units used in these processes are a flash tank to concentrate the hydrogen iodide (i.e., HI-FT unit) and a decomposition reactor to decompose the concentrated hydrogen iodide into hydrogen and iodine. Based on the literature (Chapter 2), the tubular reactor is the best type of reactor to decompose hydrogen iodide into hydrogen and iodine. To maximize the production of hydrogen a Hydrogen Iodide Decomposer (HI-DE) reactor is designed.

The hydroiodic acid solution coming from the Bunsen Section will first enter the HI-FT unit. Hydrogen iodide is vaporized while water including the unreacted iodine is sent out as the bottom output of the flash tank. The vaporized hydrogen iodide is then fed to the HI-DE reactor. In the HI-DE reactor, the hydrogen iodide is decomposed into iodine and hydrogen over catalyst; HI-DE reactor is of multi-tubular configuration where catalyst pellets are packed inside the tubes. The iodine is recycled back to Section I of the SITC plant whereas the product hydrogen is sent to a storage tank.

6.1.1 Reaction Mechanisms

The overall chemical reaction of Hydrogen Iodide Section is given as follows,

$$2HI(l) + 4I_2(l) + 6H_2O(l) \rightleftharpoons H_2(g) + 5I_2(l) + 6H_2O(l) \quad (6.1)$$

The reaction is an endothermic reversible reaction. Suitable decomposition temperatures range from 350 to 550 ^{o}C. Note that this section often demonstrates complex nonlinear behaviour because the HIx $(HI - I_2 - H_2O)$ system includes multiple liquid phases, with the possibility of forming azeotropes and solid precipitation. The binary $HI - H_2O$ mixture is known to be a strongly non-ideal solution which partially immiscible with other phases in the system, and for these reasons are very difficult to model and predict their thermodynamic behaviour. By introducing the optimum feed molar ratio (between 0.333 and 0.538) to the Bunsen reactor in the Section I, the presence of an azeotrope in the binary $HI - H_2O$ can be eliminated as well as avoiding the occurrence of solid precipitation (Lee et al., 2008b). Therefore, a binary separation via a flash tank is sufficient for this section. The design of this flash tank is described in the next section.

6.2 Hydrogen Iodide Flash Tank (HI-FT)

The section presents the design of a flash tank for the vaporization of hydrogen iodide from hydroiodic acid solution. Figure 6-1 shows the schematic diagram of the hydrogen iodide flash tank (HI-FT) unit. The methodology adopted in the dynamic modelling of HI-FT unit is similar to the one used in the dynamic modelling of SA-FT unit (in Chapter 5). Note that, the activity coefficients and non-randomness parameters of the hydrogen iodide solution are different due to the different characteristic of chemical species involved. Since the information of these parameters is scarce in the literature, a simulation in Aspen Plus is first carried out to estimate their values. Figure 6-2 shows the simulation diagram of a plant scale HI-FT in the Aspen Plus software. Table 6.1 is a stream table printed out from the Aspen Plus simulation after the HI-FT simulation. Table 6.1 lists all information for the HI-FT process including the vapor and liquid flowrates as well as the required energy balance parameters.

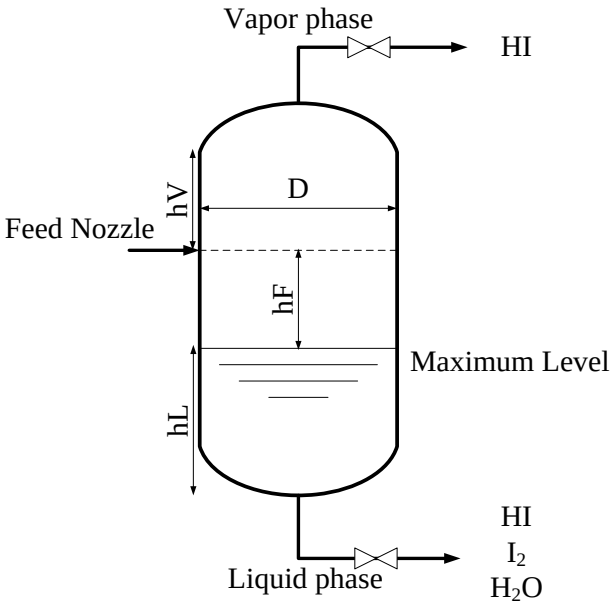

Figure 6-1: Schematic diagram of hydrogen iodide flash tank (HI-FT)

An extension of Table 6.1 may be generated to determine the activity coefficient and the non-randomness parameters. Table 6.2 shows the activity coefficients and the NRTL parameters generated from the Aspen Plus simulation. These values will be used in the complete dynamic modelling and simulation of the HI-FT in the MATLAB Simulink environment.

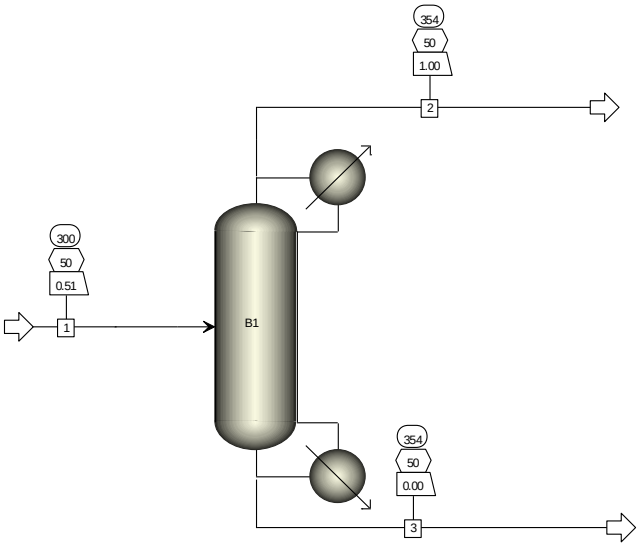

Figure 6-2: HI-FT simulation diagram in Aspen Plus.

Table 6.1: Stream table of HI-FT simulation in Aspen Plus

Heat and Material Balance Table				
Stream ID		**1**	**2**	**3**
From			B1	B1
To		B1		
Phase		MIXED	VAPOR	LIQUID
Sub-stream: MIXED				
Mole Flow	kmol/hr			
Hydrogen Iodide		7.39	2.81	4.58
Water		25.85	1.55	24.30
Iodine		18.46	1.11	17.35
Total flow	kmol/hr	51.70	5.47	46.23
Total flow	kg/hr	6096.28	668.26	5428.02
Total flow	l/min	370.75	83.53	49.97
Temperature	C	300	354.33	354.33
Pressure	bar	50	50	50
Vapor fraction		0.51	1.00	0.00
Liquid fraction		0.49	0.00	1.00
Solid fraction		0.00	0.00	0.00
Enthalpy	cal/mol	-24513.51	-8026.73	-27157.20
Entropy	cal/mol.K	2.96	13.72	0.09
Density	g/m3	0.27	0.13	1.81
Average MW		117.92	122.24	117.41
Liq Vol (60F)		32.81	4.08	28.73

Table 6.2: Non-randomness and dimensionless interaction parameter for hydrogen iodide/hydroiodic acid separation in HI-FT from Aspen Plus simulation.

Parameters (subscript: 1- HI, 2- HIx)	**Value**
Non-randomness parameter, α_{12}	16.1
Non-randomness parameter, α_{21}	1.6
Dimensionless interaction parameter, τ_{12}	0.1
Dimensionless interaction parameter, τ_{21}	0.1

6.3 Hydrogen Iodide Decomposition (HI-DE) Reactor

The hydrogen iodide decomposition (HI-DE) reactor is used to break down hydrogen iodide into iodine and hydrogen molecules. The design of HI-DE reactor is modified from the decomposer zone of the SA-IBSD reactor (see Chapter 5), previously constructed of ceramics and other corrosion resistant materials. The HI-DE reactor designed is a catalytic multi-tubular type, with catalyst pellets packed inside the tubes while heating fluid outside the tubes. Figure 6-3 shows the schematic diagram of the HI-DE reactor.

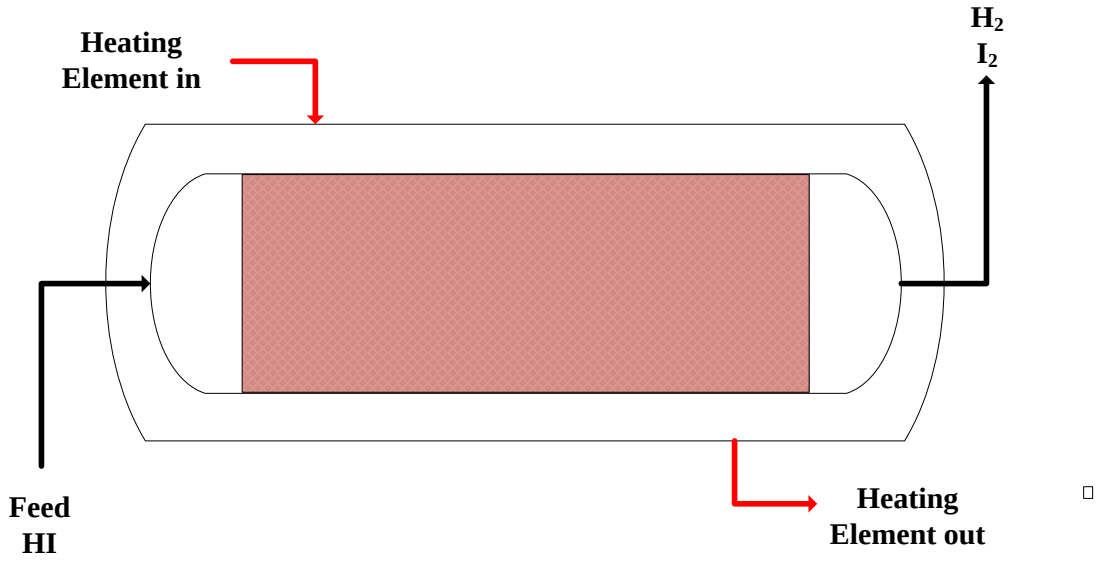

Figure 6-3: Schematic diagram of HI-DE reactor

6.3.1 Dynamic Modelling of HI-DE Reactor

6.3.1.1 Model Assumption

The assumptions made for the HI-DE reactor simulation are as follows:

A.6.3.1: The HI-DE reactor is designed as a long catalytic packed bed tubular reactor and considered as pseudo-homogenous in the reaction zone.

A.6.3.2: The mass of the catalyst is uniformly distributed throughout the packed bed where the chemical reaction only occurs in the catalyst (solid) phase.

A.6.3.3: The flow is assumed to be in gas phase.

A.6.3.4: The pressure is assumed constant in all zones.

A.6.3.5: The reactor is assumed as a plug flow type reactor in both reaction zone and external jacket zone

Remark: The modelling is based on fundamental mass and energy balances using lumped parameter approach for reasons of simplicity. Normally a multi-tubular reactor is to be divided into a few zones of equal volumes, where each zone is assumed to be completely-mixed, hence ordinary differential equations are applicable to each zone. For the small reactor, only a single zone is applied. For the large reactor a few zones are often adopted.

6.3.1.2 Mass and Energy Balances

The hydrogen iodide vapor from the HI-FT unit enters the HI-DE reactor at temperature and pressure of about 300 ^{o}C and 10 bars respectively. Before sending hydrogen to the hydrogen storage tank, the outlet from the HI-DE reactor is first sent to an iodine absorber facility. The absorbed iodine is recycled back to Section I of SITC plant.

The power law is used to describe the rate law. The reaction type is assumed to follow a first order as follows

$$2HI(g) \rightleftharpoons H_2(g) + I_2(g), \quad r_a = k_{fA} A_{cat} P \tag{6.2}$$

where,

$HI = Component\ a$

$H_2 = Component\ b$

$I_2 = Component\ c$

Table 6.3 provides the values of parameters and constants used in the simulation of HI-DE reactor.

Table 6.3: Parameters involved in the simulation of HI-DE reactor

Parameters or Constants	**Value**	**Reference**
Diameter of tank, D_{HID}	2.5 cm	(Choi et al., 2014b).
Total height of HI Decomposer, H_{THID}	45 cm	(Choi et al., 2014b).
Area of tank, A_{HID}	$0.25\pi D_E^2$ m^2	
Volumetric flow rate, v	0.1 mL/min	(Choi et al., 2014b).
Bed porosity, ε	0.8	
Area of a Catalyst, Ni/Al Catalyst (supported on porous alumina) , Acat	107.1 m^2/g	(Choi et al., 2014b).
Mass of a Catalyst, Ni/Al Catalyst (supported on porous alumina), Wcat	2200 g	(Choi et al., 2014b).
Heat capacity of feed mixture, Cp_{HID}	159 kJ/kmol.K	Aspen Plus simulation (Table 6.1)
Average Molecular weight. MW	117.9 kg/kmol	Aspen Plus simulation (Table 6.1)
Enthalpy, H_{rHID}	5882 kJ/mol	Aspen Plus simulation (Table 6.1)

The general mass balance in terms of input and output concentrations (kmol/m^3.hr) is as follows

$$V_{HID}\frac{dC_a}{dt} = \dot{M}_T\left(\frac{C_{ao}}{\rho_{ginHID}} - \frac{C_a}{\rho_{goutHID}}\right) - 2r_a W_{cat} \tag{6.3}$$

$$V_{HID}\frac{dC_b}{dt} = \dot{M}_T\left(\frac{C_{bo}}{\rho_{ginHID}} - \frac{C_b}{\rho_{goutHID}}\right) + r_a W_{cat} \tag{6.4}$$

$$V_{HID}\frac{dC_c}{dt}=\dot{M}_T\left(\frac{C_{co}}{\rho_{ginHID}}-\frac{C_c}{\rho_{goutHID}}\right)+r_aW_{cat} \tag{6.5}$$

Based on the energy balance (kJ/hr) the following equation is obtained

$$\frac{\varepsilon V_{HID}\rho_{goutHID}C_{po}}{\overline{MW}}\frac{dT}{dt}=\dot{M}_T\left(\frac{C_{po}T_oC_a}{\rho_{ginHID}}-\frac{C_pTC_a}{\rho_{goutHID}}\right)-r_a\Delta H_{HID}W_{cat}+Q_{EJ} \tag{6.6}$$

Where

$$Q_{EJ}=A_{rEJ}h_{rEJ}(T_{EJ}-T) \tag{6.7}$$

Notations: r_a is the total reaction rate, C_i is the concentration of component-i, V_{HID} is the volume of reaction zone HI-DE, C_p is the specific heat capacity, $\dot{M}_T$ is the total feed flowrate, ρ_{ginHID} is the density of the inlet mixture, $\rho_{goutHID}$ is the density of the outlet mixture, ΔH_{HID} is the reaction enthalpy, Q_{EJ} is the heat transfer from external jacket, A_{rEJ} is the heat transfer cross section area, W_{cat} is the catalyst weight, h_{rEJ} is the heat transfer coefficient, T_{EJ} is the temperature of the external jacket, ε is the voidage factor, T is the temperature of the HI-DE and $\overline{MW}$ is the average molecular weight. The subscript o denote the input.

6.3.2 Scale-up Procedure of HI-DE Reactor

The scaling-up procedure for the HI-DE reactor is carried out based on the objective to achieve a minimum of 1000 kg/hr of H_2 production. Figure 6-4 depicts the scaling-up procedure of HI-DE reactor. Given the product flow rate from the Bunsen Section, the size of Section III unit is adjusted accordingly.

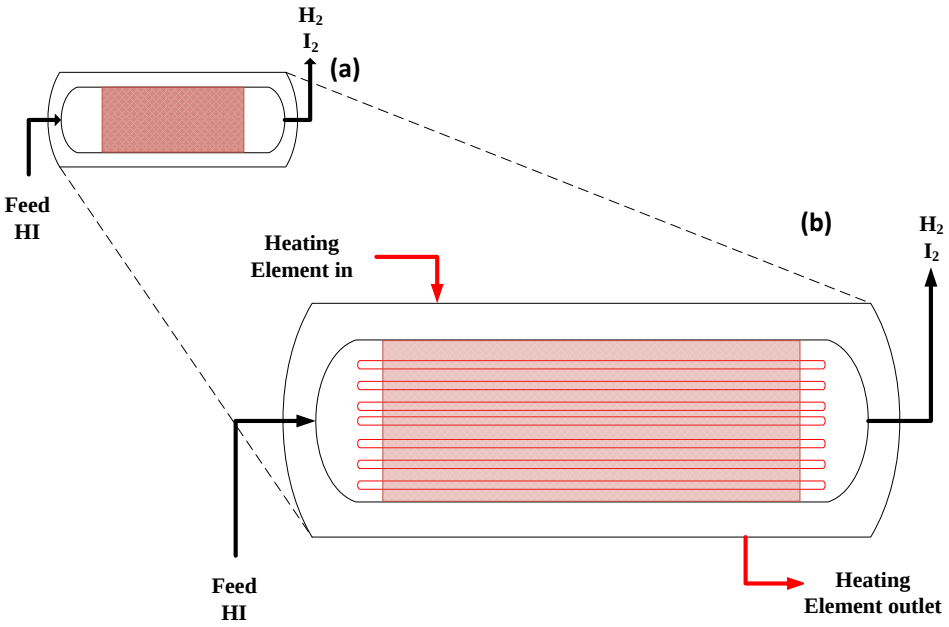

Figure 6-4: Scaling-up schematic diagram for HI-DE reactor: a) the laboratory scale HI-DE reactor, b) the plant scale multi-tubes HI-DE reactor.

This minimum 1,000 kg/hr H_2 production rate shall be accomplished by adjusting the feed flow rate and operating conditions accordingly via trial-and-error simulation. Once the estimated feedstock amount is calculated, the operating conditions can be optimized based on the desired feed and production rates. The optimization is done via graphical optimization of following the RSM methodology (Chapter 3). The kinetic parameters used for both laboratory scale and plant scale are the same, except for the amount of catalysts. The height is scaled based on the L/D ratio proposed by Moore, et.al (2011). The total cross section area is calculated based on the area of the total tubes in the HI-DE reactor. The number of tubes is calculated based on a trial-and-error simulation. The chosen number of tubes is the one that can produce the desired minimum production rate of hydrogen. Table 6.4 lists the values of parameters of HI-DE reactor model, both for laboratory scale and plant scale.

Table 6.4: Parameters of HI-DE reactor models for laboratory scale and plant scale production.

HI-DE reactor Parameters	**Laboratory Scale**	**Plant Scale**
Number of tube	1	100
External Jacket diameter, D_{EJ}	$0.0397\ m$	$2.07\ m$
Tube diameter, D_D	$0.025\ m$	$0.0381\ m$
Maximum length, L	$4\ m$	$10.7\ m$
Feed flow rate, F_{oHI}	$6 \times 10^{-6}\ \frac{m^3}{hr}$	$645.5\ \frac{kg}{hr}$
Voidage factor, ε	0.8	0.8
Mass of Ni/Al Catalyst, W_{cat}	$10\ kg$	$2264\ kg$
Hydrogen iodide conversion	0.40	0.68
Feed external jacket temperature, T_{EJo}	$1053\ K$	$1053\ K$
Outlet reactor temperature, T	$750\ K$	$760\ K$
Pressure, P	$100\ kPa$	$1000\ kPa$

6.4 Loop Gain Controllability Analysis of HI-DE Reactor

The HI-DE simulation is carried out using ode15s solver in MATLAB since reactor model is considered a stiff system. For the purpose of controller design, the reactor model is linearized at two pre-defined operating conditions; the corresponding transfer function models are presented in Table 6.5. The pairings are shortlisted based on a sensitivity study analysis; RSM analysis. Overall, there are three inputs and two outputs of HI-DE reactor. The inputs are feed flowrate, feed jacket temperature and feed temperature. Meanwhile, the outputs are product flowrate (hydrogen) and reactor temperature. Considering the feed temperature as a disturbance variable, thus the remaining two inputs are left as the potential manipulated variables. Based on the RSM analysis, all of the three inputs have significant influences on both reactor outputs. The best model (pairings) is indicated by the highest LGC value as well as RGA index close to unity, which in this case is the Model 1 as presented in Table 6.6. Based on the

transfer functions, it is demonstrated that Model 1 has unstable poles. Unstable poles usually will lead to a challenging dynamic behaviour and difficult to control. However, the LGC index of 7.6475 revealed that it is possible for an unstable model to be controllable by a PID controller despite its unstable pole characteristic.

Table 6.5: HI-DE transfer function models and its input-output pairing

No	**HI-DE reactor Model**	**Input-Output pairing**
1	$Model\ 1 = \begin{bmatrix} \frac{1.0850 \times 10^{-4} e^{-0.473s}}{1.4726s + 1} & \frac{0.3424e^{-0.507s}}{1.4726s + 1} \\ \frac{0.0455e^{-0.473s}}{4.02 \times 10^{-4}s - 1} & \frac{-4.8399e^{-0.507s}}{4.021 \times 10^{-4}s - 1} \end{bmatrix}$	Feed Flowrate **(MV1)** Feed Jacket Temperature **(MV2)** Product Flowrate **(CV1)** Reactor Temperature **(CV2)**
2	$Model\ 2 = \begin{bmatrix} \frac{0.3424e^{-0.5072s}}{1.4726s + 1} & \frac{0.385e^{-1.5565s}}{1.4726s + 1} \\ \frac{-4.8404e^{-0.507s}}{4.021 \times 10^{-4}s - 1} & \frac{-10.1809e^{-1.5565s}}{4.02 \times 10^{-4}s - 1} \end{bmatrix}$	Feed Flowrate **(MV2)** Feed Temperature **(MV1)** Reactor Temperature **(CV2)** Product Flowrate **(CV1)**

Table 6.6: Controllability analysis for HI-DE reactor

Model HI-DE	**Sensitivity study analysis**		$\boldsymbol{\theta_{eotf}}$	**LGC**	RGA
	Input	Output			
Model 1	Feed Flowrate **(MV1)**	Product Flowrate **(CV1)**	0.4730	7.6475	$\begin{bmatrix} 0.9674 & 0.0326 \\ 0.0326 & 0.9674 \end{bmatrix}$
		Reactor Temperature			
	Feed Jacket Temperature **(MV2)**	Product Flowrate			
		Reactor Temperature (CV2)			
	Feed temperature	Product Flowrate			
		Reactor Temperature			
Model 2	Feed Flowrate (MV2)	Product Flowrate	0.507	0.8996	$\begin{bmatrix} 2.1485 & -1.1485 \\ -1.1485 & 2.1485 \end{bmatrix}$
		Reactor Temperature **(CV2)**			
	Feed Jacket Temperature	Product Flowrate			
		Reactor Temperature			
	Feed temperature **(MV1)**	Product Flowrate (CV1)			
		Reactor Temperature			

6.5 Process Controller Design of HI-DE Reactor

The control objectives of the HI-DE reactor are:

a) To achieve desired production flowrate.

b) To keep the temperature as minimum as possible but not violating the constraints.

A SISO controller will be developed for the HI-DE reactor. The SISO type controller is chosen because it is shown in the Table 6.6 that, the feed flow rate (as the manipulated variable) has direct effects on both product (hydrogen) flowrate and the reactor temperature. Hence, controlling one loop is sufficient because the controller can directly affect the other controller variable (CV). Based on the LGC index in Table 6.6, Model 1 shows a higher controllability performance than that of Model 2. The chosen manipulated flowrate (MV) is feed flow rate and the CV is the reactor temperature. According to the value of LGC (7.6475), it is estimated that a PID controller can produce a high performance in controlling the HI-DE reactor. The Robust-PI controller setting from MATLAB Control Design toolbox is as follows

$$G_{ROBUST\text{-}PID} = 90.362\left(\frac{1+100}{s}\right) \tag{6.8}$$

Table 6.7 gives the nominal values and the constraints of the output variables.

Table 6.7: Nominal values and the constraints of the HI-DE reactor output variables.

Variables	**Nominal value**	**Constraints**
Reactor temperature, T_{HIDE} (K)	750	Input: Min: 1033 , Max: 1083
Hydrogen flowrate, m_{H2} (kg/hr)	1138	Output: Min: 1000

6.6 Controller Performance of HI-DE Reactor

The setpoint tracking is carried out via a sequential setpoint change tests. The reactor temperature (CV2) changes from its nominal steady state which is 750 K to 800 K at 450th hour, followed by 800 K to 700 K at the 700th hour and then finally set back to the original state value for the rest of simulation hours.

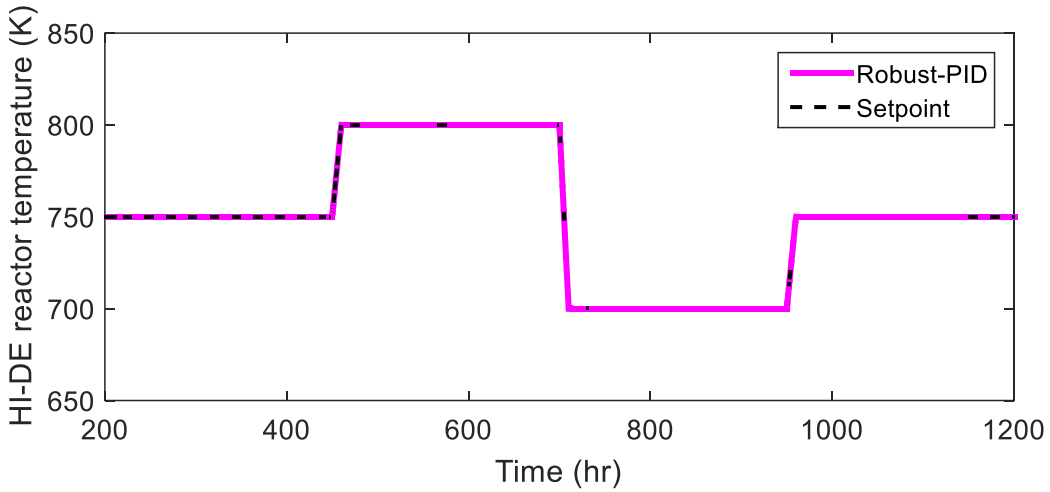

Figure 6-5: Response of Robust-PID controller for setpoint changes in CV2, temperature of HI-DE reactor.

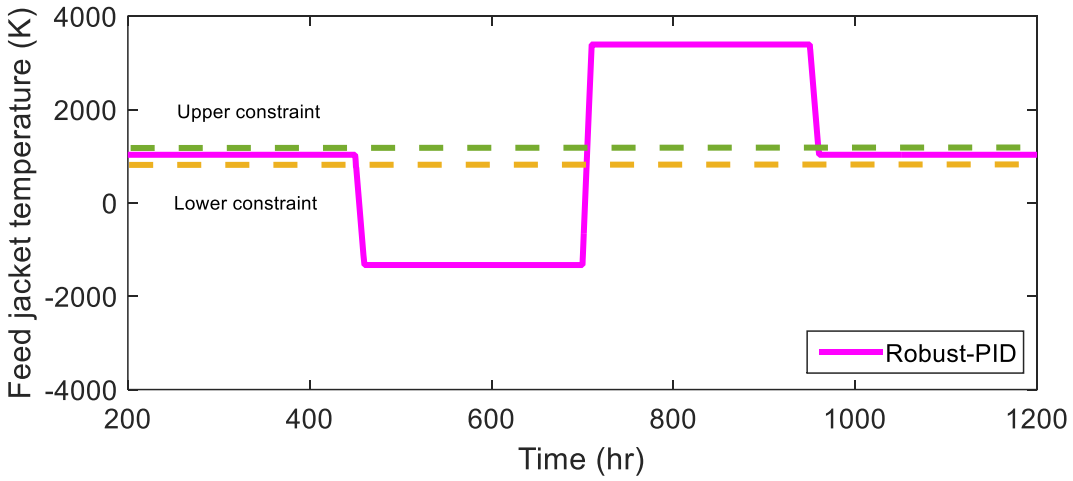

Figure 6-6: MV2 response of Robust-PID controller for setpoint changes in CV2, feed jacket temperature of HI-DE reactor.

Figure 6-5 shows that the Robust-PID is able to drive the process outputs to their desired setpoint with a fast response. However, Figure 6-6 revealed that the Robust-PID controller violates both upper and lower constraint of the feed jacket temperature. The feed jacket temperature cannot exceed the upper constraint as well as cannot be lower than the lower constraint since it can adversely affect the conversion and operation.

Due to the input constraint violation, it can be concluded that the Robust-PID is not practical to control the HI-DE reactor with the given input constraints. Alternatively, a MIMO MPC is designed to control the HI-DE reactor instead. Two types of MPC is developed; NARX based MPC and state-space (SS) based MPC. The NARX-MPC represents a nonlinear controller while the SS-MPC represents a standard linear MPC. The MPC design steps can be retrieved from Chapter 4. A similar setpoint tracking test is carried as that for the previous Robust-PID controller to evaluate the two different MPC controller performances.

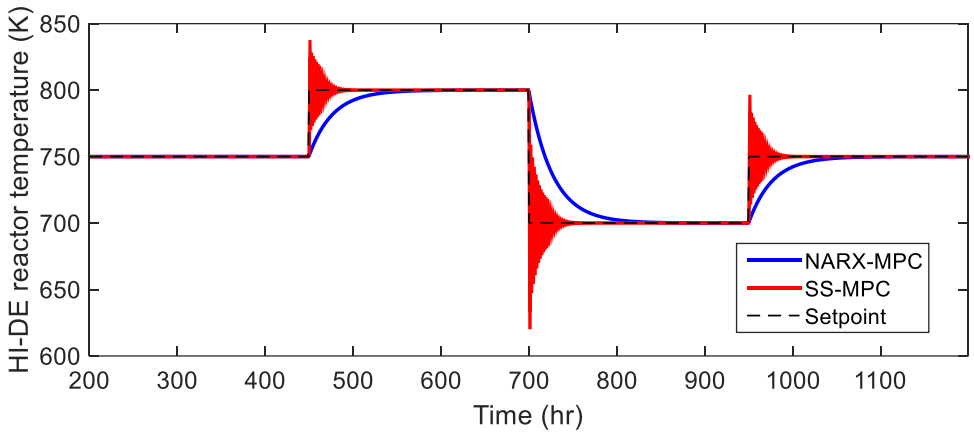

Figure 6-7: Response of SS-MPC and NARX-MPC for setpoint changes in CV2, HI-DE reactor temperature.

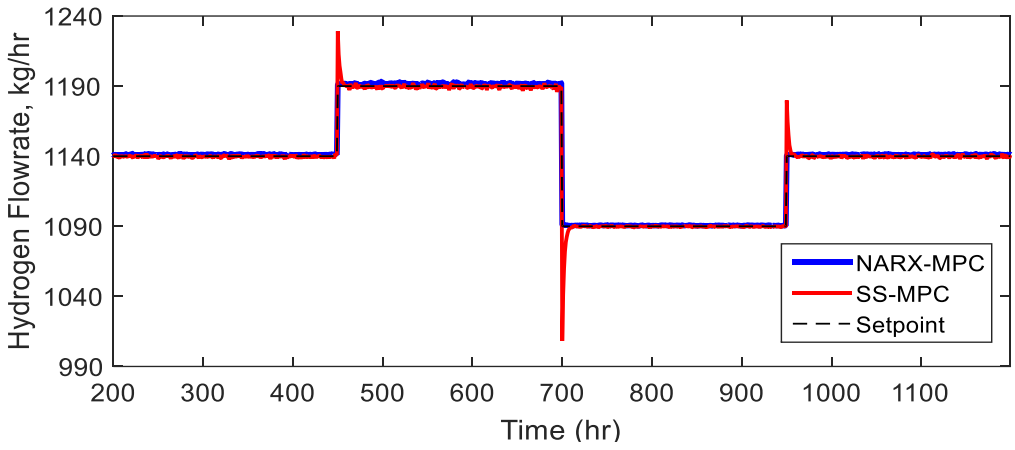

Figure 6-8: Response of SS-MPC and NARX-MPC for setpoint changes in CV1, hydrogen flowrate.

Figure 6-7 and 6-8 show the responses of both SS-MPC and NARX-MPC in the presence of setpoint changes in CV2 and CV1. Both controllers are able to drive the process outputs to its desired setpoint with a fast response without that much delay. However, it is shown that SS-MPC produces a large overshoot compared to that of nonlinear MPC. The spike overshoot behaviour on the CV response is agreed to be influenced by the constraint in the MV (Wang, 2009).

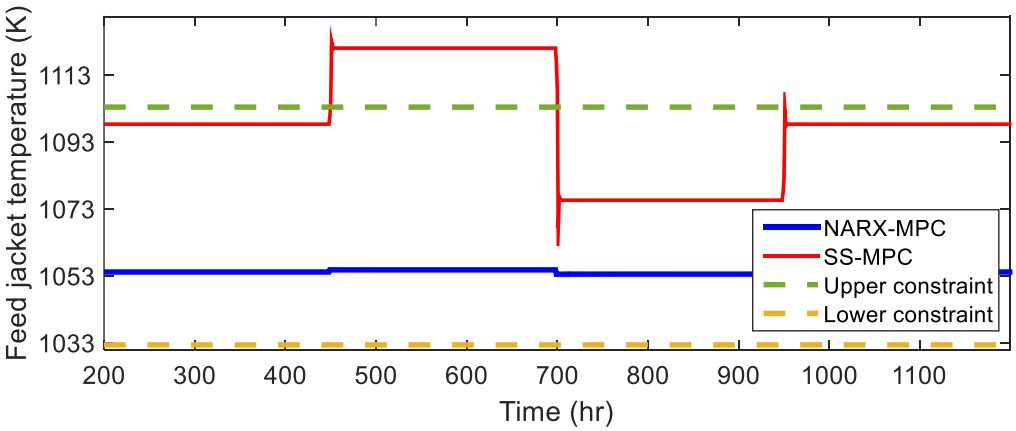

Figure 6-9: Response changes of SS-MPC and NARX-MPC for setpoint changes in MV2, feed jacket temperature.

Figure 6-9 explain the reason for the large overshoots produced by SS-MPC. It seems that SS-MPC is not able to drive the MV between the constraints limit, hence violating the upper constraint. On the other hand, the NARX-MPC can successfully keep the MV within n the allocated constraints, i.e., 1033 K to 1083 K.

Another test is carried out to see the performance of NARX-MPC. A disturbance is introduced at 800th hour of simulation time. The disturbance variable which is the feed temperature increases by 10%. Figure 6-10 shows that NARX-MPC can successfully reject the disturbance after less than 100 hours of simulation time. As a conclusion, NARX-MPC is a suitable to controller to control the HI-DE reactor. Nevertheless, the NARX model can be further improved hence improving the overall NARX-MPC performance in estimating the dynamic behavior of the real process as well as able to reject the disturbance efficiently. Otherwise, a cascade or feedforward controller may be introduced to compare their performance in controlling the HI-DE reactor.

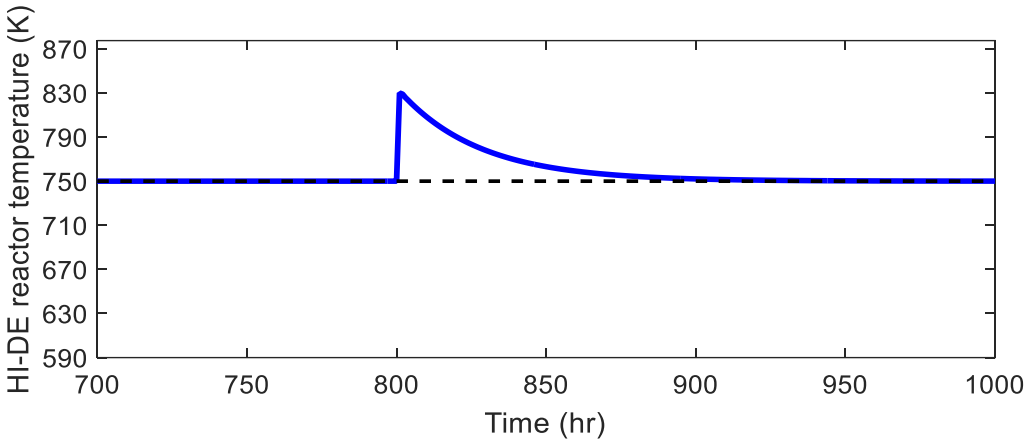

Figure 6-10: Disturbance rejection test of NARX-MPC for 10% increase in the feed temperature.

6.7 Summary

To the best of our knowledge, so far, there has been no report on the detailed fundamental models and scale-up for the HI-FT unit and HI-DE reactor of this section. The summary of this chapter is as follows,

a) The sensitivity analysis for HI-DE reactor revealed that there are three significant inputs and two outputs of HI-DE reactor. The inputs are feed flowrate, feed jacket temperature and feed temperature. Meanwhile, the outputs are product concentration and reactor temperature. Based on the RSM analysis, all of the three inputs have significant effects on both outputs.
b) Two possible sets of manipulated variables-controlled variables were identified and the LGC analysis was conducted to determine which one has the most favorable controllability property.
c) The LGC value of Model 1 (feed flowrate (MV1), feed jacket temperature (MV2), product flowrate (CV1), reactor temperature (CV2)) is 7.6475.
d) The LGC value of Model 2 (feed flowrate (MV2), feed temperature (MV1), reactor temperature (CV2), product flowrate (CV1)) is 0.8996.
e) Input-output pairing of Model 1 was chosen for the controller design of the HI-DE reactor. Since the value of LGC based on the Model 1 is large, a good PID controller performance for HI-DE reactor is anticipated. It was proven that the

PID controller can indeed successfully track the desired setpoint. However, the PID leads to possible violation of the feed jacket temperature constraints.

f) As an alternative control system to PID, two MPC schemes have been developed, NARX-MPC and SS-MPC to control the HI-DE reactor.

g) Based on the performance evaluation, it was shown that the NARX-MPC outperforms the SS-MPC in both setpoint tracking and constraint handling. It can be concluded that the application of NARX model is adequate enough to capture the main nonlinear dynamics of the HI-DE reactor.

7 Industrial SITC Plant Flowsheet

Based on the developed flowsheet of all the SITC sections reported in the previous Chapters 4, 5 and 6, a complete SITC plant flowsheet was developed in this chapter. All sections were assembled to form a complete industrial scale SITC plant. Additionally, this chapter presents summaries on chemical reactions in the SITC process, updated flowsheet for each section as well as for the entire SITC plant, process optimization of the entire SITC plant and the plant capital cost analysis.

7.1 Chemical Reactions in SITC Plant

There are three main chemical reactions taking place in the SITC process. These reactions are distinctively categorized into three sections, i.e., each section represents one main reaction. The sections involved are described as follows.

1) Section I (Bunsen Section)

   This is also known as the Bunsen Reaction Section, which is exothermic and reversible in nature with the enthalpy of reaction, $\Delta H_1 = -165\ kJ/mol$. Note that, this section is very important as a first step to producing the desired intermediate product, Hydrogen Iodide (HI). The general reaction scheme can be represented by

$$I_2(l) + SO_2(g) + 2H_2O(l) \rightleftharpoons H_2SO_4(l) + 2HI(l) \qquad (7.1)$$

   The reactants participating in this reaction are iodine (I_2), sulfur dioxide (SO_2) and water (H_2O). One of the key challenges in this section is to produce sufficiently high yield of HI as to avoid complex azeotropic mixture of HIx (i.e., $HI - I_2 - H_2O$ mixture), which can lead to a very difficult and high cost of separation process prior to feeding the HI intermediate to the HI decomposition section (Section III).

2) Section II

The purpose of this section is to decompose sulfuric acid (H_2SO_4) produced in the Section I into gaseous SO_2, O_2 and H_2O. This decomposition reaction is endothermic and reversible in nature with the enthalpy of reaction, $\Delta H_2 = 371\ kJ/mol$. The general reaction scheme can be expressed as follows

$$H_2SO_4(l) \rightleftharpoons SO_2(g) + 0.5O_2(g) + H_2O(g) \quad (7.2)$$

Note that, the product of the decomposition, i.e., SO_2 is recycled back to the Section I. The major challenge in this section is to provide sufficient amount of high-temperature thermal energy in the range of $800 - 1000^oC$. Note that, a catalyst is required for the sulfuric acid decomposition reaction to occur. More details can be found in Chapter 5.

3) Section III

In this section, the decomposition reaction takes place where the intermediate product HI molecules are broken into H_2 and I_2 molecules in a catalytic multi-tubular reactor. This reaction is strongly endothermic with the enthalpy of reaction, $\Delta H_3 = 173\ kJ/mol$. It is also a reversible reaction.

$$2HI(l) \rightleftharpoons H_2(g) + I_2(g) \quad (7.3)$$

A major issue in this section is related to the difficulty to purify HI solution (coming from the Bunsen Section) before it is being fed into the decomposing reactor. In this work, this issue is resolved by feeding an optimized amount of I_2/H_2O to the Bunsen reactor so that the produced HIx solution is well above the azeotropic HIx composition. Therefore, the produced HIx solution can be concentrated in a flash tank. On the contrary, if the HIx solution is closed to its azeotropic composition ($[HI/(HI + H_2O)] < 0.16$) (Lee et al., 2008a), then a more complicated separation scheme is needed, e.g., using a reactive distillation.

7.1.1 Section I

7.1.1.1 Process Flowsheet Description

The flowsheet of Section I is shown in Figure 7.1. Notice that, the gaseous SO_2 is fed into the Bunsen reactor from the bottom, so that the gas will bubble through the liquid iodine-water mixture. Note that, iodine and water mixture enters from the top at 393 K in a liquid form. Since the reaction is exothermic, it is required to maintain the Bunsen reactor temperature using an external cooling jacket. Two immiscible layers consisting of hydrogen iodide and sulfuric acid solutions may be formed in the reactor under insufficient mixing. The formation of separate layers can be prevented by applying adequate mixing inside the reactor. Please note that, for the purpose of modelling (Chapter 4), it has been assumed that there is no formation of separate layers in the reactor, i.e., homogeneous mixing. An excess of iodine to water molar ratio is introduced between 0.33 to 0.54 (minimum and maximum limits) to maintain an over-azeotropic (Lee et al., 2009) mixture of HIx. The two layers consisting of a heavy phase (HI in I_2) and a light phase (aqueous H_2SO_4) are then formed in the liquid-liquid (L-L) separator. The HI mixture is sent to Section III while the aqueous H_2SO_4 is sent to Section II in the SITC plant. In the Bunsen reactor, the SO_2 is selected as a limiting reactant and it is assumed to undergo complete conversion under the optimal reactor condition.

Once a plant cycle is completed, the fresh feed (I_2 and H_2O) to the Bunsen reactor is mixed with the two recycle streams from the Section II and Section III. The recycle line from Section II consists of a mixture of water, sulfur dioxide, oxygen, and the unconverted sulfuric acid. Oxygen is vented out as gas from the Bunsen reactor and stored in a storage tank. Meanwhile, the recycle line from Section III consists of a mixture of water, iodine and the unconverted hydrogen iodide. Before being mixed with the fresh feed and fed to the Bunsen reactor, both recycle lines are first cooled down to the desired feed temperature of the Bunsen reactor. The materials used for Bunsen reactor and L-L separator are assumed to be titanium and nickel alloys trade which have demonstrated high resistance to sulfuric acid.

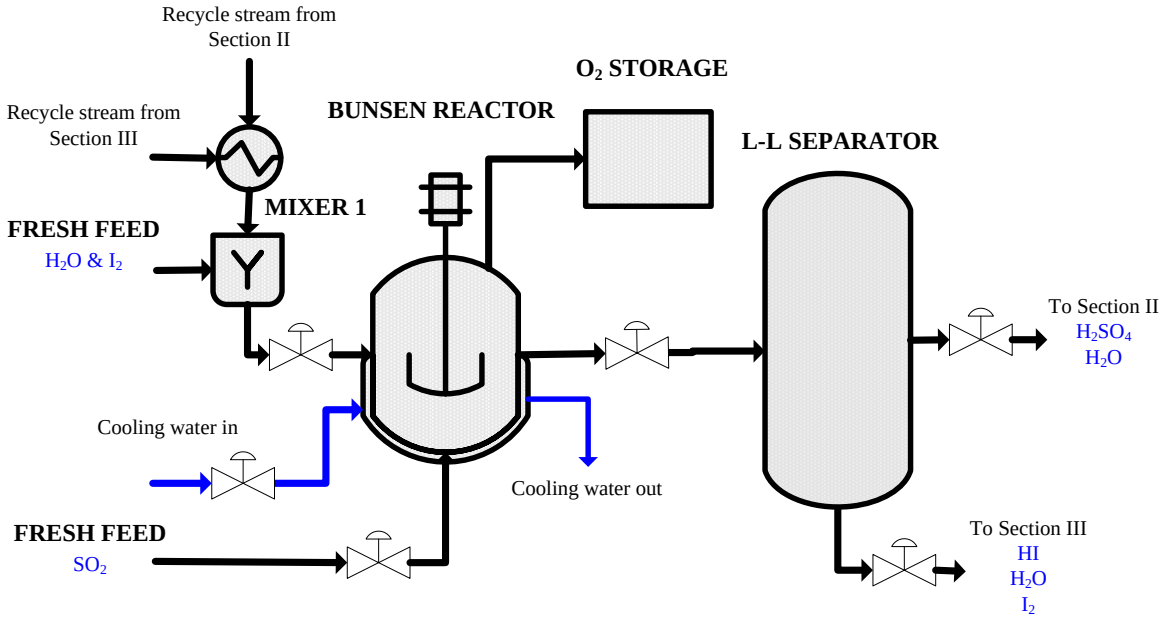

Figure 7-1: Bunsen Section (Section I) flowsheet

7.1.2 Section II

7.1.2.1 Process Flowsheet Description

The light phase mixture leaving the L-L separator of the Bunsen Section is subsequently sent to Section II; first the stream is fed to a flash tank (SA-FT) to concentrate the acid. The mixture is heated up in the flash tank to remove substantial amount of water and to attain a desired sulfuric acid concentration. The design operating pressure in the flash tank is set to be 101 kPa as this is a favorable value, for which the corresponding cost of the equipment is acceptable. In addition, this condition leads to minimising the difficulty in designing and controlling the unit. Please note that the desired sulfuric acid final concentration value is based on the optimized value from sensitivity study via RSM analysis. Bear in mind that, a concentration exceeding 90% (wt) will lead to impractically high energy consumption. The water evaporated from the SA-FT unit is recycled back to the Section I while the concentrated acid is fed to the SA-IBSD reactor. The materials used for the SA-FT unit are assumed to be titanium and nickel alloys which have been demonstrated to be highly resistance to sulfuric acid.

In some articles by researchers from General Atomic and Aachen University, it was proposed that the sulfuric acid is to be decomposed in extractive and reactive distillation columns respectively (Vitart et al., 2006). Unfortunately, this option is very energy intensive and involves high capital cost as the equipment must be able to cope under high temperature in the range of 800-1000℃. Generally, the sulfuric acid decomposition happens via three stages, which in a more conventional flowsheet, the stages involves a boiler or evaporator, a superheater and a catalytic decomposer. In the boiler stage, the sulfuric acid is heated up to remove any remaining water. In the superheater stage, the concentrated sulfuric acid is further heated up to a desired feed temperature prior to feeding the gas to the decomposer stage. In the decomposer stage, the gaseous sulfuric acid is catalytically decomposed into oxygen and sulfur dioxide. Thus, for this conventional flowsheet, three units are required to carry out the sulfuric acid decomposition. It is interesting to note that these three units can be replaced by a single reactor, i.e., bayonet reactor (Moore et al., 2011; Nagarajan et al., 2014).

In this work, an integrated reactor which is called Sulfuric Acid-Integrated Boiler Superheater Decomposer (SA-IBSD) reactor is designed for the sulfuric acid decomposition. In the SA-IBSD reactor, three stages are integrated into one equipment where integrating evaporator with the decomposer has been proven able to reduce energy demand (Liberatore et al., 2012).

The boiler or evaporator zone in the SA-IBSD reactor functions to purify the sulfuric acid from impurities, which include traces of hydrogen iodide as well as excess water at a temperature of more than 400 ℃. In the SA-IBSD reactor, the evaporated product from the evaporator zone which consists of water and sulfur trioxide, are then sent into the catalytic decomposer zone. After the superheater zone and evaporator zone, the gas is passed over a catalyst bed under high pressure in the range of 1,000-10,000 kPa and temperature no more than 1,123 K. In this reactive zone, the sulfur trioxide is decomposed into oxygen and sulfur dioxide.

The schematic diagram of this Section II is shown in Figure 7.2. As can be seen from the diagram, the effluent of SA-IBSD reactor consists of water, oxygen, sulfur dioxide, and unconverted sulfuric acid. The SA-IBSD output is then sent to the Section

I as a recycle stream. To utilize the extra heating energy from the SA-IBSD reactor, the outlet stream (heating fluid) from the SA-IBSD external jacket is sent to Section III, as a source of thermal energy in the HI decomposition reactor, which involves highly endothermic reaction but requiring a lower reaction temperature. The materials of construction for the SA-IBSD are either ceramic or silicon carbide (Moore et al., 2011), which have demonstrated highly resistance to sulfuric acid under high pressure and temperature conditions.

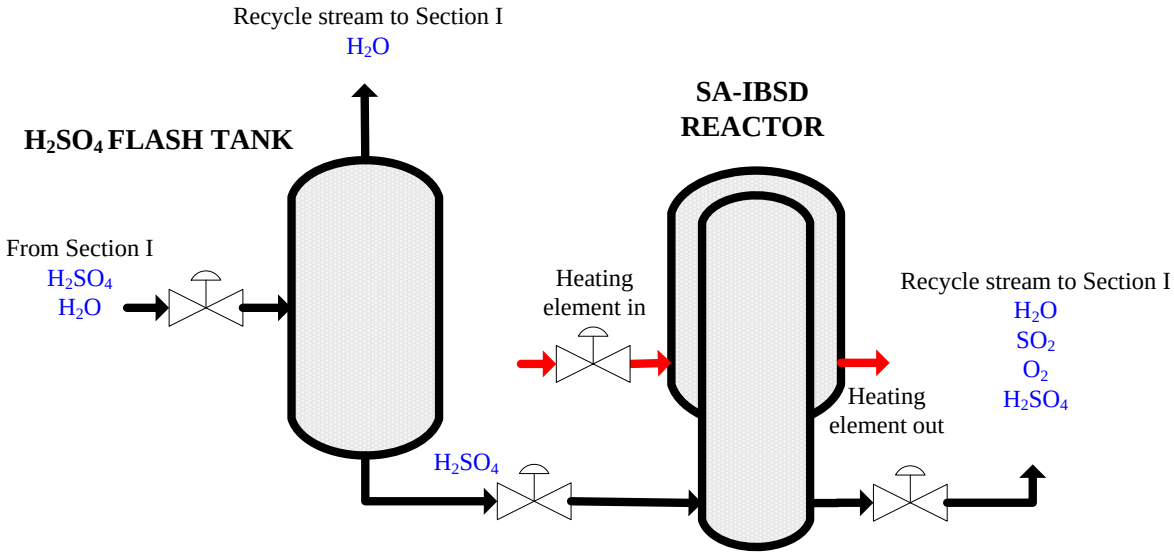

Figure 7-2: H_2SO_4 Section (Section II) flowsheet

7.1.3 Section III

7.1.3.1 Process Flowsheet Description

Figure 7.3 shows the main units involved in the HI decomposition section. By introducing excess iodine and water in the Bunsen section, the potential azeotropic issue of $HI - I_2 - H_2O$ (HIx) solution can be avoided, hence eliminating the need for using a complicated separation system, e.g., electrodialysis and reactive distillation. However, the large excess of iodine and water from the Bunsen reaction still contributes to substantial energy demand in the HI separation system, i.e., in the flash tank. Consequently, an effective design of HI section is very crucial to reduce the energy consumption and the unit capital cost.

In the *HI* section, the heavy liquid phase (*HI* mainly in I_2) from the Bunsen section is sent to the flash tank (HI-FT) to evaporate hydrogen iodide from the HIx mixture. The evaporated hydrogen iodide is then sent to the decomposer (HI-DE), in which *HI* is decomposed into hydrogen and iodine over catalyst pallets. In the HI-DE reactor, the hydrogen iodide decomposition occurs over a catalyst, at pressure of about 1,000 kPa and temperature range of 723 K to 770 K. Since the HI-DE reactor involves a highly endothermic reaction, the required heating source is supplied by the exit heating medium from the SA-IBSD reactor. The HI-DE reactor effluent is then sent to an absorber to remove iodine from the stream before sending the purified hydrogen to a storage tank. Meanwhile, the bottom mixture containing mainly hydrogen iodide, water and iodine are also treated in the absorber, before the treated stream is recycled back to Section I.

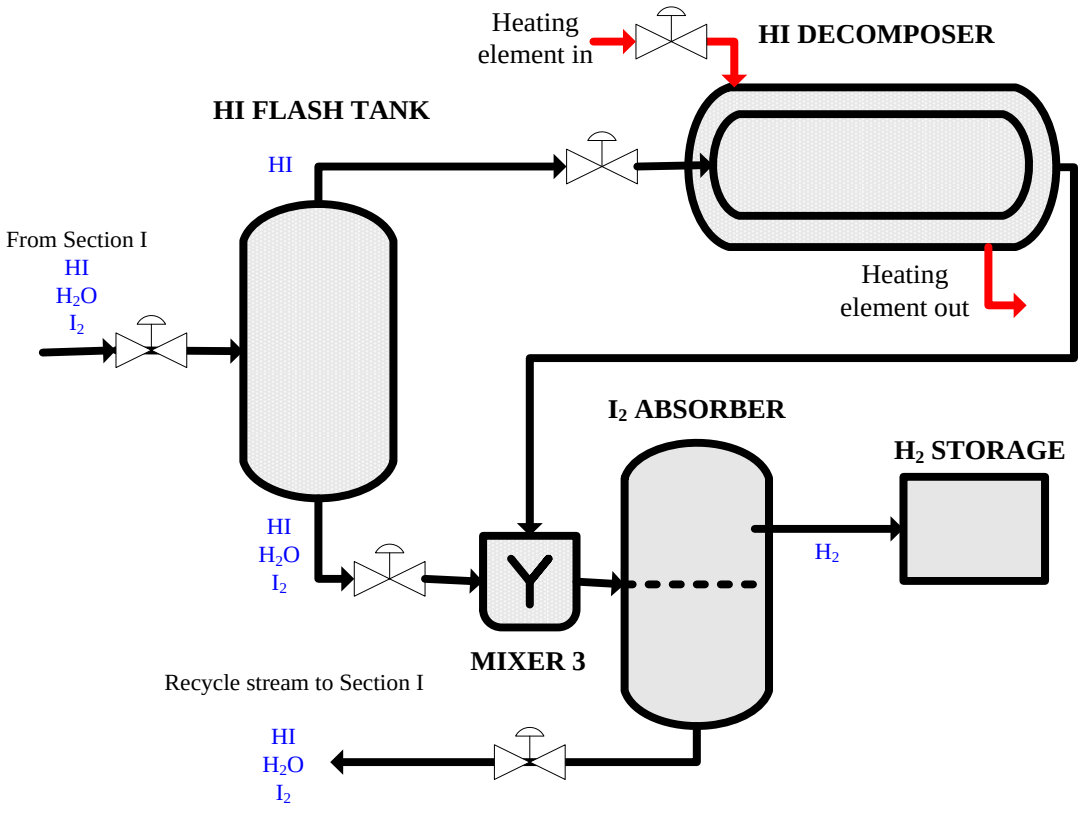

Figure 7-3: HI Section (Section III) flowsheet.

7.2 Plantwide SITC Flowsheet

A major issue in the application of plantwide control (PWC) design is related to the availability of a reliable plantwide model (Downs and Skogestad, 2009). Generally, for most plant design, modifying a steady-state model into a dynamic model is already an enormous effort. Extending an elementary dynamic model by taking into account the details and components needed to describe the plantwide dynamics is another time consuming task. Our approach in this work is that for each unit or equipment, a fundamental dynamic model is first developed. The dynamic models are based on laboratory scale unit. It should be noted that, industrial scale dynamic models of most of the units involved are not available in the open literature where most data in the literature are derived under laboratory scale studies. Once the laboratory scale dynamic model is successfully initialized, converged and validated (in MATLAB environment), then the unit is scaled up to industrial size. After scaling up, the model is ready to be connected with the next equipment/section model. For the subsequent section, equipment or unit based simulation is repeated to compare the unit model prediction with its corresponding laboratory scale data. For the CSTR, flash tank and decomposers, preliminary Aspen Plus simulations are first carried out to obtain basic information relating to the energy balance parameters, and physical/chemical properties as well as for some validation purposes. Once these basic data are obtained, our goal is to perform the plantwide simulation and control entirely in the MATLAB environment. The reason for choosing MATLAB because it offers a broad range of engineering tools, which enable rigorous analysis of the system.

In this work, the data and procedure reported by Liberatore et.al (2012) are used as the guideline for the overall plant scale-up. The heat transfer surface of the external jacket in both SA-IBSD reactor (Section II) and HI decomposer (Section III) are based on the heat transfer coefficient deduced from the flow rate and configuration i.e.: number of tubes in the shell (see Chapter 5 and 6). As for the evaporator zone in the SA-IBSD reactor, the heat transfer coefficient is estimated based on the necessary heat load. For the flash tanks, the maximum diameters should be chosen such that it

corresponds to 60% of the flooding rate. The summary of design material (Kasahara et al., 2017) and sizes of all units involved are tabulated in Table 7.1.

Figure 7.4 shows the complete flowsheet diagram of the proposed industrial scale SITC plant. This plant consists of six primary units which have been designed based on their first principle models. That is include two external heaters, two storage tanks, an iodine absorber, a hold up tank and 21 streamlines including two recycle lines. There is heat integration between Section II (SA-IBSD reactor) and Section III (HI-DE reactor) in red line.

Table 7.1: The equipment design material, size, production capacity and design operating condition of industrial scale SITC plant

Equipment	**Maximum volume (m^3)**	**Material of construction (MoC)**	**Production capacity (kg/hr)**	**Design operating condition**
Section I				
Bunsen reactor	300	Titanium and nickel alloy trade	10,000	P: 101 kPa T: 350 K
L-L separator	500	Titanium and nickel alloy trade	10,000	P: 101 kPa T: 350 K
Section II				
Flash tank	1,500	Titanium and nickel alloy trade	3,000	P: 101 kPa T: 550 K
SA-IBSD reactor	400	Ceramic or silicon carbide	1,000	P: 10,000 kPa T: 1,400 K
Section III				
Flash tank	1,500	Titanium and nickel alloy trade	6,000	P: 201 kPa T: 350 K
HI-DE reactor	200	Ceramic or silicon carbide	2,500	P: 1,000 kPa T: 900 K

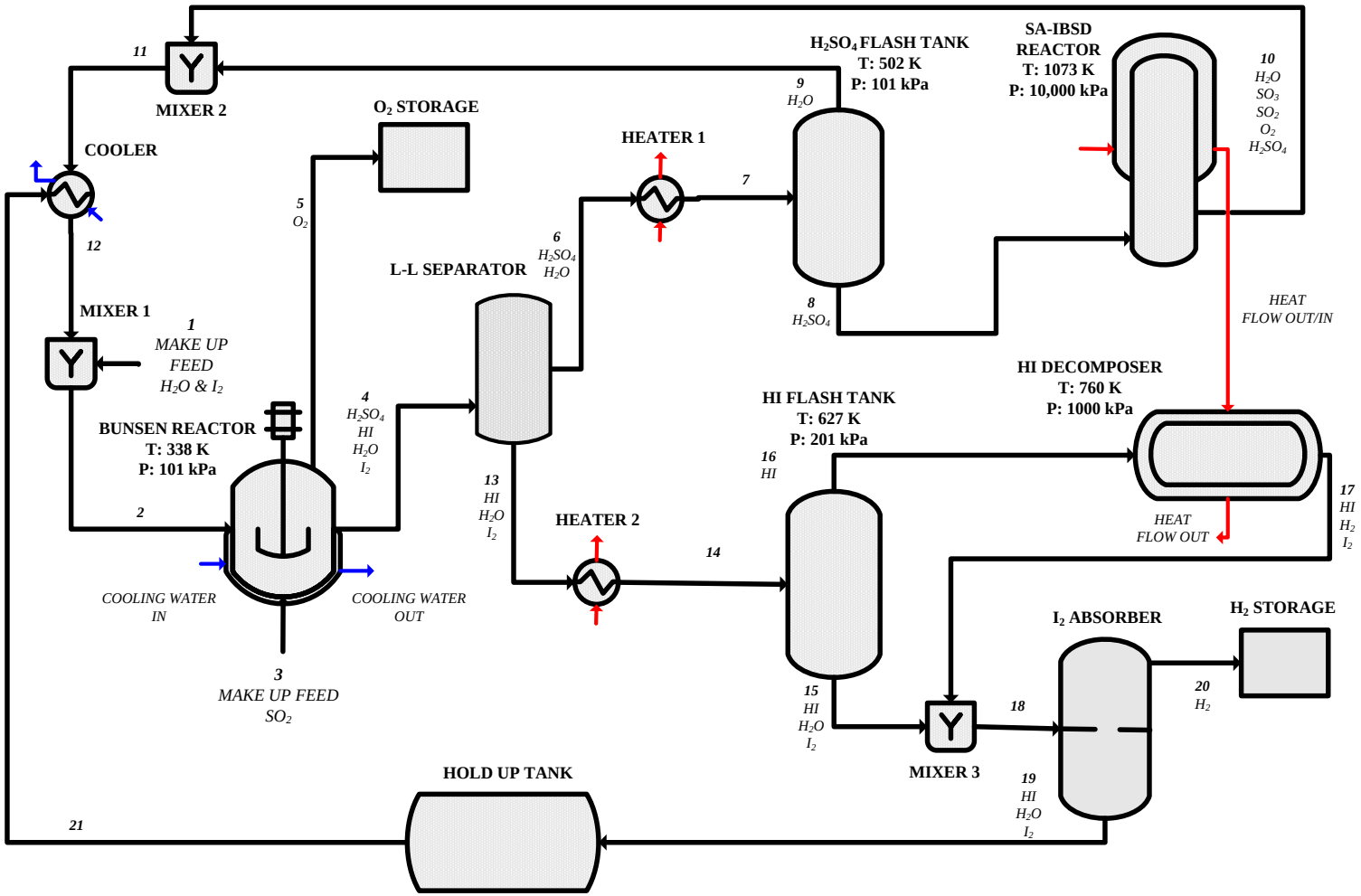

Figure 7-4: A complete industrial scale SITC plant flowsheet.

7.3 SITC Process Optimization and Sensitivity Analysis

7.3.1 Process Optimization via Response Surface Methodology (RSM)

Process optimization is carried out using Design Expert Software. There are 13 factors and 14 responses that are studied. The factors and responses are listed in the Table 7.2. These are considered independent variables which determine the kinetic of reactions and selectivity of the process, hence influencing the quantity and quality of products. The optimization is based on Box-Behnken method and consist of 210 simulations (computer experimental) runs. The desired optimum steady-state criterion is generated based on the hydrogen flowrate, feed molar iodine, and feed jacket flowrate of the SA-IBSD reactor and jacket temperature of the SA-IBSD reactor. The data generated from the computer experiments is then analyzed using statistical method. Figure 7-5 and 7-6 show the 3D plots generated from RSM analysis. The 3D plots revealed the optimum value of hydrogen flowrate, oxygen flowrate, HI-DE temperature and SA-IBSD jacket temperature.

From the overall data analysis, the ANOVA suggests that a quadratic order statistical model is sufficient to represent the effects of the aforementioned 13 factors on all 14 responses. The adjusted *R-square* for the model is 0.99, thus indicating it is significant. There are nine factors that cause the significant effects (p-value < 0.05) on all responses, the results which are given in Table 7.4. For reasons of simplicity, all responses are coded as R1 to R14. Based on the post sensitivity analysis, a coefficient table is presented in Table 7.5. The significant input variable affecting output variables ($p<0.05$) is represented by a check mark. From Table 7.5 it can be observed that the main products; hydrogen and by product; oxygen are affected by:

a) I_2/H_2O feed molar ratio
b) Valve opening of LLS
c) Valve opening of SA-FT
d) External jacket flowrate of SA-IBSD reactor
e) Valve opening of HI-FT. The valves opening are controlling the tank level.

Table 7.2: The responses (output) and factors (input) in the SITC process optimization

Code	Responses
R1	L_{BR} represented level of Bunsen reactor (BR)
R2	T_{BR} presented the temperature of BR
R3	L_{HLS} represented the level of heavy phase liquid in L-L separator (LLS)
R4	L_{LLS} represented the level of light phase liquid in LLS
R5	L_{LCLS} represented the level of light phase liquid in collecting chamber of LLS
R6	L_{SAFT} represented the level in the sulfuric acid section flash tank
R7	T_{SAFT} represented the temperature of sulfuric acid section flash tank
R8	L_{HIFT} represented the level in the hydrogen iodide section flash tank
R9	T_{HIFT} represented the temperature of hydrogen iodide section flash tank
R10	m_{O2} represented the oxygen flowrate
R11	TJ_{SAIBSD} represented the temperature of external jacket SA-IBSD reactor
R12	T_{SAIBSD} represented the temperature of SA-IBSD reactor
R13	m_{H2} represented the hydrogen flowrate
R14	T_{HIDE} represented the hydrogen iodide decomposer (HI-DE)
	Factors
A	T_{oBR} represented the feed temperature of BR
B	N_{oBR} represented the iodine molar feed
C	F_{oBR} represented the feed flowrate of BR
D	F_{SO2BR} represents the sulfur dioxide feed flowrate to BR
E	FJ_{oBR} represented the feed jacket flowrate of BR
F	V_{1LLS} represented the valve opening of LLS
G	V_{1SAFT} represented the valve opening of SA-FT
H	Ts_{SAFT} represented the steam temperature of SA-FT
J	FJ_{SAIBSD} represented jacket flowrate of SA-IBSD
K	V_{1HIFT} represented the valve opening of HI-FT
L	Ts_{HIFT} represented the steam temperature of HI-FT
M	FJ_{HIDE} represented jacket flowrate of HI-DE
N	V_{rec} represented the valve opening of recycle stream

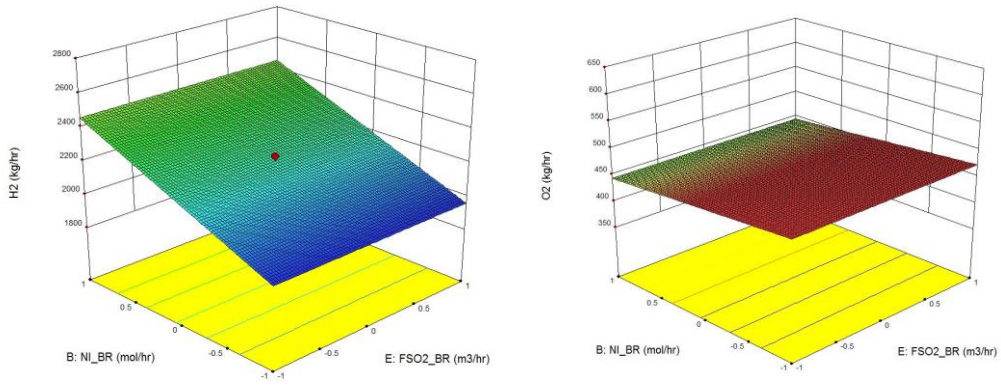

Figure 7-5: 3D Plots of (a) optimum molar hydrogen flow rate (b) optimum oxygen flow rate.

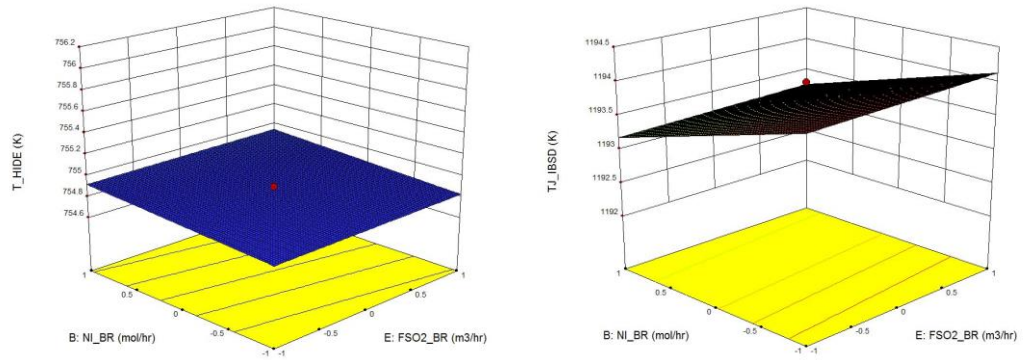

Figure 7-6: 3D Plots of (a) optimum HI-DE temperature (b) optimum SA-IBSD jacket temperature.

Table 7.3: Desired process optimization criteria of the SITC plant using RSM in Design Expert software

No	Input or output variables	Desired criteria
1	Hydrogen production, kg/hr	Maximum (2,400 kg/hr)
2	Feed Molar of Iodine, kmol/hr	Between the optimal range (0.33 to 0.54)
3	Feed Jacket Flowrate of SA-IBSD Reactor, m^3/hr	Minimum (4,500)
4	Jacket Temperature of SA-IBSD reactor, K	Minimum (1,203)

Table 7.4: Optimum values obtained for SITC plant variables based on RSM optimization

No	Variables	Optimum values
1	Feed Bunsen Reactor Temperature, K	338.8
2	Feed Molar of Iodine, kmol/hr	1,409.3
3	Feed Flowrate of Water, m^3/hr	0.12
4	Feed Jacket Flowrate of Bunsen Reactor, m^3/hr	1.47
5	Feed Sulfur Dioxide Flowrate, m^3/hr	0.48
6	Feed Steam Temperature to Flash Tank Section II, K	529.3
7	Feed Jacket Flowrate of SA-IBSD Reactor, m^3/hr	9,499.2
8	Feed Steam Temperature to Flash Tank Section III, K	527.3
9	Feed Jacket Flowrate of HI-DE Reactor, m^3/hr	768.9

7.3.2 Input-Output Sensitivity via Principle Component Analysis (PCA)

Principal Component Analysis (PCA) analysis method is utilized as part of the method to optimize the SITC plant. Here, the PCA analyzes the extents of the effect of input on output variables. The advantage of PCA is that it enables one to quickly determine the dominant input variables which critically affect the plant performance and main output

variables (possibly to be controlled). Figure 7.7 shows a principal component plot while Figure 7.8 shows a Pareto plot from the PCA analysis for SITC plant. Based on the result in RSM and PCA Pareto plot, Table 7.5 and 7.6 are generated. Table 7.5 presents the significant input variables which can critically affects the output variables as represented by a check mark. From Table 7.6 it can be observed that the main products, which are hydrogen and by product, oxygen are affected by:

a) Feed BR temperature,
b) I_2/H_2O feed molar ratio,
c) Valve opening of SA-FT,
d) Steam temperature of SA-FT,
e) Eternal jacket flowrate of SA-IBSD reactor,
f) Valve opening of HI-FT and
g) external jacket flowrate of HI-DE.

The additional important factors identified via the PCA in addition to that the RSM analysis are the feed temperatures of BR and SA-FT. As a result, both analysis are mutually complementing each others. One may deduce the significant output variables to be controlled as tabulated in Table 7.7. The results on significant controlled variables will be utilize in Chapter 8; PWC structure development.

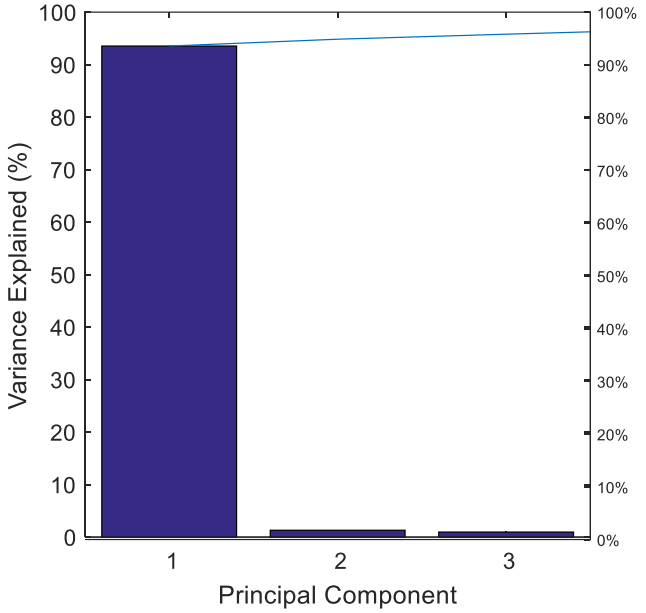

Figure 7-7: Principal component plots of PCA analysis

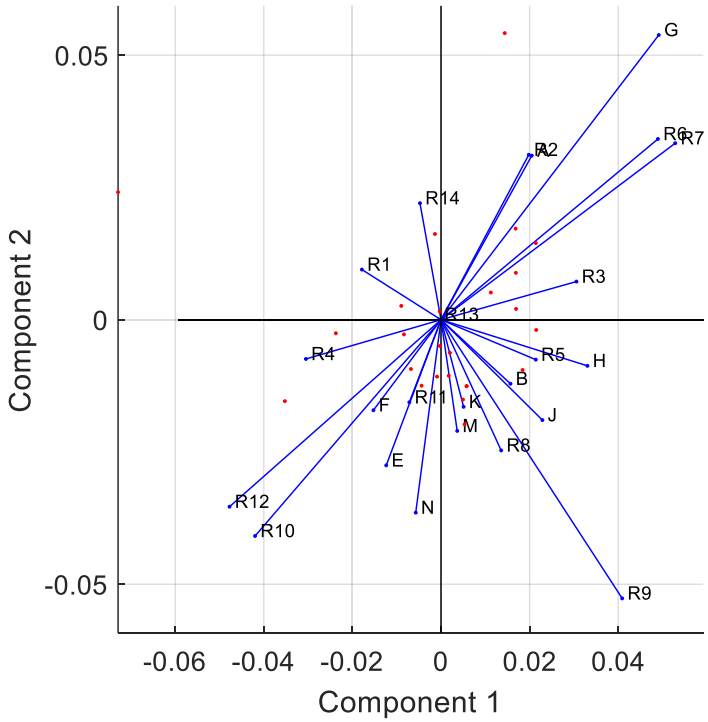

Figure 7-8: 2D Pareto plot of PCA analysis

Table 7.5: Sensitivity analysis of input-output variables coefficient table of SITC plant via RSM analysis: Checked box present significant effect ($p<0.05$)

Variables: Input (top) and Output	**A:** T_{oBR}	**B:** N_{oBR}	**C:** F_{oBR}	**D:** FJ_{oBR}	**E:** F_{SO2oBR}	**F:** V_{1LLS}	**G:** V_{1SAFT}	**H:** T_{sSAFT}	**J:** FJ_{SAIBSD}	**K:** V_{1HIFT}	**L:** T_{sHIFT}	**M:** FJ_{HIDE}	**N:** V_{REC}
R1: L_{BR}	√	√											
R2: T_{BR}	√	√			√		√						√
R3: L_{HLS}		√				√							
R4: L_{LLS}		√				√							
R5: L_{LCLS}	√	√				√							√
R6: L_{SAFT}		√				√	√	√					
R7: T_{SAFT}		√				√	√						
R8: L_{FTHI}		√				√				√			
R9: T_{FTHI}		√								√			
R10: m_{O2}		√				√	√	√	√				
R11: TJ_{SAIBSD}	√	√					√		√				
R12: T_{SAIBSD}		√				√	√	√					
R13: m_{H2}		√								√			
R14: T_{HIDE}												√	
Total	4/14	13/14	-	-	1/14	8/14	6/14	3/14	2/14	3/14	-	1/14	2/14
Rank (pre-estimated)	4	1			10	2	3	6	7	5		9	8

Table 7.6: Sensitivity analysis of input-output variables coefficient table of SITC plant via PCA analysis: Checked box represent significant effect

Variables: Input (top) and Output	**A:** T_{oBR}	**B:** N_{oBR}	**C:** F_{oBR}	**D:** FJ_{oBR}	**E:** F_{SO2oBR}	**F:** V_{1LLS}	**G:** V_{1FTSA}	**H:** T_{sFTSA}	**J:** FJ_{SAIBSD}	**K:** V_{1FTHI}	**L:** T_{sFTHI}	**M:** FJ_{HIDE}	**N:** V_{REC}
R1: L_{BR}		√						√	√	√		√	
R2: T_{BR}					√	√							√
R3: L_{HLS}					√	√							√
R4: L_{LLS}	√						√						
R5: L_{LCLS}													
R6: L_{FTSA}					√	√							√
R7: T_{FTSA}					√	√							√
R8: L_{FTHI}													
R9: T_{FTHI}													
R10: m_{O2}	√						√						
R11: TJ_{SAIBSD}	√						√						
R12: T_{SAIBSD}	√						√						
R13: m_{H2}		√						√	√	√		√	
R14: T_{HIDE}		√						√	√	√		√	
Total	4/14	3/14	-	-	4/14	4/14	4/14	3/14	3/14	3/14	-	3/14	4/14
Rank (pre-estimated)	4/2	1/8			10/4	2/3	3/1	6/6	7/7	5/9		9/10	8/5

Table 7.7: Input-output sensitivity analysis via PCA method

Output Variables	**Components (Input and Output Variables)**	
	Same quadrant	**Orthogonal quadrant**
R1: L_{BR}	R14, R13	R9, H, J, R5, B, R8, K, M
R2: T_{BR}	G, R7, R6, R3, A	R12, R10, R4, F, E, R11, N
R3: L_{HLS}	G, R7, R6, R2, A	R12, R10, R4, F, E, R11, N
R4: L_{LLS}	R12, R10, F, E, R11, N	R7, G, R6, R3, A, R2
R5: L_{LCLS}	R9, H, J, B, R8, K, M	R1, R14
R6: L_{SAFT}	G, R7, R2, R3, A	R12, R10, R4, F, E, R11, N
R7: T_{SAFT}	G, R6, R2, R3, A	R12, R10, R4, F, E, R11, N
R8: L_{HIFT}	R9, H, J, R5, B, K, M	R1, R14
R9: T_{HIFT}	R8, H, J, R5, B, K, M	R1, R14
R10: m_{O2}	R12, R4, F, E, R11, N	R7, G, R6, R3, A, R2
R11: TJ_{SAIBSD}	R12, R10, R4, F, E, N	R7, G, R6, R3, A, R2
R12: T_{SAIBSD}	R11, R10, R4, F, E, N	R7, G, R6, R3, A, R2
R13: m_{H2}	R1, R14	R9, H, J, R5, B, R8, K, M
R14: T_{HIDE}	R1, R13	R9, H, J, R5, B, R8, K, M

7.4 Economic Analysis

In this section, the economic analysis of the proposed industrial SITC plant is carried out. In the following section, the costing of entire plants is presented including both capital and operating costs.

7.4.1 Plant Investment, Specification and Targets

This work presents the costing details of the hydrogen production plant assuming a total capacity of 1000 kg/hr of hydrogen, hence a total 24 metric tons/day for a plant operating 24 hr/day for 300 days in a year. Thus, the annual production of hydrogen is 7,200,000 tons. The fresh feedstock consists of fresh make-up water and iodine and fresh sulfur dioxide. It is assumed that the plant lifetime is 20 years. Note that, the plant is modelled using Aspen Plus® (steady-state assessment) and MATLAB® software (for dynamics simulation).

7.4.2 Capital Cost Estimation

The costs of equipment and other expenses related to capital investment play a crucial role in a plant design. The capital costs of a newfangled plant comprise primarily of the Fixed Capital Investment (FCI), the land cost and the working capital costs. The FCI consists of the equipment purchase costs; which we will refer to as the Bare Module Cost (BMC), and all the necessary supplementary costs required to construct the plant. These additional costs are associated to the BMC. BMC is the sum of the direct and indirect cost of the purchase price. Direct cost includes material cost, labor cost, and equipment price while indirect cost includes freight, insurance, taxes, construction, overhead and contractor engineering expenses. The BMC is defined as:

$$C_{BM} = C_P F_{BM} \quad (7.4)$$

where C_{BM} = Bare module equipment cost: direct and indirect cost for each unit

C_P = Purchase cost for the base condition: equipment made of the most common material, usually carbon steel and operating at near ambient pressures

F_{BM} = Bare module cost factor

7.4.3 Equipment Cost Summary for the Whole Plant

The purchase costs of this work are based on the basis of Chemical Engineering Plant Cost Index (CEPCI) 2016 which is 558 (Chemical Engineering, 2016). Pre-design capital cost estimates are usually gathered from old price data. Thus, because of inflation, correction indices are needed to adjust old data to the current values. The total BMC, C_{TBM} is equal to $ 62,832,000.

7.4.4 Fixed Capital Investment

A detail of process design is crucial to capital cost estimation. An optimal process design with complete mass balance, energy balance, equipment sizing, materials of construction and process control configurations plus piping, instrumentation and electrical equipment are used to estimate the capital cost. Following this method of estimation, the bare module cost of all equipment is obtained from the correlation method which has been presented in the Table 7.12, in the previous sub-section. Meanwhile, the equation for the total capital investment by the Guthrie method (Guthrie, 1969) is given as below:

$$C_{TCI} = C_{TPI} + C_{WC} \quad (7.5)$$

$$C_{TCI} = 1.18(C_{TBM} + C_{site} + C_{building} + C_{offsitefacilities}) + C_{WC} \quad (7.6)$$

where,

C_{TCI} = Total capital investment cost, $

C_{TPI} = Total permanent investment cost, $

C_{WC} = Working capital, $

C_{TBM} = Total bare module cost, $ (Section 7.4.3)

Step 1: Estimation of site development cost, C_{site}

For grass-roots plant, we assume the site development cost is 10% of C_{TBM}

$C_{site} = 0.10 C_{TBM}$

$C_{site} = 0.10\ x\ \$62{,}832{,}000$

$C_{site} = \$\ 6{,}283{,}200$

Step 2: Estimation of building cost, $C_{bulding}$

For grassroots plant, the building cost can be estimated as 20% of C_{TBM} which including process building and non-process building

$C_{bulding} = 0.20 C_{TBM}$

$C_{bulding} = 0.20\ x\ \$62{,}832{,}000$

$C_{bulding} = \$\ 12{,}566{,}400$

Step 3: Estimation of offsite facilities cost, $C_{offsitefacilities}$

$$C_{offsitefacilities} = C_{utilities} + 0.05C_{TBM}$$

$$C_{offsitefacilities} = \$\ 11{,}700{,}000 + 0.05C_{TBM}$$

Table 7.8: List of main equipment of SITC plant

Equipment Tag	**Equipment Name**	**Purchase Cost ($)**	**Bare Module Factor (F_{BM})**	**Bare Module Cost ($)**
R-101	Section I Bunsen Reactor	25,800	1.50	38,800
S-102	Section I L-L Separator	20,600	6.17	127,000
H-201	Section II Heat Exchanger	4,750	1.81	92,000
F-202	Section II Flash Tank	27,100	7.97	216,000
E-203	Section II SA-IBSD reactor (Evaporator + Decomposer)	27,100	7.97	216,000
D-204		27,100	9.74	264,000
H-301	Section III Heat Exchanger	4,750	19.37	92,000
F-302	Section III Flash Tank	27,100	7.97	216,000
D-303	Section III Decomposer	27,100	7.97	216,000
A-304	Section III Absorber	17,000	8.06	137,000
Bare Module Cost C_{BM}				1,350,800
Total Bare Module Cost C_{TBM}				1,350,800 (558) / (12) = 62,832,000

$C_{offsitefacilities} = \$\ 14{,}841{,}600$

Step 4: Estimation of total permanent investment cost, C_{TPI}

Total permanent investment**,**

$C_{TPI} = 1.18\left(C_{TBM} + C_{site} + C_{bulding} + C_{offsitefacilities}\right) = \$\ 96,523{,}200$

Step 5: Estimation of working capital cost, C_{WC}

$C_{WC} = 0.176C_{TPI} = \$\ 16{,}988{,}083$

Step 6: Estimation of total capital investment, C_{TCI}

$C_{TCI} = \$\ 113{,}511{,}283$

From this section, the total capital investment C_{TCI} has been estimated to be $ 113,511,283.

7.5 Summary

In this chapter, a complete SITC plant flowsheet has been developed based on combining the unit based flowsheets presented in Chapters 4 to 6. Based on the sensitivity analyses via RSM and PCA, it has been identified that the main product hydrogen and by product oxygen are strongly affected by the following input variables:

a) Feed BR temperature,
b) I_2/H_2O feed molar ratio,
c) Valve opening of SA-FT,
d) Steam temperature of SA-FT,
e) External jacket flowrate of SA-IBSD reactor,
f) Valve opening of HI-FT and external jacket flowrate of HI-DE.

Detailed ecpnomic analysis showed that the cost to build a SITC plant with the nominal production capacity of 1,000 kg/hr is US$ 113.5 million. This calculation has been done by assuming certain prices on materials of construction for certain units, which have to

operate under high temperature and pressure conditions, and corrosive nature of the sulfuric acid, e.g., the SA-IBSD reactor for the sulfuric acid decomposition.

8 Plantwide Control of Industrial SITC Plant

Plantwide Control (PWC) deals with the synthesis and development of a complete control system of a given plant. This complete control system often involves multiple layers in a control hierarchy: at the basic level is called a regulatory layer while the layer above it is called the supervisory layer. In this chapter, both regulatory and supervisory layers were described and developed for the SITC plant. Note that, the PWC study of the SITC process has never been reported before. To address this uncharted territory, a set of preliminary steps was proposed prior to the PWC structure design. The Skogestad's Self-Optimizing Control structure was then adopted in the PWC design of the plant. This chapter describes the PWC objectives, PWC preliminary steps and PWC structure of the SITC plant.

8.1 PWC Objectives

PWC problem can be divided into two major elements: (1) control structure selection, and (2) controller design. It has been well recognized that the first element has a far reaching impact on the plantwide control performance compared to the second element. In the control structure selection, the key questions to be answered are: (1) which outputs to be controlled, (2) which variables to be manipulated, and (3) what are the connections between the sets of controlled and manipulated variables?

The PWC structure design starts with defining the process control objectives. In this work, there are three process control objectives to be fulfilled for the SITC plant:

a) To achieve a production rate of minimum 1 tons/hr of hydrogen under specified operating conditions. The amount of hydrogen production rate chosen is comparable with that of the currently operational electrolysis industrial scale plant (Zeng and Zhang, 2010) and the JAEA industrial scale thermochemical cycle (Kasahara et al., 2017).

b) To keep molar feed flow I_2/H_2O into the Bunsen Section at an optimum ratio. Lee et, al (2008) proposed an optimum operating window for I_2/H_2O molar feed flow ratio in the Section I to be between 0.333 and 0.538. The significance of maintaining the optimum I_2/H_2O ratio is to produce a HIx liquid solution that is well above its azeotropic composition in order to:
    i. Allows for spontaneous liquid-liquid (HI in I_2 and aqueous H_2SO_4) phase separation in the L-L Separator,
    ii. Eliminates the need to concentrating the HI gas (via an energy intensive electro electrodialysis (EED) or Reactive Distillation Column).

c) To retain the SA-IBSD temperature as minimum as possible for plant safety and to reduce high-temperature energy utilization but subject to attaining minimum SA-IBSD reactor conversion of 36%. The SITC process becomes a less favorable renewable energy production method if it consumes an excessively high amount of high-temperature thermal energy. Keep in mind that, the aforementioned temperature corresponds to the reaction zone temperature inside the SA-IBSD reactor – this is the hottest zone in the reactor.

In summary, the major constraints in the SITC plant operation are the production specification, SA-IBSD (reactive zone) temperature and molar feed ratio of I_2/H_2O. The values of these constraints are displayed in Table 8.1.

Table 8.1: Variables specification of SITC

Variables	**Constraint Specification**
Hydrogen flowrate, $\dot{m}_{H2}$ (kg/hr)	≥ 1000
Temperature SA-IBSD reactor, $T_{SA-IBSD}$ (K)	≤ 1200
Ratio of feed molar flowrate I_2/H_2O, R_{nI_2/H_2O}	$0.33\ to\ 0.54$

In this work, the Self-Optimizing Control (SOC) procedure proposed by Skogestad is applied to design a PWC structure of the SITC plant. SOC procedure consists of two sections (Skogestad, 2012, 2004, 2000b):

1) Top-down analysis, including specifications of operational objectives and degrees of freedom (see Chapter 3). This analysis mostly focuses on the economics and steady-state evaluations of the given plant.
2) Bottom-up design of the control system, which starting with the design of stabilizing control layer. This analysis is focuses on the dynamic performance of the plant.

The Principal Component Analysis (PCA) analysis method (Nandong et al., 2010) is utilized as part of the top down analysis and bottom up design. It is to identify the input-output variables that have the self-optimizing property. The decision of SITC plant structure may be retrieved from previous Chapter 4 to 7. In the next sections, the details of PWC design for the SITC plant are discussed.

8.2 PWC Preliminary Steps

8.2.1 Significance of Preliminary Steps

The SOC approach provides a rigorous step by step procedure to design a PWC structure for an existing plant. For a plant that is not yet designed at the industrial stage, it is important to conduct some PWC preliminary steps to determine the essential information before applying any PWC structure procedure. PWC preliminary steps identify steady-state mass balance, analysis of total energy, analysis of utilities, scaling-up the SITC plant production rate, scaling-up each unit and testing via dynamic simulations. These analyzes are essential to ensure the integrity of the plant design and operation prior to the PWC structure development. The PWC preliminary procedure is proposed as follows.

8.2.2 Step by Step Procedure

8.2.2.1 Pre-Step 1: Identifying steady-state mass balance

The steady-state mass balance is important to identify the total inflow and outflow of the entire plant regardless it's dynamic. Figure 8-1 shows the plant input and output signals at steady-state condition. In this figure, the solid lines indicate the external inputs and outputs while the dotted lines indicate the recycle streams in the plant.

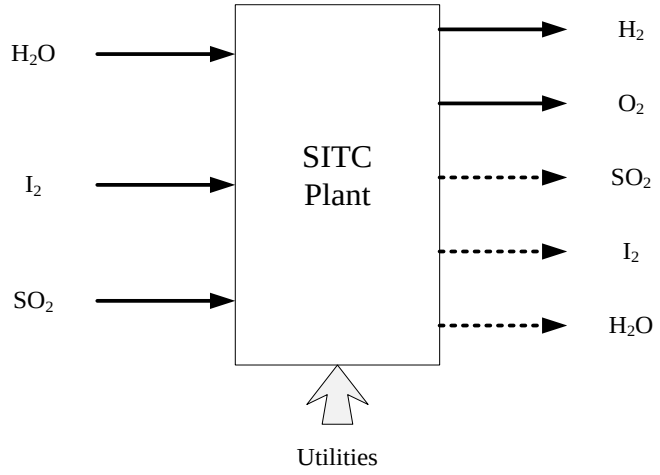

Figure 8-1: Steady-state input and output mass flow of SITC plant.

Based on Figure 8-1, the steady-state mass balance equation is

$$F_{H_2O} + F_{I_2} + F_{SO_2} = F_{H_2} + F_{O_2} + F_{H_2O} + F_{I_2} + F_{SO_2} \quad (8.1)$$

where F represents flowrate.

Table 8.2 displays the details of inflow and outflow shown in Figure 8-1. In this step, it is desired to optimize both the inflow and outflow of each unit in the SITC plant. Process optimization is carried out via RSM analysis to attain the optimum values for the inflow and outflow, as well as the other operating conditions. The details of process optimization of the entire SITC plant are presented in Chapter 7.

Table 8.2: Optimized steady-state flowrate of SITC plant

Component	**Flowrate (kg/hr)**
Input	
Water	139,860
Iodine	720,900
Sulfur Dioxide	30,400
Output	
Hydrogen	≥1,000
Oxygen	≥450
Recycle	
Water	138,461
Iodine	716,661
Sulfur Dioxide	30,096
Conversion	
Section I	0.99
Section II	0.40
Section III	0.99

8.2.2.2 Pre-Step 2: Analysis of total energy

It is desired through this step to analyze the total energy requirement by the SITC plant, H_T necessary to meet the conversion criteria as in the Table 8.2. Table 8.3 shows the energy required in the Bunsen reactor. The energy to be absorbed by the cooling jacket of Bunsen reactor is calculated as follows

Section I (Exothermic): $H_{E1} = F_{cE1} C_{pE1} (T_{c1} - T_{c2})$ (8.2)

where F_{cE1} and C_{pE1} are the cooling water flow rate and its specific heat capacity, while T_{c1} and T_{c2} are its inlet and outlet temperatures.

Table 8.3: Total energy required in the Bunsen reactor

Bunsen Reactor	**Value**
Energy to be absorbed by jacket, Q_{BR} or H_{E1}	2.4191 kJ
Operating temperature, T_{BR}	60 ºC -120 ºC
Exit temperature, $T_{BR_{exit}}$	60 ºC -120 ºC

Based on the calculation as in Equation (8.2) the energy to be absorbed by jacket at the reactor temperature between 60 ℃ -120 ℃ is 2.4191 kJ.

Table 8.4 lists the energy required by the SA-IBSD reactor. The energy required by the SA-IBSD reactor is represented as follows

Section II (Endothermic): $H_{E2} \equiv Thermal\ energy$ (8.3)

In Equation 8.3, the term 'thermal energy' is used since the heating medium is not finalized either nuclear or solar energy.

Table 8.4: Total energy required for SA-IBSD reactor

SA-IBSD Reactor	Value
Energy required, $Q_{SA-IBSD}$ or H_{E2}	5.1×10^6 kJ
Operating temperature, $T_{SA-IBSD}$	800 ºC - 950 ºC
Exit temperature, $T_{SA-IBSD_{exit}}$	800 ºC - 950 ºC
Energy released at exit temperature, $Q_{HE2_{SA-IBSD}} = F_{pE2}C_{pE2}(T_{SA-IBSD_{exit}} - T_{SA-IBSD})$	2.9×10^9 kJ

where F_{pE2} and C_{pE2} are the heating medium flow rate and its specific heat capacity.

For SA-IBSD reactor, a specified amount of energy is supplied until the desired product conversion is achieve. The energy required by SA-IBSD from external thermal energy $5.1\times 10^6\ kJ$.

Table 8.5 lists the energy required for HI Decomposer. The calculation of energy required is important to ensure that the energy integration between HI decomposer and SA-IBSD reactor is feasible. The heat integration is feasible only if there is much more energy remains after it is utilized by the HI decomposer. The required energy by the HI decomposer calculation is as follows.

Section III (Endothermic): $H_{E3} = F_{sE3} C_{psE3} (\lambda_{E3})$ (8.4)

where F_{sE3} the heating element flow rate (from the SA-IBSD reactor), C_{psE3} is its heat capacity and λ_{E3} is the sensible heat.

Table 8.5: Total energy required for HI Decomposer

HI Decomposer	Value
Energy required, Q_{HI-DE} or H_{E3}	9.5×10^4 kJ
Operating temperature, T_{HI-DE}	450 ^oC -500 ^oC
Exit temperature, $T_{HI\_DE_{exit}}$	450 ^oC -500 ^oC
Balance energy remains, $Q_{HI-DE_{add}} = Q_{HI-DE} - Q_{HE2_{SA-IBSD}}$	-2.9×10^9 kJ

From calculation in Equation (8.4) it is known that the energy required to decompose hydrogen iodide is $9.5 \times 10^4\ kJ$. The energy is supplied by the exhaust thermal energy from SA-IBSD reactor in Section II.

The total energy required by the SITC plant is given as

$$H_{TE} = H_{E1} + H_{E2} + H_{E3} = 5.011 \times 10^6\ kJ \quad (8.5)$$

Based on the analysis, it is proven that the heat integration between Section II and III is feasible. Total energy releases by Section II is $2.9 \times 10^9\ kJ$. This amount is as double as the required amount of energy needed in the Section III which is only $9.5 \times 10^4\ kJ$. For Section I, there is no additional energy required since it is an exothermic reaction.

8.2.2.3 Pre-Step 3: Analysis on utilities

Based on the calculated energy requirement, H_{TE} in the previous step, the required utilities energy, E_T can be estimated as follows:

$$H_{TE} \cong E_T = 1403\ kWh$$

8.2.2.4 Pre-Step 4: Scale-up of SITC plant production

Prior to applying the scale-up procedure (see Chapter 3), each equipment is first designed individually based on laboratory scale. The scaling-up of each sections were presented in Chapter 4,5 and 6. Compilation of all unit models according to pre-defined flowsheet (unit-based approach) has been covered in Chapter 7. Once the design of all laboratory scale units is completed, they will be assembled and then the entire process flowsheet based on laboratory scale is developed and simulated. In this work, the target production rate is more than 1 tons/hr of hydrogen.

8.2.2.5 Pre-Step 5: Scale-up equipment unit

After deciding the desired production rate, the unit scale-up is carried out. The procedure is presented in Chapter 3 while the results can be retrieved from to Chapter 4 to 6. The scale-up dimension of main units are listed in Table 8.6.

Table 8.6: Scale up volume of SITC equipment

Equipment	**Maximum Volume**
Bunsen Reactor volume	300 m^3
Liquid-Liquid Separator volume	500 m^3
Sulfuric Acid Flash Tank volume	1500 m^3
SA-IBSD Reactor volume	400 m^3
Hydrogen Iodide Flash Tank volume	1500 m^3
HI Decomposer volume	200 m^3

8.2.2.6 Pre-Step 6: Dynamic model and MATLAB program simulation

Note that, the dynamic model of each unit is developed individually by mean of fundamental modelling approach (refer Chapter 4 to 6 for details). These dynamic models are translated into m-files and s-functions in MATLAB environment. After the dynamic model of each equipment is successfully converged and validated, then the individually dynamic models are assembled into a main file to form a complete process flowsheet based on the laboratory scale unit. The laboratory-scale dynamic model is then modified further, mainly on the sizing, feed flowrates and heat duties in order to form a dynamic model of the plant-scale equipment. The plantwide model is simulated via the MATLAB Simulink.

8.3 PWC Structure Development

8.3.1 Skogestad Top-down Analysis

8.3.1.1 Step 1: Cost Function and Constraints

Typically, one of the primary objectives of PWC is to achieve the pre-defined scalar cost function J that should be minimized. A typical cost function is represented as follows.

$$J = cost\ feed + cost\ utilities\ (energy) - value\ products$$

J can be written in the following form

$$P = -J = p_p P - p_{F_o} F_o - p_V V - p_D D \tag{8.6}$$

where $P(US\$/kg)$ is the profit, $p_p(US\$/kg)$ is the product price, $p_{Fo}(US\$/kg)$ the feedstock price, $p_V(US\$/kg)$ is the energy cost, and $p_D(US\$/kg)$ is the recycle cost. The fixed costs and capital costs are not included because based on the hourly timescale basis, they usually has no effect on both costs (Skogestad, 2012). The prices ($/kg) involved are listed in Table 8.7. The cost of utilities is often time varying and subjected to the location and proximity of their sources. For example, a company may purchase

the utilities or build their own utility plants; the cost will be different for different options. Meanwhile, cooling water it is often withdrawn from a nearby river and filtered or treated before use. The feedstock water however must be purified so as to avoid undesired impurities that may disrupt chemical reaction or causing damages to reactor. The utilities considered (see Table 8.7) are electricity, process and cooling water and by product credit (in this case is oxygen). The recycle cost usually can be neglected if it does not involve a gas-phase system with compression (Larsson et al., 2003).

Table 8.7: Cost of products, feedstock and utilities

Item	**Price**
Products	
Hydrogen, H_2	
Oxygen, O_2	
Total	5.26 **($/kg)**
Feedstock	
Water, H_2O	
Sulfur dioxide, SO_2	
Iodine, I_2	
Total	0.38 **($/kg)**
Utilities	
Total	0.11 (Liberatore et al., 2012) **($/kWh)**

Based on the equation (8.6) and information in Tables 8.2 and 8.7, with assumption that at least 99% of feedstock; water, sulfur dioxide and iodine, are recycled with minimum hydrogen production rate, the steady-state cost function $-J$ which is equal to gross profit, P, is as follows

$$P = -J = (5.26)(1140) - (0.38)(3900) - (0.11)(1403) \cong 4400\ US\$/hr$$

The minimum gross profit, P estimated is US$ 34,800,000 per annum. This value is including an estimates thermal energy; solar energy, (Liberatore et al., 2012) price for Section II.

8.3.1.2 Step 2: Control Degree of Freedom (CDOF) analysis

The next step in PWC structure design is the determination of control degree of freedom (CDOF), which is a step ahead after carrying out the degree of freedom (DOF) analysis. The purpose of CDOF is essentially to find out the number of input variables that can be manipulated. In many cases, the CDOF (N_m) is equal to the number of manipulated variables (Murthy Konda and Rangaiah, 2012). One of the techniques for analyzing the CDOF is the flowsheet-oriented method by (Murthy Konda et al., 2006). This technique is briefly explained as follows:

$$N_m = N_{streams} - \sum_{1}^{all\ the\ units} (N_{restraining}) - N_{redundant} \tag{8.7}$$

$N_{redundant}$ and $N_{restraining}$ are applicable in a reference table developed by Konda and Rangaiah (Murthy Konda and Rangaiah, 2012). Once the N_m is obtained, another analysis is carried out, which is the optimization of the degrees of freedom (ODOF), N_{ss}. The ODOF is the degrees of freedom that has impact on the specified cost function, $J\ (US\$/hr)$ and is given by,

$$N_{SS} = N_m - (N_{om} + N_{oy}) \tag{8.8}$$

Here, N_{0m} is the number of manipulated (input) variables which ideally shall have no steady-state effect on the cost function. On the contrary, N_{0y} is the number of output variables that need to be controlled but ideally shall have no steady-state impact on the plant cost. Table 8.8 displays the CDOF of the SITC plant. There are at most 19 CDOF and 14 ODOF identified for the SITC plant.

Table 8.8: CDOF and ODOF of SITC plant

DOF of SITC Plant	N_m	N_{0m}	N_{0y}	N_{ss}
Section				
Section I	7	0	3	4
Section II	7	0	1	6
Section III	5	0	1	4
Total	19	0	5	14
Full plant				
All 3 Sections	19	0	5	14

Following the identification 14 CDOF, the next task is to list the output variables based on the N_{ss} values. The selected controlled variables are listed in Table 8.9. The complete control structure of industrial scale SITC plant is shown in Figure 8-2.

Table 8.9: Controlled variables, manipulated variables and controller type of SITC plant

No	Controlled Variable	Manipulated Variable	Controller type
Section I			
1	Bunsen reactor temperature	Feed flow rate of cooling water	NMPC
2	Bunsen reactor conversion	Feed flow rate SO_2	NMPC
3	Bunsen reactor level	Total feed flow rate	PID
4	Heavy phase level in L-L separator	Outlet heavy phase flow of L-L separator	MSC
5	Light phase level in separating chamber of L-L separator	Inlet flowrate	MSC
Section II			
6	H_2SO_4 flash tank temperature	Feed flow rate of heating element 1	PID
7	H_2SO_4 flash tank level	Feed flow rate to flash tank	PID
8	SA-IBSD reactor temperature	Feed flow rate of external jacket	MSC
Section III			
9	HI flash tank temperature	Feed flow rate of heating element 2	PID
10	HI flash tank level	Feed flow rate to flash tank	PID
11	HI decomposer temperature	Feed flow rate of heating element	NMPC
12	Hydrogen production rate	Feed flow rate I_2/H_2O	NMPC

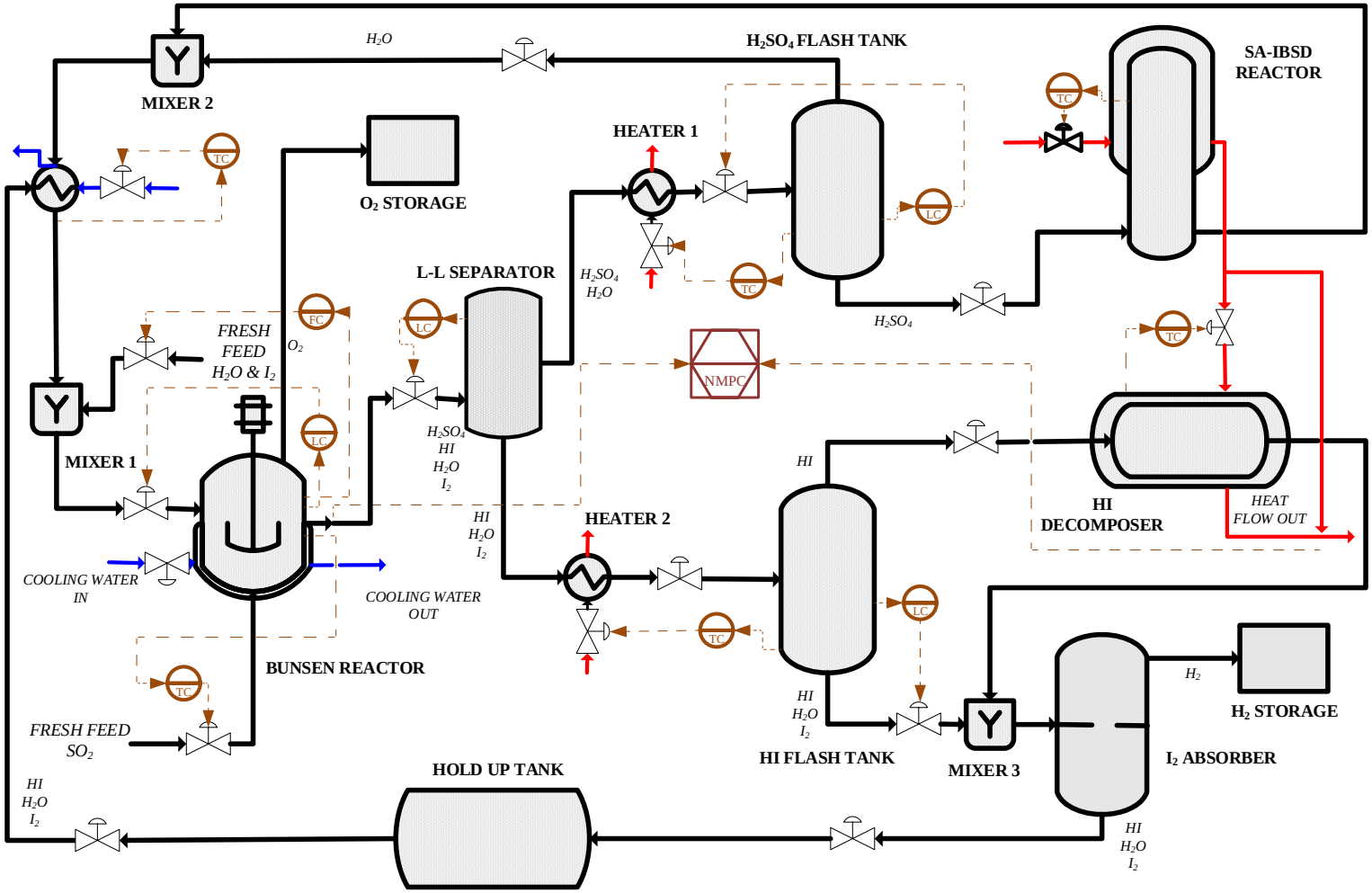

Figure 8-2: Industrial scale SITC plant with control loops

8.3.1.3 Step 3: Identify Primary Controlled Variables

The yields of main product (hydrogen) and by product (oxygen) are affected by the BR holdup liquid level, BR temperature, LLS separator holdup liquid levels, SA-FT holdup liquid level, SA-FT temperature, external jacket temperature of SA-IBSD, temperature of SA-IBSD and temperature of HI-DE. In conclusion, all of these output variables are significant and, therefore, they should output to be controlled.

8.3.1.4 Step 4: Select the Location of Throughput Manipulator (TPM)

The position of TPM is an important as it links the top-down and bottom-up parts of SOC procedure (Skogestad, 2012). In this section, the TPM is selected based on the PCA analysis (see Chapter 7, Table 7.4 and 7.5). The analysis reveal that the feed I_2/H_2O molar ratio is the most significant input affecting the SITC plant production. Therefore, the first TPM will be chosen is feed I_2/H_2O molar ratio. Table 8.10 shortlisted the potential inputs based on the PCA. Recall the process optimization described in Chapter 7 Section 7.3; by the optimization one can deduce the significant input variables having effects on the oxygen and hydrogen production rates. It follows that, both T_{oBR} and F_{SO2oBR} from Bunsen reactor are identified as the potential inputs for the TPM. Additional, there is another significant input from the SA-IBSD reactor which is the external jacket flowrate, FJ_{SAIBSD}. However, the FJ_{SAIBSD} is a utilities flow rate, hence it is not suitable as a manipulated input. Based on Skogestad (2012), the objective of TPM is to determine the amount of mass flow through the plant which can be usually expressed as a feed rate or product rate. Based on the PCA results, the significant mass flow affecting the hydrogen production is the iodine and water feeds to the Bunsen reactor. As it is desired that the reactor operating conditions (i.e.: temperature) be fixed by optimization, the best alternative choice is to select the sulphur dioxide feed flowrate as the second TPM of SITC plant. Please note that, it is quite common to have more than one TPMs for a given plant. Since both the feed I_2/H_2O molar ratio, $N_{I2/H2O}$ and feed sulfur dioxide flowrate, F_{SO2oBR} are introduced to Bunsen reactor, one may reduce these two TPMs into one TPM by specifying optimal feed

ratio of both TPMs; ratio of feed I_2/H_2O to sulfur dioxide flowrate or choosing only one TPM; either feed I_2/H_2O or sulfur dioxide flowrate. The later approached is adopted in this study. The coefficient value of PCA relate to how strong is the correlation between the input and a given output. Larger magnitude implies stronger correlation. The opposite quadrant of PCA plot implies a strong correlation.

Table 8.10: Potential inputs and their PCA coefficient values in relation to oxygen and hydrogen flowrates.

Output	**Potential Input**	**PCA Coefficient**
Oxygen Flowrate	A: T_{oBR}	0.0013
	E: F_{SO2oBR}	0.00076
	J: FJ_{SAIBSD}	-0.00038
Hydrogen Flowrate	A: T_{oBR}	-0.03
	E: F_{SO2oBR}	-0.00275
	J: FJ_{SAIBSD}	-0.0189

8.3.2 Skogestad Bottom-up Design

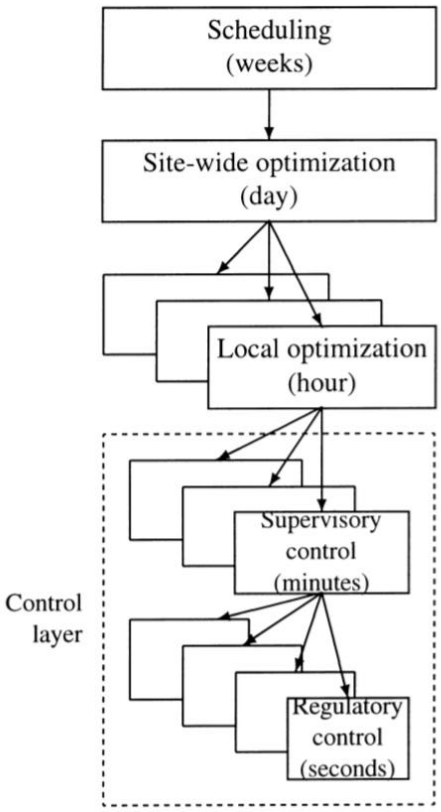

Figure 8-3: Control hierarchy of a chemical plant (Skogestad, 2000a)

Figure 8-3 depicts the typical control hierarchy in a modern chemical plant. The hierarchy consists of supervisory and regulatory layers. This control hierarchical structure can be developed based on the SOC bottom-up design as follows.

8.3.2.1 Step 5: Select the Structure of Regulatory Control Layer

The objective of regulatory control layer is to 'stabilize' the given plant, which can be achieved by controlling flow rates, liquid levels, pressures and temperatures. For the SITC plant, this regulatory control objective can be achieved by controlling the Bunsen reactor level, L-L separator level and flash tank levels. The constraints on regulatory control layer are often imposed by the higher level supervisory control layer.

8.3.2.2 Step 6: Select the Structure of the Supervisory Control Layer

The objective of supervisory control layer is to control the main production in the SITC plant. The supervisory control layer is directly linked to the economic performance of the plant. In this case, the oxygen and hydrogen production rates as well as all reactor temperatures are selected to be under the supervisory control layer. In Chapter 4, 5 and 6, NARX-MPC (NMPC) is designed for controlling the oxygen and hydrogen flowrate. To test the robustness of the NMPC in the supervisory layer, a load change is introduced for at 300th hour for a period of 100 hours to the TPM at the Bunsen reactor. Figure 8-4 shows that the controller took a while to reject the disturbance but still able to drive the hydrogen flowrate to its desired setpoint. Even under the influence of disturbance, the controller still able to maintain the hydrogen flowrate as per objective of the PWC structure where it is desired to maintain the hydrogen production rate more than 1,000 kg/hr. Figure 8-5 shows the MV profile corresponding to the robustness test. It is shown that the controller does not violate the constraints. These results prove that the NMPC controller is robust towards load change. A robust controller verifies that the selection of TPM is the right decision to obtain a self-optimize control structure.

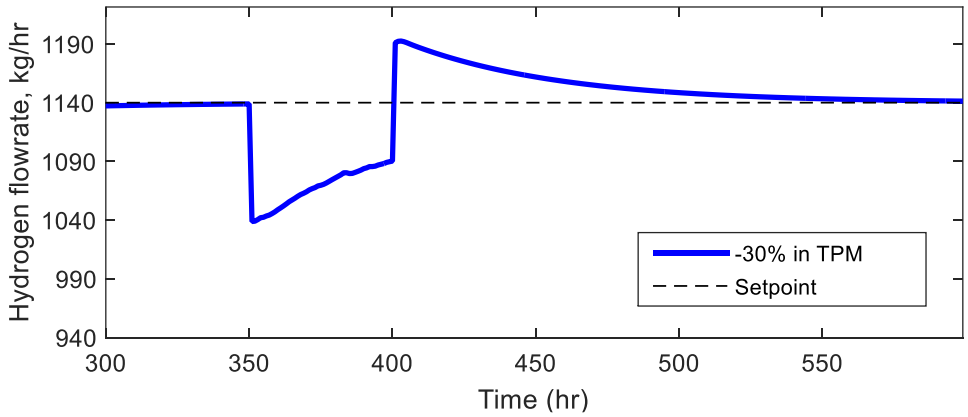

Figure 8-4: CV profile: Robustness test of NMPC for -30% load change in the TPM on hydrogen flowrate.

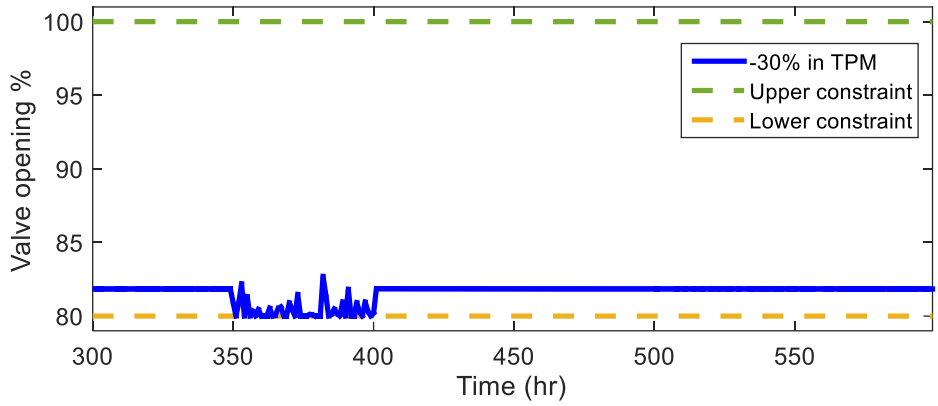

Figure 8-5: MV profile: Robustness test of NMPC for -30% load change in the TPM.

Another test is carried out which is setpoints change test. The setpoints change test objective is also to test the robustness of the NMPC in controlling both hydrogen iodide mixture, HIx and hydrogen flowrate, m_{H2}. Figures 8-6 and 8-7 demonstrate that the NMPC is able to drive the ratio of hydrogen iodide mixture, $HIx/(HI + H_2O)$ and hydrogen flowrate, m_{H2} to their desired setpoints respectively, with a fast response and no delay. The spikes in the controlled variable (CV) profiles are due to the NMPC constraint implemented to the manipulated variable (MV). The spike phenomenon is common in the MPC which has been discussed in Liuping (2009). Figure 8-8 shows the MV profiles with upper and lower limit. It is shown that the MV which is feed I_2/H_2O molar ratio is not violating the specified constraint; 0.32 to 0.54.

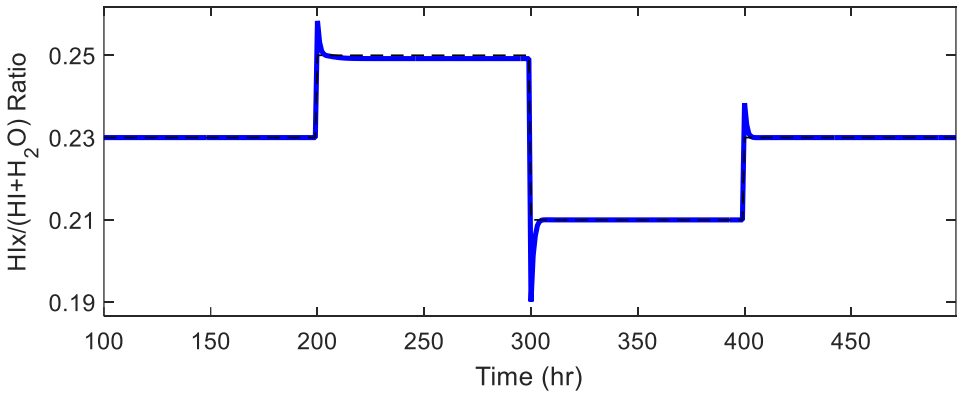

Figure 8-6: CV1 profile: Performance of NMPC for setpoint change on ratio of hydrogen iodide mixture, $HIx/(HI + H_2O)$

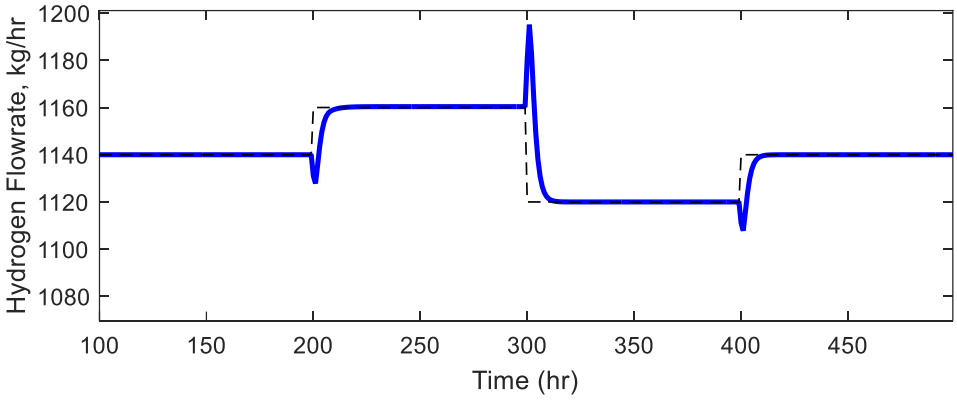

Figure 8-7: CV2 profile: Performance of NMPC for setpoint change on hydrogen flowrate, m_{H2}

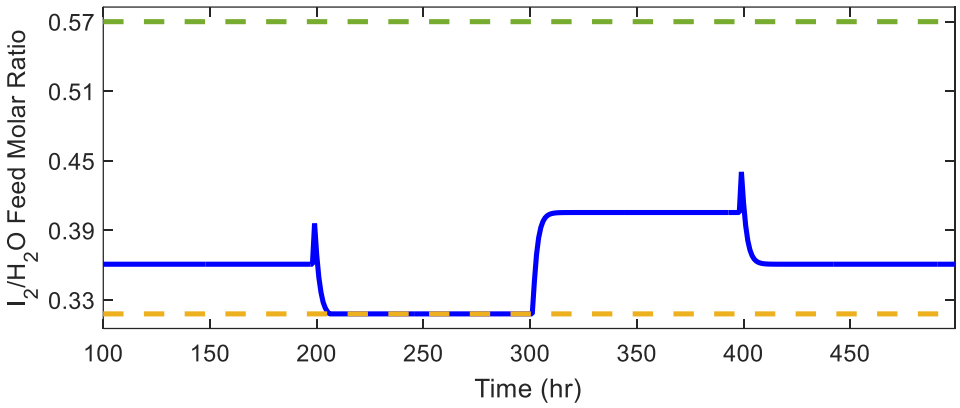

Figure 8-8: MV profile: Performance of NMPC for setpoint change on the feed I_2/H_2O molar ratio.

8.3.2.3 Step 7: Select the Structure of Optimization Layer

In the industry, the trade-off between optimality and practicality presents a difficult assessment to make (Downs, 2012). In this work, the optimality is defined as achieving the optimum production rate by setting the optimum input (operating parameters). Oppositely, the practicality is another feature that covers a wide range of definitions where one of them may be represented by controllability feature. Since there is a no work on the optimality and practicality assessments of the SITC industrial plant in the literature, this study proposed an optimization function to achieve the trade-off for both features namely Optimal-Practical Plant Wide (OPPWIDE) optimization.

The OPPWIDE optimization function, $J_{OPPWIDE}$ is to achieve a trade-off between optimum steady-state economic (represents optimality) and dynamic controllability (represents practicality) of the SITC plant. Figure 8-9 presents the flowchart of OPPWIDE optimization approach. The optimality feature identifies the optimum values of the operating and design parameters. The objective is to seek the effect of each variable onto the plant operation to achieve optimum production profit. Meanwhile, the practicality

feature is based on the controllability index; a higher LGC value represents a more controllable plant.

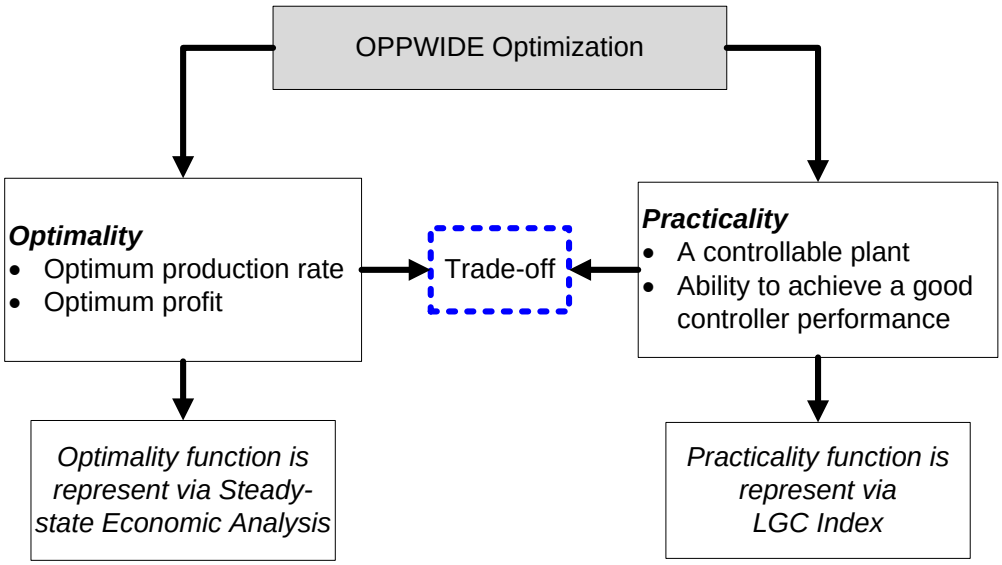

Figure 8-9: Flowchart of OPPWIDE optimization approach

8.3.2.3.1 Twin Plot SOC Method

Twin Plot SOC method is a tool applied in the OPPWIDE optimization procedure. The objective of Twin Plot SOC method is to obtain self-optimize cost function, J_{SOC}, of a particular plant. There are two plots involved in this method, (1) Skogestad's SOC plot, (2) PCA Pareto plot. Figure 8-10 shows a Skogestad SOC plot. This plot illustrates loss imposed by changing the setpoint; CV. It is desired that the cost function is kept at an optimal value if a disturbance is introduced. This idea is known as 'self-optimizing' control. In Figure 8-10, the one with smaller amount of loss is a preferable choice of cost function. In this case it is clear that J_B has a smaller amount of loss as compare to J_A. The next step is to find the manipulated variable (MV) to obtain a self-optimize cost function as J_B. The selection of MV will be based on the second plot; PCA Pareto plot.

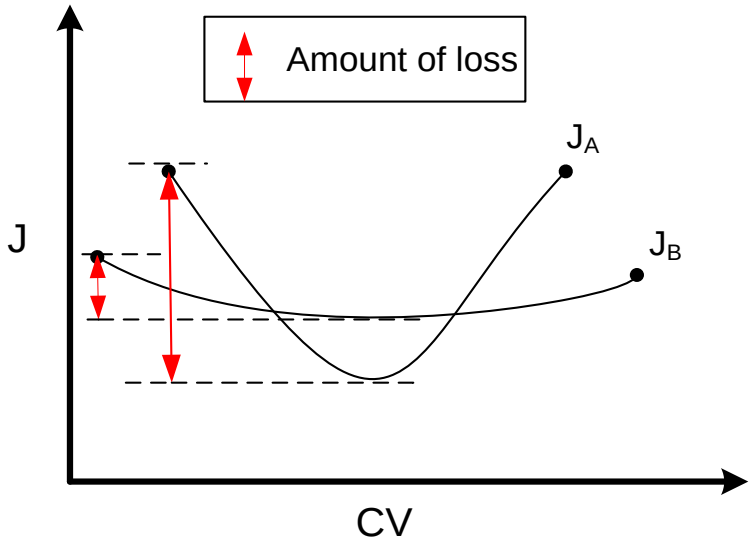

Figure 8-10: Skogestad SOC plot

Figure 8-11 illustrates a PCA Pareto plot. A PCA Pareto plot consists of four quadrants, i.e., quadrant A, quadrant B, quadrant C and quadrant D. Quadrant A and D are opposite, as well as quadrant B and C. There are two criteria of a variables correlation, (1) variables in the same quadrant (2) variables in the opposite quadrant, e.g., variables in quadrant B are correlated to variables in quadrant C. As can be seen from Figure 8-11, quadrant B has three variables which are controlled variable 1 (CV1), controlled variable 2 (CV2), and a cost function, *J*. Based on this plot, one may deduce that the variables *J*, CV1 and CV2 (quadrant B) are highly correlated to variables MV1 and MV2 (quadrant C) since they are in the opposite quadrant. The length of each variable represents a coefficient value. A longer variable represents higher coefficient value. Hence it has a greater influence onto the variables in the opposite quadrant and its own quadrant. In this case, CV1 has a greater effect on the process as compare to CV2. Therefore, CV1 is chosen as the primary control variable. In order to control CV1, a manipulated variable (MV) will be selected from the quadrant C. MV2 has a smaller PCA coefficient than MV1 (see Figure 8-11; MV2 is shorter than MV1) indicating that MV2 has a smaller correlation to CV1 as compare to MV1.

Hence, MV2 is a preferable manipulated variable for CV1. As a result, a self-optimize cost function is obtained where J_B is a function of CV1 and MV2.

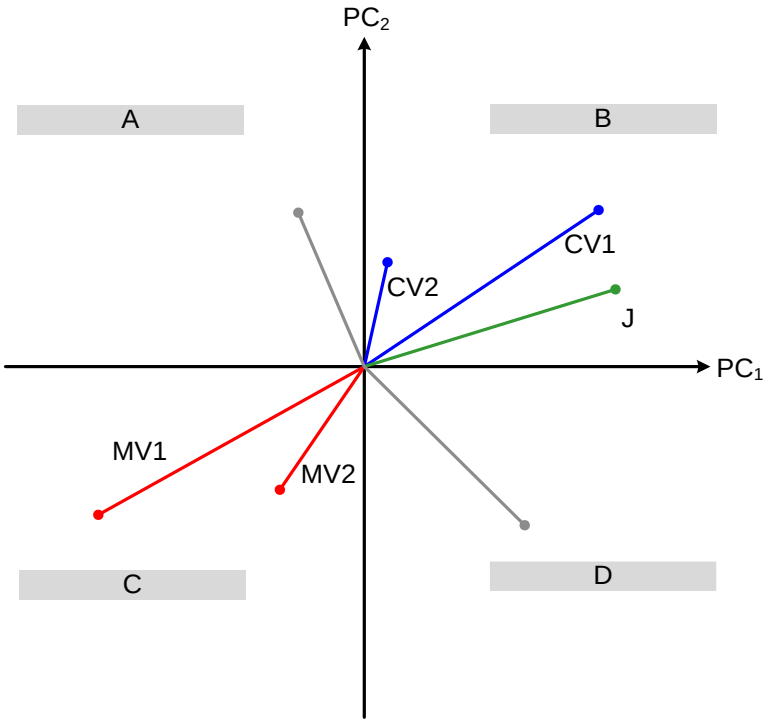

Figure 8-11: PCA Pareto plot

In this work, the manipulated variables and controlled variables for LGC index are selected based on Twin Plot SOC method. This method will help to reduce the number of variables to be included in the PWC structure, hence saving a lot of time (due to reduced complexity) and simulation effort. The application of Twin Plot SOC method and LGC index is the reason why the OPPWIDE optimization is a unique and efficient way to perform a PWC optimization. Table 8.11 shows the optimization results of two SITC models. Model 1 is optimized based on the PWC structure. Model 2 is optimized based on solely sensitivity study analysis. For Model 1, the LGC index is 0.1096. This indicates that the Model 1 is controllable. The smaller the value of LGC (less than unity) means the harder to control the system using the conventional PID controller. While the profit corresponding to Model 1 is $ 8070 per hour, demonstrated that Model 1 is a profitable model scheme. The profit

(economic) of Model 2 is comparable to that of Model 1. However, for Model 2, the LGC is negative. This implies that the system based on Model 2 is not controllable. Therefore, it is made to known that a profitable plant is not an assurance that it is a controllable plant. By applying the proposed optimization method, one is able to seek for a profitable yet controllable plant scheme. It this case it is proven that the control structure developed based on PWC structure satisfies both optimality (economic) and practicality (controllability) performance criteria.

Table 8.11: The optimization performance of two SITC models.

SITC model		**Controllability performance (LGC) (ψ_1)**	**Economic performance ($/hr H_2) (ψ_2)**
Model 1			
MV1: Feed molar ratio I_2/H_2O MV2: Feed flowrate sulfur dioxide	CV1: Hydrogen flowrate CV2: Temperature HI-DE reactor	0.1096	8070
Model 2			
MV1: Feed molar ratio I_2/H_2O MV2: Feed flowrate sulfur dioxide	CV1: Hydrogen flowrate CV2: Temperature HI-DE reactor	-1.009	8019

8.4 PWC Performance Assessment

In 2012, Liberatore et al. (2012) carried out an economic and energy analyzes for a solar energy based industrial scale SITC plant. The SITC plant by Liberatore et al. (2012) was designed for a production capacity of 100 metric ton/day of hydrogen, which achieved 34% thermal efficiency with the hydrogen production cost of 10.25 $/kg.

By applying the SOC PWC structure on the presently developed SITC plant, the thermal efficiency that can be achieved at the maximum production rate of hydrogen (2400 kg/hr H_2) is calculated as follows:

$$\eta = \frac{H_{HHV}}{H_{heat2400kg/hrH2}} = \frac{285.8\ kJ/mol}{416.7\ kJ/mol} H_2 = 0.686$$

while at a minimum production rate (1140 kg/hr H_2) is,

$$\eta = \frac{H_{HHV}}{H_{heat1140kg/hrH2}} = \frac{285.8\ kJ/mol}{869.6\ kJ/mol} H_2 = 0.329$$

Note that, H_{HHV} denotes the higher heating value of H_2 and

H_{heat} the heat required to produce the desired hydrogen production rate (calculated based on preliminary PWC steps).

As shown by the above calculations, the achievable thermal efficiency for the proposed SITC plant lies between 32.9% and 68.6%. It should be noted that, by applying process optimization and efficient controller design, the plant thermal efficiency can be increased beyond the currently reported values in the literature. The gross profit is estimated to be US$ 34,800,000 per annum with the hydrogen production cost of 4.19 $/kg. The production cost has assumed that the external heating energy for Section II is similar to the value in Liberatore et.al (2012). As compared to the work of Liberatore et.al (2012), it is shown that the application of the PWC is able to reduce the production cost of hydrogen via the SITC

process. This result is parallel to the main property of SOC, where the configuration of the supervisory layer and regulatory layer shall decrease the losses due to reactor operations (manipulated variables) (Seki and Naka, 2008).

8.5 Summary

The summary of Chapter 8 is as follows,

a) There is a number of PWC development methods available in the literature but very little work has been reported on the PWC preliminary steps. The application of PWC preliminary steps prior to applying an established PWC structure development enables us to check for a practical PWC structure for the SITC plant that has not yet existed at the industrial scale.
b) This work proposed a Twin Plot SOC method embedded into a new PWC optimization method (OPPWIDE) to access self-optimizing cost function.
c) Simulation result showed that the performance of the SITC plant under the developed SOC structure is better in terms of controllability and economic than that of the unit-based PWC structure (Chapter 7). It is worth highlighting that, under the given SOC structure, the SITC plant can attain a maximum production capacity of 2,400 kg/hr of hydrogen with a thermal efficiency reaching up to 69%. Presently, the highest thermal efficiency of a SITC plant reported in the literature is 34% (Liberatore et.al. 2012). At the minimum production rate of about 1,000 kg/hr of hydrogen, the gross profit was estimated to be US$ 34.8 million per annum with the hydrogen production cost of 4.18 $/kg.

9 Conclusion and Recommendations

9.1 Conclusions

In this PhD study, several open questions pertaining to the SITC have been addressed:

a) Which section/s in the SITC plant that impose the most difficult challenges (i.e., bottleneck) to the operation and control of the plant?
b) Will the heat integration between sulfuric acid decomposition and hydrogen iodide decomposition sections be technically feasible?
c) How to efficiently analyze the controllability of the SITC plant?
d) What is the workable PWC structure of the industrial SITC plant?

The answers to the above mentioned questions are summarized in the following sections.

9.1.1 Development of Industrial Scale of SITC Plant Flowsheet

In this work, the dynamic models of all the major units in the SITC sections have been developed based on the fundamental approach as presented in Chapters 4, 5 and 6. These unit models have been combined to represent a complete SITC plant. Based on the extensive simulation (unit-based and plantwide), it has been revealed that the Section I (Bunsen reactor) imposes the most difficult challenges (bottlenecks) to the operation and control of the plant. One of the challenges is to ensure that the HIx solution is always well above the azeotropic compositions. Otherwise, the failure to do so will cause the plant operation to fail, i.e., the flash tank will not be able to achieve required separation between HI and water. Since it has been shown via the LGC analysis that the Bunsen reactor cannot be effectively controlled using the traditional PID control system, i.e., due to the critical constraints and nonlinearity, a nonlinear MPC has been used instead. This nonlinear MPC has demonstrated capability to providing effective control of this reactor, hence making the plant operation smooth and reliable (shown by plantwide simulation, Chapter 8).

Pertaining to the second question above, a steady-state analysis conducted in Chapter 8 has shown that it is possible to apply a simple heat integration between Section II and III. In other words, the heating medium leaving the SA-IBSD reactor (Section II) possesses more than enough thermal energy than what is required by the hydrogen iodide reactor (Section III). It should be noted that, this simple heat integration has substantially reduced the total amount of high-temperature thermal energy input, hence increasing the thermal efficiency up to 69% when the plant is running at its maximum capacity of 2,400 kg/hr (or 58 ton/day) of hydrogen. Even when the plant is running at its minimum (baseline) production capacity of 1,000 kg/hr (24 ton/day) of hydrogen, the gross profit attainable is equivalent to US$ 37.8 million per annum; at this minimum production capacity, the thermal efficiency is 33%. Note that, the total investment cost to building the SITC plant that is capable of producing maximum 58 ton/day of hydrogen was estimated to be US$114 million. It is important to point out that, the plant performance is guaranteed under the implemented Self-Optimizing Control (SOC) structure, which ensures minimum loss of the economic (profit) in the face of disturbances. As a result, the proposed SITC flowsheet has successfully demonstrated a stable and economical operation.

9.1.2 Process Optimization and Controllability Analysis of SITC Process

In order to answer the third question above, process optimization and controllability analyses have been conducted on all sections and the entire SITC plant. Results from the process optimization suggest that the main product (hydrogen) and by product (oxygen) are affected mostly by the variables from the Bunsen Section. By using the LGC index, we have managed to identify the most suitable control configuration and type for each SITC section. In addition to assessing the controllability of each section, the LGC index has also been used to assess the controllability of the overall SITC plant – it has been shown that the SOC implementation can give better controllability performance than that of the unit-based control structure/strategy.

9.1.3 PWC Structure Development of the SITC Process

Finally, to answer the fourth question above, plantwide control (PWC) design based on the SOC structure approach has been performed. The governing concept of SOC structure is to find suitable sets of manipulated and controlled variables, which lead to minimum loss of cost function (i.e., in the present study, gross profit) in the face of disturbances and setpoint changes. Before applying the SOC structure method, a PWC preliminary procedure has been proposed. After the execution of PWC preliminary procedure, the next task was to identify the control structure which gives a minimum economic loss. Note that, in the original Skogestad's SOC structure method, the optimization technique was proposed to obtain the suitable structure. However, the method on how to find a cost function with a minimum loss is still an open ended question. To facilitate the finding of the suitable structure, this work proposed a Twin Plot SOC method embedded into a new PWC optimization method (OPPWIDE) to access the self-optimizing cost function. Thus, a modified SOC structure method (Chapter 8).

By using this modified SOC structure method, it is quite easy to identify the suitable sets of manipulated and controlled variables which possess the self-optimizing characteristic. Indeed, based on the performance evaluation, it has been shown that the SITC plant developed based on the proposed SOC structure can produce better performance in terms of controllability and economic as compared to the unit-based structure. Most importantly, the developed SITC industrial plant based on the PWC structure has demonstrated a high thermal efficiency up to 69%. To the best of our knowledge, this thermal efficiency is higher than the presently highest value reported in the literature, i.e., 34%.

9.1.4 New Contributions

Some new contributions made in this PhD work can be summarized as follows:

a) A novel controllability analysis called the Loop Gain Controllability (LGC) index. The LGC index can be used to assess the controller pairings which possess the highest performance margin. This index can be used together with the traditional RGA analysis.
b) A complete industrial scale SITC plant design with PWC control strategy. Both economics and controllability factors have been taken into consideration in the flowsheet design.
c) A plantwide dynamics model of the SITC plant. Most analysis reported in the literature only relies on the steady-state model, i.e., applicable to steady-state economic analysis only. The developed SITC plantwide model (in MATLAB) allows for rigorous dynamics simulation, thus enabling the evaluation of a given control strategy. MATLAB environment has been chosen since some of the reactor configurations and kinetics used in the model cannot be run on some commercial software, e.g., Aspen Plus.
d) Modified Self-Optimizing Control Structure method. The modification enables easy identification of the suitable sets of manipulated and controlled variables via the RSM and PCA.
e) Optimal-Practical Plantwide optimization (OPPWIDE) methodology. This work proposed a Twin Plot SOC method embedded into a new PWC optimization method (OPPWIDE) to access the self-optimize cost function (Chapter 8). The application of Twin Plot SOC method and LGC index made the OPPWIDE optimization as an exceptional and efficient way to perform PWC optimization.

From this study, we can conclude that the implementation of an industrial scale of SITC plant capable of producing minimum 24 tons/day to maximum 58 ton/day of hydrogen is viable, on the grounds of economics and controllability (optimality and practicality). However, it should be noted that this evaluation is based on some limited assumptions due to the presently lack of data on the materials of constructions for some units in the plant. Thus, for an example, we have assumed that the materials of construction for the SA-IBSD

reactor is available and can stand the high pressure, temperature and corrosive conditions in this reactor. Recommendations for future study presented in the next section.

9.2 Recommendations

The following are some recommendations for possible future research to expand the current study.

a) **Multi-scale dynamic modelling**. The study of the process behavior of each equipment in the SITC could be expanded to the multi scale dynamic modelling. For example, an extensive study on the modelling and design of SA-IBSD and HI-DE reactors would be able to give deeper understanding on the SITC process. This will improve the control development process because they might give great impact whether the process is exhibiting problematic dynamics among its variables that imposes severe limitations on the control system performance.

b) **Explore the plantwide control study based on different flowsheets**. Beside the proposed flowsheet in this work, there are a few other flowsheets for the SITC plant. A number of current available flowsheets use reactive distillation or electro-dialysis for acid purification. The modified SOC structure method can be used for these different flowsheets.

c) **Expanding the economic assessment of SITC plant**. In this work, the type of external thermal energy source is not finalized due to a few limitations. The economic assessment can be expanded further by integrating the external thermal energy to the plant. The developed industrial SITC plant on this work can be integrated to either a nuclear, solar or hydroelectric power plant and the economic assessment can be carried out.

References

Abbasi, T., Abbasi, S. a., 2011. “Renewable” hydrogen: Prospects and challenges. Renew. Sustain. Energy Rev. 15, 3034–3040. doi:10.1016/j.rser.2011.02.026

Adamantiades, A., Kessides, I., 2009. Nuclear power for sustainable development: Current status and future prospects. Energy Policy 37, 5149–5166. doi:10.1016/j.enpol.2009.07.052

Al-Dabbagh, A.W., Lu, L., 2010. Dynamic flowgraph modeling of process and control systems of a nuclear-based hydrogen production plant. Int. J. Hydrogen Energy 35, 9569–9580. doi:10.1016/j.ijhydene.2010.06.059

Alberto, L., Suárez, P., Georgieva, P., Feyo, S., Azevedo, D., 2010. Chemical Engineering Research and Design Nonlinear MPC for fed-batch multiple stages sugar crystallization 9, 753–767. doi:10.1016/j.cherd.2010.10.010

Almogren, S., Veziroglu, T.N., 2004. Solar-hydrogen energy system for Saudi Arabia. Int. J. Hydrogen Energy 29, 1181–1190. doi:10.1016/j.ijhydene.2003.11.010

Ananthraman, R., Bolland, O., Gundersen, T., 2010. Energy Integration of an IGCC Plant for Combined Hydrogen and Electricity Production — Methodology and Tools Integration. Taylor and Francis Group.

Andress, R.J., Huang, X., Bequette, B.W., Martin, L.L., 2009. A systematic methodology for the evaluation of alternative thermochemical cycles for hydrogen production. Int. J. Hydrogen Energy 34, 4146–4154. doi:10.1016/j.ijhydene.2008.11.118

Arefi, M.M., Montazeri, A., Poshtan, J., Jahed-Motlagh, M.R., 2008. Wiener-neural identification and predictive control of a more realistic plug-flow tubular reactor. Chem. Eng. J. 138, 274–282. doi:10.1016/j.cej.2007.05.044

Ashoori, A., Moshiri, B., Khaki-sedigh, A., Reza, M., 2009. Optimal control of a nonlinear fed-batch fermentation process using model predictive approach. J. Process Control 19, 1162–1173. doi:10.1016/j.jprocont.2009.03.006

Baykara, S.Z., 2004. Hydrogen production by direct solar thermal decomposition of water, possibilities for improvement of process efficiency. Int. J. Hydrogen Energy 29, 1451–1458. doi:10.1016/j.ijhydene.2004.02.014

Bennur, R., Dhere, N., 2008. Use of Solar Energy to Produce Hydrogen, in: Hydrogen Fuel. CRC Press, pp. 227–282. doi:doi:10.1201/9781420045772.ch7

Chang, J., Shin, Y., Lee, K., Kim, Y., Youn, C., 2012. Development of a dynamic simulation code for the sulfur-iodine process coupled to a very high-temperature gas-cooled nuclear reactor. Simulation 89, 139–155. doi:10.1177/0037549712464716

Chin, W., Song, H., Lee, J.H., Ramkrishna, D., 2010. Control Engineering Practice Hybrid cybernetic model-based simulation of continuous production of lignocellulosic ethanol : Rejecting abruptly changing feed conditions. Control Eng. Pract. 18, 177–189. doi:10.1016/j.conengprac.2009.09.002

Cho, W.C., Park, C.S., Kang, K.S., Kim, C.H., Bae, K.K., 2009. Conceptual design of sulfur-iodine hydrogen production cycle of Korea Institute of Energy Research. Nucl. Eng. Des. 239, 501–507. doi:10.1016/j.nucengdes.2008.11.017

Choi, J.Y., Kim, Y.S., Sah, I., No, H.C., Jang, C., 2014a. Corrosion resistances of alloys in high temperature hydrogen iodide gas environment for sulfur-iodine thermochemical cycle. Int. J. Hydrogen Energy 39, 14557–14564. doi:10.1016/j.ijhydene.2014.07.082

Choi, J.Y., No, H.C., Kim, Y.S., 2014b. Stability of nickel catalyst supported by mesoporous alumina for hydrogen iodide decomposition and hybrid decomposer development in sulfur-iodine hydrogen production cycle. Int. J. Hydrogen Energy 39, 3606–3616. doi:10.1016/j.ijhydene.2013.12.153

Choi, J.Y., NO, H.C., Kim, Y.S., 2014c. Stability of nickel catalyst supported by mesoporous alumina for hydrogen iodide decomposition and hybrid decomposer development in sulfur–iodine hydrogen production cycle. Int. J. Hydrogen Energy 39, 3606–3616. doi:10.1016/j.ijhydene.2013.12.153

Chonwattana, W., Panjapornpon, C., Tawai, A., Dechakupt, T., 2018. Model-based estimation and control of interface level in a two-phase vertical decanter: A case study of palm-oil/water system. Comput. Chem. Eng. 108, 372–381. doi:10.1016/j.compchemeng.2017.10.022

Cipriani, G., Di Dio, V., Genduso, F., La Cascia, D., Liga, R., Miceli, R., Ricco Galluzzo, G., 2014. Perspective on hydrogen energy carrier and its automotive applications. Int. J. Hydrogen Energy 39, 8482–8494. doi:10.1016/j.ijhydene.2014.03.174

Costa, A.C., Meleiro, L.A.C., Filho, R.M., 2002. Non-linear predicti v e control of an extracti v e alcoholic fermentation process 38, 743–750.

Deepa, S.N., Baranilingesan, I., 2017. Optimized deep learning neural network predictive controller for continuous stirred tank reactor. Comput. Electr. Eng. 0, 1–16. doi:10.1016/j.compeleceng.2017.07.004

Deshpande, A.P., Patwardhan, S.C., Narasimhan, S.S., 2009. Intelligent state estimation for fault tolerant nonlinear predictive control. J. Process Control 19, 187–204. doi:10.1016/j.jprocont.2008.04.006

Doizi, D., Dauvois, V., Roujou, J.L., Delanne, V., Fauvet, P., Larousse, B., Hercher, O., Carles, P., Moulin, C., Hartmann, J.M., 2007. Total and partial pressure measurements for the sulphur-iodine thermochemical cycle. Int. J. Hydrogen Energy 32, 1183–1191. doi:10.1016/j.ijhydene.2006.11.039

Don, W.G., Perry, R.H., 1984. Perry’s Chemical Engineers Handbook. McGraw-Hill, New York.

Dote, Y., Ovaska, S.., 2001. Industrial applications of soft computing: a review, in: IEEE. pp. 1243–1265.

Downs, J.J., 2012. Industrial Perspective on Plantwide Control, in: Rangaiah, G.P., Kariwala, V. (Eds.), Plantwide Control: Recent Developments and Applications. John Wiley and Sons Ltd, pp. 11–17.

Downs, J.J., Skogestad, S., 2009. An industrial and academic perspective on plantwide control. IFAC Proc. Vol. 7, 117–128. doi:10.1016/j.arcontrol.2011.03.006

Duigou, A. Le, Borgard, J.M., Larousse, B., Doizi, D., Allen, R., Ewan, B.C., H. Priestman, G., Elder, R., Devonshire, R., Ramos, V., Cerri, G., Salvini, C., Giovannelli, A., De Maria, G., Corgnale, C., Brutti, S., Roeb, M., Noglik, A., Rietbrock, P.M., Mohr, S., de Oliveira, L., Monnerie, N., Schmitz, M., Sattler, C., Martinez, A.O., de Lorenzo Manzano, D., Cedillo Rojas, J., Dechelotte, S., Baudouin, O., 2007. HYTHEC: An EC funded search for a long term massive hydrogen production route using solar and nuclear technologies. Int. J. Hydrogen Energy 32, 1516–1529. doi:10.1016/j.ijhydene.2006.10.047

Fino, D., 2014. Advances in Hydrogen Production, Storage and Distribution, Advances in Hydrogen Production, Storage and Distribution. Elsevier. doi:10.1533/9780857097736.1.85

Froisy, J.B., 2006. Model predictive control — Building a bridge between theory and practice 30, 1426–1435. doi:10.1016/j.compchemeng.2006.05.044

Funk, J.E., 2001. Thermochemical hydrogen production: Past and present. Int. J. Hydrogen Energy 26, 185–190. doi:10.1016/S0360-3199(00)00062-8

Gabbar, H. a., Hussain, S., Hosseini, A.H., 2014. Simulation-based fault propagation analysis-Application on hydrogen production plant. Process Saf. Environ. Prot. 92, 723–731. doi:10.1016/j.psep.2013.12.006

Garcia, C.E., Prett, D.M., Morari, M., 1989. Model predictive control: Theory and practice-a survey,. Automatica 335–348.

Goldstein, S., Borgard, J.M., Vitart, X., 2005. Upper bound and best estimate of the efficiency of the iodine sulphur cycle. Int. J. Hydrogen Energy 30, 619–626. doi:10.1016/j.ijhydene.2004.06.005

Guo, H., Kasahara, S., Onuki, K., Zhang, P., Xu, J., 2011. Simulation study on the distillation of hyper-pseudoazeotropic HI-I 2-H2O mixture. Ind. Eng. Chem. Res. 50, 11644–11656. doi:10.1021/ie200448m

Guo, H., Zhang, P., Chen, S., Wang, L., Xu, J., 2014. Review of Simulation Methods of the Distillation Column and Thermodynamic Models in the Hi Decomposition Section of the Iodine-Sulfur Process. Chem. Eng. Commun. 201, 751–789. doi:10.1080/00986445.2013.790814

Guo, H., Zhang, P., Lan, S., Chen, S., Wang, L., Xu, J., 2012. Study on the phase separation characteristics of HI–I2–H2SO4–H2O mixture at 20°C. Fluid Phase Equilib. 324, 33–40. doi:10.1016/j.fluid.2012.03.019

Guo, Y., Wang, S., Huelsman, C.M., Savage, P.E., 2014. Kinetic model for reactions of indole under supercritical water gasification conditions. Chem. Eng. J. 241, 327–335. doi:10.1016/j.cej.2013.11.012

Guthrie K.M. Capital Cost Estimating. Chem. Eng., 76(6), pp. 114-142 (1969).

Gupta, R., Pant, K.K., 2008a. Hydrogen Storage in Metal Hydrides, in: Hydrogen Fuel. CRC Press, pp. 381–407. doi:doi:10.1201/9781420045772.ch11

Gupta, R., Pant, K.K., 2008b. Fundamentals and Use of Hydrogen as a Fuel, in: Hydrogen Fuel. CRC Press, pp. 2–32. doi:doi:10.1201/9781420045772.ch1

Harris, T.., Yu, W., 2007. Controller assessment for a class of nonlinear system. J. Process

Control 17, 607–619.

Haykin, S., 1999. Neural Networks: A Comprehensive Foundation, Second. ed. Prentice-Hall International, Englewood Cliffs.

Henson, M.A., 2003. Dynamic modeling and control of yeast cell populations in continuous biochemical reactors 27, 1185–1199. doi:10.1016/S0098-1354(03)00046-2

Hodotsuka, M., Yang, X., Okuda, H., Onuki, K., 2008. Vapor−Liquid Equilibria for the HI + H_2O System and the HI + H_2O + I_2 System. J. Chem. Eng. Data 53, 1683–1687. doi:10.1021/je700544w

Hong, T., Zhang, J., Morris, A.J., Martin, E.B., Karim, M.N., n.d. Neural Based Predictive Control of a Multivariable Microalgae Fermentation 345–350.

Huang, C., T-Raissi, A., 2005. Analysis of sulfur-iodine thermochemical cycle for solar hydrogen production. Part I: Decomposition of sulfuric acid. Sol. Energy 78, 632–646. doi:10.1016/j.solener.2004.01.007

Japan Atomic Energy Agency (JAEA) [WWW Document], 2017. URL https://www.jaea.go.jp/04/o-arai/nhc/en/_top/top.htm (accessed 11.14.17).

Jonghwa, C.;, Yong-Wan, K.;, KI-Young, L.;, Lee, Y.-W., Won Jae, L., Jae-Man, N., Min-Hwan, K., Hong-Sik, L., Young-Joon, S., KI-Kwang, B., Jung, K.-D., 2007. A Study of Nuclear Hydrogen Production Demonstration Plant. Nucl. Eng. Technol. 39, 111–122.

Karami, G., Amidpour, M., Sheibani, B.H., Salehi, G.R., 2015. Distillation column controllability analysis through heat pump integration. Chem. Eng. Process. Process Intensif. 97, 23–37. doi:10.1016/j.cep.2015.08.005

Kasahara, S., Iwatsuki, J., Takegami, H., Tanaka, N., Noguchi, H., Kamiji, Y., Onuki, K.,

Kubo, S., 2017. Current R&D status of thermochemical water splitting iodine-sulfur process in Japan Atomic Energy Agency. Int. J. Hydrogen Energy 42, 13477–13485. doi:10.1016/j.ijhydene.2017.02.163

Kasahara, S., Kubo, S., Hino, R., Onuki, K., Nomura, M., Nakao, S.I., 2007. Flowsheet study of the thermochemical water-splitting iodine-sulfur process for effective hydrogen production. Int. J. Hydrogen Energy 32, 489–496. doi:10.1016/j.ijhydene.2006.05.005

Kim, C.S., Hong, S.D., Kim, Y.W., Kim, J.H., Jae Lee, W., Chang, J., 2008. Thermal design of a laboratory-scale SO3 decomposer for nuclear hydrogen production. Int. J. Hydrogen Energy 33, 3688–3699. doi:10.1016/j.ijhydene.2008.04.049

Kim, Y.S., No, H.C., Choi, J.Y., Yoon, H.J., 2013. Stability and kinetics of powder-type and pellet-type iron (III) oxide catalysts for sulfuric acid decomposition in practical Iodine-Sulfur cycle. Int. J. Hydrogen Energy 38, 3537–3544. doi:10.1016/j.ijhydene.2013.01.039

Kookos, I.K., Perkins, J.D., 2002. Regulatory control structure selection of linear systems. Comput. Chem. Eng. 26, 875–887. doi:10.1016/S0098-1354(02)00013-3

Kubo, S., Nakajima, H., Kasahara, S., Higashi, S., Masaki, T., Abe, H., Onuki, K., 2004. A demonstration study on a closed-cycle hydrogen production by the thermochemical water-splitting iodine - Sulfur process. Nucl. Eng. Des. 233, 347–354. doi:10.1016/j.nucengdes.2004.08.025

Kubo, S., Tanaka, N., Iwatsuki, J., Kasahara, S., Imai, Y., Noguchi, H., Onuki, K., 2012. R&D status on thermochemical IS process for hydrogen production at JAEA. Energy Procedia 29, 308–317. doi:10.1016/j.egypro.2012.09.037

Lan, S.R., Guo, H.F., Zhang, P., Chen, S.Z., Wang, L.J., Xu, J.M., 2013. Phase separation characteristics of HI-I-2-H2SO4-H2O mixture at elevated temperatures. Fluid Phase

Equilib. 342, 1–7. doi:DOI 10.1016/j.fluid.2012.12.015

Larsson, T., Govatsmark, M.S., Skogestad, S., Yu, C.C., 2003. Control structure selection for reactor, separator, and recycle processes. Ind. Eng. Chem. Res. 42, 1225–1234. doi:10.1021/ie0200860

Larsson, T., Skogestad, S., 2000. Plantwide control - a review and a new design procedure. Model. Identif. Control 21, 209–240. doi:10.4173/mic.2000.4.2

Lattin, W.C., Utgikar, V.P., 2009. Global warming potential of the sulfur-iodine process using life cycle assessment methodology. Int. J. Hydrogen Energy 34, 737–744. doi:10.1016/j.ijhydene.2008.10.059

Lee, B.J., Cheon NO, H., Joon Yoon, H., Jun Kim, S., Soo Kim, E., 2008a. An optimal operating window for the Bunsen process in the I-S thermochemical cycle. Int. J. Hydrogen Energy 33, 2200–2210. doi:10.1016/j.ijhydene.2008.02.045

Lee, B.J., Cheon NO, H., Joon Yoon, H., Jun Kim, S., Soo Kim, E., 2008b. An optimal operating window for the Bunsen process in the I-S thermochemical cycle. Int. J. Hydrogen Energy 33, 2200–2210. doi:10.1016/j.ijhydene.2008.02.045

Lee, B.J., No, H.C., Yoon, H.J., Jin, H.G., Kim, Y.S., Lee, J.I., 2009. Development of a flowsheet for iodine-sulfur thermo-chemical cycle based on optimized Bunsen reaction. Int. J. Hydrogen Energy 34, 2133–2143. doi:10.1016/j.ijhydene.2009.01.006

Levene, J.I., Mann, M.K., Margolis, R.M., Milbrandt, A., 2007. An analysis of hydrogen production from renewable electricity sources. Sol. Energy 81, 773–780. doi:10.1016/j.solener.2006.10.005

Liberatore, R., Lanchi, M., Giaconia, A., Tarquini, P., 2012. Energy and economic assessment of an industrial plant for the hydrogen production by water-splitting through the sulfur-iodine thermochemical cycle powered by concentrated solar energy. Int. J. Hydrogen Energy 37, 9550–9565. doi:10.1016/j.ijhydene.2012.03.088

Mjalli, B.F.S., Al-asheh, S., 2005. Neural-Networks-Based Feedback Linearization versus Model Predictive Control of Continuous Alcoholic Fermentation Process 1191–1200. doi:10.1002/ceat.200500166

Moaveni, B., Kariwala, V., 2012. Input-Output Pairing Selection for Design of Decentralized Controller, in: Plantwide Control: Recent Developments and Applications. John Wiley and Sons Ltd, pp. 73–96.

Mohd, N., Aziz, N., 2016. Performance and robustness evaluation of Nonlinear Autoregressive with Exogenous input Model Predictive Control in controlling industrial fermentation process. J. Clean. Prod. 136, 42–50. doi:10.1016/j.jclepro.2016.06.191

Mohd, N., Nandong, J., 2017. Multi-scale Control of Bunsen Section in Iodine-Sulphur Thermochemical Cycle Process. Chem. Prod. Process Model. doi:10.1515/cppm-2017-0036

Moore, R., Pickard, P.S., Pharma Jr, E.J., Vernon, M.E., Gelbard, F., Lenard, R.X., 2011. United States Patent: Integrated Boiler, Superheater and Decomposer for Sulfuric Acid Decomposition 2, 19–35. doi:10.1145/634067.634234.

Moriarty, P., Honnery, D., 2009. Hydrogen's role in an uncertain energy future. Int. J. Hydrogen Energy 34, 31–39. doi:10.1016/j.ijhydene.2008.10.060

Mu, J., Rees, D., Liu, G.., 2005. Advanced controller design for aircraft gas turbine engines. Control Eng. Pract. 13, 1001–1015.

Murthy Konda, N.V.S.., Rangaiah, G.P., 2012. Control Degrees of Freedom Analysis for Plantwide Control of Industrial Process, in: Rangaiah, G.P., Kariwala, V. (Eds.), Plantwide Control: Recents Development and Applications. John Wiley and Sons Ltd, pp. 22–42.

Murthy Konda, N.V.S.N., Rangaiah, G.P., Krishnaswamy, P.R., 2006. A simple and

effective procedure for control degrees of freedom. Chem. Eng. Sci. 61, 1184–1194. doi:10.1016/j.ces.2005.08.026

Nagarajan, V., Chen, Y., Hung, T.-C., Wang, Q., Ponyavin, V., 2014. Numerical modeling of bayonet-type heat exchanger and decomposer for the decomposition of sulfuric acid to sulfur dioxide. Heat Transf. Eng. 35, 589–599. doi:10.1080/01457632.2013.837644

Nagarajan, V., Ponyavin, V., Chen, Y., Vernon, M.E., Pickard, P., Hechanova, A.E., 2009. CFD modeling and experimental validation of sulfur trioxide decomposition in bayonet type heat exchanger and chemical decomposer for different packed bed designs. Int. J. Hydrogen Energy 34, 2543–2557. doi:10.1016/j.ijhydene.2008.10.094

Nagy, Z., Agachi, S., 1997. Model predictive control of a PVC batch reactor 21, 571–591.

Nagy, Z.K., Mahn, B., Allgo, F., 2007. Evaluation study of an efficient output feedback nonlinear model predictive control for temperature tracking in an industrial batch reactor $ 15, 839–850. doi:10.1016/j.conengprac.2006.05.004

Nandong, J., 2015. Heuristic-based multi-scale control procedure of simultaneous multi-loop PID tuning for multivariable processes. J. Process Control 35, 101–112. doi:10.1016/j.jprocont.2015.08.015

Nandong, J., 2014. A Multi-scale Control Approach for PID Controller Tuning based on Complex Models.

Nandong, J., Samyudia, Y., 2009. PCA-BASED METHOD OF IDENTIFICATION OF DOMINANT 1–10.

Nandong, J., Yudi, S., Moses O, T., 2010. Novel PCA-Based Technique for Identification of Dominant Variables for Partial Control. Chem. Prod. Process Model. 5.

Nandong, J., Zang, Z., 2013a. High-performance multi-scale control scheme for stable,

integrating and unstable time-delay processes. J. Process Control 23, 1333–1343. doi:10.1016/j.jprocont.2013.08.007

Nandong, J., Zang, Z., 2013b. Novel Multiscale Control Scheme for Nonminimum-Phase Processes.

Nandong, J., Zhuquan, Z., 2013. Multi-scale control: Improved technique to overcome time-delay limitation. Ind. Electron. Appl. (ICIEA), 2013 8th IEEE Conf. on, 19-21 June 2013.

Niederlinski, a., 1971. A heuristic approach to the design of linear multivariable interacting control systems. Automatica 7, 691–701. doi:10.1016/0005-1098(71)90007-0

Noguchi, H., Terada, A., Onuki, K., Hino, R., 2014. Boiling heat transfer characteristics of a sulfuric-acid flow in thermochemical iodine–sulfur cycle. Chem. Eng. Res. Des. 92, 1659–1663. doi:10.1016/j.cherd.2013.12.014

Nowotny, J., Veziroglu, T.N., 2011. Impact of hydrogen on the environment. Int. J. Hydrogen Energy 36, 13218–13224. doi:10.1016/j.ijhydene.2011.07.071

O'Keefe, D., Allen, C., Besenbruch, G., Brown, L., Norman, J., Sharp, R., McCorkle, K., 1982. Preliminary results from bench-scale testing of a sulfur-iodine thermochemical water-splitting cycle. Int. J. Hydrogen Energy 7, 381–392. doi:10.1016/0360-3199(82)90048-9

Pan, T., Li, S., Cai, W.J., 2007. Lazy learning-based online identification and adaptive PID control: A case study for CSTR process. Ind. Eng. Chem. Res. 46, 472–480. doi:10.1021/ie0608713

Park, J., Cho, J.H., Jung, H., Jung, K.D., Kumar, S., Moon, I., 2013. Simulation and experimental study on the sulfuric acid decomposition process of SI cycle for hydrogen production. Int. J. Hydrogen Energy 38, 5507–5516. doi:10.1016/j.ijhydene.2013.03.027

Paul, M.M., Brown, L.C., Technology, A., Park, T.C., 2003a. Thermodynamics of the Sulfur-Iodine Cycle for Thermochemical Hydrogen Production. Outlook.

Paul, M.M., Brown, L.C., Technology, A., Park, T.C., 2003b. Thermodynamics of the Sulfur-Iodine Cycle for Thermochemical Hydrogen Production.

Pearson, R.K., 2003. Selecting nonlinear model structures for computer control 13, 1–26.

Pearson, R.K., 1995. Nonlinear input / output modelling 5, 197–211.

Perret, R., 2011a. Solar Thermochemical Hydrogen Production Research (STCH) Thermochemical Cycle Selection and Investment Priority. Sandia Rep. 1–117.

Perret, R., 2011b. Solar Thermochemical Hydrogen Production Research (STCH) Thermochemical Cycle Selection and Investment Priority.

Ping, Z., Laijun, W., Songzhe, C., Jingming, X., 2016a. Progress of nuclear hydrogen production through the iodine-sulfur process in China. Renew. Sustain. Energy Rev. 1–11. doi:10.1016/j.rser.2017.05.275

Ping, Z., Laijun, W., Songzhe, C., Jingming, X., 2016b. Progress of nuclear hydrogen production through the iodine-sulfur process in China. Renew. Sustain. Energy Rev. 1–11. doi:10.1016/j.rser.2017.05.275

Prakash, J., Srinivasan, K., 2009. Design of nonlinear PID controller and nonlinear model predictive controller for a continuous stirred tank reactor. ISA Trans. 48, 273–282. doi:10.1016/j.isatra.2009.02.001

Prausnitz, J.M., Tavares, F.W., 2004. Thermodynamics of Fluid-Phase Equilibria for Standard Chemical Engineering Operations. AIChE J. 50, 739–761. doi:10.1002/aic.10069

Proll, T., Karim, M.N., 1994. Nonlinear control of bioreactor model using exact and U0

linerization. Int. J. Control 60, 499–519.

Prosini, P.P., Cento, C., Giaconia, A., Caputo, G., Sau, S., 2009. A modified sulphur-iodine cycle for efficient solar hydrogen production. Int. J. Hydrogen Energy 34, 1218–1225. doi:10.1016/j.ijhydene.2008.11.011

Puebla, H., Hernandez-Martinez, E., Hernandez-Suarez, R., Ramirez-Muñoz, J., Alvarez-Ramirez, J., 2013. A simple feedback control approach for output modulation of spatiotemporal patterns in a class of tubular reactors. Ind. Eng. Chem. Res. 52, 17517–17528. doi:10.1021/ie4013562

Rangaiah, G.P., Kariwala, V., 2012. Plantwide Control Recents Developments and Applications, First. ed. John Wiley and Sons Ltd, United Kingdom.

Rangaiah, G.P., Saha, P., Tadé, M.O., 2002. Nonlinear model predictive control of an industrial four-stage evaporator system via simulation. Chem. Eng. J. 87, 285–299. doi:10.1016/S1385-8947(01)00240-6

Rao, K.R., 2012. Companion Guide to the ASME Boiler and Pressure Vessel Code, Volume 2, 4th ed. ASME, United States.

Rashkeev, S.N., Ginosar, D.M., Petkovic, L.M., Farrell, H.H., 2009. Catalytic activity of supported metal particles for sulfuric acid decomposition reaction. Catal. Today 139, 291–298. doi:10.1016/j.cattod.2008.03.029

Ratlamwala, T.A.H., Dincer, I., 2014. Comparative energy and exergy analyses of two solar-based integrated hydrogen production systems. Int. J. Hydrogen Energy. doi:10.1016/j.ijhydene.2014.10.123

Rodriguez-Toral, M.A., Morton, W., Mitchell, D.R., 2000. Using new packages for modelling, equation oriented simulation and optimization of a cogeneration plant. Comput. Chem. Eng. 24, 2667–2685. doi:10.1016/S0098-1354(00)00620-7

Rosen, M., 1998. Comparative efficiency assessments for a range of hydrogen production processes. Int. J. Hydrogen Energy 23, 653–659. doi:10.1016/S0360-3199(97)00080-3

Rosen, M. a., 1996. Thermodynamic comparison of hydrogen production processes. Int. J. Hydrogen Energy 21, 349–365. doi:10.1016/0360-3199(95)00090-9

Säck, J.P., Roeb, M., Sattler, C., Pitz-Paal, R., Heinzel, a., 2012. Development of a system model for a hydrogen production process on a solar tower. Sol. Energy 86, 99–111. doi:10.1016/j.solener.2011.09.010

Sakaba, N., Kasahara, S., Ohashi, H., Sato, H., Kubo, S., Terada, a., Nishihara, T., Onuki, K., Kunitomi, K., 2006. Hydrogen production by thermochemical water-splitting IS process utilizing heat from high-temperature reactor HTTR. Whec 16 1–11.

Sakaba, N., Kasahara, S., Onuki, K., Kunitomi, K., 2007. Conceptual design of hydrogen production system with thermochemical water-splitting iodine-sulphur process utilizing heat from the high-temperature gas-cooled reactor HTTR. Int. J. Hydrogen Energy 32, 4160–4169. doi:10.1016/j.ijhydene.2007.06.005

Sakaba, N., Sato, H., Ohashi, H., Nishihara, T., Kunitomi, K., 2012. Development Scenario of the Iodine-Sulphur Hydrogen Production Process to be Coupled with VHTR System as a Conventional Chemical Plant Development Scenario of the Iodine-Sulphur Hydrogen Production Process to be C. J. Nucl. Sci. Technol. 45, No 9, 962–969.

Sato, H., Kubo, S., Yan, X.L., Tachibana, Y., Kato, Y., 2011. Control strategies for transients of hydrogen production plant in VHTR cogeneration systems. Prog. Nucl. Energy 53, 1009–1016. doi:10.1016/j.pnucene.2011.04.013

Satyapal, S., Thomas, G., 2008. Targets for Onboard Hydrogen Storage Systems, in: Hydrogen Fuel. CRC Press, pp. 327–340. doi:doi:10.1201/9781420045772.ch9

Schultz, K., 2003. Thermochemical Production of Hydrogen from Solar and Nuclear Energy Presentation to the Stanford Global Climate and Energy Project.

Seborg, D.E., Edgar, T.F., Mellichamp, D.A., 2004. Process Dynamics and Control, Second. ed. John Wiley & Sons, Inc, United States.

Seer, Q.H., Nandong, J., 2017a. Stabilization and PID tuning algorithms for second-order unstable processes with time-delays. ISA Trans. 67, 233–245.

Seer, Q.H., Nandong, J., 2017b. Stabilising PID tuning for a class of fourth-order integrating nonminimum-phase systems. Int. J. Control 1–17.

Seferlis, P., Georgiadis, M.C., 2004. The Integration of Process Design and Control. Amsterdam Elsevier.

Seki, H., Naka, Y., 2008. Optimizing control of CSTR/distillation column processes with one material recycle. Ind. Eng. Chem. Res. 47, 8741–8753. doi:10.1021/ie800183a

Shafiee, G., Arefi, M.M., Jahed-Motlagh, M.R., Jalali, A.A., 2008. Nonlinear predictive control of a polymerization reactor based on piecewise linear Wiener model. Chem. Eng. J. 143, 282–292. doi:10.1016/j.cej.2008.05.013

Shakeri, E., Latif-Shabgahi, G., Abharian, A.E., 2017. Design of an intelligent stochastic model predictive controller for a continuous stirred tank reactor through a Fokker-Planck observer. Trans. Inst. Meas. Control 014233121771258. doi:10.1177/0142331217712583

Shen, Y., Cai, W., Li, S., 2010. Multivariable Process Control: Decentralized, Decoupling, or Sparse? 761–771.

Shin, Y., Lee, K., Kim, Y., Chang, J., Cho, W., Bae, K., 2012. A sulfur-iodine flowsheet using precipitation, electrodialysis, and membrane separation to produce hydrogen. Int. J. Hydrogen Energy 37, 16604–16614. doi:10.1016/j.ijhydene.2012.02.082

Singh, a., Al-Raqom, F., Klausner, J., Petrasch, J., Sato, H., Kubo, S., Yan, X.L., Tachibana, Y., Kato, Y., Säck, J.P., Roeb, M., Sattler, C., Pitz-Paal, R., Heinzel, a., Nguyen, T.D.B., Gho, Y.K., Cho, W.C., Kang, K.S., Jeong, S.U., Kim, C.H., Park, C.S., Bae, K.K., Giraldi, M.R., François, J.L., Castro-Uriegas, D., Gabbar, H. a., Hussain, S., Hosseini, A.H., Al-Dabbagh, A.W., Lu, L., Revankar, S.T., Nguyen, T.D.B., Gho, Y.K., Cho, W.C., Kang, K.S., Jeong, S.U., Kim, C.H., Park, C.S., Bae, K.K., Giraldi, M.R., François, J.L., Castro-Uriegas, D., Gabbar, H. a., Hussain, S., Hosseini, A.H., Fruehauf, P.S., Chien, I.L., Lauritsen, M.D., Al-Dabbagh, A.W., Lu, L., 2012. Development of a system model for a hydrogen production process on a solar tower. Int. J. Hydrogen Energy 37, 99–111. doi:10.1016/j.solener.2011.09.010

Skogestad, S., 2012. Economic Plantwide Control, in: Rangaiah, G.P., Kariwala, V. (Eds.), Plantwide Control: Recent Developments and Applications. John Wiley and Sons Ltd, pp. 230–251.

Skogestad, S., 2004. Control structure design for complete chemical plants. Comput. Chem. Eng. 28, 219–234. doi:10.1016/j.compchemeng.2003.08.002

Skogestad, S., 2000a. Self-optimizing control: the missing link between steady-state optimization and control. Comput. Chem. Eng. 24, 569–575. doi:10.1016/S0098-1354(00)00405-1

Skogestad, S., 2000b. Plantwide control: The search for the self-optimizing control structure. J. Process Control 10, 487–507. doi:10.1016/S0959-1524(00)00023-8

Smitkova, M., Janíček, F., Riccardi, J., 2011a. Life cycle analysis of processes for hydrogen production. Int. J. Hydrogen Energy 36, 7844–7851. doi:10.1016/j.ijhydene.2011.01.177

Smitkova, M., Janíček, F., Riccardi, J., 2011b. Life cycle analysis of processes for hydrogen production. Int. J. Hydrogen Energy 36, 7844–7851. doi:10.1016/j.ijhydene.2011.01.177

Str??hle, S., Haselbacher, A., Jovanovic, Z.R., Steinfeld, A., 2014. Transient discrete-granule packed-bed reactor model for thermochemical energy storage. Chem. Eng. Sci. 117, 465–478. doi:10.1016/j.ces.2014.07.009

Temengfl, K.O., Schnelle, P.D., Mcavoy, T.J., 1995. Model predictive control of an industrial packed bed reactor using neural networks. J. Process Control. 5, 19–27.

Terada, A., Iwatsuki, J., Ishikura, S., Noguchi, H., Kubo, S., Okuda, H., Kasahara, S., Tanaka, N., Ota, H., Onuki, K., Hino, R., 2007. Development of hydrogen production technology by thermochemical water splitting IS process pilot test plan. J. Nucl. Sci. Technol. 44, 477–482. doi:10.1080/18811248.2007.9711311

Vitart, X., Le Duigou, a., Carles, P., 2006. Hydrogen production using the sulfur-iodine cycle coupled to a VHTR: An overview. Energy Convers. Manag. 47, 2740–2747. doi:10.1016/j.enconman.2006.02.010

Vural, I.H., Altinten, A., Hapołlu, H., Erdołan, S., Alpbaz, M., 2015. Application of pH control to a tubular flow reactor. Chinese J. Chem. Eng. 23, 154–161. doi:10.1016/j.cjche.2014.10.002

Wang, L., 2009. Model Predictive Control System Design and Implementation Using MATLAB, 1st ed. Springer-Verlag, London.

Wang, L., Li, D., Zhang, P., Chen, S., Xu, J., 2012. The HI catalytic decomposition for the lab-scale H2 producing apparatus of the iodine-sulfur thermochemical cycle. Int. J. Hydrogen Energy 37, 6415–6421. doi:10.1016/j.ijhydene.2012.01.052

Wang, L., Zhang, P., Chen, S., Xu, J., 2014a. Overview of the development of catalysts for HI decomposition in the iodine–sulfur thermochemical cycle at INET. Nucl. Eng. Des. 271, 60–63. doi:10.1016/j.nucengdes.2013.11.010

Wang, L., Zhang, P., Chen, S., Xu, J., 2014b. Overview of the development of catalysts for HI decomposition in the iodine–sulfur thermochemical cycle at INET. Nucl. Eng. Des.

271, 60–63. doi:10.1016/j.nucengdes.2013.11.010

Willis, M., 2000. Review of methods for non-linear control. Lorien.Ncl.Ac.Uk.

World Nuclear Association, n.d. World Nuclear Association [WWW Document]. URL www.world-nuclear.org (accessed 11.25.17).

Xu, L., Wang, L., Zhang, P., Hu, S., Li, D., Chen, S., 2017a. INET's catalysts study for HI decomposition in the thermochemical water-splitting iodine???sulfur process for hydrogen production. Int. J. Hydrogen Energy 42, 3593–3597. doi:10.1016/j.ijhydene.2016.08.042

Yadav, D., Banerjee, R., 2016a. A review of solar thermochemical processes. Renew. Sustain. Energy Rev. 54, 497–532. doi:10.1016/j.rser.2015.10.026

Yadav, D., Banerjee, R., 2016b. A review of solar thermochemical processes. Renew. Sustain. Energy Rev. 54, 497–532. doi:10.1016/j.rser.2015.10.026

Yoon, H.J., Kim, S.J., Cheon No, H., Lee, B.J., Kim, E.S., 2008. A thermo-physical model for hydrogen-iodide vapor-liquid equilibrium and decomposition behavior in the iodine-sulfur thermo-chemical water splitting cycle. Int. J. Hydrogen Energy 33, 5469–5476. doi:10.1016/j.ijhydene.2008.05.107

Yoon, H.J., No, H.C., Lee, J., Choi, J.Y., Pyon, C.U., 2015. Experimental validation of an optimal operating window in the Bunsen reaction section of the iodine–sulfur cycle. Int. J. Hydrogen Energy 1–9. doi:10.1016/j.ijhydene.2015.05.104

Zeng, K., Zhang, D., 2010. Recent progress in alkaline water electrolysis for hydrogen production and applications. Prog. Energy Combust. Sci. 36, 307–326. doi:10.1016/j.pecs.2009.11.002

Zhang, P., Chen, S.Z., Wang, L.J., Yao, T.Y., Xu, J.M., 2010a. Study on a lab-scale hydrogen production by closed cycle thermo-chemical iodine-sulfur process. Int. J.

Hydrogen Energy 35, 10166–10172. doi:10.1016/j.ijhydene.2010.07.150

Zhang, P., Chen, S.Z., Wang, L.J., Yao, T.Y., Xu, J.M., Yoon, H.J., No, H.C., Lee, J.I., Choi, J.Y., Pyon, C.U., Cheon No, H., Kim, Y.Y.S., Jin, H.G., Lee, J.I., Lee, B.J., Wang, Z.L., Naterer, G.F., Gabriel, K.S., Gravelsins, R., Daggupati, V.N., Shin, Y., Chang, J., Lee, T., Lee, K., Kim, Y.Y.S., Murphy IV, J.E., O'Connell, J.P., Leybros, J., Gilardi, T., Saturnin, a., Mansilla, C., Carles, P., Lee, B.J., Cheon No, H., Joon Yoon, H., Jun Kim, S., Soo Kim, E., Kubo, S., Tanaka, N., Iwatsuki, J., Kasahara, S., Imai, Y., Noguchi, H., Onuki, K., Giaconia, A., Caputo, G., Sau, S., Prosini, P.P., Pozio, A., De Francesco, M., Tarquini, P., Nardi, L., Ceroli, a., Diamanti, M., Barbarossa, V., Tarquini, P., Sau, S., Cerri, G., Salvini, C., Corgnale, C., Giovannelli, A., De Lorenzo Manzano, D., Martinez, A.O., Le Duigou, A., Borgard, J.M., Mansilla, C., Cementizi, M., 2010b. Study on a lab-scale hydrogen production by closed cycle thermo-chemical iodine-sulfur process. Int. J. Hydrogen Energy 35, 7939–7948. doi:10.1016/j.ijhydene.2008.11.009

Zhang, Y., Peng, P., Ying, Z., Zhu, Q., Zhou, J., Wang, Z., Liu, J., Cen, K., 2014. Experimental investigation on multiphase bunsen reaction in the thermochemical sulfur-iodine cycle. Ind. Eng. Chem. Res. 53, 3021–3028. doi:10.1021/ie4038856

Zhang, Z., Wu, Z., Durand, H., Albalawi, F., Christofides, P.D., 2018. On integration of feedback control and safety systems: Analyzing two chemical process applications. Chem. Eng. Res. Des. 132, 616–626. doi:10.1016/j.cherd.2018.02.009

Zhao, D., Zhu, Q., Dubbeldam, J., 2015. Terminal sliding mode control for continuous stirred tank reactor. Chem. Eng. Res. Des. 94, 266–274. doi:10.1016/j.cherd.2014.08.005

Zhu, G., Henson, M.A., Ogunnaike, B.A., 2000. A hybrid model predictive control strategy for nonlinear plant-wide control 10, 449–458.

Zhu, Q., Zhang, Y., Ying, Z., Wang, S., Wang, Z., Zhou, J., Cen, K., 2013. Kinetic and

thermodynamic studies of the Bunsen reaction in the sulfur-iodine thermochemical process. Int. J. Hydrogen Energy 38, 8617–8624. doi:10.1016/j.ijhydene.2013.04.110

Every reasonable effort has been made to acknowledge the owners of copyright materials. I would be pleased to hear from any copyright owner who has been omitted or incorrectly acknowledge.

Appendix A

Equation (3.18) can be simplified into a polynomial form

$$f_6 s^6 + \left(f_5 + K_{L_1} h_5\right)s^5 + \left(f_4 + K_{L_1} h_4\right)s^4 + \quad \left(f_3 + K_{L3} h_3\right)s^3 + \left(f_2 + K_{L_2} h_2\right)s^2 + \left(f_1 + K_{L_1} h_1\right)s + K_{L_1} h_0 = 0$$

Given that,

$$f_6 = a_4 \tau_{11} \tau_{I_1}$$

$$f_5 = (a_3 \tau_{11} + a_4)\tau_{J_1}$$

$$f_4 = (a_2 \tau_{11} + a_3)\tau_{I_1}$$

$$f_3 = (a_1 \tau_{11} + a_2)\tau_{I_1}$$

$$f_2 = (\tau_{11} + a_1)\tau_{I_1}$$

$$f_1 = \tau_{I_1}$$

General equation

$$f_k = (a_{k-2} \tau_{11} + a_{k-1})\tau_{I_1} \qquad for\ k = 1,2,\ldots,6$$

$$h_5 = \tau_{I_1}(b_{14} - \psi_1 b_{24})$$

$$h_4 = \tau_{I_1}(b_{13} - \psi_i b_{23}) + b_{14} - \psi_1 b_{24}$$

$$h_3 = \tau_{I_1}(b_{12} - \psi_1 b_{22}) + b_{13} - \psi_1 b_{23}$$

$$h_2 = \tau_{I_1}(b_{11} - \psi_1 b_{21}) + b_{12} - \psi_1 b_{22}$$

$$h_1 = \tau_{I_1}(b_{10} - \psi_1 b_{20}) + b_{11} - \psi_1 b_{21}$$

$$h_0 = 1 - \psi_1$$

General equation

$$h_k = \tau_{I_1}(b_{1(k-1)} - \psi_1 b_{2(k-1)}) + b_{1k} - \psi_1 b_{2k} \qquad for\ k = 0.1,\ldots,5$$

The parameters in definition are

$$a_{-1} = 0$$

$$a_0 = 1$$

$$a_1 = \tau_{12} + \tau_{21} + \alpha_{11} + \alpha_{I_1}$$

$$a_2 = \tau_{12}\tau_{21} + (\tau_{12} + \tau_{21})(\alpha_{11} + \alpha_{I_1}) + \alpha_{11}\alpha_{I_1}$$

$$a_3 = \tau_{12}\tau_{21}(\alpha_{11} + \alpha_{I_1}) + \alpha_{11}\alpha_{I_1}(\tau_{12} + \tau_{21})$$

$$a_4 = \tau_{12}\tau_{21}\alpha_{11}\alpha_{I_1}$$

$$b_{1(-1)} = b_{2(-1)} = 0$$

$$b_{10} = b_{20} = 1$$

$$b_{11} = \alpha_{I_1} - \alpha_{11} + \tau_{12} + \tau_{21}$$

$$b_{12} = -\alpha_{11}\alpha_{I_1} + (\alpha_{I_1} - \alpha_{11})(\tau_{12} + \tau_{21}) + \tau_{12}\tau_{21}$$

$$b_{13} = -\alpha_{11}\alpha_{I_1}(\tau_{12} + \tau_{21}) + (\alpha_{I_1} - \alpha_{11})\tau_{12}\tau_{21}$$

$$b_{14} = -\alpha_{11}\alpha_{I_1}\tau_{12}\tau_{21}$$

$$b_{21} = \tau_{11} + \tau_{22} + \alpha_{11} - \alpha_{I_1}$$

$$b_{22} = \tau_{11}\tau_{22} + (\tau_{11} + \tau_{22})(\alpha_{11} - \alpha_{I_1}) - \alpha_{11}\alpha_{I_1}$$

$$b_{23} = \tau_{11}\tau_{22}(\alpha_{11} - \alpha_{I_1}) - \alpha_{11}\alpha_{I_1}(\tau_{11} + \tau_{22})$$

$$b_{24} = -\tau_{11}\tau_{22}\alpha_{11}\alpha_{I_1}$$

The condition for P-controller,

$$\left.\begin{aligned} K_{upperk} &= \frac{(a_{k-1}\tau_{11} + a_k)}{|f_k|} \\ K_{lowerk} &= -\inf \end{aligned}\right\} if \;\; f_k < 0, \; for \; k = 1,2,3,4$$

$$\left.\begin{aligned} K_{upperk} &= \frac{-(a_{k-1}\tau_{11} + a_k)}{f_k} \\ K_{lowerk} &= -\inf \end{aligned}\right\} if \;\; f_k > 0, \; for \; k = 1,2,3,4$$

The condition for PI-controller,

$$\left.\begin{aligned} K_{upperk} &= \frac{(a_{k-2}\tau_{11} + a_{k-1})\tau_{I_1}}{|f_k|} \\ K_{lowerk} &= -\inf \end{aligned}\right\} if \;\; f_k < 0, \; for \; k = 1,2,3,4,5,6$$

$$\left.\begin{aligned} K_{upperk} &= \frac{-(a_{k-2}\tau_{11} + a_{k-1})\tau_{I_1}}{f_k} \\ K_{lowerk} &= -\inf \end{aligned}\right\} if \;\; f_k < 0, \; for \; k = 1,2,3,4,5,6$$

Finally, the limit or stability region can be calculate

$$\overline{K}_{\min} = \min(K_{upperk})$$

$$\underline{K}_{\max} = \max(K_{lowerk})$$

By providing three desired inputs; process gains, time constants and time delays, one may calculate the limits ($\overline{K}_{min}$ and $\underline{K}_{max}$) via an m-file in the MATLAB software.

Appendix B

Figure 3.7, 'calculcoeffa' file

```
function [A,B,C,L11,LGCs] = calculcoeffa(K,T,D)
%Characteristic polynomial
% Af(s) + Kl*(Bf(s) - Cf(s)) = 0
% Kl = Kc*K1/L11; Loop gain
% This function to calculate coefficient ai, i = 1, 2, ...,5
% where Af(s) = A(n)*s^n + ... + A(2)*s^2 + A(1)*s + 1;
% Process gain
k11 = K(1,1);
k12 = K(1,2);
k21 = K(2,1);
k22 = K(2,2);
% Time constant
t11 = T(1,1);
t12 = T(1,2);
t21 = T(2,1);
t22 = T(2,2);
% Deadtime
d11 = D(1,1);
d12 = D(1,2);
d21 = D(2,1);
d22 = D(2,2);
% RGA
L11 = k11/(k11 - (k12*k21/k22));
% SISO upper limit
LGCs = (t11 + 0.5*d11)/(0.5*d11); % SISO upper limit
% Assume pade approx exp(-D*s) = (1 - alp*s)/(1 + alp*s); alp = 0.5*D
alp1 = d11/2;
alpI = (d12 + d21 - d22)/2;
%
a1 = alp1 + alpI + t12 + t21;
a2 = alp1*alpI + t12*t21 + (alp1+alpI)*(t12+t21);
a3 = alp1*alpI*(t12+t21) +t12*t21*(alp1+alpI);
a4 = t12*t21*alp1*alpI;
%
A = [t11 + a1;
     a1*t11 + a2;
     a2*t11 + a3;
     a3*t11 + a4;
     a4*t11];
%
% Calculate coefficient bi, i = 1, 2, ...4
% Bf(s) = B(n)*s^b +  B(1)*s + 1;
b1 = alpI - alp1 + t12 + t21;
b2 = t12*t21 - alp1*alpI + (alpI-alp1)*(t12 + t21);
b3 = (alpI-alp1)*t12*t21 - alp1*alpI*(t12 + t21);
b4 = -alp1*alpI*t12*t21;
```

```
B = L11*[b1;b2;b3;b4];
%
% Calculate coefficient ci, i = 1, 2, ..., 4
% Cf(s) = C(n)*s^n + ... C(1)*s + 1;
c1 = alp1 - alpI + t11 + t22;
c2 = t11*t22 - alp1*alpI + (alp1-alpI)*(t11+t22);
c3 = (alp1-alpI)*t11*t22 - alp1*alpI*(t11+t22);
c4 = alp1*alpI*t11*t22;
C = (L11-1)*[c1;c2;c3;c4];
%
end
%
```

Figure 3.7, 'LGCcalc' file

```
function [Kulmin,Kllmax,L11,LGCs,Klb1,Klb2,Klc,Kld] = LGCcalc(K,T,D)
%
% This function is to calculate the upper and lower limits
% Characteristic polynomial is given by
% Af(s) + Kl*(Bf(s) - Cf(s)) = 0;
% Calculate coefficients in Af, Bf, and Cf
% Express characteristic polynomial as (for power up to 5)
% (f5 + Kl*h5)*s^5 + ... (f1 + Kl*h1)*s + (f0 + Kl*h0) = 0
% where fi = A(i) and h(i) = B(i) - C(i); f0 = 1 and h0 = 1
% ---------------------------------------------------------
[A,B,C,L11,LGCs] = calculcoeffa(K,T,D);
%
f = A;
h = [B - C];
% length of h;
n = length(h);
for i = 1:n
    if h(i) < 0
        Kul(i) = f(i)/abs(h(i));
        Kll(i) = -inf;
    else
        Kll(i) = -f(i)/h(i);
        Kul(i) = inf;
    end
end
% Note that the coeffcient of s^0 alaways lead to lower limit Kll = -1;
%
% Determine maximum lower limit
Kllmax = max([-1,Kll]);
% Determine minimum upper limit
Kulmin = min(Kul);
% End of function
%
Klb1 = fzero(@costb1,0.1*Kulmin);
Klb2 = fzero(@costb2,0.1*Kulmin);
Klc = fzero(@costc,0.1*Kulmin);
Kld = fzero(@costd,0.1*Kulmin);
%
    function Jb1 = costb1(Klb1)
        Jb1 = ( (f(4)+Klb1*h(4))*(f(3)+Klb1*h(3)) - ...
            (f(5)*(f(2)+Klb1*h(2))) )/(f(4)+Klb1*h(4));
    end
    function Jb2 = costb2(Klb2)
        Jb2 = ( (f(4)+Klb2*h(4))*(f(1)+Klb2*h(1)) - f(5)
)/(f(4)+Klb1*h(4));
    end
    function Jc = costc(Klc)
       coefb1 = ( (f(4)+Klc*h(4))*(f(3)+Klc*h(3)) - ...
                  (f(5)*(f(2)+Klc*h(2))) )/(f(4)+Klc*h(4));
```

```
       coefb2 = ( (f(4)+Klc*h(4))*(f(1)+Klc*h(1)) - f(5)
)/(f(4)+Klc*h(4));
       Jc = coefb1*(f(2)+Klc*h(2)) - coefb2*(f(4)+Klc*h(4));
    end
    function Jd = costd(Kld)
       coefb1 = ( (f(4)+Kld*h(4))*(f(3)+Kld*h(3)) - ...
                  (f(5)*(f(2)+Kld*h(2))) )/(f(4)+Kld*h(4));
       coefb2 = ( (f(4)+Kld*h(4))*(f(1)+Kld*h(1)) - f(5)
)/(f(4)+Kld*h(4));
        coefc1 = (coefb1*(f(2)+Kld*h(2)) -
coefb2*(f(4)+Kld*h(4)))/coefb1;
        Jd = coefc1*coefb2 - coefb1;
    end
%
end
%
```